(19) Europäisches Patentamt
European Patent Office
Office européen des brevets

(11) EP 1 001 437 A1

(12) EUROPEAN PATENT APPLICATION

(43) Date of publication:
17.05.2000 Bulletin 2000/20

(51) Int Cl.[7]: **H01F 1/153**

(21) Application number: **99308538.0**

(22) Date of filing: **28.10.1999**

(84) Designated Contracting States:
AT BE CH CY DE DK ES FI FR GB GR IE IT LI LU MC NL PT SE
Designated Extension States:
AL LT LV MK RO SI

(30) Priority: **10.11.1998 JP 31966298**
10.11.1998 JP 31966398
10.11.1998 JP 31966498
20.11.1998 JP 33176298
20.11.1998 JP 33177298
20.11.1998 JP 33177398
20.11.1998 JP 33177498
20.11.1998 JP 33177598
02.12.1998 JP 34347398
02.12.1998 JP 34347498

(71) Applicants:
- **ALPS ELECTRIC CO., LTD.**
  Ota-ku Tokyo 145 (JP)
- **Inoue, Akihisa**
  Sendai-shi, Miyagi-ken (JP)
- **Masumoto, Tsuyoshi**
  Miyagi-ken (JP)

(72) Inventors:
- **Makino, Akihiro**
  Nagaoka-shi, Niigata-ken (JP)
- **Bito, Teruo**
  Honjo-shi, Akita-ken (JP)
- **Murakami, Junichi**
  Mitsuke-shi, Niigata-ken (JP)
- **Yamamoto, Yutaka**
  Nagaoka-shi, Niigata-ken (JP)
- **Kojima, Akinori**
  Nagaoka-shi, Niigata-ken (JP)
- **Takadate, Kinshiro**
  Nagaoka-shi, Niigata-ken (JP)
- **Akihisa, Inoue**
  Aoba-ku, Sendai-shi, Miyagi-ken (JP)
- **Masumoto, Tsuyoshi**
  Sendai-shi, Miyagi-ken (JP)

(74) Representative: **Kensett, John Hinton**
Saunders & Dolleymore,
9 Rickmansworth Road
Watford, Hertfordshire WD1 7HE (GB)

(54) Fe-based soft magnetic alloy , magnetic core using the same, and method for making the same

(57) A Fe-based soft magnetic alloy is represented by the formula: $Fe_aZr_xNb_yB_\beta$ or $(Fe_{1-a}Q_a)_bB_\beta$ $M_\lambda Zn_z$, wherein Q is at least one of Co and Ni; M is at least one selected from the group consisting of Ti, Zr, Hf, V, Nb, Ta, Mo and W; the subscripts satisfy the relationships; $a \leq 0.05$, 80 atomic percent $\leq b$; 5 atomic percent $\leq x + y \leq 7.5$ atomic percent; $1.5/6 \leq x/(x+y) \leq 2.5/6$; and 5 atomic percent $\leq \beta \leq 12.5$ atomic percent. The Fe-based soft magnetic alloy has a fine crystalline texture composed of at least 50% of the fine crystalline texture of a bcc-Fe phase as the major component and the balance being an amorphous phase. The soft magnetic alloy has high saturation magnetic flux density and low iron loss. The alloy is suitable for magnetic cores.

FIG. 1

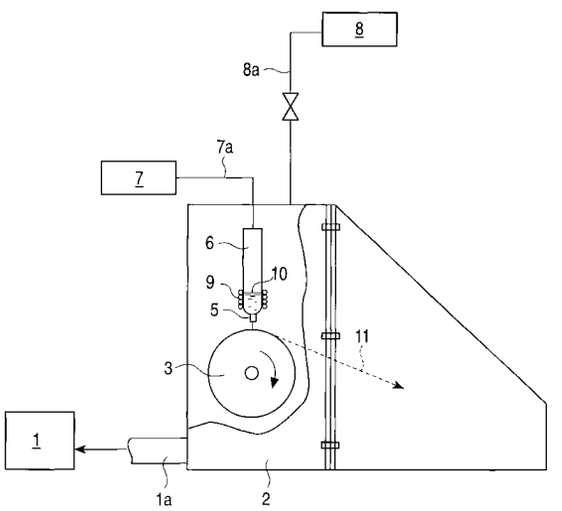

EP 1 001 437 A1

Description

[0001] The present invention relates to a Fe-based soft magnetic alloy having high saturation magnetic flux density and low iron loss used in magnetic heads, transformers, and choke coils, to a magnetic core using the alloy, and to a method for making the alloy.

[0002] Typical magnetic characteristics required for soft magnetic alloys which are used in magnetic heads, transformers and choke coils include high magnetic flux density, high permeability, and low coercive force. In addition, soft magnetic alloys for transformers require low iron loss.

[0003] Various soft magnetic alloy systems have been investigated in view of these requirements. Examples of conventional alloys used in the above fields include Fe-Si alloys and Fe-Ni alloys. In recent years, Fe- or Co-based amorphous alloys have been used.

[0004] Since Fe-Si alloys have large iron loss, transformers using the alloys lose large amounts of electrical power, although the alloys have high saturation magnetic flux density. Fe-Ni alloys designed so as to have satisfactory soft magnetic properties inevitably have low saturation magnetic flux density. Fe-based amorphous alloys undergo large changes in magnetic characteristics over time due to low thermal stability thereof, although the alloys have high saturation magnetic flux density and low iron loss. Since Co-based amorphous alloys have low saturation magnetic flux density, the alloys are not suitable for use in transformers for power conversion.

[0005] Important magnetic characteristics for soft magnetic alloys for transformers are low iron loss and high saturation magnetic flux density. Silicon steel generally used in transformers has an iron loss of 1.0 W/kg at 1.7 T and 50 Hz, and a saturation magnetic flux density of 2.0 T. Thus, the iron loss must be further decreased to satisfy the above requirements.

[0006] A Fe-based amorphous alloy, which is used in particular types of transformers, has an iron loss of 0.25 W/kg at 1.4 T and 50 Hz and a saturation magnetic flux density of 1.56 T. Thus, a lower iron loss and a higher saturation magnetic flux density are required for the Fe-based amorphous alloy.

[0007] The present inventors have applied for patents on Fe-based soft magnetic alloys having high saturation magnetic flux density, in view of the above, as disclosed in Japanese Examined Patent Publication (Kokoku) No. 7-65145 and Japanese Unexamined Patent Publication (Kokai) No. 5-93249. One of these alloys has the following composition:

$$(Fe_{1-a1}Q_{a1})_bB_{x1}T_{y1}$$

wherein Q is Co and/or Ni; T is at least one selected from the group consisting of Ti, Zr, Hf, V, Nb, Ta, Mo and W, and includes Zr and/or Hf as essential components; $a1 \leq 0.05$; $b \leq 93$ atomic percent, $x1 = 0.5$ to 8 atomic percent; and $y1 = 4$ to 9 atomic percent.

[0008] Another alloy has the following composition:

$$Fe_bB_{x2}T_{y2}$$

wherein T is at least one selected from the group consisting of Ti, Zr, Hf, V, Nb, Ta, Mo and W, and includes Zr and/or Hf as essential components; $b \leq 93$ atomic percent, $x2 = 0.5$ to 8 atomic percent; and $y2 = 4$ to 9 atomic percent.

[0009] In these alloys, desired soft magnetic characteristics are achieved by adding other elements and controlling the compositions. Production processes are also essential factors for achieving desired soft magnetic characteristics. For example, when an alloy substantially composed of an amorphous phase is produced by a singe-roller liquid quenching method using a cooling roller and a crucible with a nozzle, the annealing conditions for the resulting amorphous alloy significantly affect properties of the alloy. That is, the properties of the alloy are affected by the annealing temperature and the heating program or heating rate up to the annealing temperature. Also, the temperature of the alloy melt ejected through the nozzle (the ejection temperature) significantly affects properties of the resulting alloy.

[0010] When a soft magnetic alloy is used in transformers, the alloy is inevitably allowed to stand in a heated state for long periods in a production step. Such long heating periods will significantly change magnetic characteristics of the soft magnetic alloy over time. When the soft magnetic alloy is used in compact electronic devices, such as magnetic heads, the stationary detecting current will be increased so as to increase the output. Such a high current results in heating of the magnetic head to a temperature higher than 200°C. Thus, magnetic characteristics of the soft magnetic alloy change significantly over time. Accordingly, the product will be unreliable.

[0011] The present inventors have developed Fe-based soft magnetic alloys having various compositions, and have discovered that specific Zr and Nb content in the alloy contribute to superior soft magnetic characteristics of the alloy. That is, an alloy of the specific Zr and Nb content has significantly decreased iron loss in a frequency range of several hundreds Hz or less. Accordingly, the present inventors have completed the present invention.

[0012] It is an object of the present invention to provide a Fe-based soft magnetic alloy having excellent soft magnetic characteristics, such as high saturation magnetic flux density and low iron loss, large fracture strain, and satisfactory moldability and workability.

[0013] It is another object of the present invention to provide a Fe-based soft magnetic alloy which has a saturation magnetic flux density of 1.5 T or more, an iron loss of 0.10 W/kg or less at 1.4 T and 50 Hz, and in which magnetic characteristics change only slightly over time when the alloy is heated for long periods, and facilitates bending working in the production of transformers, etc.

[0014] It is another object of the present invention to provide a method for making a Fe-based soft magnetic alloy having excellent soft magnetic characteristics, such as low coercive force, high permeability, and high saturation magnetic flux density.

[0015] It is another object of the present invention to provide a method for making a Fe-based soft magnetic alloy having superior soft magnetic characteristics and in which magnetic characteristics change only slightly over time when the alloy is allowed to stand at high temperatures for long periods, and facilitating working in production of transformers, etc.

[0016] In a first aspect of the present invention, a Fe-based soft magnetic alloy (first soft magnetic alloy) is provided, having high saturation magnetic flux density and low iron loss, represented by the following formula and having a fine crystalline texture formed by annealing an amorphous alloy substantially composed of an amorphous phase; at least 50% of the fine crystalline texture being composed of a bcc-Fe phase (body-centered-cubic-Fe phase) as the major component having an average crystal grain size of 100 nm or less:

$$Fe_aZr_xNb_yB_z$$

wherein the subscripts satisfy the relationships; 80 atomic percent $\leq a$; 5 atomic percent $\leq x + y \leq 7$ atomic percent; $1.5/6 \leq x/(x+y) \leq 2.5/6$; and 5 atomic percent $\leq z \leq 12.5$ atomic percent.

[0017] Preferably, the subscripts satisfy the relationships 83 atomic percent $\leq a$; 5.7 atomic percent $\leq x + y \leq 6.5$ atomic percent; $1.5/6 \leq x/(x+y) \leq 2.5/6$; and 6 atomic percent $\leq z \leq 9.5$ atomic percent.

[0018] More preferably, the subscripts satisfy the relationships 85 atomic percent $\leq a \leq 86$ atomic percent; 5.7 atomic percent $\leq x + y \leq 6.5$ atomic percent; $x/(x+y) = 2/6$; and 8 atomic percent $\leq z \leq 9$ atomic percent.

[0019] Most preferably, the subscripts x and y satisfy the relationships 1.5 atomic percent $\leq x \leq 2.5$ atomic percent; and 3.5 atomic percent $\leq z \leq 5.0$ atomic percent.

[0020] Preferably, the crystallization temperature T_{X1} of the bcc-Fe phase, the crystallization temperature T_{X2} of a compound phase which is crystallized at a temperature higher than T_{X1}, and the difference $\Delta T_X = T_{X2} - T_{X1}$ of the crystallization temperatures satisfy the relationship $200°C \leq \Delta T_X$.

[0021] Preferably, the saturation magnetic flux density of the Fe-based soft magnetic alloy is at least 1.5 T; the iron loss, when a magnetic flux of 1.4 T at a frequency of 50 Hz is applied, is 0.15 W/kg or less; and the change in iron loss after aging at 200°C for 500 hours is 10% or less.

[0022] Preferably, the fracture strain of the Fe-based soft magnetic alloy is 1.0×10^{-2} or more.

[0023] This Fe-based soft magnetic alloy has improved permeability and saturation magnetic flux density and decreased iron loss. In particular, iron loss and the change rate of iron loss are significantly decreased in a low-frequency region of several hundreds Hz or less.

[0024] In addition, the Fe content is relatively high, that is, 80 atomic percent or more, preferably 83 atomic percent or more and more preferably 85 atomic percent or more. Thus, the Fe-based soft magnetic alloy has improved soft magnetic characteristics.

[0025] The above-specified B content suppresses the formation of a FeB compound during the deposition of the fine crystalline texture in an annealing treatment of the alloy and can maintain soft magnetic characteristics at high levels.

[0026] Furthermore, a difference ΔT_X in crystallization temperatures of 200°C or more facilitates annealing the alloy at an optimized temperature which promotes precipitation of only the bcc-Fe phase and suppresses precipitation of the other compound phases. Thus, the alloy has improved soft magnetic characteristics.

[0027] In a second aspect of the present invention, a Fe-based soft magnetic alloy (a second soft magnetic alloy) is provided, having high saturation magnetic flux density and low iron loss, represented by the following formula and having a fine crystalline texture comprising at least 50% of fine bcc-Fe crystal grains having an average crystal grain size of 100 nm or less and the balance being an amorphous phase; the bcc-Fe crystal grains being precipitated by heating to a temperature higher than the crystallization temperature and then cooling a substantially single amorphous phase which is formed by quenching an alloy melt:

$$(Fe_{1-a}Q_a)_bB_xM_yZn_z$$

wherein Q is at least one of Co and Ni; M is at least one selected from the group consisting of Ti, Zr, Hf, V, Nb, Ta, Mo and W; the subscripts satisfy the relationships $0 \leq a \leq 0.05$, 80 atomic percent $\leq b$; 5 atomic percent $\leq x \leq 12.5$ atomic percent; 5 atomic percent $\leq y \leq 7$ atomic percent; and 0.025 atomic percent $\leq z \leq 0.2$ atomic percent.

[0028] In a third aspect of the present invention, a Fe-based soft magnetic alloy (also referred to as a second alloy) is provided, having high saturation magnetic flux density and low iron loss, represented by the following formula and having a fine crystalline texture comprising at least 50% of fine bcc-Fe crystal grains having an average crystal grain size of 100 nm or less and the balance being an amorphous phase; the bcc-Fe crystal grains being precipitated by heating to a temperature higher than the crystallization temperature and then cooling a substantially single amorphous phase which is formed by quenching an alloy melt:

$$(Fe_{1-a}Q_a)_bB_xH_yZn_zM'_u$$

wherein Q is at least one of Co and Ni; M is at least one selected from the group consisting of Ti, Zr, Hf, V, Nb, Ta, Mo and W; M' is at least one selected from the group consisting of Cr, Ru, Rh and Ir; the subscripts satisfy the relationships $0 \leq a \leq 0.05$, 80 atomic percent $\leq b$; 5 atomic percent $\leq x \leq 12.5$ atomic percent; 5 atomic percent $\leq y \leq 7$ atomic percent; 0.025 atomic percent $\leq z \leq 0.2$ atomic percent; and $u \leq 5$ atomic percent.

[0029] In the second Fe-based soft magnetic alloys in the second and third aspects, preferably the change in iron loss after heating at 320°C for 100 hours is 20% or less, the saturation magnetic flux density is 1.5 T or more, and the permeability is 30,000 or more.

[0030] Preferably, the magnetostriction of the Fe-based soft magnetic alloy is 10×10^{-3} or more.

[0031] In a fourth aspect of the present invention, a Fe-based soft magnetic alloy (third Fe based soft magnetic alloy) is provided, having high saturation magnetic flux density and low iron loss, comprising Fe, Zr, Nb, B, and Zn, and having a texture comprising at least 50% of bcc-Fe fine crystal grains having an average crystal grain size of 100 nm or less and the balance being an amorphous phase.

[0032] Preferably, the change in iron loss of the Fe-based soft magnetic alloy after heating at 320°C for 100 hours is 20% or less, the saturation magnetic flux density is 1.5 T or more, and the permeability is 30,000 or more.

[0033] Preferably, the Fe-based soft magnetic alloy is represented by the following formula and has a fine crystalline texture comprising at least 50% of fine bcc-Fe crystal grains having an average crystal grain size of 100 nm or less and the balance being an amorphous phase; the bcc-Fe crystal grains being precipitated by heating to a temperature higher than the crystallization temperature and then cooling a substantially single amorphous phase which is formed by quenching an alloy melt:

$$(Fe_{1-a}Q_a)_bZr_xNb_yB_tZn_z$$

wherein Q is at least one of Co and Ni; the subscripts satisfy the relationships $0 \leq a \leq 0.05$, 80 atomic percent $\leq b$; 1.5 atomic percent $\leq x \leq 2.5$ atomic percent; 3.5 atomic percent $\leq y \leq 5.0$ atomic percent; 5 atomic percent $\leq t \leq 12.5$ atomic percent, 0.025 atomic percent $\leq z \leq 0.2$ atomic percent; 5.0 atomic percent $\leq x + y \leq 7.5$ atomic percent; and $1.5/6 \leq x/(x+y) \leq 2.5/6$.

[0034] Alternatively, the Fe-based soft magnetic alloy may be represented by the following formula and has a fine crystalline texture comprising at least 50% of fine bcc-Fe crystal grains having an average crystal grain size of 100 nm or less and the balance being an amorphous phase; the bcc-Fe crystal grains being precipitated by heating to a temperature higher than the crystallization temperature and then cooling a substantially single amorphous phase which is formed by quenching an alloy melt:

$$(Fe_{1-a}Q_a)_bZr_xNb_yB_tZn_zM'_u$$

wherein Q is at least one of Co and Ni; M' is at least one selected from the group consisting of Cr, Ru, Rh and Ir; the subscripts satisfy the relationships $0 \leq a \leq 0.05$, 80 atomic percent $\leq b$; 1.5 atomic percent $\leq x \leq 2.5$ atomic percent; 3.5 atomic percent $\leq y \leq 5.0$ atomic percent; 5 atomic percent $\leq t \leq 12.5$ atomic percent, 0.025 atomic percent $\leq z \leq 0.2$ atomic percent; $u \leq 5$ atomic percent; 5.0 atomic percent $\leq x + y \leq 7.5$ atomic percent; and $1.5/6 \leq x/(x+y) \leq 2.5/6$.

[0035] Preferably, the magnetostriction is 10×10^{-2} or more.

[0036] In a fifth aspect of the present invention, a low-iron-loss magnetic core is provided, comprising the Fe-based soft magnetic alloy described in any one of the first to fourth aspects.

[0037] Preferably, the saturation magnetic flux density of the Fe-based soft magnetic alloy is at least 1.5 T, the iron loss, when a magnetic flux of 1.4 T at a frequency of 50 Hz is applied, is 0.15 W/kg or less, and the change in iron loss

after aging at 200°C for 500 hours is 10% or less.

[0038] Preferably, the magnetic core comprises a ribbon of the Fe-based soft magnetic alloy having a fracture strain of the 1.0×10^{-2} or more.

[0039] Preferably the magnetic core comprises at least one ring formed of a ribbon of the Fe-based soft magnetic alloy.

[0040] Preferably the magnetic core comprises an annular ring formed by winding a ribbon of the Fe-based soft magnetic alloy.

[0041] In a sixth aspect of the present invention, a method for making a Fe-based soft magnetic alloy is provided, comprising the steps of quenching an alloy melt comprising Fe as the major component, B, and at least one metal M selected from the group consisting of Ti, Zr, Hf, V, Nb, Ta, Mo, W and Mn to form a substantially amorphous phase; and heating the alloy to a predetermined annealing temperature at a heating rate of 10°C/min to 200°C/min to form a texture comprising at least 50% of fine bcc-Fe crystal grains having an average crystal grain size of 100 nm and the balance being an amorphous phase (hereinafter, this method is referred to as the first method).

[0042] Preferably, the predetermined annealing temperature is in a range of 490°C to 670°C. More preferably, the predetermined annealing temperature is in a range of 500°C to 560°C.

[0043] In a seventh aspect of the present invention, a method for making a Fe-based soft magnetic alloy is provided, comprising the steps of melting an alloy melt comprising Fe as the major component, B, and at least one metal M selected from the group consisting of Ti, Zr, Hf, V, Nb, Ta, Mo, W and Mn, in a crucible; ejecting the melt at less than 1,350°C onto a cooling roller through a nozzle to quench and solidify the melt on the roller to form an alloy ribbon substantially composed of an amorphous phase; and annealing the alloy ribbon at an annealing temperature which is higher than the crystallization temperature so as to form a texture comprising at least 50% of fine bcc-Fe crystal grains having an average crystal grain size of 100 nm and the balance being an amorphous phase (hereinafter, this method is referred to as the second method).

[0044] Preferably, the melt is ejected at a temperature of 1,240°C or more.

[0045] In an eighth aspect of the present invention, a method for making a Fe-based soft magnetic alloy comprising a first annealing step for annealing an amorphous alloy comprising: Fe as the major component, B, and at least one metal M selected from the group consisting of Ti, Zr, Hf, V, Nb, Ta, Mo, W and Mn to form a fine crystalline alloy composed of fine bcc-Fe crystal grains having an average crystal grain size of 30 nm and containing an amorphous phase; and a second annealing step for annealing the fine crystalline alloy at an annealing temperature which is 100°c or more and lower than the holding temperature at the first annealing step (hereinafter referred to as the third method).

[0046] Preferably, the annealing temperature is in a range of 200°C to 400°C.

[0047] Preferably, the second annealing step is performed for 0.5 to 100 hours. More preferably, the second annealing step is performed for 1 to 30 hours.

[0048] Preferably, the first annealing step is performed at a heating rate of 10 to 200°C/min.

[0049] Preferably, the first annealing step is performed at an annealing temperature of 500 to 800°C.

[0050] Embodiments of the invention will now be described, by way of example only, with reference to the accompanying schematic drawings in which:

Fig. 1 is a schematic view of an apparatus for making a ribbon of a soft magnetic alloy in accordance with the present invention;

Fig. 2 is a graph showing the relationship between the zinc content in the ribbon and the amount of zinc fed into a crucible used for production of an alloy in accordance with the present invention;

Fig. 3 is an exploded view of a low-iron-loss magnetic core of an embodiment of the present invention;

Fig. 4 is an exploded view of a low-iron-loss magnetic core of another embodiment of the present invention;

Fig. 5 is an isometric view of a magnet core of the present invention, which is applied to a common-mode choke coil;

Fig. 6 is a graph of an annealing pattern in a third method for making a Fe-based soft magnetic alloy;

Fig. 7 is a graph of an annealing pattern in a third method for making a Fe-based soft magnetic alloy;

Fig. 8 shows an X-ray diffraction pattern of a quenched soft magnetic alloy having a composition of $Fe_{86.76}Zr_2Nb_4B_{8.25}$;

Fig. 9 shows an X-ray diffraction pattern of an annealed soft magnetic alloy having a composition of $Fe_{86.76}Zr_2Nb_4B_{8.25}$;

Fig. 10 is a graph showing the relationship between the composition of a soft magnetic alloy containing zirconium and niobium in a total amount of 5 atomic percent and the coercive force (Hc);

Fig. 11 is a graph showing the relationship between the composition of a soft magnetic alloy containing zirconium and niobium in a total amount of 5 atomic percent and the permeability (μ') at 1 kHz;

Fig. 12 is a graph showing the relationship between the composition of a soft magnetic alloy containing zirconium and niobium in a total amount of 5 atomic percent and the saturation magnetic flux density (B_{10}) in a magnetic field of 10 Oe;

Fig. 13 is a graph showing the relationship between the composition of a soft magnetic alloy containing zirconium and niobium in a total amount of 5 atomic percent and the remanent magnetization (Br);

Fig. 14 is a graph showing the relationship between the composition of a soft magnetic alloy containing zirconium and niobium in a total amount of 5.5 atomic percent and the coercive force (Hc);

Fig. 15 is a graph showing the relationship between the composition of a soft magnetic alloy containing zirconium and niobium in a total amount of 5.5 atomic percent and the permeability (μ');

Fig. 16 is a graph showing the relationship between the composition of a soft magnetic alloy containing zirconium and niobium in a total amount of 5.5 atomic percent and the saturation magnetic flux density (B_{10}) in a magnetic field of 10 Oe;

Fig. 17 is a graph showing the relationship between the composition of a soft magnetic alloy containing zirconium and niobium in a total amount of 5.5 atomic percent and the remanent magnetization (Br);

Fig. 18 is a graph showing the relationship between the composition of a soft magnetic alloy containing zirconium and niobium in a total amount of 5.5 atomic percent and the annealing temperature (Ta) when the coercive force (Hc) is minimized;

Fig. 19 is a graph showing the relationship between the composition of a soft magnetic alloy containing zirconium and niobium in a total amount of 5.5 atomic percent and the annealing temperature (Ta) when the permeability (μ') is maximized;

Fig. 20 is a graph showing the relationship between the composition of a soft magnetic alloy containing zirconium and niobium in a total amount of 5.5 atomic percent and the crystallization temperature (T_{X1}) of the bcc-Fe phase;

Fig. 21 is a graph showing the relationship between the composition of a soft magnetic alloy containing zirconium and niobium in a total amount of 5.5 atomic percent and the crystallization temperature ($T_{X1'}$) of the compound phase precipitated at a temperature which is higher than the crystallization temperature of the bcc-Fe phase;

Fig. 22 is a graph showing the relationship between the composition of a soft magnetic alloy containing zirconium and niobium in a total amount of 5.5 atomic percent and the crystallization temperature (T_{X2}) of the FeB_x phase;

Fig. 23 is a graph showing the relationship between the composition of a soft magnetic alloy containing zirconium and niobium in a total amount of 5.5 atomic percent and the difference (ΔT_X) between the crystallization temperatures;

Fig. 24 is a graph showing the relationship between the composition of a soft magnetic alloy containing zirconium and niobium in a total amount of 6 atomic percent and the coercive force (Hc);

Fig. 25 is a graph showing the relationship between the composition of a soft magnetic alloy containing zirconium and niobium in a total amount of 6 atomic percent and the permeability (μ');

Fig. 26 is a graph showing the relationship between the composition of a soft magnetic alloy containing zirconium and niobium in a total amount of 6 atomic percent and the saturation magnetic flux density (B_{10}) in a magnetic field of 10 Oe;

Fig. 27 is a graph showing the relationship between the composition of a soft magnetic alloy containing zirconium and niobium in a total amount of 6 atomic percent and the remanent magnetization (Br);

Fig. 28 is a graph showing the relationship between the composition of a soft magnetic alloy containing zirconium and niobium in a total amount of 6 atomic percent and the average grain size of the bcc-Fe phase;

Fig. 29 is a graph showing the relationship between the composition of a soft magnetic alloy containing zirconium and niobium in a total amount of 6 atomic percent and the magnetostriction constant (λ_s);

Fig. 30 is a graph showing the relationship between the composition of a soft magnetic alloy containing zirconium and niobium in a total amount of 6 atomic percent and the annealing temperature (Ta) when the coercive force (Hc) is minimized;

Fig. 31 is a graph showing the relationship between the composition of a soft magnetic alloy containing zirconium and niobium in a total amount of 6 atomic percent and the annealing temperature (Ta) when the permeability (μ') is maximized;

Fig. 32 is a graph showing the relationship between the composition of a soft magnetic alloy containing zirconium and niobium in a total amount of 6 atomic percent and the crystallization temperature (T_{X1}) of the bcc-Fe phase;

Fig. 33 is a graph showing the relationship between the composition of a soft magnetic alloy containing zirconium and niobium in a total amount of 6 atomic percent and the crystallization temperature (T_{X2}) of the FeB_x phase;

Fig. 34 is a graph showing the relationship between the composition of a soft magnetic alloy containing zirconium and niobium in a total amount of 6 atomic percent and the crystallization temperature ($T_{X1'}$) of the compound phase precipitated at a temperature which is higher than the crystallization temperature of the bcc-Fe phase;

Fig. 35 is a graph showing the relationship between the composition of a soft magnetic alloy containing zirconium and niobium in a total amount of 6 atomic percent and the difference (ΔT_X) between the crystallization temperatures;

Fig. 36 is a graph showing the relationship between the composition of a soft magnetic alloy containing zirconium and niobium in a total amount of 6.5 atomic percent and the coercive force (Hc);

Fig. 37 is a graph showing the relationship between the composition of a soft magnetic alloy containing zirconium

and niobium in a total amount of 6.5 atomic percent and the permeability (μ');

Fig. 38 is a graph showing the relationship between the composition of a soft magnetic alloy containing zirconium and niobium in a total amount of 6.5 atomic percent and the saturation magnetic flux density (B_{10}) in a magnetic field of 10 Oe;

Fig. 39 is a graph showing the relationship between the composition of a soft magnetic alloy containing zirconium and niobium in a total amount of 6.5 atomic percent and the remanent magnetization (Br);

Fig. 40 is a graph showing the relationship between the composition of a soft magnetic alloy containing zirconium and niobium in a total amount of 6.5 atomic percent and the average grain size of the bcc-Fe phase;

Fig. 41 is a graph showing the relationship between the composition of a soft magnetic alloy containing zirconium and niobium in a total amount of 6.5 atomic percent and the magnetostriction constant (λ_s);

Fig. 42 is a graph showing the relationship between the composition of a soft magnetic alloy containing zirconium and niobium in a total amount of 6.5 atomic percent and the annealing temperature (Ta) when the coercive force (Hc) is minimized;

Fig. 43 is a graph showing the relationship between the composition of a soft magnetic alloy containing zirconium and niobium in a total amount of 6.5 atomic percent and the annealing temperature (Ta) when the permeability (μ') is maximized;

Fig. 44 is a graph showing the relationship between the composition of a soft magnetic alloy containing zirconium and niobium in a total amount of 6.5 atomic percent and the crystallization temperature (T_{X1}) of the bcc-Fe phase;

Fig. 45 is a graph showing the relationship between the composition of a soft magnetic alloy containing zirconium and niobium in a total amount of 6.5 atomic percent and the crystallization temperature ($T_{X1'}$) of the compound phase precipitated at a temperature which is higher than the crystallization temperature of the bcc-Fe phase;

Fig. 46 is a graph showing the relationship between the composition of a soft magnetic alloy containing zirconium and niobium in a total amount of 6.5 atomic percent and the crystallization temperature (T_{X2}) of the FeB_x phase;

Fig. 47 is a graph showing the relationship between the composition of a soft magnetic alloy containing zirconium and niobium in a total amount of 6.5 atomic percent and the difference (ΔT_X) between the crystallization temperatures;

Fig. 48 is a graph showing the relationship between the composition of a soft magnetic alloy containing zirconium and niobium in a total amount of 7 atomic percent and the coercive force (Hc);

Fig. 49 is a graph showing the relationship between the composition of a soft magnetic alloy containing zirconium and niobium in a total amount of 7 atomic percent and the permeability (μ');

Fig. 50 is a graph showing the relationship between the composition of a soft magnetic alloy containing zirconium and niobium in a total amount of 7 atomic percent and the saturation magnetic flux density (B_{10}) in a magnetic field of 10 Oe;

Fig. 51 is a graph showing the relationship between the composition of a soft magnetic alloy containing zirconium and niobium in a total amount of 7 atomic percent and the remanent magnetization (Br);

Fig. 52 is a graph showing the relationship between the composition of a soft magnetic alloy containing zirconium and niobium in a total amount of 7 atomic percent and the average grain size of the bcc-Fe phase;

Fig. 53 is a graph showing the relationship between the composition of a soft magnetic alloy containing zirconium and niobium in a total amount of 7 atomic percent and the magnetostriction constant (λ_s);

Fig. 54 is a graph showing the relationship between the composition of a soft magnetic alloy containing zirconium and niobium in a total amount of 7 atomic percent and the annealing temperature (Ta) when the coercive force (Hc) is minimized;

Fig. 55 is a graph showing the relationship between the composition of a soft magnetic alloy containing zirconium and niobium in a total amount of 7 atomic percent and the annealing temperature (Ta) when the permeability (μ') is maximized;

Fig. 56 is a graph showing the relationship between the composition of a soft magnetic alloy containing zirconium and niobium in a total amount of 7 atomic percent and the crystallization temperature (T_{X1}) of the bcc-Fe phase;

Fig. 57 is a graph showing the relationship between the composition of a soft magnetic alloy containing zirconium and niobium in a total amount of 7 atomic percent and the crystallization temperature (T_{X2}) of the FeB_x phase;

Fig. 58 is a graph showing the relationship between the composition of a soft magnetic alloy containing zirconium and niobium in a total amount of 7 atomic percent and the crystallization temperature ($T_{X1'}$) of the compound phase precipitated at a temperature which is higher than the crystallization temperature of the bcc-Fe phase;

Fig. 59 is a graph showing the relationship between the composition of a soft magnetic alloy containing zirconium and niobium in a total amount of 7 atomic percent and the difference (ΔT_X) between the crystallization temperatures;

Fig. 60 is a graph showing the relationship between the coercive force (Hc) and the relative contents of the Zr and Nb;

Fig. 61 is a graph showing the relationship between the difference in the crystallization temperature (ΔT_X) and the relative contents of the Zr and Nb;

Fig. 62 is a graph showing the relationship between the difference in crystallization temperatures (ΔT_X) and the fracture strain (λ_f) of soft magnetic alloys represented by $Fe_{85.5}Zr_2Nb_4B_{8.5}$, $Fe_{90}Zr_7B_3$, and $Fe_4Nb_7B_9$;

Fig. 63 is a graph showing the relationship between the iron loss and the magnetic flux density (Bm) of soft magnetic alloys represented by $Fe_{85}Zr_{1.75}Nb_{4.25}B_9$, $Fe_{85.5}Zr_2Nb_4B_{8.5}$, $Fe_{85.75}Zr_{2.25}Nb_{3.75}B_{8.25}$, and $Fe_{78}Si_9B_{13}$;

Fig. 64 is a graph showing the relationship between the iron loss and the magnetic flux density (Bm) of soft magnetic alloys represented by $Fe_{85}Zr_{1.75}Nb_{4.25}B_9$ and $Fe_{78}Si_9B_{13}$;

Fig. 65 is a graph showing changes in iron losses over time of soft magnetic alloys represented by $Fe_{85}Zr_{1.75}Nb_{4.25}B_9$, $Fe_{85.75}Zr_{2.25}Nb_{3.75}B_{8.25}$ and $Fe_{78}Si_9B_{13}$;

Fig. 66 is a graph showing the relationship between the change rate of iron loss and the magnetic flux density (Bm) of soft magnetic alloys represented by $Fe_{85}Zr_{1.75}Nb_{4.25}B_9$, $Fe_{85.5}Zr_2Nb_4B_{8.5}$, $Fe_{85.75}Zr_{2.25}Nb_{3.75}B_{8.25}$ and $Fe_{78}Si_9B_{13}$;

Fig. 67 is a graph showing changes in iron losses over time of soft magnetic alloys represented by $Fe_{85.5}Zr_2Nb_4B_{8.5}$ and $Fe_{78}Si_9B_{13}$;

Fig. 68 is a graph showing changes in iron losses over time of soft magnetic alloys represented by $Fe_{85.5}Zr_2Nb_4B_{8.5}$ and $Fe_{78}Si_9B_{13}$;

Fig. 69 is a graph of X-ray diffraction patterns of an alloy of the present invention represented by $(Fe_{0.8575}Zr_{0.02}Nb_{0.04}B_{0.0825})_{99.88}Zn_{0.12}$ before annealing and after annealing;

Fig. 70 is a triangular diagram of coercive forces (Hc) of a $Fe_cZr_dNb_eB_f$ alloy ribbon and a $(Fe_cZr_dNb_eB_f)_{100-z}Zn_z$ containing 0.034 to 0.142 atomic percent of zinc;

Fig. 71 is a triangular diagram of permeability (μ': real number section of permeability) at 1 KHz of the alloys shown in Fig. 70;

Fig. 72 is a triangular diagram of the saturation magnetic flux densities (B_{10}) of the alloys shown in Fig. 71, which are determined from magnetization curves obtained by applying a magnetic field of 10 Oe;

Fig. 73 is a triangular diagram of the remanent magnetization (Br) of the alloys;

Fig. 74 is a triangular diagram of the first crystallization temperature (T_{X1}) of the bcc-Fe in the alloys;

Fig. 75 is a triangular diagram of the intermediate crystallization temperature ($T_{X1'}$) of the compound phase in the alloys;

Fig. 76 is a triangular diagram of the second crystallization temperature (T_{X2}) of the compound phase in the alloys;

Fig. 77 is a triangular diagram of the difference ($\Delta T_X = T_{X2} - T_{X1}$) in the crystallization temperature in the alloys;

Fig. 78 is a triangular diagram of the crystal grain size in the alloys having compositions, which are similar to the composition in accordance with the present invention, and not containing zinc;

Fig. 79 is a triangular diagram of the magnetostriction (λ_S) in the alloys having compositions, which are similar to the composition in accordance with the present invention, and not containing zinc;

Fig. 80 is a graph of the dependence of the crystal grain size (D) on the zinc content in zinc-containing alloys in accordance with the present invention;

Fig. 81 is a graph of the dependence of the magnetostriction (λs) on the zinc content in zinc-containing alloys in accordance with the present invention;

Fig. 82 is a graph of iron loss of ribbons prepared by adding 0.12 or 0.13 atomic percent of zinc to a base alloy represented by $Fe_{85.75}Zr_2Nb_4B_{8.25}$ and a ribbon for comparison represented by $Fe_{78}Si_9B_{13}$;

Fig. 83 is a graph of a change in iron loss over time of an alloy ribbon represented by $(Fe_{0.8575}Zr_{0.02}Nb_{0.04}B_{0.0825})_{99.88}Zn_{0.12}$ in accordance with the present invention and ribbons for comparison represented by $Fe_{78}Si_9B_{13}$, $Fe_{85}Zr_{1.75}Nb_{4.25}B_9$, $Fe_{85.5}Zr_2Nb_4B_{8.5}$, and $Fe_{85.75}Zr_{2.25}Nb_{3.75}B_{8.25}$;

Fig. 84 is a graph of the iron loss at room temperature of the alloys which are shown in Fig. 83 and heated to 320°C for a predetermined time;

Fig. 85 is a graph of a change rate of the iron loss over time of the alloys shown in Fig. 84;

Fig. 86 is a graph of the relationship between the fracture strain and the bending diameter of various alloy ribbons;

Fig. 87 is a graph of the dependence of the Curie temperature on the zinc content in an amorphous phase of an annealed alloy;

Fig. 88 is a graph of the dependence of the Curie temperature on the zinc content in an as-quenched alloy;

Fig. 89 is a graph of the dependence of the coercive force on the zinc content in FeNbB-based alloys;

Fig. 90 is a graph of the dependence of the permeability on the zinc content in FeNbB-based alloys;

Fig. 91 is a graph of the dependence of the coercive force on the zinc content in FeZrNbB-based alloys;

Fig. 92 is a graph of the dependence of the permeability on the zinc content in FeZrNbB-based alloys;

Fig. 93 is a triangular diagram of coercive forces of an alloy ribbon containing 4 atomic percent in total of zirconium and niobium;

Fig. 94 is a graph of the relationships among the permeability μ', the heating rate and the annealing temperature of an annealed alloy represented by $Fe_{85.5}Zr_2Nb_4B_{8.5}$ in which the holding time at the annealing temperature is zero;

Fig. 95 is a graph of the relationships among the coercive force Hc, the heating rate and the annealing temperature of an annealed alloy represented by $Fe_{85.5}Zr_2Nb_4B_{8.5}$ in which the holding time at the annealing temperature is zero;

Fig. 96 is a graph of the relationships among the permeability μ', the heating rate and the annealing temperature of the annealed alloy shown in Fig. 94 in which the holding time at the annealing temperature is 5 minutes;

Fig. 97 is a graph of the relationships among the coercive force Hc, the heating rate and the annealing temperature of the annealed alloy shown in Fig. 94 in which the holding time at the annealing temperature is 5 minutes;

Fig. 98 is a graph of the relationships among the permeability μ', the heating rate and the annealing temperature of the annealed alloy shown in Fig. 94 in which the holding time at the annealing temperature is 10 minutes;

Fig. 99 is a graph of the relationships among the coercive force Hc, the heating rate and the annealing temperature of the annealed alloy shown in Fig. 94 in which the holding time at the annealing temperature is 10 minutes;

Fig. 100 is a graph of the relationships among the permeability μ', the heating rate and the annealing temperature of the annealed alloy shown in Fig. 94 in which the holding time at the annealing temperature is 30 minutes;

Fig. 101 is a graph of the relationships among the coercive force Hc, the heating rate and the annealing temperature of the annealed alloy shown in Fig. 94 in which the holding time at the annealing temperature is 30 minutes;

Fig. 102 is a graph of the relationships among the permeability μ', the heating rate and the annealing temperature of the annealed alloy shown in Fig. 94 in which the holding time at the annealing temperature is 60 minutes;

Fig. 103 is a graph of the relationships among the coercive force Hc, the heating rate and the annealing temperature of the annealed alloy shown in Fig. 94 in which the holding time at the annealing temperature is 60 minutes;

Fig. 104 is a graph of the permeabilities of the annealed alloys shown in Figs. 94, 96, 98, 100 and 102;

Fig. 105 is a graph of the coercive forces of the annealed alloys shown in Figs. 95, 97, 99, 101 and 103;

Fig. 106 is a graph of the permeabilities of the annealed alloys for the holding times of 0, 10 and 60 minutes which are extracted from Fig. 104;

Fig. 107 is a graph of the coercive forces of the annealed alloys for the holding times of 0, 10 and 60 minutes which are extracted from Fig. 105;

Fig. 108 is a graph of the permeabilities of the annealed alloys for the holding times of 5 and 30 minutes which are extracted from Fig. 104;

Fig. 109 is a graph of the coercive forces of the annealed alloys for the holding times of 5 and 30 minutes which are extracted from Fig. 105;

Fig. 110 is a graph of the permeabilities of the annealed alloys for the ejection temperature of 1,320°C which are extracted from Figs. 94, 96, 98, 100 and 102;

Fig. 111 is a graph of the coercive forces of the annealed alloys for the ejection temperature of 1,320°C which are extracted from Figs. 95, 97, 99, 101 and 103;

Fig. 112 is a graph of the permeabilities of the annealed alloys for the holding times of 0, 10 and 60 minutes which are extracted from Fig. 110;

Fig. 113 is a graph of the coercive forces of the annealed alloys for the holding times of 0, 10 and 60 minutes which are extracted from Fig. 111;

Fig. 114 is a graph of the permeabilities of the annealed alloys for the holding times of 5 and 30 minutes which are extracted from Fig. 110;

Fig. 115 is a graph of the coercive forces of the annealed alloys for the holding times of 5 and 30 minutes which are extracted from Fig. 111;

Fig. 116 is a graph of the relationships among the permeability μ', the heating rate and the annealing temperature of an annealed alloy represented by $Fe_{85.5}Zr_2Nb_4B_{8.5}$ in which the holding time at the annealing temperature is 5 minutes;

Fig. 117 is a graph of the relationships among the coercive force Hc, the heating rate and the annealing temperature of an annealed alloy represented by $Fe_{85.5}Zr_2Nb_4B_{8.5}$ in which the holding time at the annealing temperature is 5 minutes;

Fig. 118 is a graph of the permeability μ' of the annealed alloy shown in Fig. 116 in which the composition is changed to $(Fe_{85.5}Zr_2Nb_4B_{8.5})_{99}Zn_1$;

Fig. 119 is a graph of the coercive force Hc of the annealed alloy shown in Fig. 117 in which the composition is changed to $(Fe_{85.5}Zr_2Nb_4B_{8.5})_{99}Zn_1$;

Fig. 120 is a graph of the permeability μ' of the annealed alloy shown in Fig. 116 in which the composition is changed to $(Fe_{85.5}Zr_2Nb_4B_{8.5})_{98}Zn_2$;

Fig. 121 is a graph of the coercive force Hc of the annealed alloy shown in Fig. 117 in which the composition is changed to $(Fe_{85.5}Zr_2Nb_4B_{8.5})_{98}Zn_2$;

Fig. 122 is a graph of the permeability μ' of the annealed alloy shown in Fig. 116 in which the composition is changed to $(Fe_{85.5}Zr_2Nb_4B_{8.5})_{97}Zn_3$;

Fig. 123 is a graph of the coercive force Hc of the annealed alloy shown in Fig. 117 in which the composition is

changed to $(Fe_{85.5}Zr_2Nb_4B_{8.5})_{97}Zn_3$;

Fig. 124 is a graph of summarized permeabilities μ' at an ejection temperature of 1,260°C, which are shown in Figs. 116, 118, 120 and 122;

Fig. 125 is a graph of summarized coercive forces Hc at an ejection temperature of 1,260°C, which are shown in Figs. 117, 119, 121 and 123;

Fig. 126 is a graph of summarized permeabilities μ' at an ejection temperature of 1,300°C, which are shown in Figs. 116, 118, 120 and 122;

Fig. 127 is a graph of summarized coercive forces Hc at an ejection temperature of 1,300°C, which are shown in Figs. 117, 119, 121 and 123;

Fig. 128 is a graph showing the dependence of the coercive force (Hc) on the annealing time of the second annealing treatment; and

Fig. 129 is a graph showing the dependence of the permeability on the annealing time.

[0051] A first Fe-based soft magnetic alloy having high saturation magnetic flux density and low iron loss in accordance with the present invention will now be described.

[0052] The first Fe-based soft magnetic alloy having high saturation magnetic flux density and low iron loss is represented by the following formula:

$$Fe_aZr_xNb_yB_z$$

wherein the subscripts satisfy the relationships 80 atomic percent ≤ a; 5 atomic percent ≤ x + y ≤ 7 atomic percent; 1.5/6 ≤ x/(x+y) ≤ 2.5/6; and 5 atomic percent ≤ z ≤ 12.5 atomic percent. The Fe-based soft magnetic alloy has a fine crystalline texture formed by annealing an amorphous alloy substantially composed of an amorphous phase. At least 50% (preferably at least 70%) of the fine crystalline texture is composed of a bcc-Fe phase as the major component having an average crystal grain size of 100 nm or less (preferably 30 nm or less).

[0053] The Fe-based soft magnetic alloy having the above fine crystalline texture can be generally produced by the quenching step for quenching the melt having the composition described in the first aspect to form an alloy substantially comprising an amorphous phase and by the annealing step for heating and then cooling the alloy to precipitate a fine crystalline texture comprising fine crystal grains.

[0054] This Fe-based soft magnetic alloy is composed of the fine crystalline phase of bcc-Fe crystal grains as the major component and an amorphous phase, and thus has low magnetostriction, high saturation magnetic flux density and superior permeability.

[0055] Fe (iron) as the primary component in the alloy has magnetism and is essential for high saturation magnetic flux density and superior soft magnetic characteristics. In the above formula, the Fe content represented by the subscript "a" is at least 80 atomic percent. When the Fe content is less than 80 atomic percent, the saturation magnetic flux density is less than 1.5 T, which is an unsatisfactory level in the present invention. The Fe content is more preferably at least 83 atomic percent and most preferably in a range of 85 atomic percent to 86 atomic percent.

[0056] A saturation magnetic flux density of 1.5 T or more is achieved by adding as much Fe as possible in consideration of the preferred concentrations of other components. That is, a saturation magnetic flux density of 1.4 T or more is achieved by adding 80 atomic percent or more of Fe and a saturation magnetic flux density of 1.6 T or more is achieved by adding 85 atomic percent or more of Fe.

[0057] When the Fe content exceeds 86 atomic percent, the amorphous phase is barely formed in the alloy by a liquid quenching process of the melt. When such an alloy is annealed, the resulting alloy has an inhomogeneous texture which does not have high permeability. Thus, the upper limit of the Fe content is preferably 86 atomic percent.

[0058] A part of the Fe may be replaced with Co or Ni to adjust magnetostriction of the alloy. The Co or Ni content is preferably 10% or less and more preferably 5% or less. A higher content will result in deterioration of permeability.

[0059] In this embodiment, Zr (zirconium) and Nb (niobium) are essential components for facilitating the formation of the amorphous phase. These elements have high formability of the amorphous phase. In addition, B (boron) is an essential component in the alloy of the present invention. Boron also facilitates the formation of the amorphous phase in the Fe-based soft magnetic alloy of the present invention and suppresses the formation of the compound phase, which adversely affects magnetic characteristics, during the annealing step.

[0060] Zirconium and niobium facilitate the formation of the amorphous phase in the alloy when the melt is quenched and the precipitation of fine crystal grains composed of the bcc-Fe phase in the amorphous phase when the amorphous alloy is annealed. As a result, compatibility of a saturation magnetic flux density of at least 1.5 T and a high permeability is achieved.

[0061] The total content x+y of the zirconium content "x" and the niobium content "y" is at least 5 atomic percent in the present invention to form a required amount of amorphous phase. A total content x+y exceeding 7 atomic percent

results in undesirable deterioration of saturation magnetic flux density and soft magnetic characteristics.

[0062] When the Zr content "x" and the Nb content "y" satisfy the relationship $1.5/6 \leq x/(x+y) \leq 2.5/6$, the Fe-based soft magnetic alloy has improved permeability and saturation magnetic flux density and remarkably decreased iron loss. In particular, in a low-frequency region of 100 Hz or less, iron loss is significantly decreased and a change in iron loss over time is decreased.

[0063] The total content x+y of zirconium and niobium is preferably in a range of 5 atomic percent to 7 atomic percent, and more preferably 5.7 atomic percent to 6.5 atomic percent. Furthermore, the ratio x/(x+y) of these elements is preferably 2/6.

[0064] For achieving superior soft magnetic characteristics, the Zr content "x" is preferably in a range of 0.5 atomic percent to 3.5 atomic percent, and more preferably 1.5 atomic percent to 2.5 atomic percent, and the Nb content "y" is preferably in a range of 3 atomic percent to 5.5 atomic percent, and more preferably 3.5 atomic percent to 5.0 atomic percent.

[0065] As described above, boron (B) also has formability of the amorphous phase. Addition of an excessive amount of boron, however, tends to decrease permeability and to form a compound phase with iron which adversely affects the soft magnetic characteristics. Thus, the boron content z is preferably in a range of 5 atomic percent to 12.5 atomic percent, more preferably 6 atomic percent to 9.5 atomic percent, and most preferably 8 atomic percent to 9 atomic percent.

[0066] It is believed that Zirconium and niobium are not substantially dissolved in bcc-Fe in an ordinary state. These elements can, however, be dissolved in the bcc-Fe in a supersaturated state by quenching the alloy melt to form an amorphous alloy and then annealing the amorphous alloy to form a crystalline phase. The amounts of these elements dissolved into the bcc-Fe phase are controlled so that a fine crystalline texture is precipitated during the annealing. The resulting Fe-based alloy has improved soft magnetic characteristics and an alloy ribbon thereof has decreased magnetostriction.

[0067] The presence of an amorphous phase in the grain boundaries is essential for precipitation of the fine crystalline texture and suppression of coarsening of crystal grains in the fine crystalline texture. The amorphous phase inhibits growth of crystal grains.

[0068] In addition, it is believed that the boundary amorphous phase includes Zr and Nb excluded from the bcc-Fe phase as the temperature increases during annealing and suppresses the formation of a Fe-Zr or Fe-Nb compound phase. Accordingly, addition of boron to a Fe-Zr, Fe-Nb or Fe-Zr-Nb alloy is essential.

[0069] The alloy may contain at least one platinum element, e.g., Ru, Rh, Pd, Os, Ir and Pt to improve corrosion resistance of the alloy. A content of more than 5 atomic percent, however, causes significant deterioration of saturation magnetic flux density. Thus, the content of the platinum element is limited to 5 atomic percent or less.

[0070] In addition, the Fe-based soft magnetic alloy may contain miscellaneous elements, e.g., Y, La, Ce, Pr, Nd, Pm, Sm, Eu, Gd, Tb, Dy, Ho, Er, Tm, Yb, Lu, Zn, Cd, In, Sn, Pb, As, Sb, Bi, Se, Te, Li, Be, Mg, Ca, Sr, and Ba, if necessary, in order to adjust magnetostriction.

[0071] The Fe-based soft magnetic alloy having the above composition may contain trace amounts of incidental impurities, such as H, N, O and S within ranges which do not deteriorate the above-mentioned magnetic characteristics. The allowable upper limit of the total content of the impurities is approximately 0.1 atomic percent.

[0072] Preferably, the crystallization temperature T_{X1} of the bcc-Fe phase, the crystallization temperature T_{X2} of a compound phase which is crystallized at a temperature higher than T_{X1}, and the difference $\Delta T_X = T_{X2} - T_{X1}$ of the crystallization temperatures satisfy the relationship $200^\circ C \leq \Delta T_X$. The compound phase can be regarded as a phase which is crystallized subsequent to the bcc-Fe phase at a temperature higher than T_{X1}. The composition of the compound phase is believed to be Fe_3B or Fe_2B.

[0073] The alloy is formed by quenching and is substantially composed of an amorphous phase. When the alloy is heated, an exothermic reaction occurs at a primary stage due to crystallization of the bcc-Fe phase, and then another exothermic reaction occurs at a higher temperature due to crystallization of the compound phase. These exothermic reactions can be observed by, for example, differential thermal analysis (DTA) of the quenched alloy. The crystallization temperatures T_{X1} and T_{X2} of the bcc-Fe phase and the compound phase, respectively, and the difference ΔT_X between these crystallization temperatures are determined from the exothermic peaks of a DTA thermogram.

[0074] When the difference ΔT_X is at least $200^\circ C$, the alloy can be annealed at optimized conditions so as to precipitate only the bcc-Fe phase and to suppress precipitation of the compound phase. The resulting Fe-based soft magnetic alloy has high saturation magnetic flux density and low iron loss. Under optimal conditions, the preferred annealing temperature T_a of the alloy lies in a range of $T_{X1} \leq T_a \leq T_{X2}$.

[0075] According to the DTA, another phase (third phase) will be deposited at a temperature between T_{X1} and T_{X2} in some cases. The composition of this phase is not clear. The deposition of the third phase depends on the composition of the Fe-based soft magnetic alloy. In particular, a high boron content facilitates the precipitation of the third phase. Thus, the composition of the third phase is believed to be a compound phase of boron and other elements.

[0076] When the crystallization of the third phase is $T_{X1'}$, it is preferable that the difference $\Delta T_X = T_{X1'} - T_{X1}$ in crys-

tallization temperatures be at least 200°C. Furthermore, the preferred annealing temperature T_a of the alloy lies in a range of $T_{X1} \leq T_a \leq T_{X1'}$.

[0077] The preferred heating rate is at least 10°C/min, more preferably in a range of 10°C/min to 200°C/min, and most preferably in a range of 30°C/min to 100°C/min. The preferred annealing temperature T_a is in a range of 490°C to 670°C and more preferably 500°C to 560°C. The preferred holding time at the annealing temperature is in a range of 0 to 1 hour. A vacuum or inert gas annealing atmosphere is preferable to avoid oxidation of the alloy.

[0078] The resulting Fe-based soft magnetic alloy having the above-described composition has a saturation magnetic flux density of at least 1.5 T, an iron loss of 0.15 or less when a magnetic flux of 1.4 T at a frequency of 50 Hz is applied, and a change rate in iron loss after aging at 200°C for 500 hours of 10% or less. Furthermore, the Fe-based soft magnetic alloy has a fracture strain of at least 1.0×10^{-2}.

[0079] The Fe-based soft magnetic alloy (hereinafter referred to as a second alloy), having high saturation magnetic flux density and low iron loss, of the second embodiment is represented by the following formula:

$$(Fe_{1-a}Q_a)_bB_xM_yZn_z$$

wherein Q is at least one of Co and Ni; M is at least one selected from the group consisting of Ti, Zr, Hf, V, Nb, Ta, Mo and W; the subscripts satisfy the relationships $0 \leq a \leq 0.05$, 80 atomic percent $\leq b$; 5 atomic percent $\leq x \leq 12.5$ atomic percent; 5 atomic percent $\leq y \leq 7$ atomic percent; and 0.025 atomic percent $\leq z \leq 0.2$ atomic percent. The Fe-based soft magnetic alloy has a fine crystalline texture comprising at least 50% of fine bcc-Fe crystal grains having an average crystal grain size of 100 nm or less and the balance being an amorphous phase. The bcc-Fe crystal grains are precipitated by heating to a temperature higher than the crystallization temperature and then cooling a substantially single amorphous phase which is formed by quenching an alloy melt.

[0080] The second Fe-based soft magnetic alloy may be represented by the formula $Fe_bB_xM_yZn_z$ when the alloy does not contain the component Q.

[0081] The Fe-based soft magnetic alloy, having high saturation magnetic flux density and low iron loss, as a modification of the second embodiment is represented by the following formula:

$$(Fe_{1-a}Q_a)_bB_xM_yZn_zM'_u$$

wherein Q is at least one of Co and Ni; M is at least one selected from the group consisting of Ti, Zr, Hf, V, Nb, Ta, Mo and W; M' is at least one selected from the group consisting of Cr, Ru, Rh and Ir; the subscripts satisfy the relationships $0 \leq a \leq 0.05$, 80 atomic percent $\leq b$; 5 atomic percent $\leq x \leq 12.5$ atomic percent; 5 atomic percent $\leq y \leq 7$ atomic percent; 0.025 atomic percent $\leq z \leq 0.2$ atomic percent; and $u \leq 5$ atomic percent. The Fe-based soft magnetic alloy also has a fine crystalline texture comprising at least 50% of fine bcc-Fe crystal grains having an average crystal grain size of 100 nm or less and the balance being an amorphous phase. The bcc-Fe crystal grains are precipitated by heating to a temperature higher than the crystallization temperature and then cooling a substantially single amorphous phase which is formed by quenching an alloy melt.

[0082] This Fe-based soft magnetic alloy is generally produced by a quenching step for quenching an alloy melt to form an amorphous alloy ribbon or powder which is substantially composed of an amorphous single phase or composed of an amorphous phase partly containing a crystalline phase, and an annealing step for annealing the amorphous ribbon or powder to precipitate fine crystal grains. Since zinc (Zn) is easily vaporized compared to other constituents, the zinc content is preferably set to be higher than the above-mentioned range when the alloy melt is prepared.

[0083] The quenched alloy may be in the form of a ribbon or powder. The quenched alloy may be shaped to a desired form by molding or working and then may be annealed.

[0084] Boron (B) is added as an essential element in the Fe-based soft magnetic alloy. Boron facilitates the formation of the amorphous phase in the Fe-based soft magnetic alloy, enhances thermal stability of the Fe-M-based fine crystalline alloy (wherein M is Zr, Hf, Nb or the like), functions as a barrier to crystal grain growth, and facilitates the remaining of thermally stable amorphous phases in the grain boundaries. Thus, a texture primarily composed of fine bcc-crystal grains having a particle size of 100 nm or less and preferably 30 nm or less can be formed in a wide range of annealing temperatures of 400 to 750°C during the annealing step described below. Such a texture does not adversely affect magnetic characteristics. The boron content is preferably in a range of 5 atomic percent to 12.5 atomic percent, more preferably 6 atomic percent to 9.5 atomic percent, and most preferably 8 atomic percent to 9.0 atomic percent.

[0085] The Fe-based soft magnetic alloy may contain miscellaneous elements, e.g., Y, La, Ce, Pr, Nd, Pm, Sm, Eu, Gd, Tb, Dy, Ho, Er, Tm, Yb, Lu, Cd, In, Sn, Pb, As, Sb, Bi, Se, Te, Li, Be, Mg, Ca, Sr, and Ba, if necessary, in order to adjust magnetostriction.

[0086] In addition, the Fe-based soft magnetic alloy may contain elements facilitating the formation of the amorphous

phase, for example, Al, Si, C and P, within ranges which do not cause not cause deterioration of the above-described magnetic characteristics. The content of these constituents is preferably 1 atomic percent or less. The Fe-based soft magnetic alloy may also contain trace amounts of incidental impurities, such as H, N, O and S within ranges which do not deteriorate the above-mentioned magnetic characteristics. The allowable upper limit of the total content of the impurities is approximately 0.1 atomic percent.

[0087] Among the constituents M, that is, Ti, Zr, Hf, V, Nb, Ta, Mo, and W, at least one of Zr, Hf and Nb is preferably used. These elements have further facilitates the formation of the amorphous phase. The Zr, Hf or Nb may be partly replaced with Ti, V, Ta, Mo or W among Groups IVA to VIA elements.

[0088] Zirconium and niobium are not substantially dissolved in bcc-Fe in an ordinary state. These elements can, however, be dissolved in the bcc-Fe in a supersaturated state by quenching the alloy melt to form an amorphous alloy and then annealing the amorphous alloy to form a crystalline phase. The magnetostriction of the alloy can be reduced by controlling the amounts of these elements dissolved in the bcc-Fe phase. That is, the amounts of the dissolved Zr and Nb are controlled by the annealing conditions so that the resulting Fe-based alloy has decreased magnetostriction.

[0089] It is important that a fine crystalline texture can be formed under wide annealing conditions in order to achieve low magnetostriction. The addition of boron facilitates the formation of a fine crystalline texture under wider annealing conditions. Since the alloy has small magnetostriction and small crystalline magnetic anisotropy, the alloy has superior magnetic characteristics.

[0090] Controlling the ratio of Zr and Nb is particularly effective for decreasing the iron loss. When Zr and Nb are added as the elements M, the total content of these elements preferably satisfies the relationship 5 atomic percent ≤ (Zr content + Nb content) ≤ 7.5 atomic percent, and more preferably 5.7 atomic percent ≤ (Zr content + Nb content) ≤ 6.5 atomic percent. Preferably, the ratio (Zr content)/(Zr content + Nb content) is in a range of 1.5/6 to 2.5/6, that is, 1.5/6 ≤ (Zr content)/(Zr content + Nb content) ≤ 2.6/6. Most preferably, the ratio (Zr content)/(Zr content + Nb content) is 2/6.

[0091] The Fe-based soft magnetic alloy may contain at least one selected from the group consisting of Cr, Ru, Rh, and Ir to improve corrosion resistance. It is preferable that the content of these elements be 5 atomic percent or less in order to ensure high saturation magnetic flux density, and be 1 atomic percent or less in view of compatibility among the saturation magnetic flux density, soft magnetic characteristics, and iron loss.

[0092] The present inventors disclosed the formation of a fine crystalline texture by partial crystallization of a Fe-M (= Zr, Hf) based amorphous alloy in "Conference on Metallic Science and Technology, Budapest", pages 217 to 221, in 1980. The Fe-based soft magnetic alloy also has similar advantages to those of the Fe-M based alloy. The reason for the formation of the fine crystalline structure is believe to be that perturbation of the composition occurs in the quenched amorphous alloy and such a perturbation causes the formation of many fine and uniform nuclei.

[0093] The Fe content or the total content of Fe, Co and Ni in the Fe-based soft magnetic alloy is 80 atomic percent or more. In addition, it is preferable that the content be less than 90 atomic percent. When the content exceeds 90 atomic percent, the Fe-based soft magnetic alloy does not have high permeability. It is more preferable that the content be in a range of 83 to 87 atomic percent, and most preferably 85 to 86 atomic percent in order to achieve a saturation magnetic flux density of 1.55 T or more. A desired saturation magnetic flux density is achieved when the Fe content is at least 80 atomic percent.

[0094] It is preferable that the Zn content in the Fe-based soft magnetic alloy be in a range of 0.025 to 0.2 atomic percent. When the Zn content lies in this range, the coercive force and the iron loss of the alloy can be decreased while maintaining a high saturation magnetic flux density of 1.5 T or more. In addition, the permeability can be increased. It is more preferable that the Zn content in the Fe-based soft magnetic alloy be in a range of 0.034 to 0.16 atomic percent. When the Zn content lies in the more preferable range, the Fe-based soft magnetic alloy has lower iron loss, high saturation magnetic flux density, and a decreased change in iron loss over time.

[0095] Zinc has a melting point of 419.5°C and a boiling point of 908°C. The alloy is generally melted in a crucible at a temperature of 1,240 to 1,350°C. When an alloy having the above-mentioned composition is melted at such a high temperature, most of the zinc is lost by vaporization.

[0096] In production of the amorphous alloy from the melt, the melt may be jetted onto a cooling member such as a cooling roller or jetted into a cooling gas medium (atomizing method) to quench the melt. Zinc is excessively added to the alloy fed into the crucible so that the quenched alloy contains the above-specified content of zinc.

[0097] It is preferable that zinc be added to the alloy in an amount which is at least 20 times the final target content, when a ribbon or powdered alloy is formed by a melt-quenching process at a temperature of 1,240 to 1,350°C.

[0098] Fig. 1 is a schematic view of an apparatus for making a ribbon of a soft magnetic alloy in accordance with the present invention. A copper or steel cooling roller 3 is placed in a chamber 2. The chamber 2 can be evacuated through an evacuation pipe la connected to a vacuum pump 1. A crucible 6 having a nozzle 5 made of, for example, quartz is placed on the cooling roller 3. The crucible 6 is connected to a gas feeder 7 by a gas supply pipe 7a so as to supply argon gas and to pressurize the interior of the crucible 6. The chamber 2 is connected to a gas feeder 8 by a gas supply pipe 8a so as to supply a nonoxidative gas, such as argon gas. The crucible 6 has a lid connected to the gas supply

pipe 7a, so that the internal pressure of the crucible 6 and the internal pressure of the chamber 2 are independently adjustable.

[0099] The raw materials placed in the crucible 6 are melted by a heater 9 provided on the outer periphery of the bottom section of the crucible 6. The argon gas is fed into the crucible 6 through the gas feeder 7 to jet the melt from the nozzle 5 onto the rotating cooling roller 3. The melt is cooled on the cooling roller 3 to form a ribbon 11.

[0100] Using the apparatus shown in Fig. 1, the interior of the chamber 2 is filled with an argon atmosphere of approximately 160 Torr, and melts of alloys represented by the formula $(Fe_{0.94-t}Zr_{0.02}Nb_{0.04}B_t)_{100-z}Zn_z$, wherein t = 0.08, 0.0825, and 0.085 and having different Zn contents "z" of 1, 2 and 3 atomic percent, are jetted on the rotating cooling roller 3 to form ribbons. Fig. 2 is a graph showing the relationship between the zinc content in the ribbon and the amount of zinc fed to the crucible.

[0101] The results shown in Fig. 2 demonstrates that the ribbon prepared from the melt containing 1 atomic percent of zinc contains 0.035 to 0.0575 atomic percent of residual zinc, the ribbon prepared from the melt containing 2 atomic percent of zinc contains 0.07 to 0.125 atomic percent of residual zinc, and the ribbon prepared from the melt containing 3 atomic percent of zinc contains 0.12 to 0.170 atomic percent of residual zinc. Thus, 0.5 to 4.0 atomic percent of zinc must be fed to the raw materials for the alloy in order to prepare a quenched ribbon containing 0.025 to 0.2 atomic percent of zinc in accordance with the present invention.

[0102] Based on these results, zinc in an amount which is approximately 20 times the final target content is fed to the crucible in the present invention and a ribbon is produced by the apparatus shown in Fig. 1, in the EXAMPLES described below so as to prepare soft magnetic alloys containing 0.025 to 0.2 atomic percent of zinc.

[0103] When a thin film alloy is produced, the film is preferably deposited using a target or an evaporation source containing zinc in an excess amount.

[0104] The resulting Fe-based soft magnetic alloy has high saturation magnetic flux density and low iron loss. The permeability of the alloy is further increased due to the addition of zinc. In addition, the alloy has low coercive force, large fracture strain, and high bending resistance.

[0105] A third Fe-based soft magnetic alloy in accordance with the present invention contains Fe (as the major component), Zr, Nb, B, and Zn, and has a texture composed of at least 50% of bcc-Fe fine crystal grains having an average crystal grain size of 100 nm or less and the balance being an amorphous phase.

[0106] Preferably, the Fe-based soft magnetic alloy is represented by the following formula:

$$(Fe_{1-a}Q_a)_bZr_xNb_yB_tZn_z$$

wherein Q is at least one of Co and Ni; the subscripts satisfy the relationships $0 \le a \le 0.05$, 80 atomic percent $\le b$; 1.5 atomic percent $\le x \le 2.5$ atomic percent; 3.5 atomic percent $\le y \le 5.0$ atomic percent; 5 atomic percent $\le t \le 12.5$ atomic percent, 0.025 atomic percent $\le z \le 0.2$ atomic percent; 5.0 atomic percent $\le x + y \le 7.5$ atomic percent; and $1.5/6 \le x/(x+y) \le 2.5/6$. The alloy has a fine crystalline texture comprising at least 50% of fine bcc-Fe crystal grains having an average crystal grain size of 100 nm or less and the balance being an amorphous phase, and the bcc-Fe crystal grains are precipitated by heating to a temperature higher than the crystallization temperature and then cooling a substantially single amorphous phase which is formed by quenching an alloy melt.

[0107] Alternatively, the Fe-based soft magnetic alloy may be represented by the following formula:

$$(Fe_{1-a}Q_a)_bZr_xNb_yB_tZn_zM'_u$$

wherein Q is at least one of Co and Ni; M' is at least one selected from the group consisting of Cr, Ru, Rh and Ir; the subscripts satisfy the relationships $0 \le a \le 0.05$, 80 atomic percent $\le b$; 1.5 atomic percent $\le x \le 2.5$ atomic percent; 3.5 atomic percent $\le y \le 5.0$ atomic percent; 5 atomic percent $\le t \le 12.5$ atomic percent, 0.025 atomic percent $\le z \le 0.2$ atomic percent; $u \le 5$ atomic percent; 5.0 atomic percent $\le x + y \le 7.5$ atomic percent; and $1.5/6 \le x/(x+y) \le 2.5/6$. This alloy also has a fine crystalline texture comprising at least 50% of fine bcc-Fe crystal grains having an average crystal grain size of 100 nm or less and the balance being an amorphous phase, and the bcc-Fe crystal grains are precipitated by heating to a temperature higher than the crystallization temperature and then cooling a substantially single amorphous phase which is formed by quenching an alloy melt.

[0108] This Fe-based soft magnetic alloy is generally produced by a quenching step for quenching an alloy melt to form an amorphous alloy ribbon or powder which is substantially composed of an amorphous single phase or composed of an amorphous phase partly containing a crystalline phase, and an annealing step for annealing the amorphous ribbon or powder to precipitate fine crystal grains. Since zinc (Zn) is easily vaporized compared to other constituents, the zinc content is preferably set to be higher than the above-mentioned range when the alloy melt is prepared, as described in the second embodiment. The adjustment of the zinc content is necessary when a thin film is produced.

[0109] The quenched alloy may be in the form of a ribbon or powder. The quenched alloy may be shaped to a desired form by molding or working and may then be annealed.

[0110] Boron (B) is added as an essential element in this Fe-based soft magnetic alloy. Boron facilitates the formation of the amorphous phase in the Fe-based soft magnetic alloy, enhances thermal stability of the Fe-M-based fine crystalline alloy (wherein M is Zr, Hf, Nb or the like), functions as a barrier to crystal grain growth, and facilitates the remaining of thermally stable amorphous phases in the grain boundaries. Thus, a texture primarily composed of fine bcc-crystal grains having a particle size of 100 nm or less and preferably 30 nm or less can be formed in a wide range of annealing temperatures of 400 to 750°C during the annealing step described below. Such a texture does not adversely affect magnetic characteristics. The boron content is preferably in a range of 5 atomic percent to 12.5 atomic percent, more preferably 6 atomic percent to 9.5 atomic percent, and most preferably 8 atomic percent to 9.0 atomic percent.

[0111] The Fe-based soft magnetic alloy may contain miscellaneous elements, e.g., Y, La, Ce, Pr, Nd, Pm, Sm, Eu, Gd, Tb, Dy, Ho, Er, Tm, Yb, Lu, Cd, In, Sn, Pb, As, Sb, Bi, Se, Te, Li, Be, Mg, Ca, Sr, and Ba, if necessary, in order to adjust magnetostriction.

[0112] In addition, the Fe-based soft magnetic alloy may contain elements facilitating the formation of the amorphous phase, for example, Al, Si, C and P, within ranges which do not cause not cause deterioration of the above-described magnetic characteristics. The content of these constituents is preferably 0.5 atomic percent or less. The Fe-based soft magnetic alloy may also contain trace amounts of incidental impurities, such as H, N, O and S within ranges which do not deteriorate the above-mentioned magnetic characteristics. The allowable upper limit of the total content of the impurities is approximately 0.1 atomic percent.

[0113] The soft magnetic alloy contains Zr (zirconium) and Nb (niobium) as essential components to facilitate the formation of the amorphous phase.

[0114] Zirconium and niobium are not substantially dissolved in bcc-Fe in an ordinary state. These elements can, however, be dissolved in the bcc-Fe in a supersaturated state by quenching the alloy melt to form an amorphous alloy and then annealing the amorphous alloy to form a crystalline phase. The magnetostriction of the alloy can be reduced by controlling the amounts of these elements dissolved into the bcc-Fe phase. That is, the amounts of the dissolved Zr and Nb are controlled by the annealing conditions so that the resulting Fe-based alloy has decreased magnetostriction.

[0115] It is important that a fine crystalline texture can be formed under wide annealing conditions in order to achieve low magnetostriction. The addition of boron facilitates the formation of a fine crystalline texture under wider annealing conditions. Since the alloy has small magnetostriction and small crystalline magnetic anisotropy, the alloy has superior magnetic characteristics.

[0116] Controlling the ratio of Zr and Nb is particularly effective for decreasing the iron loss. When Zr and Nb are added as the elements M, the total content of these elements preferably satisfies the relationship, 5 atomic percent ≤ (Zr content + Nb content) ≤ 7.5 atomic percent, and more preferably 5.7 atomic percent ≤ (Zr content + Nb content) ≤ 6.5 atomic percent. Preferably, the ratio (Zr content)/(Zr content + Nb content) is in a range of 1.5/6 to 2.5/6, that is, 1.5/6 ≤ (Zr content)/(Zr content + Nb content) ≤ 2.6/6. Most preferably, the ratio (Zr content)/(Zr content + Nb content) is 2/6.

[0117] For achieving superior soft magnetic characteristics, the Zr content "x" is preferably in a range of 0.5 atomic percent to 3.5 atomic percent, and more preferably 1.5 atomic percent to 2.5 atomic percent, and the Nb content "y" is preferably in a range of 3 atomic percent to 5.5 atomic percent, and more preferably 3.5 atomic percent to 5.0 atomic percent.

[0118] The Fe-based soft magnetic alloy may contain at least one selected from the group consisting of Cr, Ru, Rh, and Ir to improve corrosion resistance thereof. It is preferable that the content of these elements be 5 atomic percent or less in order to ensure high saturation magnetic flux density, and be 1 atomic percent or less in view of compatibility among the saturation magnetic flux density, soft magnetic characteristics, and iron loss.

[0119] A fine crystalline texture can be formed by partial crystallization of a Fe-M (= Zr, Hf) based amorphous alloy, as described in the second embodiment.

[0120] The Fe content or the total content of Fe, Co and Ni in the Fe-based soft magnetic alloy is preferably 80 atomic percent or more. In addition, it is preferable that the content be less than 90 atomic percent. When the content exceeds 90 atomic percent, the Fe-based soft magnetic alloy does not have high permeability. It is more preferable that the content be in a range of 83 to 87 atomic percent, and most preferably 85 to 86 atomic percent in order to achieve a saturation magnetic flux density of 1.55 T or more. A desired saturation magnetic flux density is achieved when the Fe content is at least 80 atomic percent.

[0121] It is preferable that the Zn content in the Fe-based soft magnetic alloy be in a range of 0.034 to 0.16 atomic percent. When the Zn content lies in this range, the soft magnetic alloy has lower iron loss, high saturation magnetic flux density, and a small change in iron loss over time.

[0122] Zinc has a melting point of 419.5°C and a boiling point of 908°C. The alloy is generally melted in a crucible at a temperature of 1,240 to 1,350°C. When an alloy having the above-mentioned composition is melted at such a high

temperature, most of the zinc is lost by vaporization, as described above. Thus, the Fe-based soft magnetic alloy is preferably produced by the method for controlling the zinc content described in the second embodiment.

[0123] The resulting Fe-based soft magnetic alloy containing Zr and Nb in the above-specified amounts has high saturation magnetic flux density and low iron loss. The permeability of the alloy is further increased due to the addition of zinc. In addition, the alloy has low coercive force, large fracture strain, and high bending resistance.

[0124] A low-iron-loss magnetic core as a fourth embodiment will now be described.

[0125] The low-iron-loss magnetic core in accordance with the present invention may be, for example, troidal. Such a troidal magnetic core can be produced as follows. A ribbon of any one the above first to third Fe-based soft magnetic alloys can be produced by a quenching process described below. The ribbon is press-punched to form rings and the required rings are stacked to form a magnetic core. Alternatively, the ribbon is wound to form an annular ring. The magnetic core is preferably covered with a resin such as an epoxy resin or placed into a resin case for insulation, and then a coil is wound therearound.

[0126] An EI-type magnetic core may be formed as follows. The thin ribbon is pressed to form E-type pieces and I-type pieces. E-type pieces or I-type pieces are stacked to form an E-type core or I-type core. Required portions of the E-type core and the I-type core are covered with a resin or these core are placed into resin cases for insulation, and then these are joined to each other to form an EI-type magnetic core. The magnetic core may be a combination of two E-type cores, a U-type core and an I-type core, or two U-type cores.

[0127] Figs. 3 and 4 are exploded views of troidal low-iron-loss magnetic cores in accordance with the present invention. In the configuration shown in Fig. 3, a magnetic core 22 formed by stacking rings of a Fe-based soft magnetic alloy ribbon is contained in a lower case 21 and an upper case 20, these forming a hollow annular ring. In the configuration shown in Fig. 4, a magnetic core 24 of a wound ribbon 23 is contained in a lower case 21 and an upper case 20, these forming a hollow annular ring, and the entire member is covered with a resin. The upper and lower cases 20 and 21 may be omitted to form a magnetic core only by resin coating in some cases.

[0128] Fig. 5 is an isometric view of a magnet core of the present invention, which is applied to a common-mode choke coil. A choke coil 25 for three phases is used as a noise filter etc., and includes a magnetic core 26 of a wound ribbon of the low-iron-loss Fe-based soft magnetic alloy covered with a resin, three coils 27 wound on the magnetic core 26, and a bobbin 28 mounted in the magnetic core 26.

[0129] The Fe-based soft magnetic alloy constituting the ribbon is composed of at least 50% and preferably at least 70% of a fine crystalline texture of fine crystal grains consisting of a bcc-Fe phase as the major component having an average grain size of 100 nm or less and preferably 30 nm or less, and the balance being an amorphous texture. Thus, the Fe-based soft magnetic alloy has low magnetostriction, high saturation magnetic flux density and satisfactory permeability.

[0130] This Fe-based soft magnetic alloy is generally produced by a quenching step for quenching an alloy melt to form an amorphous alloy which is substantially composed of an amorphous phase, and an annealing step for annealing the amorphous ribbon or powder to precipitate fine crystal grains. The compositions of the Fe-based soft magnetic alloys suitable for the magnetic core in this embodiment are described in the first to third embodiments.

[0131] The magnetic core has satisfactory soft magnetic characteristics and low iron loss, and is used as magnetic cores of various transformers, such as low-frequency transformers, pulse transformers, power transformers, and pole-mounted transformers, and of various coils, such as choke coils and inductance coils.

[0132] When this low-iron-loss magnetic core is used in a transformer, loss of electrical power is reduced and heating of the magnetic core is also reduced.

[0133] Since the Fe-based soft magnetic alloy has a large fracture strain, that is, at least 1.0×10^{-2}, the ribbon formed of the alloy has excellent bending workability. Thus, a ring magnetic core can be easily formed by winding the ribbon.

[0134] A fifth embodiment of the present invention relates to the first method. In this embodiment, the amorphous alloy ribbon produced using the apparatus shown in Fig. 1 is annealed to precipitate a fine crystalline texture of a bcc-Fe phase as the major component. The heating rate to a predetermined annealing temperature is set to 10°C/min to 200°C/min, preferably 20°C/min to 100°C/min, and more preferably 30°C/min to 40°C/min. When the heating rate is lower than the lower limit, the annealing time is prolonged, and satisfactory magnetic characteristics may not be achieved. When the heating rate is higher than the upper limit, the temperature in the annealing furnace will not follow such a high heating rate or thermal conduction will become nonuniform. Thus, a homogeneous crystalline texture will not be easily formed, and magnetic characteristics will be deteriorated. In addition, annealing of an alloy having a large size at a high and uniform heating rate requires a complicated heating furnace mechanism, resulting in increased facility costs.

[0135] In the present invention, a moderate heating rate of the alloy for achieving satisfactory magnetic characteristics was discovered and is applied to the above method.

[0136] An alloy having superior characteristics can be produced in the present invention, based on the following standard regarding the annealing temperature. When the crystallization temperature of bcc-Fe is T_{X1} [°C] and the crystallization temperature of the compound phase which can be crystallized at a higher temperature is T_{X2} [°C], the

temperature difference T_x (= T_{X2} - T_{X1}) is preferably as large as possible. More preferably, T_x is at least 200°C in order to avoid undesired crystallization of the compound phase during the heating process up to T_{X2}, in view of the formation of bcc-Fe fine crystal grains in the amorphous phase. When the T_x is large, the alloy can be annealed under optimal conditions which are capable of facilitating precipitation of the bcc-Fe phase and suppressing precipitation of other compound phases. The resulting Fe-based soft magnetic alloy has improved soft magnetic characteristics. The annealing temperature Ta preferably satisfies the relationship $T_{X1} < Ta < T_{X2}$. In the case of the above first to third Fe-based soft magnetic alloys, the compound phases, which are crystallized at T_{X2}, are believed to be Fe_3B, Fe_2B and the like.

[0137] At an intermediate temperature T_{X1}, between T_{X1} and T_{X2}, another compound phase may be crystallized. Although the composition of this compound phase is not clear, the precipitation of this compound phase depends on the composition of the Fe-based soft magnetic alloy. In particular, this compound phase is readily precipitated when the boron content is increased. Thus, this compound phase is believed to be composed of boron and other elements. When crystallization due to this compound phase is observed at $T_{X1'}$, it is preferable that Tx (= $T_{X1'}$ - T_{X1}) be at least 200°c and the annealing temperature Ta of the alloy satisfy $T_{X1} < Ta < T_{X1'}$.

[0138] The first method is preferably applied to production of the above first to third Fe-based soft magnetic alloys.

[0139] A sixth embodiment of the present invention relates to the second method. In this embodiment, a single-roller quenching process using the apparatus shown in Fig. 1 is preferably employed. An alloy melt having a predetermined composition is jetted onto a rotating cooling roller made of steel through a quartz nozzle placed on the cooling roller by a pressure of argon gas to quench the melt. A ribbon is thereby formed. The temperature of the melt ejected from the nozzle (ejection temperature) is less than 1,350°C in the present invention. In addition, the ejection temperature is preferably at least 1,240°C to avoid clogging in the nozzle due to decreased viscosity of the melt. The second method is preferably applied to production of the above first to third Fe-based soft magnetic alloys. When Fe-based soft magnetic alloys contains zinc according to the second and third embodiments, most of the zinc is lost by vaporization, because the ejection temperature, 1,240 to 1,350°C, is higher than the melting point and the boiling point of the zinc, 419.5°C and 908°C. Thus, zinc is added in excess to the alloy fed into the crucible so that the quenched alloy contains the above-specified content of zinc. It is preferable that zinc be added to the alloy in an amount which is at least 20 times the final target content, that is 0.025 to 0.2 atomic percent.

[0140] A seventh embodiment of the present invention relates to the third method. In this embodiment, an alloy melt containing Fe as the major component, at least one metal M selected from the group consisting of Ti, Zr, Hf, V, Nb, Ta, Mo and W, and B is quenched to form an amorphous alloy ribbon. The amorphous alloy ribbon may be any well-known process. A typical process is ejection of the alloy melt onto a moving cooling medium, such as a rotating cooling roller, using the apparatus shown in Fig. 1.

[0141] The resulting amorphous alloy ribbon is subjected to a first annealing treatment at a holding or annealing temperature of 500 to 800°C. When the amorphous alloy ribbon is heated, a fine crystalline phase substantially composed of bcc-Fe crystal grains having an average grain size of 30 nm is deposited at a temperature which is higher than a certain temperature. In the present invention, the temperature at which the bcc-Fe fine crystal phase is precipitated is called a first crystallization temperature. The first crystallization temperature depends on the composition of the alloy, and generally lies in a range of approximately 480 to 550°C.

[0142] When the alloy ribbon is heated to a certain temperature which is higher than the first crystallization temperature, a compound phase or second crystalline phase, which is composed of Fe_3B and Fe_3Zr in the case of the Zr-containing alloy, is deposited. In the present invention, the temperature at which such a compound phase is precipitated is called a second crystallization temperature. The second crystallization temperature depends on the composition of the alloy, and generally lies in a range of approximately 740 to 810. The compound phase causes deterioration of soft magnetic characteristics.

[0143] Accordingly, the annealing temperature during the first annealing treatment of the amorphous alloy ribbon is preferably set to be in a range of 500 to 800°C so as to facilitate deposition of the bcc-Fe fine crystalline phase and to inhibit precipitation of the compound phase, in view of the alloy composition.

[0144] The holding or annealing time of the amorphous alloy is 20 minutes or less. The annealing time may be zero in some alloy compositions. In such a case, the alloy is cooled immediately after the alloy reaches the annealing temperature. The resulting alloy has high permeability by such annealing. When the alloy does not contain silicon or copper, high permeability is achieved during a shorter annealing time of 10 minutes or less. When the alloy contains silicon, a long annealing time is required so that silicon is sufficiently dissolved into iron. Although the annealing time may be further prolonged, the prolonged annealing time will not result in improvement in magnetic characteristics, but will result in decreased productivity.

[0145] In the first annealing treatment, the heating rate of the amorphous alloy ribbon from room temperature to the annealing temperature is 10°C or more, more preferably in a range of 10 to 200°C, and most preferably 30 to 100°C. Although a higher heating rate is preferable in view of the production time, it is difficult to achieve a heating rate of more than 200°C/min as long as a currently available heating apparatus is used.

[0146] After the first annealing treatment, the alloy ribbon is cooled to a predetermined temperature, is subjected to a second heating treatment, and is then cooled by air cooling or the like to room temperature. This method including the second annealing treatment in the middle of the cooling process after the first annealing is referred to as a two-stage annealing.

[0147] The predetermined temperature is a holding or annealing temperature of the second annealing treatment. The annealing temperature of the second annealing treatment is 100°C to a temperature less than the annealing temperature of the first annealing treatment, and more preferably 200 to 400°C. When the annealing temperature of the second annealing treatment is less than 100°C, satisfactory soft magnetic characteristics are not obtained due to insufficient annealing effects. When the annealing temperature of the second annealing treatment is higher than the annealing temperature of the first annealing treatment, a compound phase (second crystal phase) composed of Fe_3B and Fe_3Zr etc., which deteriorates soft magnetic characteristics, is deposited.

[0148] During the second heating treatment, the annealing time of the alloy ribbon is 0.5 to 100 hours and more preferably 1 to 30 hours. An annealing time less than 0.5 hours will produce large coercive force which inhibits improvement in soft magnetic characteristics such as high permeability. On the other hand, an annealing time exceeding 100 hours causes large changes in magnetic characteristics over time.

[0149] The two-stage cooling step causes significant improvement in soft magnetic characteristics and slight changes in magnetic characteristics over time when the Fe-based soft magnetic alloy is allowed to stand at high temperatures for long periods.

[0150] The alloy ribbon may be subjected to the second annealing treatment by heating the alloy ribbon to a predetermined temperature after the alloy ribbon is cooled by air cooling or the like from the annealing temperature of the first annealing treatment to room temperature. In this case, the second annealing treatment is called a low-temperature annealing treatment. When the low-temperature annealing is performed after the deposition of the fine bcc-Fe crystal grain phase having an average grain size of 30 nm in an amorphous phase in the first annealing treatment, soft magnetic characteristics are significantly improved. Thus, the resulting Fe-based soft magnetic alloy has slight changes in magnetic characteristics when the alloy is allowed to stand at high-temperatures for long periods.

[0151] Preferable annealing patterns in this embodiment are as follows.

[0152] Fig. 6 is a graph of an annealing pattern or program for the two-stage annealing treatment. The amorphous alloy ribbon is heated from room temperature to the annealing temperature of the first annealing treatment, maintained at the annealing temperature for the predetermined time, cooled to the annealing temperature of the second annealing treatment, maintained at the annealing temperature of the second annealing treatment for the predetermined time, and then cooled by air cooling or the like to room temperature.

[0153] Fig. 7 is a graph of an annealing pattern or program for the low-temperature annealing treatment. The amorphous alloy ribbon is heated from room temperature to the annealing temperature of the first annealing treatment, maintained at the annealing temperature for the predetermined time, cooled by air cooling or the like to room temperature, the annealing temperature of the second annealing treatment, heated from room temperature to the annealing temperature of the second annealing treatment, maintained at the annealing temperature of the second annealing treatment for the predetermined time, and then cooled by air cooling or the like to room temperature.

[0154] As described above, the alloy ribbon after the first annealing treatment has a texture including a fine crystalline phase composed of fine bcc-Fe crystal grains having an average grain size of 30 nm or less, and a boundary amorphous phase which is present in the grain boundaries. Since this texture contains no compound phase, which causes deterioration of soft magnetic characteristics of the alloy, the annealed alloy ribbon has superior soft magnetic characteristics.

[0155] Furthermore, the second annealing treatment further improves soft magnetic characteristics of the Fe-based soft magnetic alloy, and the resulting alloy has slight changes in magnetic characteristics when the alloy is allowed to stand at high temperatures for long periods.

[0156] It is believed that superior soft magnetic characteristics of the alloy produced by the method according to this embodiment are due to significantly small apparent magnetocrystalline anisotropy. That is, magnetocrystalline anisotropy is a factor deteriorating soft magnetic characteristics of conventional crystalline materials. In the present invention, however, the bcc crystal grains deposited during the first annealing treatment are fine and thus magnetocrystalline anisotropy will be moderated by magnetic interaction between the bcc grains.

[0157] When the average crystal grain size exceeds 30 nm, the magnetocrystalline anisotropy is not sufficiently moderated and the soft magnetic characteristics are deteriorated.

[0158] The residual stress in the alloy which is formed during the first annealing treatment is believed to be relaxed in the second annealing treatment.

[0159] The Fe-based soft magnetic alloy preferably contains Fe as the major component; at least one metal M selected from the group consisting of Ti, Zr, Hf, V, Nb, Ta, Mo, W and Mn; and B. The third method is preferably applied to production of the above first to third Fe-based soft magnetic alloys.

[0160] The third method is also preferably applicable to alloys represented by the following formulas:

$$(Fe_{1-a}Z_a)_bB_xM_y$$

$$(Fe_{1-a}Z_a)_bB_xM_yX_z$$

$$(Fe_{1-a}Z_a)_bB_xM_yT_t$$

$$(Fe_{1-a}Z_a)_bB_xM_yX_zT_t$$

wherein Z is at least one of Ni and Co; M is at least one selected from the group consisting of Ti, Zr, Hf, V, Nb, Ta, Mo, W and Mn; T is at least one selected from the group consisting of Cu, Ag, Au, Pd and Pt; X is at least one selected from the group consisting of Si, Al, Ge and Ga; subscripts a, b, x, y, t and z satisfy the relationships $0 \le a \le 0.1$; 75 atomic percent $\le b \le$ 93 atomic percent; 0.5 atomic percent $\le x \le$ 18 atomic percent; 4 atomic percent $\le y \le$ 9 atomic percent; $t \le 5$ atomic percent; and $z \le 5$ atomic percent. These alloys may be used in the above first and second methods.

[0161] The first to third methods may be performed alone or in combination of at least two methods.

EXAMPLE 1 [Texture of Fe-based Soft Magnetic Alloy having High Saturation Magnetic Flux Density and Low Iron Loss]

[0162] An alloy ribbon essentially composed of an amorphous phase was prepared by a single-roller liquid quenching process. A melt was jetted onto a rotating steel roller through a nozzle by pressure of argon gas to form a ribbon by quenching. The resulting ribbon had a width of approximately 15 mm and a thickness of approximately 20 μm.

[0163] The ribbon was heated at 180°C/min and maintained at 535°C for 5 minutes to precipitate a fine crystalline texture.

[0164] The texture of the resulting soft magnetic alloy ribbon was identified by X-ray diffractometry. The permeability (μ'), coercive force (Hc), and saturation magnetic flux density (B_{10}) of the alloy ribbon were measured. The ribbon was worked to form rings with an outer diameter of 10 mm and an inner diameter of 6 mm, the rings were stacked, and a coil was wound around the stacked rings. The permeability (μ') of the stacked rings was measured at 5 mOe and 1 kHz using an impedance analyzer. The coercive force (Hc) and the saturation magnetic flux density (B_{10}) were measured using a direct-current B-H loop tracer.

[0165] Fig. 8 shows an X-ray diffraction pattern of a quenched soft magnetic alloy ribbon having a composition of $Fe_{86.76}Zr_2Nb_4B_{8.25}$ which is formed by quenching a melt, and Fig. 9 shows an X-ray diffraction pattern of the annealed soft magnetic alloy ribbon having the same composition.

[0166] In Fig. 8, a halo diffraction pattern indicating the presence of an amorphous phase is observed in a quenched ribbon, whereas, in Fig. 9, a diffraction pattern indicating the presence of a bcc-Fe crystalline phase is observed in an annealed ribbon. These results show the texture of the alloy changed from an amorphous state to a body-centered-cubic crystal structure. According to transmittance electron microscopic observation, the texture after the annealing is composed of fine crystal grains having a grain size of approximately 10 nm.

[0167] Accordingly, the Fe-based soft magnetic alloy having the above composition has a fine crystalline texture primarily composed of fine crystal grains which are formed by annealing of the amorphous alloy.

[0168] Quenched ribbons having the compositions for comparison of $Fe_{86}Nb_7B_7$, $Fe_{91}Zr_7B_2$, $Fe_{89}Zr_7B_4$, and $Fe_{89}Zr_5B_6$ and having the compositions according to the present invention of $Fe_{86}Zr_2Nb_4B_8$, $Fe_{85.75}Zr_2Nb_4B_{8.25}$ and $Fe_{85.5}Zr_2Nb_4B_{8.5}$, respectively, were prepared, heated at a heating rate of 180°C/min, and maintained at a temperature of 510 to 650°C for 5 minutes to 1 hour to provide soft magnetic alloys. The permeability (μ'), the coercive force (Hc) and the saturation magnetic flux density (B_{10}) of each alloy were measured. The result is shown in Table 1.

[0169] The results in Table 1 show that the soft magnetic alloys $Fe_{86}Zr_2Nb_4B_8$, $Fe_{85.75}Zr_2Nb_4B_{8.25}$ and $Fe_{85.5}Zr_2Nb_4B_{8.5}$ containing specific amounts of zirconium and niobium have a higher permeability (μ') and a lower coercive force (Hc) than those of alloys for comparison containing either zirconium or niobium. Thus, the Fe-based soft magnetic alloys in accordance with the present invention have satisfactory soft magnetic characteristics. In particular, the alloy $Fe_{85.75}Zr_2Nb_4B_{8.25}$ has a significantly high permeability (μ') of 57,800 and a significantly low coercive force (Hc) of 0.043 Oe, and has superior soft magnetic characteristics.

EXAMPLE 2 [Relationship between Alloy Composition and Magnetic Characteristics]

[0170] Quenched alloy ribbons having different compositions were prepared as in EXAMPLE 1 and were annealed at a heating rate of 180°C/min and an annealing time of 5 minutes unless otherwise specified. A variety of soft magnetic

alloy ribbons were thereby prepared.

[0171] The coercive force (Hc), permeability (μ') at 1 kHz, and saturation magnetic flux density (B_{10}) in a magnetic field of 10 Oe, and remanent magnetization (Br) of each soft magnetic alloy ribbon were measured. Furthermore, the magnetostriction constants (λ_s) of parts of the ribbons were measured.

[0172] The annealing temperature at which the coercive force (Hc) is minimized and the permeability (μ') is maximized was measured during the annealing within a range of 500°C to 700°C.

[0173] An average crystal grain size in the fine crystalline texture of each of some annealed ribbons was determined by X-ray diffractometry.

[0174] The crystallization temperatures (T_{X1}, T_{X2} and T_{X1}') of the bcc-Fe phase and the compound phases of each of some quenched ribbons were measured to determine the difference (ΔT_X) between the crystallization temperatures by differential thermal analysis (DTA).

[0175] The results are shown in Figs. 10 to 59. Figs. 10 to 13 show magnetic characteristics of a soft magnetic alloy containing zirconium and niobium in a total amount of 5 atomic percent; Figs. 14 to 23 show magnetic and thermal characteristics of a soft magnetic alloy containing zirconium and niobium in a total amount of 5.5 atomic percent; Figs. 24 to 35 show various properties including magnetic and thermal characteristics of a soft magnetic alloy containing zirconium and niobium in a total amount of 6 atomic percent; Figs. 36 to 47 show various properties including magnetic and thermal characteristics of a soft magnetic alloy containing zirconium and niobium in a total amount of 6.5 atomic percent; and Figs. 48 to 59 show various properties including magnetic and thermal characteristics of a soft magnetic alloy containing zirconium and niobium in a total amount of 7 atomic percent. In these graphs, white circle (○) indicates a ribbon having diffraction peaks of (200) plane of the bcc-Fe phase at a quenched state, whereas black circle (●) indicates a ribbon having no diffraction peak of (200) plane of the bcc-Fe phase at a quenched state. That is, ribbons represented by the white circle (○) are obtained by annealing of quenched ribbons in which crystalline phases are partly deposited in amorphous phases, and ribbons represented by the black circle (●) are obtained by annealing of quenched ribbons composed of substantially amorphous single-phases.

(Soft Magnetic Alloy of Zr + Nb = 5 atomic percent)

[0176] With reference to Fig. 10, soft magnetic alloys in which the total amount of zirconium and niobium is 5 atomic percent have coercive forces (Hc) of 59 to 1,055 mOe. The alloy having a coercive force (Hc) of 59 mOe is represented by $Fe_{87}Zr_{2.5}Nb_{2.5}B_8$.

[0177] With reference to Fig. 11, soft magnetic alloys in which the total amount of zirconium and niobium is 5 atomic percent have permeabilities (μ') of 300 to 33,000. The alloy having a permeability (μ') of 33,000 is represented by $Fe_{87}Zr_{2.5}Nb_{2.5}B_8$.

[0178] With reference to Fig. 12, soft magnetic alloys in which the total amount of zirconium and niobium is 5 atomic percent have saturation magnetic flux densities (B_{10}) of 1.59 to 1.72 T. The alloys having saturation magnetic flux densities (B_{10}) higher than 1.5 T have compositions of 1 to 2.5 atomic percent of zirconium, 6.75 to 11 atomic percent of boron, and 88 to 90.75 atomic percent in total of iron and niobium (84 to 88.5 atomic percent of iron). The alloy represented by $Fe_{87}Zr_{2.5}Nb_{2.5}B_8$ has a significantly high saturation magnetic flux density (B_{10}), 1.72 T.

[0179] With reference to Fig. 13, soft magnetic alloys in which the total amount of zirconium and niobium is 5 atomic percent have remanent magnetizations (Br) of 0.47 to 1.36 T.

[0180] The graphs shown in Figs. 10 to 13 demonstrate that alloys having satisfactory soft magnetic characteristics contain 1 to 2.5 atomic percent of zirconium, 6.75 to 11 atomic percent of boron, and 88 to 90.75 atomic percent in total of iron and niobium. In particular, the alloy represented by $Fe_{87}Zr_{2.5}Nb_{2.5}B_8$ has superior soft magnetic characteristics.

(Soft Magnetic Alloy of Zr + Nb = 5.5 atomic percent)

[0181] With reference to Fig. 14, soft magnetic alloys in which the total amount of zirconium and niobium is 5.5 atomic percent have coercive forces (Hc) of 94 to 211 mOe. The alloys having coercive forces (Hc) less than 200 mOe have compositions of not less than 1 atomic percent of zirconium and not more than 90 atomic percent in total of iron and niobium. The alloys having coercive forces (Hc) less than 100 mOe have compositions of not less than 1.5 atomic percent of zirconium and not more than 88.5 atomic percent in total of iron and niobium.

[0182] With reference to Fig. 15, soft magnetic alloys in which the total amount of zirconium and niobium is 5.5 atomic percent have permeabilities (μ') of 8,400 to 25,400. The graph suggests that the permeability (μ') depends on the relative contents of Fe, Zr and Nb, but does not depend on the content of boron. The alloys having permeabilities (μ') of 10,000 or more have compositions of not more than 90.5 atomic percent in total of iron and niobium, and not less than 0.5 atomic percent of zirconium. The alloys having permeabilities (μ') of 20,000 or more have compositions of not more than 89 atomic percent in total of iron and niobium, and not less than 1 atomic percent of zirconium.

[0183] The graphs shown in Figs. 14 and 15 demonstrate that these alloys have satisfactory soft magnetic characteristics, that is, high permeability (μ') and low coercive force (Hc).

[0184] With reference to Fig. 16, soft magnetic alloys in which the total amount of zirconium and niobium is 5.5 atomic percent have saturation magnetic flux densities (B_{10}) of 1.60 to 1.68 T.

[0185] With reference to Fig. 17, soft magnetic alloys in which the total amount of zirconium and niobium is 5.5 atomic percent have remanent magnetizations (Br) of 0.44 to 0.62 T.

[0186] Fig. 18 shows optimized annealing temperatures of soft magnetic alloys to achieve minimum coercive forces (Hc) in which the total amount of zirconium and niobium is 5.5 atomic percent. The alloy ribbons having minimum coercive forces (Hc) at a temperature of 550°C or less contain not less than 1 atomic percent of zirconium, 10 atomic percent of boron, and 88.5 to 89 atomic percent in total of iron and niobium.

[0187] A lower annealing temperature is advantageous for mass production of alloys. The soft magnetic alloys in accordance with the present invention can be annealed at a temperature lower than the annealing temperature for conventional fine crystalline alloys.

[0188] Fig. 19 shows optimized annealing temperatures of soft magnetic alloys to achieve maximum permeabilities (μ') in which the total amount of zirconium and niobium is 5.5 atomic percent. The alloy ribbons having maximum permeabilities (μ') at a temperature of 550°C or less contain not less than 1 atomic percent of zirconium, 10 atomic percent of boron, and 88.5 to 89 atomic percent in total of iron and niobium.

[0189] The graphs shown in Figs. 18 and 19 suggest that alloy ribbons containing not less than 1 atomic percent of zirconium, 10 atomic percent of boron, and 88.5 to 89 atomic percent in total of iron and niobium have optimized coercive force (Hc) and optimized permeability (μ') even when the ribbons are annealed at 550°C or less. Thus, the fine crystalline soft magnetic alloys have high productivity. The optimized composition range shown in Figs. 18 and 19 substantially includes the optimized composition range for coercive force (Hc) and permeability (μ') shown in Figs. 14 and 15, respectively.

[0190] Fig. 20 shows the crystallization temperature (T_{X1}) of the bcc-Fe phase; Fig. 22 shows the crystallization temperature (T_{X2}) of a compound phase; and Fig. 21 shows the crystallization temperature ($T_{X1'}$) of another compound phase. These crystallization temperatures satisfy the relationship $T_{X1} < T_{X1'} < T_{X2}$. Fig. 23 shows the difference in the crystallization temperatures $\Delta T_X = T_{X2} - T_{X1}$.

[0191] As shown in Fig. 20, T_{X1} lies in a range of 462 to 484°C, depend on the relative contents of iron, niobium and zirconium, and does not depend on the boron content.

[0192] As shown in Fig. 23, the difference in the crystallization temperature (ΔT_X) lies in a range of 331 to 227°C. Since these alloys have large differences in the crystallization temperatures (ΔT_X), that is, more than 320°C, only the bcc-Fe phase can be precipitated during annealing while precipitation of the compound phase which deteriorates soft magnetic characteristics of the alloys can be suppressed.

[0193] The circle without a numeral in Fig. 21 indicates an alloy not having a crystallization temperature ($T_{X1'}$) of another compound phase. Alloys having no crystallization temperature ($T_{X1'}$) generally have satisfactory magnetic characteristics.

[0194] The graphs shown in Figs. 14 to 23 show that alloys (Zr + Nb = 5.5 atomic percent) having satisfactory soft magnetic characteristics contain not less than 0.5 atomic percent and preferably not less than 1 atomic percent of zirconium, 10 atomic percent of boron, and 88.5 to 89 atomic percent in total of iron and niobium (84.5 to 87.7 atomic percent of iron). In particular, the alloys represented by $Fe_{84.5}Zr_1Nb_{4.5}B_{10}$ and $Fe_{84.5}Zr_{1.5}Nb_4B_{10}$ have superior soft magnetic characteristics.

(Soft Magnetic Alloy of Zr + Nb = 6 atomic percent)

[0195] With reference to Fig. 24, soft magnetic alloys in which the total amount of zirconium and niobium is 6 atomic percent have coercive forces (Hc) of 38 to 8,400 mOe. The alloys having coercive forces (Hc) less than 70 mOe have compositions of not less than 0.5 atomic percent and preferably not less than 1 atomic percent of zirconium, not more than 10 atomic percent of boron, and not more than 90 atomic percent in total of iron and niobium. The alloys having coercive forces (Hc) less than 50 mOe have compositions of 1.5 to 3.5 atomic percent of zirconium, 6.5 to 9.5 atomic percent and preferably 6.5 to 9 atomic percent of boron, and 89 to 90 atomic percent in total of iron and niobium (84.5 to 87.5 atomic percent of iron). The alloys having coercive forces (Hc) less than 40 mOe have compositions of 1.5 to 2.5 atomic percent and preferably 2.0 atomic percent of zirconium, 8 to 9 atomic percent of boron, and 89 to 89.5 atomic percent and preferably 89.5 atomic percent in total of iron and niobium (85 to 86 atomic percent of iron).

[0196] With reference to Fig. 25, soft magnetic alloys in which the total amount of zirconium and niobium is 6 atomic percent have permeabilities (μ') of 900 to 59,000. The alloys having permeabilities (μ') of 30,000 or more have compositions of not less than 1 atomic percent of zirconium, not more than 10 atomic percent of boron, and not more than 90 atomic percent in total of iron and niobium. The alloys having permeabilities (μ') of 40,000 or more have compositions of 1 to 3 atomic percent of zirconium, 7.5 to 9.5 atomic percent of boron, and 89 to 90 atomic percent in total of iron

and niobium (84.5 to 86.5 atomic percent of iron). The alloys having permeabilities (μ') of 50,000 or more have compositions of 1.5 to 2.5 atomic percent of zirconium, 8 to 9 atomic percent of boron, and 89 to 90 atomic percent in total of iron and niobium (85 to 86 atomic percent of iron).

[0197] The graphs shown in Figs. 24 and 25 demonstrate that when the alloy satisfies Zr + Nb = 6 atomic percent and contains 1.5 to 2.5 atomic percent of zirconium, that is, 1.5/6 to 2.5/6 of Zr/(Zr+Nb), 8 to 9 atomic percent of boron, not less than 80 atomic percent of iron, and 89 to 90 atomic percent in total of iron and niobium (the resulting Fe content is 85 to 86 atomic percent), the alloy ribbon has superior soft magnetic characteristics, that is, a high permeability (μ') of 40,000 to 50,000 and a low coercive force (Hc) of 40 mOe or less.

[0198] With reference to Fig. 26, soft magnetic alloys in which the total amount of zirconium and niobium is 6 atomic percent have saturation magnetic flux densities (B10) of 1.53 to 1.67 T. The saturation magnetic flux density (B10) tends to increase as the Fe content increases, but the relationship with the relative contents of Zr, Nb and B is not clear. In the above-mentioned composition range, the alloy has a saturation magnetic flux density (B10) of 1.5 to 1.6 T and a permeability (μ') of 40,000 to 50,000.

[0199] With reference to Fig. 27, soft magnetic alloys in which the total amount of zirconium and niobium is 6 atomic percent have remanent magnetizations (Br) of 0.39 to 1.19 T. The relationship between the remanent magnetization (Br) and the relative contents of Fe, Zr, Nb and B is not clear.

[0200] With reference to Fig. 28, average crystal grain sizes of bcc-Fe phases in soft magnetic alloys in which the total amount of zirconium and niobium is 6 atomic percent lie in a range of 10 to 12 nm. Thus, these crystal grains are significantly fine. A soft magnetic alloy having an average crystal grain size of 11 nm or less contains not more than 4 atomic percent of zirconium, 5.5 to 10 atomic percent and preferably 6 to 9 atomic percent of boron, and 88 to 92 atomic percent and preferably 90 to 92 atomic percent in total of iron and niobium (84 to 88.5 atomic percent and preferably 85 to 88 atomic percent of iron). This composition range includes the optimized composition ranges for coercive force (Hc) and permeability (μ') shown in Figs. 24 and 25. Accordingly, soft magnetic characteristics of the alloy are improved as the average crystal grain size of the bcc-Fe phase decreases.

[0201] With reference to Fig. 29, soft magnetic alloys in which the total amount of zirconium and niobium is 6 atomic percent have magnetostriction constants (λ_s) in a desirable range of -14×10^{-7} to 17×10^{-7}. The line representing a magnetostriction constant of 0 is included in a region having the highest permeability (μ') shown in Fig. 18. The magnetostriction constant (λ_s) tends to depend on the B content and is substantially zero when the B content is in a range of 8 to 9 atomic percent.

[0202] Fig. 30 shows optimized annealing temperatures of soft magnetic alloys to achieve minimum coercive forces (Hc) in which the total amount of zirconium and niobium is 6 atomic percent. The alloy ribbons having minimum coercive forces (Hc) at a temperature of 525°C or less contain 1 to 3 atomic percent of zirconium, 7.5 to 9.5 atomic percent of boron, and 89 to 90 atomic percent in total of iron and niobium (84.5 to 86.5 atomic percent of iron).

[0203] Fig. 31 shows optimized annealing temperatures of soft magnetic alloys to achieve maximum permeabilities (μ') in which the total amount of zirconium and niobium is 6 atomic percent. The alloy ribbons having maximum permeabilities (μ') at a temperature of 525°C or less contain 1.5 to 2.5 atomic percent of zirconium, 8 to 9 atomic percent of boron, and 89 to 90 atomic percent in total of iron and niobium (85 to 86 atomic percent of Fe).

[0204] The graphs shown in Figs. 30 and 31 suggest that alloy ribbons containing 0.5 to 3.5 atomic percent of zirconium, 7 to 10.5 atomic percent of boron, and not more than 90 atomic percent in total of iron and niobium have optimized coercive force (Hc) and optimized permeability (μ') even when the ribbons are annealed at 550°C or less. Thus, the fine crystalline soft magnetic alloys have high productivity. The optimized composition range shown in Figs. 30 and 31 substantially includes the optimized composition range for coercive force (Hc), permeability (μ') and the average crystal grain size of the bcc-Fe phase shown in Figs. 24, 25 and 28, respectively.

[0205] Fig. 32 shows the crystallization temperature (T_{X1}) of the bcc-Fe phase; Fig. 33 shows the crystallization temperature (T_{X2}) of a compound phase; and Fig. 34 shows the crystallization temperature ($T_{X1'}$) of another compound phase. These crystallization temperatures satisfy the relationship $T_{X1} < T_{X1'} < T_{X2}$. Fig. 35 shows the difference in the crystallization temperatures $\Delta T_X = T_{X2} - T_{X1}$.

[0206] As shown in Fig. 32, T_{X1} lies in a range of 464 to 500°C, depending on the relative content of iron, niobium and zirconium, and does not depend on the boron content.

[0207] In the composition range showing high permiability (Hc) and low permeability (μ') in Figs. 24 and 25 ($1.5/6 \leq Zr/(Zr+Nb) \leq 2.5/6$, 8 atomic percent $\leq B \leq$ 9 atomic percent, 80 atomic percent $\leq$ Fe, and $89 \leq Fe + Nb \leq 90$), T_{X1} lies in a range of 480 to 490°C.

[0208] As shown in Fig. 35, the difference in the crystallization temperature (ΔT_X) lies in a range of 313 to 344°C. These alloys have large differences in the crystallization temperatures (ΔT_X) which increase as the boron content decreases. In particular, the alloys have large differences in the crystallization temperatures (ΔT_X) of more than 330°C in a range of 1 to 2.5 atomic percent of zirconium and 9.5 atomic percent of boron, and only the bcc-Fe phase can be precipitated during annealing while precipitation of the compound phase which deteriorates soft magnetic characteristics of the alloys can be suppressed.

[0209] The circle without a numeral in Fig. 34 indicates an alloy not having a crystallization temperature ($T_{X1'}$) of another compound phase. Alloys having no crystallization temperature ($T_{X1'}$) generally have satisfactory magnetic characteristics, as shown in Figs. 24 to 26.

[0210] The graphs in Figs. 24 to 35 show that alloys (Zr + Nb = 6 atomic percent) having satisfactory soft magnetic characteristics contain 1.5 to 2.5 atomic percent of zirconium, 8 to 9 atomic percent of boron, and 89 to 90 atomic percent in total of iron and niobium (85 to 86 atomic percent of iron). More satisfactory soft magnetic characteristics are obtained when the zirconium content is 2 atomic percent.

[0211] As shown in Figs. 24 to 35, many ribbons, represented by black circles, substantially composed of an amorphous single phase in a quenched state are distributed through the above composition range, whereas ribbons, represented by white circles, having amorphous phases and crystalline phases, lie outside the above composition range.

[0212] When a ribbon composed of an amorphous phase in a quenched state is annealed, the ribbon has satisfactory magnetic characteristics.

[0213] In particular, the alloys represented by $Fe_{85.5}Zr_2Nb_4B_{8.5}$, $Fe_{85}Zr_{1.75}Nb_{4.25}B_9$, $Fe_{85.25}Zr_{1.75}Nb_{4.25}B_{8.75}$, and $Fe_{85.75}Zr_{2.25}Nb_{3.75}B_{8.25}$ have superior soft magnetic characteristics.

(Soft Magnetic Alloy of Zr + Nb = 6.5 atomic percent)

[0214] With reference to Fig. 36, soft magnetic alloys in which the total amount of zirconium and niobium is 6.5 atomic percent have coercive forces (Hc) of 43 to 108 mOe. The alloys having coercive forces (Hc) less than 100 mOe have compositions of not more than 90.5 atomic percent in total of iron and niobium. The alloys having coercive forces (Hc) less than 50 mOe have compositions of 1.6 to 3.2 atomic percent of zirconium, 6.75 to 9 atomic percent of boron, and not less than 89 atomic percent and preferably 89.5 to 90.25 atomic percent in total of iron and niobium (84.5 to 86.75 atomic percent of iron).

[0215] With reference to Fig. 37, soft magnetic alloys in which the total amount of zirconium and niobium is 6.5 atomic percent have permeabilities (μ') of 10,500 to 45,000. The alloys having permeabilities (μ') of 20,000 or more have compositions of not less than 6.0 atomic percent and preferably not less than 6.75 atomic percent of boron, and not more than 90.75 atomic percent in total of iron and niobium. The alloys having permeabilities (μ') of 30,000 or more have compositions of no less than 6.5 atomic percent and preferably 6.75 atomic percent of boron, and not more than 90.5 atomic percent and preferably not more than 90.25 atomic percent in total of iron and niobium. The alloys having permeabilities (μ') of 40,000 or more have compositions of 1.25 to 2.5 atomic percent and preferably 1.5 to 2 atomic percent of zirconium, 8 to 9.25 atomic percent and preferably 8.5 to 9 atomic percent of boron, and 89 to 90 atomic percent and preferably 89.5 atomic percent in total of iron and niobium.

[0216] The graphs shown in Figs. 36 and 37 demonstrate that when the alloy satisfies Zr + Nb = 6.5 atomic percent and contains 1.5 to 2.5 atomic percent of zirconium, 8 to 9 atomic percent and preferably 8.5 to 9 atomic percent of boron, and 84.5 to 85.5 atomic percent and preferably 84.5 to 85 atomic percent in total of iron and niobium (84.5 to 85.5 atomic percent and preferably 84.5 to 85 atomic percent of iron), the alloy ribbon has superior soft magnetic characteristics, that is, high permeability (μ') and low coercive force (Hc).

[0217] With reference to Fig. 38, soft magnetic alloys in which the total amount of zirconium and niobium is 6.5 atomic percent have saturation magnetic flux densities (B_{10}) of 1.5 to 1.6 T.

[0218] With reference to Fig. 39, soft magnetic alloys in which the total amount of zirconium and niobium is 6.5 atomic percent have remanent magnetizations (Br) of 0.37 to 0.97 T.

[0219] The saturation magnetic flux densities (B_{10}) and the remanent magnetization (Br) are satisfactory levels, although the relationships with the composition are not clear.

[0220] With reference to Fig. 40, average crystal grain sizes of bcc-Fe phases in soft magnetic alloys in which the total amount of zirconium and niobium is 6.5 atomic percent lie in a range of 9.8 to 11.5 nm. Thus, these crystal grains are significantly fine.

[0221] With reference to Fig. 41, soft magnetic alloys in which the total amount of zirconium and niobium is 6.5 atomic percent have small magnetostriction constants (λ_s) in a desirable range of -3×10^{-7} to 6×10^{-7}. The magnetostriction constant (λ_s) tends to depend on the B content and is substantially zero when the B content is in a range of 8 to 9 atomic percent.

[0222] Fig. 42 shows optimized annealing temperatures of soft magnetic alloys to achieve minimum coercive forces (Hc) in which the total amount of zirconium and niobium is 6.5 atomic percent. The optimized annealing temperature lies in a range of 550 to 650°C. With reference to Fig. 36, a low coercive force (Hc) is achieved at a low annealing temperature of 550°C.

[0223] Fig. 43 shows optimized annealing temperatures of soft magnetic alloys to achieve maximum permeabilities (μ') in which the total amount of zirconium and niobium is 6.5 atomic percent. A high permeability (μ') is achieved at a low annealing temperature of 550°C.

[0224] The graphs in Figs. 42 and 43 suggest that alloy ribbons having the optimized compositions have superior

soft magnetic characteristics when the ribbons are annealed at 550 to 650°C.

[0225] Fig. 44 shows the crystallization temperature (T_{X1}) of the bcc-Fe phase; Fig. 46 shows the crystallization temperature (T_{X2}) of a compound phase; and Fig. 45 shows the crystallization temperature ($T_{X1'}$) of another compound phase. These crystallization temperatures satisfy the relationship $T_{X1} < T_{X1}, < T_{X2}$. Fig. 47 shows the difference in the crystallization temperatures $\Delta T_X = T_{X2} - T_{X1}$.

[0226] As shown in Fig. 44, T_{X1} lies in a range of 488 to 511°C, depending on the relative content of iron, niobium and zirconium, and does not depend on the boron content.

[0227] As shown in Fig. 47, the difference in the crystallization temperature (ΔT_X) lies in a range of 305 to 325°C. These alloys have large differences in the crystallization temperatures (ΔT_X) which increase as the B content decreases. In particular, the alloys have large differences in the crystallization temperatures (ΔT_X) of more than 320°C in a range of 1.6 to 2.5 atomic percent of zirconium, 8.5 to 9 atomic percent of boron, and 90.5 atomic percent in total of iron and niobium, and only the bcc-Fe phase can be precipitated during annealing while precipitation of the compound phase which deteriorates soft magnetic characteristics of the alloys can be suppressed.

[0228] The circle without a numeral in Fig. 45 indicates an alloy not having a crystallization temperature ($T_{X1'}$) of another compound phase. Alloys having no crystallization temperature ($T_{X1'}$) generally have satisfactory magnetic characteristics.

[0229] The graphs in Figs. 36 to 47 demonstrate that alloys (Zr + Nb = 6.5 atomic percent) having satisfactory soft magnetic characteristics contain 1.5 to 2.5 atomic percent of zirconium, no less than 6.0 atomic percent, preferably not less than 6.5 atomic percent, and more preferably 8.5 to 9 atomic percent of boron, and 89 to 90.5 atomic percent and preferably 89.5 atomic percent in total of iron and niobium (not more than 87.5 atomic percent, preferably not more than 97.0 atomic percent, and more preferably 84.5 to 85 atomic percent of iron).

[0230] As shown in Figs. 36 to 47, many ribbons, represented by black circles, substantially composed of an amorphous single phase in a quenched state are distributed through the above composition range, whereas ribbons, represented by white circles, having amorphous phases and crystalline phases lie outside the above composition range. Alloys composed of amorphous single phases have superior soft magnetic characteristics compared to the alloys composed of amorphous phases and crystalline phases.

[0231] When a ribbon composed of an amorphous phase in a quenched state is annealed, the ribbon has satisfactory magnetic characteristics.

[0232] In particular, the alloys represented by $Fe_{85}Zr_{1.6}Nb_{4.4}B_9$, $Fe_{85}Zr_2Nb_{4.5}B_{8.5}$, $Fe_{86.75}Zr_3Nb_{3.5}B_{6.75}$, and $Fe_{86.75}Zr_{3.3}Nb_{3.2}B_{6.75}$ have superior soft magnetic characteristics.

(Soft Magnetic Alloy of Zr + Nb = 7 atomic percent)

[0233] With reference to Fig. 48, soft magnetic alloys in which the total amount of zirconium and niobium is 7 atomic percent have coercive forces (Hc) of 50 to 2,500 mOe. The alloys having coercive forces (Hc) less than 200 mOe have compositions of not more than 87.5 atomic percent in total of iron and niobium. The alloys having coercive forces (Hc) less than 100 mOe have compositions of not more than 10 atomic percent of boron, and 88.5 to 92 atomic percent in total of iron and niobium.

[0234] With reference to Fig. 49, soft magnetic alloys in which the total amount of zirconium and niobium is 7 atomic percent have permeabilities (μ') of 600 to 44,800. The alloys having permeabilities (μ') of 10,000 or more have compositions of not less than 10 atomic percent of boron and not less than 88.5 atomic percent in total of iron and niobium. The alloys having permeabilities (μ') of 20,000 or more have compositions of not more than 4 atomic percent and preferably not more than 3.5 atomic percent of zirconium, 6 to 9 atomic percent of boron, and not less than 89.5 atomic percent and preferably 90 to 92 atomic percent in total of iron and niobium (84 to 87 atomic percent of iron).

[0235] The graphs in Figs. 48 and 49 demonstrate that when the alloy satisfies Zr + Nb = 7 atomic percent and contains not more than 4 atomic percent and preferably not more than 3.5 atomic percent of zirconium, 6 to 9 atomic percent of boron, and not less than 89.5 atomic percent and preferably 90 to 92 atomic percent in total of iron and niobium (84 to 87 atomic percent of iron), the alloy ribbon has superior soft magnetic characteristics, that is, a high permeability (μ') of at least 20,000 and a low coercive force (Hc) of 100 mOe or less.

[0236] With reference to Fig. 50, soft magnetic alloys in which the total amount of zirconium and niobium is 7 atomic percent have saturation magnetic flux densities (B_{10}) of 1.42 to 1.68 T. The saturation magnetic flux density (B_{10}) depends on the Zr and B contents. The alloys have saturation magnetic flux densities (B_{10}) higher than 1.5 T when the boron content is not more than 9 atomic percent or higher than 1.55 T when the boron content is not more than 8.5 atomic percent and preferably not more than 8 atomic percent.

[0237] With reference to Fig. 51, soft magnetic alloys in which the total amount of zirconium and niobium is 7 atomic percent have remanent magnetizations (Br) of 0.79 to 1.44 T. The remanent magnetization (Br) depends on the boron and iron contents. When the alloy contains 7 to 9 atomic percent and preferably 8 atomic percent of boron and 88.5 atomic percent in total of iron and niobium, the alloy shows a remanent magnetization (Br) of at least 1.2 T.

[0238] With reference to Fig. 52, average crystal grain sizes of bcc-Fe phases in soft magnetic alloys in which the total amount of zirconium and niobium is 7 atomic percent lie in a range of 9.1 to 16.7 nm. The average crystal grain size substantially depends on the relative contents of Zr and Nb. When the Zr content is 5 atomic percent or less, the average crystal grain size is 14 nm or less; when the Zr content is 3 atomic percent or less, the average crystal grain size is 12 nm or less; and when the Zr content is 1 atomic percent or less, the average crystal grain size is 11 nm or less. These ribbons have fine crystalline textures.

[0239] With reference to Fig. 53, soft magnetic alloys in which the total amount of zirconium and niobium is 7 atomic percent have magnetostriction constants (λ_s) in a desirable range of -10×10^{-7} to 19×10^{-7}. The magnetostriction constant (λ_s) tends to depend on the boron content and is substantially zero when the boron content is 7.5 to 8.5 atomic percent.

[0240] Fig. 54 shows optimized annealing temperatures of soft magnetic alloys to achieve minimum coercive forces (Hc) in which the total amount of zirconium and niobium is 7 atomic percent. The alloy ribbons having minimum coercive forces (Hc) at a temperature of 650°C or less contain not more than 5 atomic percent of zirconium, not less than 5.5 atomic percent and preferably 6 to 11 atomic percent of boron, and not less than 87 atomic percent in total of iron and niobium.

[0241] Fig. 55 shows optimized annealing temperatures of soft magnetic alloys to achieve maximum permeabilities (μ') in which the total amount of zirconium and niobium is 7 atomic percent. The alloy ribbons having maximum permeabilities (μ') at a temperature of 650°C or less contain not more than 5 atomic percent of zirconium and not more than 92.5 atomic percent in total of iron and niobium. The alloy ribbons having maximum permeabilities (μ') at a temperature of 600°C or less contain not less than 2.5 atomic percent and preferably 3 to 3.5 atomic percent of zirconium, not less than 5.5 atomic percent and preferably 6 to 8 atomic percent of boron, and 89 to 91 atomic percent in total of iron and niobium (not more than 87.5 atomic percent and preferably 85 to 87 atomic percent of iron).

[0242] Fig. 56 shows the crystallization temperature (T_{X1}) of the bcc-Fe phase; Fig. 57 shows the crystallization temperature (T_{X2}) of a compound phase; and Fig. 58 shows the crystallization temperature ($T_{X1'}$) of another compound phase. These crystallization temperatures satisfy the relationship $T_{X1} < T_{X1'} < T_{X2}$. Fig. 59 shows the difference in the crystallization temperatures $\Delta T_X = T_{X2} - T_{X1}$.

[0243] As shown in Fig. 56, T_{X1} lies in a range of 491 to 533°C, depend on the relative contents of niobium and zirconium, and does not substantially depend on the boron content.

[0244] As shown in Fig. 59, the difference in the crystallization temperature (ΔT_X) lies in a range of 181 to 316°C. These alloys have large differences in the crystallization temperatures (ΔT_X) which increase as the zirconium content decreases. In particular, the alloys have large differences in the crystallization temperatures (ΔT_X) of more than 200°C in a range of not more than 5 atomic percent of zirconium and not less than 87 atomic percent in total of iron and niobium. The alloys have larger differences in the crystallization temperatures (ΔT_X) of more than 300°C in a range of not more than 3 atomic percent of zirconium, not less than 6.5 atomic percent and preferably 7 to 8 atomic percent of boron, and not less than 89 atomic percent in total of iron and niobium (not less than 85 atomic percent of iron). Only the bcc-Fe phase can be precipitated during such annealing while precipitation of the compound phase which deteriorates soft magnetic characteristics of the alloys can be suppressed.

[0245] The circle without a numeral in Fig. 58 indicates an alloy not having a crystallization temperature ($T_{X1'}$) of another compound phase. Alloys having no crystallization temperature ($T_{X1'}$) generally have satisfactory magnetic characteristics.

[0246] The graphs in Figs. 48 to 59 demonstrate that alloys (Zr + Nb = 7 atomic percent) having satisfactory soft magnetic characteristics contain not more than 4 atomic percent and preferably not more than 3 atomic percent of zirconium; 6 to 9 atomic percent and preferably 7 to 8 atomic percent of boron; and 89 to 91 atomic percent in total of iron and niobium.

[0247] In particular, the alloys represented by $Fe_{85}Zr_1Nb_6B_8$, $Fe_{85}Zr_{1.2}Nb_{5.8}B_8$, $Fe_{85}Zr_2Nb_5B_8$, and $Fe_{86}Zr_{2.4}Nb_{4.6}B_7$ have superior soft magnetic characteristics.

[0248] Fig. 60 is a graph showing the relationship between the coercive force (Hc) and the relative contents of the Zr and Nb of soft magnetic alloys ($Fe_{85.75}Zr_xNb_{5.75-x}B_{8.5}$) containing 5.75 atomic percent in total of zirconium and niobium, and 8.5 atomic percent of boron, soft magnetic alloys ($Fe_aZr_xNb_{6-x}B_z$, wherein "a" is 85 to 86 and "z" is 8 to 9) containing 6 atomic percent in total of zirconium and niobium, and 8 to 9 atomic percent of boron, soft magnetic alloys ($Fe_{85.5}Zr_xNb_{6.25-x}B_{8.25}$) containing 6.25 atomic percent in total of zirconium and niobium, and 8.25 atomic percent of boron, soft magnetic alloys ($Fe_{85}Zr_xNb_{6.5-x}B_{8.5}$) containing 6.5 atomic percent in total of zirconium and niobium, and 8.5 atomic percent of boron, and soft magnetic alloys ($Fe_aZr_xNb_{7-x}B_z$, wherein "a" is 84 to 85 and "z" is 8 to 9) containing 7 atomic percent in total of zirconium and niobium, and 8 to 9 atomic percent of boron.

[0249] The graph in Fig. 60 shows that the alloys having a Zr/(Zr+Nb) ratio of 0 to 0.4 has coercive force (Hc) of not more than 0.1 Oe, whereas the alloys having a Zr/(Zr+Nb) ratio of more than 0.5 shows deterioration of soft magnetic characteristics due to increased coercive force (Hc). Alloys containing 6 atomic percent in total of zirconium and niobium and of $0.1 < Zr/(Zr+Nb) < 0.5$ have lower coercive forces (Hc) than that in the case of Zr/(Zr+Nb) = 0. Thus, combined

use of zirconium and niobium contributes to improvements in soft magnetic characteristics. When the Zr/(Zr+Nb) ratio exceeds 0.5, the coercive force (Hc) undesirably decreases.

[0250] Fig. 61 is a graph showing the relationship between the difference in the crystallization temperature ($\Delta T_X = T_{X2} - T_{X1}$ or $= T_{X1'} - T_{X1}$) and the relative contents of the Zr and Nb in these alloys.

[0251] Fig. 61 shows that alloys have large difference in the crystallization temperatures (ΔT_X) of at least 200°C in the case of $0 \leq Zr/(Zr+Nb) \leq 0.7$ and particularly at least 300°C in the case of $0 < Zr/(Zr+Nb) < 0.4$. The difference (ΔT_X), however, significantly decreases when the Zr/(Zr+Nb) ratio is higher than 0.7 and particularly 0.8.

[0252] Accordingly, the difference (ΔT_X) decreases and compound phases other than the bcc-Fe phase are easily precipitated during annealing when the Zr/(Zr+Nb) ratio increases, and thus the coercive force (Hc) increases.

EXAMPLE 3 [Fracture Strain (λ_f)]

[0253] Three quenched ribbons with a thickness of approximately 20 μm having compositions of $Fe_{85.5}Zr_2Nb_4B_{8.5}$, $Fe_{90}Zr_7B_3$, and $Fe_4Nb_7B_9$ were produced as in EXAMPLE 1. The ribbons were heated to a temperature of 510 to 670°C at a heating rate of 180°C/min and annealed at that temperature for 5 minutes to prepare soft magnetic alloy ribbons. The fracture strain (λ_f) of each annealed ribbon was measured from a bending diameter of the ribbon at which the ribbon broke. The results are shown in Fig. 62.

[0254] Fig. 62 shows that the ribbon of the present invention containing Zr and Nb and represented by $Fe_{85.5}Zr_2Nb_4B_{8.5}$ has a fracture strain (λ_f) of higher than 10×10^{-3}, that is, 12.71×10^{-3} when the alloy is annealed at 510°C, or 11.98×10^{-3} when the alloy is annealed at 520°C. Thus, the ribbon has excellent formability.

[0255] In contrast, the ribbon represented by $Fe_{90}Zr_7B_3$ has a fracture strain (λ_f) of 8.35×10^{-3} when the ribbon is annealed at 620°C, and the ribbon represented by $Fe_{84}Nb_7B_9$ has a fracture strain (λ_f) of 9.72×10^{-3}. Thus, the fracture strains (λ_f) of these ribbons are lower than 10×10^{-3}.

EXAMPLE 4 [Iron Loss]

[0256] Three quenched ribbons having compositions of $Fe_{85}Zr_{1.75}Nb_{4.25}B_9$, $Fe_{85.5}Zr_2Nb_4B_{8.5}$, $Fe_{85\text{-}7.5}Zr_{2.25}Nb_{3.75}B_{8.25}$, and $Fe_{78}Si_9B_{13}$ (commercially available amorphous alloy) were produced as in EXAMPLE 1. The temperature of the melt was 1,260 to 1,280°C for the $Fe_{85}Zr_{1.75}Nb_{4.25}B_9$ alloy, or 1,300°C for the $Fe_{85.75}Zr_{2.25}Nb_{3.75}B_{8.25}$ alloy. Each ribbon was wound to form rings, each having an outer diameter of 10 mm and an inner diameter of 6 mm. The rings were stacked to form a core. The core was heated to 510 to 525°C at a heating rate of 180°C/min and annealed at that temperature for 5 minutes. The iron loss of the annealed core was measured.

[0257] Fig. 63 shows the iron loss of the core annealed at 510 or 520°C when a magnetic flux with a frequency of 50 Hz is applied at room temperature. The cores having the compositions represented by $Fe_{85}Zr_{1.75}Nb_{4.25}B_9$, $Fe_{85.5}Zr_2Nb_4B_{8.5}$ and $Fe_{85.75}Zr_{2.25}Nb_{3.75}B_{8.25}$ have lower iron losses than the iron loss of the $Fe_{78}Si_9B_{13}$ core. The iron losses of the cores in accordance with the present invention are not more than 0.1 W/kg when the magnetic flux density (Bm) is 1.4 T.

[0258] Fig. 64 shows the iron losses of the $Fe_{85}Zr_{1.75}Nb_{4.25}B_9$ and $Fe_{78}Si_9B_{13}$ cores which are heated or aged at 200°C for 500 hours in a nitrogen atmosphere. The iron loss of the $Fe_{78}Si_9B_{13}$ core does not substantially change by the heating treatment, whereas the iron loss of the $Fe_{85}Zr_{1.75}Nb_{4.25}B_9$ core decreases by the heating treatment when the Bm exceeds 1.4 T. Accordingly, the alloy in accordance with the present invention has high thermal stability in higher Bm regions.

[0259] Fig. 65 shows the relationship between the iron loss and the heating time (t) when the $Fe_{85}Zr_{1.75}Nb_{4.25}B_9$, $Fe_{85.75}Zr_{2.25}Nb_{3.75}B_{8.25}$ and $Fe_{78}Si_9B_{13}$ cores heated at 200°C for a heating time of 0 to 500 hours in a nitrogen atmosphere. The iron loss was measured by applying a magnetic flux density (Bm) of 1.4 T with a frequency of 50 Hz at room temperature. The coercive force (Hc) and the permeability (μ') of each core were also measured. These results are shown in Tables 2 and 3.

[0260] Fig. 65 shows that the iron losses of the cores in accordance with the present invention do not substantially change by heating, and thus have high thermal stability.

[0261] Tables 2 and 3 show that the cores in accordance with the present invention show slight decreases in permeability (μ') and slight increases in coercive force (Hc). Thus, deterioration of these cores is significantly reduced. In contrast, the $Fe_{78}Si_9B_{13}$ amorphous alloy has a large iron loss and a significant change in iron loss with the heating time.

[0262] Fig. 66 shows the relationship between the change rate of the iron loss, on the basis of the iron loss before heating in Fig. 65, and the magnetic flux density (Bm) of each core which is heated for 500 hours. Table 4 shows the results of the iron loss (Pcm), the saturation magnetic flux densities (B_{10}), the remanent magnetization (Br), the coercive force (Hc), and the permeability (μ') of the core before heating and after heating.

[0263] In the $Fe_{78}Si_9B_{13}$ core (Comparative Example), the change rate of the iron loss tends to slightly decrease towards smaller iron loss as the magnetic flux density (Bm) increases. In contrast, in the $Fe_{85}Zr_{1.75}Nb_{4.25}B_9$ and

$Fe_{85.5}Zr_2Nb_4B_{8.5}$ cores, the change rate of the iron loss significantly decreases for high magnetic flux densities (Bm).

[0264] As shown in Table 4, the permeability (μ') of each core in accordance with the present invention slightly decreases and the coercive force (Hc) tends to increase by heating. In contrast, the permeability (μ') of the $Fe_{78}Si_9B_{13}$ core is small before annealing, and decreases by 26% by heating. Thus, the $Fe_{78}Si_9B_{13}$ core has inferior thermal stability of the permeability (μ') to the Fe-based soft magnetic alloy in accordance with the present invention.

[0265] Fig. 67 is a graph showing changes in iron losses over time of the cores having the compositions $Fe_{85.5}Zr_2Nb_4B_{8.5}$ and $Fe_{78}Si_9B_{13}$, which are heated to a higher temperature, that is, 320°C for 0 to 100 hours. The iron loss was measured at room temperature while a magnetic flux of 1.4 T was applied at a frequency of 50 Hz.

[0266] As shown Fig. 60, in the core composed of an $Fe_{78}Si_9B_{13}$ amorphous alloy, the iron loss increases with an increased heating time. In contrast, in the $Fe_{85.5}Zr_2Nb_4B_{8.5}$ core, the iron loss does not substantially change with an increased heating time.

[0267] Fig. 68 shows the relationship between the change rate of the iron loss, on the basis of the iron loss before heating in Fig. 66, and the heating time. The change rate of the iron loss of the $Fe_{78}Si_9B_{13}$ core more significantly increases with the heating time than does that of the $Fe_{85.5}Zr_2Nb_4B_{8.5}$ core.

[0268] As described, in the cores having the compositions $Fe_{85}Zr_{1.75}Nb_{4.25}B_9$, $Fe_{85.5}Zr_2Nb_4B_{8.5}$ and $Fe_{85.75}Zr_{2.25}Nb_{3.75}B_{8.25}$ in accordance with the present invention, the increase in the iron loss is suppressed when the cores are heated at 200 to 320°C. Thus, these cores have small change rates of iron losses and superior thermal stability.

EXAMPLE 5 [Addition of Zinc]

[0269] The following soft magnetic alloy ribbons were prepared by a single-roller quenching process using the apparatus shown in Fig. 1. Each alloy melt having predetermined compositions was jetted onto a rotating copper roller through a nozzle by pressure from argon gas to form a quenched ribbon. The resulting ribbon had a width of approximately 15 mm and a thickness of approximately 20 μm. The quenched ribbon was substantially composed of an amorphous phase. The quenched ribbon was annealed by heating to a temperature which is higher than the crystallization temperature and then cooling to form a Fe-based soft magnetic alloy ribbon in accordance with the present invention. Each alloy for comparison was also formed in the same manner.

[0270] Rings having an outer diameter of 10 mm and an inner diameter of 6 mm were formed from each thin ribbon and were stacked. A coil was wound around the stacked rings and the permeability (μ') was measured at 5 mOe and 1 KHz using an impedance analyzer. The coercive force (Hc) and the magnetic flux densities (B_{10}) were measured at 10 Oe using a direct-current B-H loop tracer, wherein the magnetic flux densities (B_{10}) were substantially equal to the saturation magnetic flux density (Bs).

[0271] Fig. 69 is a graph of X-ray diffraction patterns of an alloy of the present invention represented by $(Fe_{0.8575}Zr_{0.02}Nb_{0.04}B_{0.0825})_{99.88}Zn_{0.12}$ before annealing and after annealing. As shown in Fig. 69, a broad halo pattern characteristic to an amorphous phase is observed in the quenched alloy ribbon, whereas a diffraction pattern assigned to the bcc-Fe is observed in the annealed ribbon. Thus, the results in Fig. 69 demonstrate that the texture of the alloy changes from the amorphous phase to the bcc crystalline phase during annealing.

[0272] Fig. 70 is a triangular diagram of coercive forces (Hc) of a $Fe_cZr_dNb_eB_f$ alloy ribbon, which has a similar composition to the composition of the present invention, and a $(Fe_cZr_dNb_eB_f)_{100-z}Zn_z$ containing 0.034 to 0.142 atomic percent of zinc.

[0273] In Fig. 70, the alloy No. (1) is represented by $(Fe_{0.855}Zr_{0.02}Nb_{0.04}B_{0.085})_{99.944}Zn_{0.056}$; the alloy No. (2) is represented by $(Fe_{0.855}Zr_{0.02}Nb_{0.04}B_{0.085})_{99.892}Zn_{0.108}$; the alloy No. (3) is represented by $(Fe_{0.855}Zr_{0.02}Nb_{0.04}B_{0.085})_{99.859}Zn_{0.141}$; the alloy No. (4) is represented by $(Fe_{0.8575}Zr_{0.02}Nb_{0.04}B_{0.0825})_{99.96}Zn_{0.04}$; the alloy No. (5) is represented by $(Fe_{0.8575}Zr_{0.02}Nb_{0.04}B_{0.0825})_{99.875}Zn_{0.125}$; the alloy No. (6) is represented by $(Fe_{0.8575}Zr_{0.02}Nb_{0.04}B_{0.0825})_{99.867}Zn_{0.133}$; the alloy No. (7) is represented by $(Fe_{0.86}Zr_{0.02}Nb_{0.04}B_{0.08})_{99.966}Zn_{0.034}$; the alloy No. (8) is represented by $(Fe_{0.86}Zr_{0.02}Nb_{0.04}B_{0.08})_{99.883}Zn_{0.117}$; and the alloy No. (9) is represented by $(Fe_{0.86}Zr_{0.02}Nb_{0.04}B_{0.08})_{99.858}Zn_{0.142}$.

[0274] In the FeZrNbB alloy containing 6 atomic percent in total of zirconium and niobium, a coercive force of less than 50 mOe is produced when the boron content is in a range of 6 to 9.5 atomic percent, and a coercive force of less than 40 mOe is produced when the boron content is in a range of 8 to 9.5 atomic percent, the zirconium content is 1.5 to 2.5 atomic percent and the total content of iron and niobium is 80 to 90 atomic percent. The alloys (1) to (9) containing zinc show coercive force of less than 100 mOe. When zinc is added to an alloy having a coercive force of approximately 40 mOe or 50 mOe, the coercive force tends to decrease.

[0275] In Fig. 70, the quenched alloy ribbons marked with ○ or Δ have (200) peaks assigned to bcc-Fe crystal grains which are partially precipitated during the quenching process. On the other hand, the quenched alloy ribbons marked with ● have no (200) peak and are thus completely composed of an amorphous phase. The completely amorphous alloy ribbons have lower coercive forces.

[0276] Fig. 71 is a triangular diagram of permeability (μ': real number section of permeability) at 1 KHz of these alloys. The alloys having the composition in accordance with the present invention containing 0.034 to 0.142 atomic percent have permeabilities of more than 30,000 and the alloys containing 0.04 to 0.142 have permeabilities of more than 40,000.

[0277] Fig. 72 is a triangular diagram of saturation magnetic flux densities (B_{10}) of these alloys, which are determined from magnetization curves obtained by applying a magnetic field of 10 Oe. Fig. 73 is a triangular diagram of remanent magnetization (Br) of these alloys.

[0278] A composition having a total content of zirconium and niobium in accordance with the present invention has a high saturation magnetic flux density of more than 1.5 T. The alloys (1) to (9) containing 0.034 to 0.142 atomic percent of zinc also show saturation magnetic flux densities of more than 1.6 T. Thus, the saturation magnetic flux density does not substantially change when zinc is added within a range of the present invention and is maintained at high levels.

[0279] Fig. 74 is a triangular diagram of the first crystallization temperature (T_{X1}) of the bcc-Fe in the alloys; Fig. 75 is a triangular diagram of the intermediate crystallization temperature ($T_{X1'}$) of the compound phase in the alloys; Fig. 76 is a triangular diagram of the second crystallization temperature (T_{X2}) of the compound phase in the alloys; and Fig. 77 is a triangular diagram of the difference ($\Delta T_X = T_{X2} - T_{X1}$) in the crystallization temperature in the alloys.

[0280] The first crystallization temperature, the intermediate crystallization temperature, and the second crystallization temperature will now be described.

[0281] When the amorphous alloy in accordance with the present invention produced by quenching is heated, a first exothermic reaction due to crystallization of the bcc-Fe phase will occur, and then another exothermic reaction (third exothermic reaction) due to crystallization of the compound phase (Fe_3B or Fe_2B) will occur. Another exothermic reaction (second exothermic reaction) will occur between these crystallization reactions in some compositions. The first exothermic reaction releases the largest amount of heat of crystallization and corresponds to the first crystallization temperature. The second exothermic reaction releases a small amount of heat of crystallization of the compound phase and corresponds to the intermediate crystallization temperature. The third exothermic reaction releases a small amount of heat of crystallization of the other compound phase and corresponds to the second crystallization temperature. The second exothermic reaction does not always occur. Alloys represented by the symbol "-" in Fig. 75 do not have the second exothermic peaks or the intermediate crystallization temperatures $T_{X1'}$. Alloys not having the second exothermic peak have superior magnetic characteristics. The crystallization temperature does not substantially change when zinc is added to these alloys.

[0282] It is preferable that the difference ΔT_X in the crystallization temperature between T_{X1} and T_{X2} be at least 200°C. The ΔT_X shown in Fig. 77 is more than 200°C. When the ΔT_X is at least 200°C, the alloy can be annealed under optimized conditions at a temperature between the crystallization temperature of the bcc-Fe phase and the crystallization temperature of the compound phase so that only the bcc-Fe phase is precipitated. The resulting alloy has superior soft magnetic characteristics. Accordingly, the annealing temperature of the alloy is preferably between the first crystallization temperature (T_{X1}) and the second crystallization temperature (T_{X2}).

[0283] Fig. 78 is a triangular diagram of the crystal grain size in the alloys having compositions, which are similar to the composition in accordance with the present invention, and not containing zinc. When zinc in an amount in accordance with the present invention is added to these compositions, the crystal grain size decreases slightly, as will be described later. The alloy in accordance with the present invention has crystal grains having grain sizes of 12 nm or less and preferably 11 nm or less.

[0284] Fig. 79 is a triangular diagram of the magnetostriction (λ_s) in the alloys having compositions which are similar to the composition in accordance with the present invention and which do not contain zinc. When zinc in an amount in accordance with the present invention is added to these compositions, the magnetostriction does not substantially change. Thus, an alloy in accordance with the present invention, which is prepared by adding zinc to an alloy shown in Fig. 79, will have a magnetostriction of near zero.

[0285] Fig. 80 is a graph of the dependence of the crystal grain size (D) on the zinc content in zinc-containing alloys in accordance with the present invention. The crystal grain size (D) slightly decreases by the addition of zinc.

[0286] Fig. 81 is a graph of the dependence of the magnetostriction (λs) on the zinc content in zinc-containing alloys in accordance with the present invention. The magnetostriction decreases distinctly but moderately by the addition of zinc.

[0287] Fig. 82 is a graph of iron loss of ribbons prepared by adding 0.12 or 0.13 atomic percent of zinc to a base alloy represented by $Fe_{85.75}Zr_2Nb_4B_{8.25}$ and a ribbon for comparison represented by $Fe_{78}Si_9B_{13}$. The iron loss was measured by an AC magnetization characteristic measuring apparatus. The results in Fig. 82 show that the iron loss of the ribbons in accordance with the present invention is lower than that of the ribbon for comparison. The iron loss of the ribbons in accordance with the present invention is lower than 0.1 W/kg at 1.5 T, and is one-tenth that of silicon steel ribbons or approximately one-fifth to one-sixth that of Fe-based amorphous alloy ribbons.

[0288] Fig. 83 is a graph of a change in iron loss over time of an alloy ribbon represented by $(Fe_{0.8575}Zr_{0.02}Nb_{0.04}B_{0.0825})_{99.88}Zn_{0.12}$ in accordance with the present invention and alloy ribbons for comparison rep-

resented by $Fe_{78}Si_9B_{13}$, $Fe_{85}Zr_{1.75}Nb_{4.25}B_9$, $Fe_{85.5}Zr_2Nb_4B_{8.5}$, and $Fe_{85.75}Zr_{2.25}Nb_{3.75}B_{8.25}$, when these alloys are heated to 200°C for a predetermined time and cooled to room temperature.

[0289] Fig. 83 shows that the alloy ribbon in accordance with the present invention has an iron loss which is significantly smaller than that of the $Fe_{78}Si_9B_{13}$ alloy ribbon for comparison and which does not substantially change over time. Furthermore, the iron loss and the change rate of the iron loss of the alloy ribbon in accordance with the present invention are lower than those of the ribbons which have similar compositions to that of the ribbon in accordance with the present invention and does not contain zinc. The ribbon in accordance with the present invention has an iron loss of less than 0.1 W/kg even after the ribbon is heated for 300 hours.

[0290] Tables 5 and 6 show the dependence of the iron loss, the coercive force and the permeability on the elapsed time of each alloy in Fig. 83. The alloy containing zinc in accordance with the present invention has a low iron loss of 0.081 to 0.90, a small change rate, a small coercive force of 0.038, and a high permeability of 60,200 to 61,200. The alloy containing a specific amount of zirconium and niobium has a low iron loss, a low coercive force, and a high permeability. The addition of zinc to this alloy, however, contributes to a lower iron loss and a higher permeability.

[0291] Fig. 84 is a graph of the iron loss at room temperature of the alloys which are shown in Fig. 83 and heated to 320°C for a predetermined time, and Fig. 85 is a graph of a change rate of the iron loss over time of the alloys shown in Fig. 84. Figs. 84 and 85 show that the change rates of the iron loss of the alloys in accordance with the present invention are significantly lower than that of the $Fe_{78}Si_9B_{13}$ alloy for comparison, and are still lower than that of the $Fe_{85.75}Zr_{2.25}Nb_{3.75}B_{8.25}$ alloy not containing zinc for comparison. Accordingly, the addition of a specific small amount of zinc to FeNbZrB alloys produces a further decreased iron loss and a decreased change rate of the iron loss.

[0292] Fig. 86 is a graph of the relationship between the fracture strain (λ_f) and the bending diameter (Df: in mm) of various alloy ribbons having a thickness of approximately 20 μm. In Fig. 86, the alloy ribbon in accordance with the present invention is represented by $(Fe_{0.855}Zr_{0.02}Nb_{0.04}B_{0.085})_{99.86}Zn_{0.14}$, and the alloy ribbons for comparison are represented by $Fe_{78}Si_9B_{13}$, $Fe_{84}Zr_{3.5}Nb_{3.5}B_8Cu_1$, $Fe_{90}Zr_7B_3$, $Fe_{84}Nb_7B_9$, $Fe_{73.5}Zr_{13.5}B_9Nb_3Cu_1$, and $Fe_{86}Zr_2Nb_4B_8$. The fracture strain means a strain when the sample is fractured, and the bending diameter means a minimum diameter in which the sample is bendable without fracture.

[0293] The fracture strain was determined as follows. A ribbon was fasten with two rods, and the rods were moved close to each other so as to bend the ribbon in a "U" shape. The fracture strain (λ_f) was defined as the ratio t/(L-t) wherein L is the distance between the rods when the ribbon is fractured by bending and t is the thickness of the ribbon.

[0294] The ribbon in accordance with the present invention has a small bending diameter when it is annealed at a preferable temperature of 510 to 520°C, and is resistive to bending fracture. The ribbons shown in Fig. 86 were annealed at different temperatures due to different crystallization temperatures, but were heated to the annealing temperature at the same heating rate of 180°C/min, held at the annealing temperature for 5 minutes, and were then cooled.

[0295] Since the ribbon in accordance with the present invention has superior bending characteristics, it can be wound to form a magnetic core having a small diameter for a transformer without the formation of cracks.

[0296] Fig. 87 is a graph of the dependence of the Curie temperature on the zinc content in an amorphous phase of an annealed alloy, and Fig. 88 is a graph of the dependence of the Curie temperature on the zinc content in an as-quenched alloy (not annealed), wherein the Curie temperature is determined by a change in magnetization with temperature.

[0297] The Curie temperature of the as-quenched alloy does not change with the zinc content, probably due to a low zinc content. On the other hand, the Curie temperature of the alloy annealed at 510°C increased with an increased zinc content. It is believed that the bcc-Fe phase is deposited by annealing and the texture of the residual amorphous phase changes.

[0298] TEM observation and component analysis confirm concentration of zinc into the residual amorphous phase. It is believed that the concentration of zinc results in an increased Curie temperature of the amorphous phase. The present inventors presume that increasing the Curie temperature of the residual amorphous phase causes enhanced exchange coupling between the bcc-Fe phases which results in increased permeability and decreased coercive force.

[0299] Fig. 89 is a graph of the dependence of the coercive force on the zinc content in soft magnetic alloys represented by $(Fe_{0.86}Nb_{0.07}B_{0.07})_{100-z}Zn_z$. The coercive force distinctly decreases with an increased zinc content, reaches a minimum value at a zinc content of 0.04 to 0.07 atomic percent, and gradually increases with an increased zinc content. An alloy containing 0.12 atomic percent of zinc has a lower coercive force than that of an alloy not containing zinc.

[0300] Fig. 90 is a graph of the dependence of the permeability on the zinc content in the soft magnetic alloys having the same compositions. The permeability increases by addition of zinc, reaches a maximum value at a zinc content of 0.07 atomic percent, and then gradually decreases.

[0301] Fig. 91 is a graph of the dependence of the coercive force on the zinc content in soft magnetic alloys represented by $(Fe_{0.86}Zr_{0.02}Nb_{0.04}B_{0.08})_{100-z}Zn_z$. The coercive force has a minimum value by addition of zinc. The coercive force of the alloy containing 0.133 atomic percent of zinc is approximately 65% of that of the corresponding alloy not containing zinc. Thus, addition of zinc contributes to decreased coercive force.

[0302] Fig. 92 is a graph of the dependence of the permeability on the zinc content in the soft magnetic alloys having the same compositions. The permeability increases by addition of zinc, and reaches a maximum value at a zinc content of 0.133 atomic percent. The alloy containing 0.025 atomic percent of zinc shows a high permiability of 29,821, and the alloy containing 0.19 atomic percent shows a high permiability of 31,769 or more. Thus, a high permeability of more than 30,000 is achieved by a zinc content of 0.025 to 0.2 atomic percent.

[0303] The alloys shown in Figs. 91 and 92 have superior coercive force and permeability compared to the alloys shown in Figs. 89 and 90, because the zirconium and niobium contents are adjusted so that superior soft magnetic characteristics are obtained.

[0304] Table 7 shows the permeability (μ') at 1 kHz, the coercive force (Hc), and the saturation magnetic flux densities (B_{10}) of a FeNbB-based alloy, a FeZrB-based alloy, a FeHfB-based alloy, and FeZrNbB-based alloys which contain zinc in accordance with the present invention or do not contain zinc for comparison.

[0305] In Table 7, the composition of the alloy No. 10 corresponds to an alloy in which 0.07 atomic percent of zinc is added to the FeNbB-based alloy No. 16. The composition of the alloy No. 11 corresponds to an alloy in which 0.1 atomic percent of zinc is added to the FeZrB-based alloy No. 17. The composition of the alloy No. 12 corresponds to an alloy in which 0.1 atomic percent of zinc is added to the FeHfB-based alloy No. 18. The composition of the alloy No. 13 corresponds to an alloy in which 0.13 atomic percent of zinc is added to the FeZrNbB-based alloy No. 19. The composition of the alloy No. 14 corresponds to an alloy in which 0.13 atomic percent of zinc is added to the FeZrNbB-based alloy No. 20. The composition of the alloy No. 15 corresponds to an alloy in which 0.14 atomic percent of zinc is added to the FeZrNbB-based alloy No. 20.

[0306] The results in Table 7 show that addition of zinc to these alloys significantly improves permeability, causes decreased coercive force and saturation magnetic flux densities of approximately 1.6 T.

[0307] When zirconium and niobium are added as elements M, the ranges of these contents and the ratio Zr/(Zr+Nb) are the same as those in the above-mentioned FeZrNb-based alloys. Since the coercive force is significantly high when the total content of zirconium and niobium is 4 atomic percent, as shown in Fig. 93, the lower limit of the total content of zirconium and niobium is assumed to be 5 atomic percent in the FeZrNbB alloys and the FeZrNbBZn alloys.

[0308] When the above-described soft magnetic alloy is used as a magnetic core, the magnetic core has low iron loss and satisfactory workability and can be made compact.

EXAMPLE 6 [First Production Method]

[0309] The following soft magnetic alloy ribbons (corresponding to the above-mentioned first to third soft magnetic alloys) were prepared by a single-roller quenching process using the apparatus shown in Fig. 1. Each alloy melt having predetermined compositions was jetted onto a rotating copper roller through a nozzle by pressure from argon gas to form a quenched ribbon. The temperature of the melt ejected from the nozzle, that is, the ejection temperature, was approximately 1,240 to 1,350°C. When the alloy contained volatile zinc, the amount of zinc added to the melt was approximately 20 times the final target content, that is, 0.025 to 0.2 atomic percent, as described above in detail.

[0310] The resulting ribbon had a width of approximately 15 mm and a thickness of approximately 20 μm. The quenched ribbon was substantially composed of an amorphous phase. The quenched ribbon was annealed by heating to a temperature Ta which is higher than the crystallization temperature T_{X1} to improve soft magnetic characteristics by precipitation of fine bcc-Fe crystal grains. A Fe-based soft magnetic alloy ribbon in accordance with the present invention was thereby formed. Each alloy for comparison was also formed in the same manner. The annealing temperature Ta was in a range of 490 to 670°C, and the heating rate to the annealing temperature was in a range of 10°C/min to 200°C/min. Alloys were also prepared at different holding time after the alloys reached the annealing temperature, for comparison.

[0311] Rings having an outer diameter of 10 mm and an inner diameter of 6 mm were formed from the soft magnetic alloy ribbon and stacked. A coil was wound around the stacked rings and the permeability μ' (real part of complex permeability) of the ribbon was measured using an impedance analyzer at 5 mOe and 1 KHz. The coercive force Hc and the saturation magnetic flux densities B_{10} were measured at 10 Oe using a DC H-H loop tracer.

[0312] The effects of the annealing temperature Ta and the heating rate on the various properties of the Fe-based soft magnetic alloy will now be described.

[0313] Figs. 94 is a graph of the relationship among the permeability μ', the heating rate and the annealing temperature of an annealed alloy represented by $Fe_{85.5}Zr_2Nb_4B_{8.5}$ in which the holding time at the annealing temperature is zero, and Fig. 95 is a graph of the relationship among the coercive force Hc, the heating rate and the annealing temperature of this alloy. Thick lines in these drawings indicate results obtained at an ejection temperature of 1,280°C and thin lines indicate results obtained at an ejection temperature of 1,320°C. Figs. 96 to 103 are similar graphs in which the holding time are different. This alloy corresponds to the above-mentioned first soft magnetic alloy.

[0314] In Fig. 94, the permeability μ' ranges from 200 to 53,800. The preferred permeability region is located near the intersection of the heating rate of 40°C/min and the annealing temperature Ta of approximately 520 to 550°C and

near the intersection of the heating rate of 40°C/min and the annealing temperature Ta of approximately 650°C. In this region, the permeability μ' is in a preferred range of 50,000 to 53,800 regardless of the ejection temperature. The permeability μ' is still high, that is, it is on the order of 40,000, in the vicinity thereof.

[0315] Two-dot lines indicated by "amor." in the drawing suggest that each alloy is substantially composed of an amorphous phase in the left sides (lower annealing temperature sides) of these dot lines, and thus no fine bcc-Fe crystal grain is formed. The permeability μ' of this alloy is significantly low as shown in the drawing. Accordingly, the bcc-Fe phase plays a vital role in the improvement in the permeability in the present invention.

[0316] The coercive force (Hc) shown in Fig. 95 lies in a range of 39 to 2,455 mOe. A particularly satisfactory region for soft magnetic characteristics is near the intersection of the annealing temperature Ta of 550°C and the heating rate of 100°C/min. A coercive force Hc of 39 mOe is observed in this region. In addition, a coercive force Hc of approximately 50 mOe is observed over substantially the entire region, other than the above-mentioned amorphous region in the left side of the drawing. In the amorphous region, the coercive force Hc is undesirably high, that is, it is on the order of hundreds to thousands mOe.

[0317] Figs. 96 to 103 show the permeabilities μ' and the coercive forces (Hc) for different holding times at the annealing temperature Ta. Figs. 96 and 97 are for a holding time of 5 minutes; Figs. 98 and 99 are for a holding time of 10 minutes; Figs. 100 and 101 are for a holding time of 30 minutes; and Figs. 102 and 103 are for a holding time of 60 minutes.

[0318] In Fig. 96, the permeability μ' is approximately 50,000 in a region near the intersection of the heating rate of 30 to 90°C/min and the annealing temperature Ta of approximately 500 to 600°C for the ejection temperature of 1,320°C, and in a slightly narrower region for the ejection temperature of 1,280°C.

[0319] In Fig. 97, the coercive force Hc is approximately 40 mOe in a region near the intersection of the heating rate of 40 to 100°C/min and the annealing temperature Ta of approximately 530°C for the ejection temperature of 1,320°C. The preferred range of the coercive force Hc for the ejection temperature of 1,280°C is slightly narrower than the above range, as in the permeability μ' in Fig. 96.

[0320] In Figs. 96 and 97, no amorphous region is observed. Also, in Figs. 98 to 103, no amorphous region is observed. Thus, it is presumed that sufficient energy facilitating bcc-Fe crystal growth is not supplied from the exterior at such low annealing temperatures in Figs. 95 and 96.

[0321] In Fig. 98, the permeability μ' is approximately 50,000 in a region near the intersection of the heating rate of 20 to 200°C/min and the annealing temperature Ta of approximately 500 to 600°C for the ejection temperature of 1,320°C, and in a slightly narrower region for the ejection temperature of 1,280°C.

[0322] In Fig. 99, the coercive force Hc is approximately 40 mOe in a region near the intersection of the heating rate of 20 to 100°C/min and the annealing temperature Ta of approximately 510 to 540°C for the ejection temperature of 1,320°C. A very similar trend is observed for the ejection temperature of 1,280, although a coercive force Hc of 40 mOe or less is not observed.

[0323] In Fig. 100, the preferred permeability μ' is observed in a region near the intersection of the heating rate of 20 to 200°C/min and the annealing temperature Ta of approximately 510 to 560°C. In Fig. 101, the coercive force Hc is approximately 45 mOe in a region near the intersection of the heating rate of 40 to 200°C/min and the annealing temperature Ta of approximately 510 to 580°C.

[0324] In Fig. 102, the permeability μ' is approximately 50,000 in a region near the intersection of the heating rate of 20 to 40°C/min and the annealing temperature Ta of approximately 500 to 550°C for the ejection temperature of 1,320°C, and in a similar region for the ejection temperature of 1,280°C.

[0325] In Fig. 103, the coercive force Hc is in a range of 40 to 49 mOe in a region near the intersection of the heating rate of 20 to 200°C/min and the annealing temperature Ta of approximately 500 to 600°C for the ejection temperature of 1,320°C. A similar coercive force Hc is observed in a lightly narrower region for the ejection temperature of 1,280°C.

[0326] Figs. 104 and 105 are graphs of the permeability μ' and coercive force Hc, respectively, of the $Fe_{85.5}Zr_2Nb_4B_{8.5}$ annealed alloy at various heating rates, various annealing temperatures, and various holding times of 0 to 60 minutes. The ejection temperature is 1,280°C. In Figs. 106 and 107, data for the holding times of 0, 10 and 60 minutes is extracted from Figs. 104 and 105. In Figs. 108 and 109, data for the holding times of 5 and 30 minutes is extracted from Figs. 104 and 105. Figs. 110 to 115 are graphs for the ejection temperature of 1,320°C, and corresponds to Figs. 104 to 109, respectively.

[0327] According to these drawings, the preferred range of the permeability μ' lies near the intersection of the heating rate of 40 to 100°C/min and the annealing temperature Ta of 500 to 560°C for the ejection temperature of 1,280°C regardless of the holding time, and the permeability μ' is approximately 50,000 in this region. The preferred range for the ejection temperature of 1,320°C is broader than that for 1,280°C. In addition, the permeability μ' is higher than 30,000 over substantially the entire region.

[0328] The preferred range of the coercive force Hc lies near the intersection of the heating rate of 100°C/min and the annealing temperature Ta of 520 to 560°C for the ejection temperature of 1,280°C. The coercive force Hc is approximately 40 mOe in this range. The preferred range for the ejection temperature of 1,320°C is broader than that for

1,280°C, and this trend is more noticeable than that in the permeability. In addition, the coercive force Hc of approximately 50 mOe lies over a relatively wide region.

[0329] Accordingly, it is preferable that the annealing temperature Ta be in a range of approximately 490 to 670°C and more preferably 500 to 560°C, and that the heating rate be in a range of 10 to 200°C/min and more preferably 30 to 100°C/min, in order to achieve a desirable permeability and coercive force regardless of the ejection temperature and the holding time.

[0330] Since the lower limit of the heating rate is 10°C/min and more preferably 30°C/min, the method in accordance with the present invention has the following two advantages. Since the Fe-based soft magnetic alloy can be produced at such a low heating rate, the alloy can be annealed using inexpensive facilities including a furnace. Furthermore, the alloy is gradually heated during the annealing process, and the annealing can be uniformly performed. Thus, in a preferred embodiment, a heating rate may be as low as possible.

[0331] As described above, the $Fe_{85.5}Zr_2Nb_4B_{8.5}$ alloy corresponds to the above-mentioned first soft magnetic alloy. Thus, the contents of these constituents satisfy the relationships specified in the first embodiment. That is, the iron content of 85.5 atomic percent is higher than 80 atomic percent; the total content of zirconium and niobium, 6 atomic percent, is in a range of 5 to 7 atomic percent and more preferably 5.7 to 6.5 atomic percent; the ratio x/(x+y), 2/6, is in a range of 1.5/6 to 2.5/6; and the boron content 8.5 atomic percent is in a range of 5 to 12 atomic percent.

[0332] Figs. 116 and 117 show the dependence of the permeability μ' and the coercive force Hc, respectively, of an alloy represented by $Fe_{85.5}Zr_2Nb_4B_{8.5}$ on the annealing temperature Ta and the heating rate for a holding time of 5 minutes. Thick lines in the drawings indicate the results for the ejection temperature of 1,260°C and thin lines indicate the results for the ejection temperature of 1,300°C.

[0333] Figs. 118 and 119 show the dependence of the permeability μ' and the coercive force Hc, respectively, of an alloy represented by $(Fe_{85.5}Zr_2Nb_4B_{8.5})_{99}Zn_1$. The other conditions are the same as those in Figs. 116 and 117. In addition, Figs. 120 and 121 show the dependence of the permeability μ' and the coercive force Hc, respectively, of an alloy represented by $(Fe_{85.5}Zr_2Nb_4B_{8.5})_{98}Zn_2$; and Figs. 122 and 123 show the dependence of the permeability μ' and the coercive force Hc, respectively, of an alloy represented by $(Fe_{85.5}Zr_2Nb_4B_{8.5})_{97}Zn_3$.

[0334] In these alloys, the subscript for zinc indicates the amount of fed zinc and thus does not indicate the final zinc content in the alloy. As described above, zinc is vaporized during the production of the alloy, and only a fraction of the zinc remains in the alloy. The actual content in the alloy is shown in Table 8.

[0335] Table 8 shows that 0.056 atomic percent of zinc remains when 1 atomic percent of zinc is fed to the $Fe_{85.5}Zr_2Nb_4B_{8.5}$ alloy. Similarly, 0.108 atomic percent of zinc remains in the alloy for 2 atomic percent of fed zinc, and 0.133 to 0.141 atomic percent of zinc remains for 3 atomic percent of fed zinc. The residual zinc contents are included in the specific range of the zinc content in the above-described third Fe-based soft magnetic alloy. The other compositions shown in Fig. 8 will be described below.

[0336] With reference to Fig. 116, the permeability μ' lies in a range of 700 to 39,800. A particularly high permeability μ' of at least 35,000 for the ejection temperature of 1,260°C is achieved in regions defined by the heating rate of 30 to 100°C/min or 200°C/min and the annealing temperature Ta of 510 to 550°C.

[0337] With reference to Fig. 117, the coercive force Hc lies in a range of 46 to 754 mOe. The preferred range of the coercive force Hc lies in regions defined by the heating rate of 50 to 100°C/min or 100°C/min and the annealing temperature Ta of 520°C.

[0338] With reference to Fig. 118, the permeability μ' lies in a range of 800 to 55,700 and is higher than 30,000 in substantially the entire region. The maximum value is higher than that in Fig. 116. The coercive force Hc in Fig. 119 lies in a range of 37 to 670 mOe, and the minimum value is lower than that in Fig. 117. These drawings show that the addition of zinc contributes to improved soft magnetic characteristics and that the permeability μ' and the coercive force Hc are at satisfactory levels over the entire region. The preferable regions in Figs. 118 and 119 are very similar to the preferable regions in Figs. 116 and 117.

[0339] The maximum permeability μ' in Fig. 120 is 57,500 and is slightly higher than that in the former cases. The permeability μ' of at least 40,000 is observed in substantially the entire region in the drawing, and thus the permeability μ' reaches a satisfactory level in this drawing. The coercive force Hc in Fig. 121 lies in a range of 37 to 219 mOe, and the minimum value is slightly lower than the former cases. The results in Fig. 121 are substantially the same as those in Fig. 119 and are generally satisfactory levels.

[0340] The maximum permeability μ' in Fig. 122 is 52,600 and the minimum coercive force Hc in Fig. 123 is 43 mOe. The permeability μ' is slightly lower than that in the former cases and the coercive force Hc is slightly higher than that in the former cases. Thus, the soft magnetic characteristics are slightly decreased in this composition.

[0341] The preferable regions in Figs. 120 to 123 are substantially the same as the regions shown in Figs. 118 and 119 and in Figs. 116 and 117.

[0342] Figs. 124 and 125 are graphs of summarized relationships between the permeability μ' and the coercive force Hc, respectively, and the annealing temperature Ta and heating rate for an ejection temperature of 1,260°C when zinc is fed in an amount of 0, 1, 2 or 3 atomic percent, which are shown in Figs. 116 to 123. Figs. 126 and 127 are similar

graphs for an ejection temperature of 1,300°C.

[0343] These graphs clearly show the effect of the addition of zinc. For example, in Fig. 124, the alloy containing 1 atomic percent of zinc has a permeability μ' region of 45,000 whereas the zinc-free alloy has a permeability μ' region of 38,000. In Fig. 125, the alloy containing 1 atomic percent of zinc has a minimum coercive force of 38 mOe whereas the zinc-free alloy has a minimum coercive force of 40 mOe. The same trends are observed in Figs. 126 and 127.

[0344] As described above, the addition of zinc contributes to improved soft magnetic characteristics. The heating rate and the annealing temperature Ta suitable for the preferred magnetic characteristics are not significantly changed. Thus, a satisfactory alloy will be produced at an annealing temperature Ta of 510 to 550°C, and a heating rate of 30 to 100°C/min or 200°C/min.

EXAMPLE 7 [Second Production Method]

[0345] An alloy ribbon having a width of 15 mm and a thickness of approximately 20 μm was prepared as in EXAMPLE 6. The quenched ribbon primarily composed of an amorphous phase was subjected to heat treatment including heating to a temperature which is higher than the crystallization temperature and then cooling to precipitate bcc-Fe fine crystal grains.

[0346] Rings having an outer diameter of 10 mm and an inner diameter of 6 mm were produced from the resulting soft magnetic alloy ribbon and were stacked. A coil was wound around the stacked rings. The permeability μ' was measured at 5 mOe and 1 kHz using an impedance analyzer. The coercive force (Hc) and the saturation magnetic flux densities (B_{10}) were measured at 10 Oe using a DC loop tracer.

[0347] Tables 9 and 10 show the peak intensity of the (200) plane of the bcc-Fe phase by X-ray diffractometry, the coercive force Hc (Oe), the saturation magnetic flux densities B_{10} (T), the remanent magnetic flux density Br (T), and the permeability μ' (real number section of permeability) of each unannealed alloy. The term "start" in Table 10 indicates an alloy which is produced immediately after the beginning of the ejection of the melt from the nozzle onto the cooling roller, and the term "end" indicates an alloy which is produced at the end of the production.

[0348] These alloy ribbons, each having high saturation magnetic flux density and low iron loss, i.e., $Fe_{85}Zr_{1.75}Nb_{4.25}B_9$, $Fe_{85.5}Zr_2Nb_4B_{8.5}$ and $Fe_{85}Zr_2Nb_{4.5}B_{8.5}$, belong to the soft magnetic alloy. The ribbons ejected at a temperature less than 1,350°C will be compared with the ribbons ejected at a temperature of 1,350°C or more.

[0349] The $Fe_{85}Zr_{1.75}Nb_{4.25}B_9$ unannealed alloys which were ejected at a temperature less than 1,350°C have no X-ray diffraction peak of a crystalline phase in both the start position and the end position (represented by "-" in Table 1). In contrast, the alloys ejected at a temperature of 1,350°C or more have (200) peaks of the bcc-Fe phase (represented by "XX" or "X" in Table 1, wherein "X" indicates a relatively weak peak intensity, and asterisk (*) indicates that a peak due to a compound phase is observed.)

[0350] The alloy ejected at a temperature less than 1,350°C is substantially composed of an amorphous phase, whereas the alloy ejected at a temperature of 1,350°C or more is partially crystallized. It is important that the texture of the unannealed alloy be composed of an amorphous phase in the present invention. Thus, an ejection temperature less than 1,350°C is suitable for production of a more desirable alloy.

[0351] The coercive force Hc is in a range of 0.038 to 0.044 at the start position or 0.038 to 0.044 at the end position for the alloys ejected at a temperature less than 1,350°C, and of 0.76 to 0.086 at the start position or 0.049 to 0.078 at the end position for the alloys ejected at a temperature of 1,350°C or more. The permeability μ' is in a range of 40,968 to 49,672 at the start position or 41,508 to 49,649 at the end position for the alloys ejected at a temperature less than 1,350°C, and of 23,812 to 24,739 at the start position or 25,594 to 38,191 at the end position for the alloys ejected at a temperature of 1,350°C or more. Thus, preferred alloys are produced at an ejection temperature less than 1,350°C. Furthermore, the saturation magnetic flux densities B_{10} at an ejection temperature less than 1,350°C is 1.5 T or more over the start and end positions. Accordingly, the alloy ejected at a temperature less than 1,350°C has superior soft magnetic characteristics.

[0352] In addition to the above viscosity of melt deteriorated when ejection temperature is less than 1240°C, and the nozzle is clogged up and is not able to make an amorphous ribbon.

[0353] Substantially the same results are obtained for the $Fe_{85.5}Zr_2Nb_4B_{8.5}$ and $Fe_{85}Zr_2Nb_{4.5}B_{8.5}$ alloys, as shown in Tables 9 and 10. In conclusion, an alloy having soft magnetic characteristics, such as low coercive force, large permeability, and sufficient saturation magnetic flux density is produced at an ejection temperature less than 1,350°C.

[0354] In Table 9, the T_{X1} (°C) indicates the crystallization temperature of bcc-Fe and the T_{X2} (°C) indicates the crystallization temperature of the compound phase which can be crystallized at a temperature higher than the T_{X1}. The T_{X1}, (°C) indicate the crystallization temperature of the other compound phase which can be crystallized at a temperature between the T_{X1} and the T_{X2}. These temperatures, T_{X1}, T_{X2} and T_{X1}' are parameters regarding annealing, and satisfy the relationship $\Delta T_X = T_{X2} - T_{X1} = T_{X1}' - T_{X1} \geq 200°C$, as described above.

[0355] In Tables 9 and 10, the relationship $\Delta T_X \geq 200°C$ is satisfied and Ta satisfies the above specific range. Thus, these alloys are annealed under desirable annealing conditions.

[0356] Tables 11 to 14 will now be described. Each alloy shown in these tables does not contain zinc (Zn) and thus belongs to the first magnetic alloy. All alloys are ejected at a temperature less than 1,350°C.

[0357] The coercive force Hc lies in a range of 0.038 to 0.116 Oe at the start position, or of 0.043 to 0.114 Oe at the end position, in Tables 11 to 14. In most cases, the coercive force Hc lies in the order of 0.04 Oe. The saturation magnetic flux densities B_{10} is 1.5 T or more in most cases (except for the end positions of lots RQ6-108 and RQ6-111 in Table 12 and the start position of lot RQ6-148 in Table 14). The permeability μ' is higher than 30,000 in most cases except for some lots.

[0358] These Fe-based magnetic alloys produced at an ejection temperature less than 1,350°C have superior soft magnetic characteristics on the whole. Of course, the crystallization temperatures T_{X1}, T_{X1}' and T_{X2} and the annealing temperature Ta satisfy the above-mentioned relationship.

[0359] Among the alloys shown in Tables 9 to 14, alloys having particularly superior soft magnetic characteristics are $Fe_{85}Zr_{1.75}Nb_{4.25}B_9$ and $Fe_{85.5}Zr_2Nb_4B_{8.5}$ in Tables 9 and 10, $Fe_{85.25}Zr_{1.75}Nb_{4.25}B_{8.75}$ and $Fe_{85.75}Zr_{2.25}Nb_{3.75}B_{8.25}$ in Tables 11 and 12, and $Fe_{86}Zr_{2.25}Nb_{3.75}B_8$ and $Fe_{85.62}Zr_2Nb_4B_{8.38}$ in Tables 13 and 14. In these alloys, the total content of zirconium and niobium is 6 atomic percent.

[0360] Tables 15 to 16 will now be described. Each alloy shown in these tables contains zinc and belongs to the above-mentioned second or third soft magnetic alloy. The coercive force Hc, the saturation magnetic flux densities B_{10} and the permeability μ' of each alloy are shown in Tables 15 and 16.

[0361] The subscript 1, 2 or 3 for zinc in each formula in Tables 15 and 16 indicates 1, 2 or 3 atomic percent, respectively, of zinc is fed when the alloy is produced. Thus, the subscript does not indicate the final zinc content in the alloy. As described above, most of the zinc is lost by vaporization during the production process of the alloy. The zinc content in each alloy is shown in Table 8.

[0362] The ejection temperature is less than 1,350°C in Tables 15 and 16. The coercive force Hc lies in a range of 0.037 to 0.131 at the start position and of 0.040 to 0.140 at the end position. The saturation magnetic flux densities B_{10} is 1.59 or more at the start position and 1.52 or more at the end position. The permeability μ' lies in a range of 23,088 to 63,337 at the start position and of 20,936 to 55,250 at the end position. The permeability μ' lies in a range of 40,000 to 50,000 in most cases, although it is on the order of 20,000 in a few cases. Accordingly, the Fe-based alloys shown in Tables 15 and 16 show superior soft magnetic characteristics including high saturation magnetic flux density and low iron loss.

[0363] No peak due to the (200) plane is observed, except for lots RQ6-172 and RQ6-170. The results suggest that most alloys have a desired texture and are composed of an amorphous phase.

[0364] Furthermore, the crystallization temperatures T_{X1} and T_{X2} and the annealing temperature Ta satisfy the above-mentioned relationship.

EXAMPLE 8 [Third Production Method]

[0365] Quenched ribbons were prepared from $Fe_{85.5}Zr_2Nb_4B_{8.5}$ and $Fe_{78}Si_9B_{13}$ (commercially available amorphous alloy) alloys, and were subjected to first annealing. Quenched ribbons were also prepared from $(Fe_{0.8575}Zr_{0.02}Nb_{0.04}B_{0.0825})_{99.88}Zn_{0.12}$ and $(Fe_{0.8575}Zr_{0.02}Nb_{0.04}B_{0.0825})_{99.87}Zn_{0.13}$ alloys, were subjected to first annealing, and then were cooled to room temperature, as in EXAMPLE 5.

[0366] In the first annealing, the $Fe_{85.5}Zr_2Nb_4B_{8.5}$, $(Fe_{0.8575}Zr_{0.02}Nb_{0.04}B_{0.0825})_{99.88}Zn_{0.12}$ and $(Fe_{0.8575}Zr_{0.02}Nb_{0.04}B_{0.0825})_{99.87}Zn_{0.13}$ alloys were annealed at a heating rate of 180°C/min, an annealing time of 5 minutes, and annealing temperatures of 510°C, 525°C and 510°C, respectively. The $Fe_{78}Si_9B_{13}$ alloy was annealed at a heating rate of 180°C/min, an annealing time of 120 minutes, and an annealing temperature of 350°C.

[0367] Each ribbon was subjected to second annealing in air while the annealing time was changed within a range of 0 to 100 hours at an annealing temperature of 320°C. The heating rate from room temperature to the annealing temperature was 20°C/min. The coercive force, the permeability, the saturation magnetic flux density B_{10} and the remanent magnetization Br of the ribbon were measured to determine the dependence of these magnetic characteristics on the annealing time. The results are shown in Tables 17 to 20. Fig. 128 shows the dependence of the coercive force (Hc) on the annealing time of the second annealing treatment. Fig. 129 shows the dependence of the permeability on the annealing time. The change rate of each magnetic characteristic in Tables 17 to 20 and Figs. 128 and 129 is calculated on the basis of the magnetic characteristic when the second annealing time is zero, in other words, when the second annealing is not performed.

[0368] The results in Table 17 and Fig. 128 show that most of the $Fe_{78}Si_9B_{13}$ alloy ribbons, which are subjected to the second annealing treatment, have a coercive force exceeding 0.05 Oe. The coercive force significantly changes with the second annealing time. In contrast, the $Fe_{85.5}Zr_2Nb_4B_{8.5}$, $(Fe_{0.8575}Zr_{0.02}Nb_{0.04}B_{0.0825})_{99.88}Zn_{0.12}$ and $(Fe_{0.8575}Zr_{0.02}Nb_{0.04}B_{0.0825})_{99.87}Zn_{0.13}$ alloys in accordance with the present invention, which are subjected to the second annealing treatment, have smaller coercive force. Thus, an alloy having a composition within the present invention and produced by the method of the present invention has a small coercive force. Accordingly, the method in

accordance with the present invention is applicable to an alloy containing a fine crystalline texture and preferably having a composition in accordance with the present invention.

[0369] The results in Table 18 and Fig. 129 show that the $Fe_{78}Si_9B_{13}$ alloy ribbons, which are subjected to the second annealing treatment, have a permeability of 5,200 or less. The permeability significantly changes with the second annealing time. In contrast, the $Fe_{85.5}Zr_2Nb_4B_{8.5}$, $(Fe_{0.8575}Zr_{0.02}Nb_{0.04}B_{0.0825})_{99.88}Zn_{0.12}$ and $(Fe_{0.8575}Zr_{0.02}Nb_{0.04}B_{0.0825})_{99.87}Zn_{0.13}$ alloys in accordance with the present invention, which are subjected to the second annealing treatment, has a permeability of 38,500 or more. The change rate of permeability is small even when the second annealing time is longer. Thus, an alloy having a composition within the ranges of the present invention and produced by the method of the present invention has a large permeability. Accordingly, the method in accordance with the present invention is applicable to an alloy containing a fine crystalline texture and preferably having a composition in accordance with the present invention.

[0370] The results in Table 19 show that the $Fe_{78}Si_9B_{13}$ alloy ribbons, which are subjected to the second annealing treatment, have a small B_{10} value of 1.57 or less, although the change rate of the B_{10} value is low. In contrast, the $Fe_{85.5}Zr_2Nb_4B_{8.5}$, $(Fe_{0.8575}Zr_{0.02}Nb_{0.04}B_{0.0825})_{99.88}Zn_{0.12}$ and $(Fe_{0.8575}Zr_{0.02}Nb_{0.04}B_{0.0825})_{99.87}Zn_{0.13}$ alloys in accordance with the present invention, which are subjected to the second annealing treatment, has a B_{10} value of 1.57 or more. The change rate of the B_{10} value is small even when the second annealing time is longer. Thus, an alloy having a composition within the present invention and produced by the method of the present invention has a saturation magnetic flux density, which is significantly larger than that of the commercially available $Fe_{78}Si_9B_{13}$ alloy.

[0371] The results in Table 20 show that the $Fe_{78}Si_9B_{13}$ alloy ribbons, which are subjected to the second annealing treatment, shows a significant change in remanent magnetic flux density with the second annealing time. In contrast, the $Fe_{85.5}Zr_2Nb_4B_{8.5}$, $(Fe_{0.8575}Zr_{0.02}Nb_{0.04}B_{0.0825})_{99.88}Zn_{0.12}$ and $(Fe_{0.8575}Zr_{0.02}Nb_{0.04}B_{0.0825})_{99.87}Zn_{0.13}$ alloys in accordance with the present invention, which are subjected to the second annealing treatment, shows a small change in remanent magnetic flux density with the second annealing time. Thus, an alloy having a composition within the present invention and produced by the method of the present invention has a high remanent saturation magnetic flux density, in addition to improved soft magnetic characteristics. In contrast, the commercially available $Fe_{78}Si_9B_{13}$ alloy has significantly deteriorated soft magnetic characteristics, although it has an increased remanent magnetic flux density.

[0372] Accordingly, the results shown in Figs. 128 and 129 and Tables 17 to 20 suggest that an alloy having a fine crystalline texture, produced by the method in accordance with the present invention, and preferably having a composition of the present invention has a small coercive force, as well as a high permeability, a high saturation magnetic flux density and a high remanent magnetic flux density. Furthermore, magnetic characteristics change little in the alloy over time.

Table 1

Alloy Composition	Permeability μ' (1 kHz)	Coercive Force Hc (Oe)	Saturation magnetic flux Density B_{10} (T)
$Fe_{86}Zr_2Nb_4B_8$	22,200	0.066	1.60
$Fe_{85.75}Zr_2Nb_4B_{8.25}$	57,800	0.043	1.63
$Fe_{85.5}Zr_2Nb_4B_{8.5}$	49,900	0.042	1.62
$Fe_{86}Nb_7B_7$ (for Comparison)	3,200	2.5	1.68
$Fe_{91}Zr_7B_2$ (for Comparison)	14,000	0.09	1.70
$Fe_{89}Zr_7B_4$ (for Comparison)	15,000	0.093	1.65
$Fe_{89}Zr_5B_6$ (for Comparison)	13,000	0.104	1.70

Table 2

Heating Time (Hours)	$Fe_{85}Zr_{1.75}Nb_{4.25}B_9$								
	Ejected at 1,260°C Annealed at 520°C			Ejected at 1,260°C Annealed at 525°C			Ejected at 1,280°C Annealed at 525°C		
	Pcm (W/kg)	Hc (Oe)	μ	Pcm (W/kg)	Hc (Oe)	μ	Pcm (W/kg)	Hc (Oe)	μ
0	0.100	0.038	45,000	0.119	0.038	48,000	0.149	0.038	41,100
1	0.095			0.108			0.139		
5	0.104			0.105			0.115		
10	0.100	0.036	43,400	0.118	0.037	45,000	0.111	0.038	42,500
30	0.104	0.038	43,400	0.119	0.037	45,200	0.118	0.038	41,000
100	0.106	0.035	43,300	0.118	0.038	44,500	0.152	0.038	41,400
200	0.106	0.035	42,900	0.121	0.038	42,100	0.124	0.038	41,600
300	0.105	0.035	41,900	0.114	0.038	44,400	0.125	0.038	41,400
500	0.105	0.035	42,200	0.113	0.038	43,600	0.111	0.039	41,100

Table 3

Heating Time (Hours)	$Fe_{85.5}Zr_2Nb_4B_{8.5}$			$Fe_{85.75}Zr_{2.25}Nb_{3.75}B_{8.25}$			$Fe_{78}Si_9B_{13}$ (Comparative Example)		
	Ejected at 1,280°C Annealed at 510°C			Ejected at 1,280°C Annealed at 510°C					
	Pcm (W/kg)	Hc (Oe)	μ	Pcm (W/kg)	Hc (Oe)	μ	Pcm (W/kg)	Hc (Oe)	μ
0	0.087	0.038	49,900	0.107	0.038	39,900	0.256	0.051	5,700
1	0.082			0.107			0.248		
5	0.085			0.107			0.264		
10	0.086	0.039	50,100	0.108	0.036	37,900	0.212	0.054	4,300
30	0.086	0.038	49,900	0.107	0.038	37,600	0.210	0.053	4,100
100	0.090	0.039	50,500	0.115	0.035	37,100	0.260	0.053	4,400
200	0.095	0.039	49,300	0.125	0.035	36,800	0.209	0.053	4,200
300	0.091	0.039	49,800	0.115	0.035	36,600	0.265	0.053	4,200
500	0.091	0.039	48,900	0.115	0.035	37,400	0.231	0.054	4,200

Table 4

	Bm(T)	$Fe_{85}Zr_{1.75}Nb_{4.25}B_9$		
		Ejected at 1,260°C Annealed at 520°C	Ejected at 1,260°C Annealed at 525°C	Ejected at 1,280°C Annealed at 510°C
Iron Loss (W/kg)	0.50	0.015 (0.015, 0%)	0.014 (0.011, 2.7%)	0.015 (0.014, 7.1%)
	0.70	0.028 (0.027, 3.7%)	0.026 (0.022, 15.4%)	0.028 (0.027, 3.7%)
	1.10	0.066 (0.061, 8.2%)	0.065 (0.059, 10.2%)	0.069 (0.061, 13.1%)
	1.25	0.084 (0.078, 7.7%)	0.084 (0.076, 10.5%)	0.090 (0.075, 20.0%)
	1.35	0.099 (0.091, 8.8%)	0.100 (0.097, 3.1%)	0.103 (0.105, -1.9%)
	1.40	0.104 (0.099, 5.0%)	0.113 (0.114, -0.9%)	0.109 (0.151, -25.5%)
	1.45	0.114 (0.109, 4.6%)	0.139 (0.167, -16.8%)	0.133 (0.255, -47.8%)
	1.50	0.129 (0.126, 2.3%)	0.198 (0.287, -31.0%)	0.188 (0.475, -60.4%)
B_{10} (T)		1.61 (1.61, 0%)	1.55 (1.55, 0%)	1.55 (1.56, 0.6%)
Br (T)		1.00 (0.99, 1.0%)	0.95 (0.93, 2.2%)	0.70 (0.67, 4.5%)
Hc (Oe)		0.039 (0.038, 2.6%)	0.035 (0.038, -7.9%)	0.038 (0.038, 0%)
μ at 1 kHz		42,200 (45,000, -6.2%)	43,600 (48,000, -9.2%)	41,100 (41,100, 0%)

The figures in parentheses indicate ("initial value", "increased rate after 500 hours)".

Table 4 (Continued)

	Bm(T)	$Fe_{85.75}Zr_{2.25}Nb_{3.75}B_{8.25}$ Ejected at 1,300°C Annealed at 525°C	$Fe_{85.5}Zr_2Nb_4B_{8.5}$ Ejected at 1,300°C Annealed at 510°C	$Fe_{78}Si_9B_{13}$ (Comparative Example)
Iron Loss (W/kg)	0.50	0.018 (0.017, 5.8%)	0.013 (0.014, -7.1%)	0.050 (0.043, 16.3%)
	0.70	0.033 (0.031, 6.5%)	0.024 (0.024, 0%)	0.083 (0.076, 9.2%)
	1.10	0.073 (0.069, 5.8%)	0.065 (0.053, 7.5%)	0.162 (0.164, -1.2%)
	1.25	0.093 (0.086, 8.1%)	0.072 (0.066, 9.1%)	0.197 (0.208, -5.3%)
	1.35	0.107 (0.099, 8.1%)	0.084 (0.077, 7.7%)	0.220 (0.240, -8.3%)
	1.40	0.115 (0.105, 7.5%)	0.091 (0.087, 4.6%)	0.231 (0.256, -9.8%)
	1.45	0.125 (0.112, 11.6%)	0.101 (0.108, -6.5%)	0.341 (0.265, -9.1%)
	1.50	0.139 (0.142, -2.1%)	0.118 (0.156, -24.3%)	0.250 (0.287, -12.9%)
B_{10} (T)		1.61 (1.61, 0%)	1.62 (1.59, 1.9%)	1.57 (1.57, 0%)
Br (T)		0.99 (1.01, -2.0%)	0.96 (0.91, 5.5%)	0.43 (0.44, -2.3%)
Hc (Oe)		0.035 (0.038, -7.9%)	0.039 (0.038, 2.6%)	0.054 (0.051, 5.9%)
μ at 1 kHz		37,400 (39,900, 6.3%)	48,900 (49,900, -2.0%)	4,200 (5,700, -26.3%)

The figures in parentheses indicate ("initial value", "increased rate after 500 hours)".

Table 5

Elapsed Time (hours)	$Fe_{85.75}Zr_{2.25}Nb_{3.75}B_{8.25}$ Ejected at 1,280°C Annealed at 510°C			$(Fe_{0.8575}Zr_{0.02}Nb_{0.04}B_{0.0825})_{99.88}Zn_{0.12}$ Ejected at 1,260°C Annealed at 525°C		
	Pcm (W/kg)	Hc (Oe)	μ	Pcm (W/kg)	Hc (Oe)	μ
0	0.107	0.038	39,900	0.081	0.038	61,200
1	0.107					
5	0.107			0.084	0.038	61,200
10	0.108	0.036	37,900	0.086	0.038	61,200
30	0.107	0.038	37,600	0.085	0.038	60,600
100	0.115	0.035	37,100	0.086	0.038	59,600
200	0.125	0.035	36,800	0.090	0.038	60,900
300	0.115	0.035	36,600	0.085	0.038	60,900
500	0.115	0.038	37,400	0.085	0.038	60,200

Magnetic characteristics were measured after heating to 200°C in a nitrogen atmosphere.

The core loss was measured at Bm = 1.4 T, f = 50 Hz, and room temperature.

Table 6

Elapsed Time (hours)	$Fe_{85}Zr_{1.75}Nb_{4.25}B_9$ Ejected at 1,280°C Annealed at 525°C			$Fe_{85.5}Zr_2Nb_4B_{8.5}$ Ejected at 1,280°C Annealed at 510°C			$Fe_{78}Si_9B_{13}$		
	Pcm (W/kg)	Hc (Oe)	μ	Pcm (W/kg)	Hc (Oe)	μ	Pcm (W/kg)	Hc (Oe)	μ
0	0.149	0.038	41,100	0.087	0.038	49,900	0.256	0.051	5,700
1	0.139			0.082			0.248		
5	0.115			0.085			0.264		
10	0.111	0.038	42,500	0.086	0.039	50,100	0.212	0.054	4,300
30	0.118	0.038	41,000	0.086	0.038	49,900	0.210	0.053	4,100
100	0.152	0.038	41,400	0.090	0.039	50,500	0.260	0.053	4,400
200	0.124	0.038	41,600	0.095	0.039	49,300	0.209	0.053	4,200
300	0.125	0.038	41,400	0.091	0.039	49,800	0.265	0.053	4,200
500	0.111	0.039	41,100	0.091	0.039	48,900	0.231	0.054	4,200

Magnetic characteristics were measured after heating to 200°C in a nitrogen atmosphere.

The core loss was measured at Bm = 1.4 T, f = 50 Hz, and room temperature.

Table 7

Alloy No.	Composition of Alloy (atomic percent)	Permeability μ' at 1 kHz	Coercive Force Hc (Oe)	Saturation magnetic flux density B_{10} (T)
Alloys of this invention				
10	$(Fe_{0.86}Nb_{0.07}B_{0.07})_{99.93}Zn_{0.07}$	7,600	0.24	1.62
11	$(Fe_{0.90}Zr_{0.07}B_{0.03})_{99.9}Zn_{0.1}$	31,000	0.055	1.63
12	$(Fe_{0.89}Hf_{0.07}B_{0.04})_{99.9}Zn_{0.1}$	35,000	0.052	1.59
13	$(Fe_{0.86}Zr_{0.02}Nb_{0.04}B_{0.08})_{99.87}Zn_{0.13}$	47,000	0.042	1.64
14	$(Fe_{0.8575}Zr_{0.02}Nb_{0.04}B_{0.0825})_{99.87}Zn_{0.13}$	61,800	0.039	1.63
15	$(Fe_{0.855}Zr_{0.02}Nb_{0.04}B_{0.085})_{99.86}Zn_{0.14}$	56,700	0.41	1.60
Alloys for Comparison				
16	$Fe_{86}Nb_7B_7$	3,200	2.5	1.68
17	$Fe_{90}Zr_7B_3$	22,000	0.070	1.63
18	$Fe_{89}Hf_7B_4$	32,000	0.070	1.59
19	$Fe_{86}Zr_2Nb_4B_8$	22,200	0.066	1.60
20	$Fe_{85.75}Zr_2Nb_4B_{8.25}$	57,800	0.043	1.63
21	$Fe_{85.5}Zr_2Nb_4B_{8.5}$	49,900	0.042	1.62

Table 8

Analyzed Zinc Content		
Composition by atomic percent	Zinc Content (percent by weight)	Zinc content (atomic percent)
$(Fe_{85.5}Zr_2Nb_4B_{8.5})_{99}Zn_1$	0.067	0.056
$(Fe_{85.5}Zr_2Nb_4B_{8.5})_{98}Zn_2$	0.13	0.108
$(Fe_{85.5}Zr_2Nb_4B_{8.5})_{98}Zn_2$	0.13	0.108
$(Fe_{85.5}Zr_2Nb_4B_{8.5})_{97}Zn_3$	0.17	0.141
$(Fe_{85.5}Zr_2Nb_4B_{8.5})_{97}Zn_3$	0.16	0.133
$(Fe_{85.75}Zr_2Nb_4B_{8.25})_{98}Zn_2$	0.15	0.125
$(Fe_{85.75}Zr_2Nb_4B_{8.25})_{98}Zn_2$	0.15	0.125
$(Fe_{85.75}Zr_2Nb_4B_{8.25})_{98}Zn_2$	0.15	0.125
$(Fe_{85.75}Zr_2Nb_4B_{8.25})_{97}Zn_3$	0.16	0.133
$(Fe_{85.75}Zr_2Nb_4B_{8.25})_{98}Zn_2$	0.16	0.133
$(Fe_{86}Zr_2Nb_4B_8)_{99}Zn_1$	0.041	0.034
$(Fe_{86}Zr_2Nb_4B_8)_{99}Zn_1$	0.041	0.034
$(Fe_{86}Zr_2Nb_4B_8)_{98}Zn_2$	0.14	0.117
$(Fe_{86}Zr_2Nb_4B_8)_{98}Zn_2$	0.14	0.117
$(Fe_{86}Zr_2Nb_4B_8)_{97}Zn_3$	0.16	0.133
$(Fe_{86}Zr_2Nb_4B_8)_{97}Zn_3$	0.17	0.142

Table 9

Composition	Ribbon Lot No.	Ingot	Ejection Temp. (°C)	T_{x1} (°C)	T_{x1}' (°C)	T_{x2} (°C)	(200) Peak Intensity	
							Start	End
$Fe_{85}Zr_{1.75}Nb_{4.25}B_9$ (Composition RQ6-45)	RQ6-64	Vacuum-melted	1,260	491	-	820	-	-
	RQ6-63		1,280	493	-	819	-	-
	RQ6-60		1,300	491	-	817	-	-
	RQ6-59		1,320	491	-	819	-	-
	RQ6-61		1,350	488	-	819	XX*	XX*
	RQ6-62		1,380	489	-	818	XX*	XX*
$Fe_{85.5}Zr_2Nb_4B_{8.5}$ (Composition RQ6-49)	RQ6-70	Vacuum-melted	1,260	494	-	819	-	-
	RQ6-69		1,280	491	-	823	-	-
	RQ6-68		1,300	490	-	821	XX	-
	RQ6-67		1,320	491	-	820	X	-
	RQ6-66		1,350	491	-	822	XX*	XX*
	RQ6-65		1,380	491	-	821	XX*	XX*
$Fe_{85}Zr_2Nb_{4.5}B_{8.5}$ (Composition RQ6-47)	RQ6-87	Vacuum-melted	1,260	499	-	821	-	-
	RQ6-86		1,280	500	-	823	-	-
	RQ6-85		1,300	497	-	822	X	-
	RQ6-84		1,320	497	-	822	-	-
	RQ6-82		1,350	498	-	822	XX*	XX
	RQ6-81		1,380	500	-	823	XX	XX

Table 10

Composition	Ribbon Lot No.	Start					End				
		Hc (Oe)	B10 (T)	Br (T)	Ta (°C)	μ'	Hc (Oe)	B10 (T)	Br (T)	Ta (°C)	μ'	Ta (°C)
$Fe_{85}Zr_{1.75}Nb_{4.25}B_9$ (Composition RQ6-45)	RQ6-64	0.038	1.61	0.99	520	40,968	0.038	1.57	0.93	525	46,808	550
	RQ6-63	0.041	1.59	0.83	520	49,672	0.038	1.55	0.70	510	45,790	575
	RQ6-60	0.044	1.58	0.79	575	45,759	0.044	1.55	0.86	510	41,508	525
	RQ6-59	0.040	1.41	0.74	520	49,061	0.043	1.56	0.70	520	49,649	525
	RQ6-61	0.086	1.54	0.37	510	23,812	0.049	1.58	0.70	510	38,191	525
	RQ6-62	0.076	1.47	0.49	510	24,739	0.078	1.51	0.48	510	25,594	525
$Fe_{85.5}Zr_2Nb_4B_{8.5}$ (Composition RQ6-49)	RQ6-70	0.042	1.62	0.97	520	49,934	0.043	1.57	0.84	525	43,142	525
	RQ6-69	0.043	1.58	0.86	520	39,122	0.040	1.62	0.89	520	44,861	520
	RQ6-68	0.041	1.60	0.85	525	49,416	0.039	1.59	0.87	510	47,232	525
	RQ6-67	0.041	1.60	0.83	520	43,881	0.040	1.58	0.68	520	42,615	525
	RQ6-66	0.085	1.62	0.50	625	26,765	0.067	1.60	0.55	575	28,910	525
	RQ6-65	0.088	1.62	0.47	625	25,634	0.075	1.54	0.42	510	26,710	525
$Fe_{85}Zr_2Nb_{4.5}B_{8.5}$ (Composition RQ6-47)	RQ6-87	0.053	1.56	0.88	650	30,262	-	-	-	-	-	-
	RQ6-86	0.055	1.53	0.97	600	32,133	-	-	-	-	-	-
	RQ6-85	0.049	1.44	0.77	600	33,041	-	-	-	-	-	-
	RQ6-84	0.049	1.49	0.96	600	28,805	0.050	1.51	0.74	600	26,263	650
	RQ6-82	0.066	1.46	0.45	625	25,238	0.063	1.47	0.60	600	25,890	650
	RQ6-81	0.064	1.55	0.69	625	27,532	0.049	1.43	0.55	600	23,577	625

Table 11

Composition	Ribbon Lot No.	Ingot	Ejection Temp. (°C)	T_{x1} (°C)	T_{x1}' (°C)	T_{x2} (°C)	(200) Peak Intensity	
							Start	End
$Fe_{85.75}Zr_2Nb_4B_{8.25}$ (8/7-1)	RQ6-92	Vacuum-melted	1,260	489	-	821	-	-
	RQ6-91		1,280	488	-	821	XX	XX
	RQ6-89		1,300	488	-	821	XX*	XX*
	RQ6-88		1,320	488	-	820	XX	X
$Fe_{85.5}Zr_2Nb_{4.25}B_{8.25}$ (8/7-2)	RQ6-96	Vacuum-melted	1,260	495	-	822	-	-
	RQ6-95		1,280	494	-	822	-	-
	RQ6-94		1,300	493	-	820	-	-
	RQ6-93		1,320	494	-	821	XX*	XX*
$Fe_{85.5}Zr_{1.75}Nb_{4.25}B_{8.5}$ (8/7-3)	RQ6-100	Vacuum-melted	1,280	489	-	820	XX*	XX
	RQ6-98		1,300	488	-	819	XX*	XX*
	RQ6-97		1,320	488	-	820	XX*	XX*
$Fe_{85.5}Zr_{1.75}Nb_4B_{8.75}$ (8/7-4)	RQ6-105	Vacuum-melted	1,260	486	-	820	-	-
	RQ6-104		1,280	487	-	820	-	-
	RQ6-103		1,300	486	-	819	-	-
	RQ6-102		1,320	485	-	820	XX*	XX
$Fe_{85.25}Zr_{1.75}Nb_{4.25}B_{8.75}$ (8/7-5)	RQ6-108	Vacuum-melted	1,280	491	-	820	-	-
	RQ6-107		1,300	491	-	820	XX*	XX*
	RQ6-106		1,320	490	-	819	XX*	-
$Fe_{85.75}Zr_{2.25}Nb_{3.75}B_{8.25}$ (8/7-6)	RQ6-115	Vacuum-melted	1,260	493	-	823	-	-
	RQ6-114		1,280	492	(794)	823	-	-
	RQ6-113		1,300	492	(796)	823	-	-
	RQ6-111		1,320	492	(796)	823	-	-

Table 12

Composition	Ribbon Lot No.	Start					End					
		Hc (Oe)	B10 (T)	Br (T)	Ta (°C)	μ'	Ta (°C)	Hc (Oe)	B10 (T)	Br (T)	Ta (°C)	μ'	Ta (°C)
$Fe_{85.75}Zr_2Nb_4B_{8.25}$ (8/7-1)	RQ6-92	0.042	1.60	0.82	525	41,300	525	0.052	1.57	0.56	550	38,332	600
	RQ6-91	0.049	1.62	0.79	525	39,490	525	0.054	1.60	0.67	550	41,330	525
	RQ6-89	0.099	1.62	0.40	600	19,324	600	0.104	1.55	0.32	575	19,324	600
	RQ6-88	0.052	1.61	0.94	525	49,333	525	0.053	1.61	0.93	525	45,083	525
$Fe_{85.5}Zr_2Nb_{4.25}B_{8.25}$ (8/7-2)	RQ6-96	0.048	1.60	0.82	510	42,860	510	0.046	1.59	0.80	520	34,696	550
	RQ6-95	0.047	1.58	0.75	520	37,765	550						
	RQ6-94	0.043	1.56	0.57	520	40,843	510	0.043	1.56	0.86	525	36,366	525
	RQ6-93	0.068	1.62	0.55	510	31,874	520	0.065	1.56	0.60	520	33,220	510
$Fe_{85.5}Zr_{1.75}Nb_{4.25}B_{8.5}$ (8/7-3)	RQ6-100	0.053	1.61	0.74	510	39,468	550	0.049	1.58	0.76	520	37,745	550
	RQ6-98	0.100	1.59	0.44	525	20,794	550	0.114	1.57	0.39	525	18,762	510
	RQ6-97	0.064	1.57	0.50	550	23,386	510	0.056	1.59	0.58	510	31,790	510
$Fe_{85.5}Zr_{1.75}Nb_4B_{8.75}$ (8/7-4)	RQ6-105	0.047	1.61	0.68	525	33,649	575						
	RQ6-104	0.048	1.65	0.82	510	35,334	510	0.053	1.62	0.72	510	32,542	510-
	RQ6-103	0.046	1.64	0.73	525	35,787	525	0.045	1.53	0.56	510	31,342	525
	RQ6-102	0.052	1.64	0.67	510	37,446	525	0.046	1.60	0.67	525	35,440	520
$Fe_{85.25}Zr_{1.75}Nb_{4.25}B_{8.75}$ (8/7-5)	RQ6-108	0.043	1.56	0.83	520	50,257	520	0.045	1.43	0.78	520	45,043	550
	RQ6-107	0.086	1.59	0.42	520	26,423	520	0.050	1.55	0.73	520	42,258	520
	RQ6-106	0.055	1.53	0.70	520	34,239	520	0.046	1.61	0.77	550	48,458	520
$Fe_{85.75}Zr_{2.25}Nb_{3.75}B_{8.25}$ (8/7-6)	RQ6-115	0.045	1.57	0.78	520	49,307	525						
	RQ6-114	0.048	1.50	0.55	520	37,217	550						
	RQ6-113	0.038	1.61	1.10	520	44,960	525	0.045	1.57	0.95	510	47,908	510
	RQ6-111	0.045	1.60	0.92	505	46,769	505	0.045	1.46	0.60	520	36,712	575

Table 13

Composition	Ribbon Lot No.	Ingot	Ejection Temp. (°C)	T_{x1} (°C)	T_{x1}' (°C)	T_{x2} (°C)	(200) Peak Intensity	
							Start	End
$Fe_{86.25}Zr_{2.5}Nb_{3.5}B_{7.75}$ (8/24-1)	RQ6-164	Vacuum-melted	1,260	491	790	821	-	-
	RQ6-157		1,280	491	793	821	-	-
	RQ6-156		1,300	490	792	824	-	-
	RQ6-155		1,320	489	796	823	XX*	XX*
$Fe_{85.75}Zr_{1.75}Nb_4B_{8.5}$ (8/24-2)	RQ6-126	Vacuum-melted	1,260	486	-	818	-	-
	RQ6-125		1,280	486	-	819	-	-
	RQ6-123		1,300	486	-	820	-	-
	RQ6-121		1,320	484	-	820	-	-
$Fe_{86}Zr_{2.25}Nb_{3.75}B_8$ (8/24-3)	RQ6-162	Vacuum-melted	1,260	489	-	822	-	-
	RQ6-161		1,280	489	-	822	-	-
	RQ6-135		1,300	491	798?	822	-	-
	RQ6-130		1,320	492	-	824	-	-
$Fe_{85.6}Zr_{1.9}Nb_4B_{8.5}$ (8/24-4)	RQ6-143	Vacuum-melted	1,260	490	-	821	-	-
	RQ6-142		1,280	490	-	821	-	-
	RQ6-141		1,300	490	-	822	-	-
	RQ6-138		1,320	489	-	821	X	-
$Fe_{85.55}Zr_{1.95}Nb_4B_{8.5}$ (8/24-5)	RQ6-150	Vacuum-melted	1,260	491	-	823	-	-
	RQ6-148		1,280	492	-	822	XX	XX
	RQ6-147		1,300	490	-	822	-	XX
	RQ6-145		1,320	489	-	820	XX	-
$Fe_{85.62}Zr_2Nb_4B_{8.38}$ (8/24-6)	RQ6-154	Vacuum-melted	1,260	489	-	821	-	-
	RQ6-153		1,280	490	-	821	-	-
	RQ6-152		1,300	491	-	822	-	-
	RQ6-151		1,320	489	-	822	X	X

Table 14

Composition	Ribbon Lot No.	Start						End					
		Hc (Oe)	B_{10} (T)	Br (T)	Ta (°C)	μ'	Ta (°C)	Hc (Oe)	B_{10} (T)	Br (T)	Ta (°C)	μ'	Ta (°C)
$Fe_{86.25}Zr_{2.5}Nb_{3.5}B_{7.75}$ (8/24-1)	RQ6-164	0.049	1.58	0.88	500	46,278	500						
	RQ6-157	0.046	1.58	0.83	520	45,587	520	0.046	1.56	0.71	520	47,204	500
	RQ6-156	0.046	1.61	1.05	525	48,947	500						
	RQ6-155	0.116	1.65	0.49	575	20,304	575	0.103	1.62	0.45	575	21,175	525
$Fe_{85.75}Zr_{1.75}Nb_4B_{8.5}$ (8/24-2)	RQ6-126	0.063	1.61	0.94	510	50,487	505	0.058	1.54	0.80	525	48,772	525
	RQ6-125	0.055	1.61 /1.66	0.96 /0.93	510	57,014	500	0.051	1.57	0.97	510	55,313	505
	RQ6-123	0.060	1.62	1.09	510	45,470	525	0.069	1.60	0.85	535	38,647	500
	RQ6-121	0.057	1.64 /1.62	1.0 /0.91	525	47,266	525	0.058	1.65	0.92	550	46,271	525
$Fe_{86}Zr_{2.25}Nb_{3.75}B_8$ (8/24-3)	RQ6-162	0.051	1.62	0.99	505	52,521	520	0.044	1.62 /1.64	0.95 /0.94	520 /550	56,396	510
	RQ6-161	0.048	1.62	1.03	525	52,520	525	0.043	1.63	0.81	550	55,286	505
	RQ6-135	0.048	1.58	0.88	510	50,382	510						
	RQ6-130	0.055	1.64 /1.64 /1.65	0.87 /0.91 /0.90	525 /535 /575	54,126	510	0.051	1.62 /1.65	0.97 /0.90	525 /575	53,305	520
$Fe_{85.6}Zr_{1.9}Nb_4B_{8.5}$ (8/24-4)	RQ6-143	0.050	1.49	0.77	525	39,952	525						
	RQ6-142	0.045	1.63	0.99	505	58,174	505						
	RQ6-141	0.055	1.60	0.99	525	55,029	525	0.050	1.61	0.96	505	55,176	505
	RQ6-138	0.051	1.64	0.94	520	48,751	525	0.049	1.59	0.82	550	45,185	535
$Fe_{85.55}Zr_{1.95}Nb_4B_{8.5}$ (8/24-5)	RQ6-150	0.051	1.51 /1.56	0.69 /0.70	520 /525	44,048	505						
	RQ6-148	0.048	1.48	0.77	500	44,752	520	0.053	1.58 /1.58	0.78 /0.78	520 /535	46,107	520
	RQ6-147	0.048	1.62	0.99	510	56,079	500	0.052	1.60	0.84	525	48,485	505
	RQ6-145	0.046	1.62	0.90	550	52,885	510	0.044	1.58	0.89	510	56,603	500
$Fe_{85.62}Zr_2Nb_4B_{8.38}$ (8/24-6)	RQ6-154	0.046	1.62	0.92	525	52,689	510	0.045	1.63	0.88	575	53,556	510
	RQ6-153	0.045	1.62	0.97	525	59,416	500	0.048	1.60 /1.62	0.95 /0.99	510 /520	53,900	520
	RQ6-152	0.048	1.62	0.96	510	51,302	510	0.048	1.61	0.95	525	50,254	520
	RQ6-151	0.047	1.62	0.87	505	51,059	510	0.045	1.60 /1.61	0.88 /0.87	500 /535	50,411	525

Table 15

Composition	Ribbon Lot No.	Ingot	Ejection Temp. (°C)	T_{x1} (°C)	T_{x1}' (°C)	T_{x2} (°C)	(200) Peak Intensity	
							Start	End
$(Fe_{85.5}Zr_2Nb_4B_{8.5})_{99}Zn_1$	RQ6-116	Vacuum-melted	1,300	488	-	820	-	-
$(Fe_{85.5}Zr_2Nb_4B_{8.5})_{99}Zn_1$	RQ6-128		1,300	489	-	821	-	-
$(Fe_{85.5}Zr_2Nb_4B_{8.5})_{99}Zn_1$	RQ6-134		1,300	490	-	821	-	-
$(Fe_{85.5}Zr_2Nb_4B_{8.5})_{98}Zn_2$	RQ6-172		1,260	487	-	821	X	-
	RQ6-170		1,300	486	-	820	X	XX
$(Fe_{85.5}Zr_2Nb_4B_{8.5})_{97}Zn_3$	RQ6-176		1,260	490	-	821	-	-
	RQ6-175		1,300	491	-	823	-	-
$(Fe_{85.75}Zr_2Nb_4B_{8.25})_{98}Zn_2$	RQ6-167		1,260	489	-	822	-	-
	RQ6-165		1,300	488	-	822	-	-
$(Fe_{85.75}Zr_2Nb_4B_{8.25})_{97}Zn_3$	RQ6-169		1,260	488	-	821	-	-
	RQ6-168		1,300	489	-	821	-	-
$(Fe_{86}Zr_2Nb_4B_8)_{99}Zn_1$	RQ6-178		1,260	483	-	822	-	-
	RQ6-177		1,300	486	-	823	-	-
$(Fe_{86}Zr_2Nb_4B_8)_{98}Zn_2$	RQ6-182		1,260	487	-	823	-	-
	RQ6-181		1,300	487	-	823	-	-
$(Fe_{86}Zr_2Nb_4B_8)_{97}Zn_3$	RQ6-180		1,260	487	-	821	-	-
	RQ6-179		1,300	487	-	820	-	-

Table 16

Composition	Ribbon Lot No.	Start					End				
		Hc (Oe)	B_{10} (T)	Br (T)	Ta (°C)	μ'	Ta (°C)	Hc (Oe)	B_{10} (T)	Br (T)	Ta (°C)	μ'	Ta (°C)
$(Fe_{85.5}Zr_2Nb_4B_{8.5})_{99}Zn_1$	RQ6-116	0.041	1.62	0.80	525	44,733	520						
$(Fe_{85.5}Zr_2Nb_4B_{8.5})_{99}Zn_1$	RQ6-128	0.045	1.61	0.89 /0.92 /0.9	510 /525 /535	46,873	525	0.048	1.54 /1.58	0.91 /0.9	520 /535	44,195	525
$(Fe_{85.5}Zr_2Nb_4B_{8.5})_{99}Zn_1$	RQ6-134	0.040	1.60	0.92	520	53,172	535						
$(Fe_{85.5}Zr_2Nb_4B_{8.5})_{98}Zn_2$	RQ6-172	0.040	1.61	0.90	525	54,987	520						
	RQ6-170	0.044	1.61	0.82	535	50,071	535	0.044	1.58	0.60	535	40,803	525
$(Fe_{85.5}Zr_2Nb_4B_{8.5})_{97}Zn_3$	RQ6-176	0.044	1.61	0.86	505	51,149	505	0.040	1.52	0.71	535	41,343	575
	RQ6-175	0.039	1.60	0.84	535	56,702	555	0.040	1.56	0.85	535	55,250	505
$(Fe_{85.75}Zr_2Nb_4B_{8.25})_{98}Zn_2$	RQ6-167	0.037	1.64	0.89	535	61,768	525	0.040	1.56	0.92	550	54,808	520
	RQ6-165	0.039	1.64	0.90	550	47,525	520	0.043	1.61	0.87	525	55,182	525
$(Fe_{85.75}Zr_2Nb_4B_{8.25})_{97}Zn_3$	RQ6-169	0.041	1.62	0.92	520	57,450	520	0.040	1.61	0.80	535	47,374	575
	RQ6-168	0.046	1.61 /1.63 /1.64 /1.65	0.94 /0.87 /0.83 /0.87	505 /520 /535 /575	63,337	510	0.041	1.61	0.90	535	52,235	520
$(Fe_{86}Zr_2Nb_4B_8)_{99}Zn_1$	RQ6-178	0.085	1.62	0.97	535	30,093	535	0.133	1.53	0.98	525	20,936	535
	RQ6-177	0.131	1.64	1.21	510	23,088	510	0.140	1.63	1.18	520	21,737	520
$(Fe_{86}Zr_2Nb_4B_8)_{98}Zn_2$	RQ6-182	0.088	1.59	0.98	520	29,417	525	0.088	1.57	0.91	525	28,434	535
	RQ6-181	0.054	1.61	1.00	520	40,014	520	0.070	1.60	0.98	535	34,739	535
$(Fe_{86}Zr_2Nb_4B_8)_{97}Zn_3$	RQ6-180	0.041	1.63	0.81	535	46,960	550	0.051	1.55	0.82	525	39,159	535
	RQ6-179	0.072	1.61	0.85	550	33,250	535	0.090	1.56	0.83	525	28,883	550

Table 17

	$Fe_{85.5}Zr_2Nb_4B_{8.5}$		$(Fe_{0.8575}Zr_{0.02}Nb_{0.04}B_{0.0825})_{99.88}Zn_{0.12}$		$(Fe_{0.8575}Zr_{0.02}Nb_{0.04}B_{0.0825})_{99.87}Zn_{0.13}$		$Fe_{78}Si_9B_{13}$	
Second Annealing Time (Hr)	Coercive Force Hc (Oe)	Change Rate of Hc (%)	Coercive Force Hc (Oe)	Change Rate of Hc (%)	Coercive Force Hc (Oe)	Change Rate of Hc (%)	Coercive Force Hc (Oe)	Change Rate of Hc (%)
0	0.041	0	0.083	0	0.047	0	0.052	0
1	0.037	-10	0.032	-16	0.044	-6	0.042	-19
5	0.036	-12	0.031	-18	0.042	-11	0.051	-2
10	0.035	-15	0.031	-18	0.043	-9	0.070	35
30	0.035	-15	0.029	-24	0.044	-6	0.119	129
100	0.037	-10	0.029	-24	0.041	-13	0.106	104

Table 18

Second Annealing Time (Hr)	$Fe_{85.5}Zr_2Nb_4B_{8.5}$		$(Fe_{0.8575}Zr_{0.02}Nb_{0.04}B_{0.0825})_{99.88}Zn_{0.12}$		$(Fe_{0.8575}Zr_{0.02}Nb_{0.04}B_{0.0825})_{99.87}Zn_{0.13}$		$Fe_{78}Si_9B_{13}$	
	Permeability (μ')	Change Rate of μ' (%)	Permeability (μ')	Change Rate of μ' (%)	Permeability (μ')	Change Rate of μ' (%)	Permeability (μ')	Change Rate of μ' (%)
0	47,900	0	61,800	0	63,900	0	4,700	0
1	49,800	4	60,900	-1	63,500	-1	5,200	11
5	53,000	11	60,000	-3	65,100	2	3,400	-28
10	47,100	-2	60,600	-2	66,400	4	3,400	-28
30	46,300	-3	59,200	-4	66,500	4	3,300	-30
100	38,500	-20	56,000	-9	64,100	0	3,000	-36

Table 19

Second Annealing Time (Hr)	$Fe_{85.5}Zr_2Nb_4B_{8.5}$		$(Fe_{0.8573}Zr_{0.02}Nb_{0.04}B_{0.0825})_{99.88}Zn_{0.12}$		$(Fe_{0.8573}Zr_{0.02}Nb_{0.04}B_{0.0825})_{99.87}Zn_{0.13}$		$Fe_{78}Si_9B_{13}$	
	B_{10} (T)	Change Rate of B_{10} (%)	B_{10} (T)	Change Rate of B_{10} (%)	B_{10} (T)	Change Rate of B_{10} (%)	B_{10} (T)	Change Rate of B_{10} (%)
0	1.58	0	1.62	0	1.63	0	1.55	0
1	1.59	1	1.60	-1	1.64	-1	1.56	1
5	1.58	0	1.61	-1	1.63	0	1.57	1
10	1.57	-1	1.60	-1	1.62	-1	1.56	1
30	1.57	-1	1.59	-2	1.62	-1	1.56	1
100	1.57	-1	1.61	-1	1.63	0	1.56	1

Table 20

	$Fe_{85.5}Zr_2Nb_4B_{8.5}$		$(Fe_{0.8575}Zr_{0.02}Nb_{0.04}B_{0.0825})_{99.88}Zn_{0.12}$		$(Fe_{0.8575}Zr_{0.02}Nb_{0.04}B_{0.0825})_{99.87}Zn_{0.13}$		$Fe_{78}Si_9B_{13}$	
Second Annealing Time (Hr)	Br (T)	Change Rate of Br (%)	Br (T)	Change Rate of Br (%)	Br (T)	Change Rate of Br (%)	Br (T)	Change Rate of Br (%)
0	0.96	0	0.93	0	0.86	0	0.42	0
1	0.94	-2	0.97	4	0.88	2	0.47	12
5	1.00	4	0.99	6	0.91	6	0.55	31
10	0.95	-1	1.00	8	0.91	6	0.62	48
30	0.90	-6	1.01	9	0.94	9	0.71	69
100	0.86	-10	1.04	12	1.00	16	0.72	71

Claims

1. A Fe-based soft magnetic alloy, having high saturation magnetic flux density and low iron loss, represented by the following formula and having a fine crystalline texture formed by annealing an amorphous alloy substantially composed of an amorphous phase; at least 50% of the fine crystalline texture being composed of a bcc-Fe phase as the major component having an average crystal grain size of 100 nm or less:

$$Fe_aZr_xNb_yB_z$$

wherein the subscripts satisfy the relationships 80 atomic percent ≤ a; 5 atomic percent ≤ x + y ≤ 7 atomic percent; 1.5/6 ≤ x/(x+y) ≤ 2.5/6; and 5 atomic percent ≤ z ≤ 12.5 atomic percent.

2. A Fe-based soft magnetic alloy according to claim 1, wherein the subscripts satisfy the relationships 83 atomic percent ≤ a; 5.7 atomic percent ≤ x + y ≤ 6.5 atomic percent; 1.5/6 ≤ x/(x+y) ≤ 2.5/6; and 6 atomic percent ≤ z ≤ 9.5 atomic percent.

3. A Fe-based soft magnetic alloy according to claim 1, wherein the crystallization temperature T_{X1} of the bcc-Fe phase, the crystallization temperature T_{X2} of a compound phase which is crystallized at a temperature higher than T_{X1}, and the difference $\Delta T_X = T_{X2} - T_{X1}$ of the crystallization temperatures satisfy the relationship 200°C ≤ ΔT_X.

4. A Fe-based soft magnetic alloy according to claim 1, wherein the saturation magnetic flux density of the Fe-based soft magnetic alloy is at least 1.5 T, the iron loss, when a magnetic flux of 1.4 T at a frequency of 50 Hz is applied, is 0.15 W/kg or less, and the change in iron loss after aging at 200°C for 500 hours is 10% or less.

5. A Fe-based soft magnetic alloy according to claim 1, wherein the fracture strain of the Fe-based soft magnetic alloy is 1.0×10^{-2} or more.

6. A Fe-based soft magnetic alloy, having high saturation magnetic flux density and low iron loss, represented by the following formula and having a fine crystalline texture comprising at least 50% of fine bcc-Fe crystal grains having an average crystal grain size of 100 nm or less and the balance being an amorphous phase; the bcc-Fe crystal grains being precipitated by heating to a temperature higher than the crystallization temperature and then cooling a substantially single amorphous phase which is formed by quenching an alloy melt:

$$(Fe_{1-a}Q_a)_bB_xM_yZn_z$$

wherein Q is at least one of Co and Ni; M is at least one selected from the group consisting of Ti, Zr, Hf, V, Nb, Ta, Mo and W; the subscripts satisfy the relationships 0 ≤ a ≤ 0.05, 80 atomic percent ≤ b; 5 atomic percent ≤ x ≤ 12.5 atomic percent; 5 atomic percent ≤ y ≤ 7 atomic percent; and 0.025 atomic percent ≤ z ≤ 0.2 atomic percent.

7. A Fe-based soft magnetic alloy according to claim 6, wherein the change in iron loss of the Fe-based soft magnetic alloy after heating at 320°C for 100 hours is 20% or less, the saturation magnetic flux density is 1.5 T or more, and the permeability is 30,000 or more.

8. A Fe-based soft magnetic alloy according to claim 6, wherein the fracture strain of the Fe-based soft magnetic alloy is 1.0×10^{-2} or more.

9. A Fe-based soft magnetic alloy, having high saturation magnetic flux density and low iron loss, represented by the following formula and having a fine crystalline texture comprising at least 50% of fine bcc-Fe crystal grains having an average crystal grain size of 100 nm or less and the balance being an amorphous phase; the bcc-Fe crystal grains being precipitated by heating to a temperature higher than the crystallization temperature and then cooling a substantially single amorphous phase which is formed by quenching an alloy melt:

$$(Fe_{1-a}Q_a)_bB_xH_yZn_zM'_u$$

wherein Q is at least one of Co and Ni; M is at least one selected from the group consisting of Ti, Zr, Hf, V, Nb, Ta,

Mo and W; M' is at least one selected from the group consisting of Cr, Ru, Rh and Ir; the subscripts satisfy the relationships $0 \le a \le 0.05$, 80 atomic percent $\le b$; 5 atomic percent $\le x \le 12.5$ atomic percent; 5 atomic percent $\le y \le 7$ atomic percent; 0.025 atomic percent $\le z \le 0.2$ atomic percent; and $u \le 5$ atomic percent.

10. A Fe-based soft magnetic alloy according to claim 9, wherein the change in iron loss of the Fe-based soft magnetic alloy after heating at 320°C for 100 hours is 20% or less, the saturation magnetic flux density is 1.5 T or more, and the permeability is 30,000 or more.

11. A Fe-based soft magnetic alloy according to claim 9, wherein the fracture strain of the Fe-based soft magnetic alloy is 1.0×10^{-2} or more.

12. A Fe-based soft magnetic alloy having high saturation magnetic flux density and low iron loss comprising Fe, Zr, Nb, B, and Zn, and having a texture comprising at least 50% of bcc-Fe fine crystal grains having an average crystal grain size of 100 nm or less and the balance being an amorphous phase.

13. A Fe-based soft magnetic alloy according to claim 6, wherein the change in iron loss of the Fe-based soft magnetic alloy after heating at 320°C for 100 hours is 20% or less, the saturation magnetic flux density is 1.5 T or more, and the permeability is 30,000 or more.

14. A Fe-based soft magnetic alloy according to claim 12, wherein the Fe-based soft magnetic alloy is represented by the following formula and has a fine crystalline texture comprising at least 50% of fine bcc-Fe crystal grains having an average crystal grain size of 100 nm or less and the balance being an amorphous phase; the bcc-Fe crystal grains being precipitated by heating to a temperature higher than the crystallization temperature and then cooling a substantially single amorphous phase which is formed by quenching an alloy melt:

$$(Fe_{1-a}Q_a)_bZr_xNb_yB_tZn_z$$

wherein Q is at least one of Co and Ni; the subscripts satisfy the relationships $0 \le a \le 0.05$, 80 atomic percent $\le$ b; 1.5 atomic percent $\le x \le 2.5$ atomic percent; 3.5 atomic percent $\le y \le 5.0$ atomic percent; 5 atomic percent $\le t \le 12.5$ atomic percent, 0.025 atomic percent $\le z \le 0.2$ atomic percent; 5.0 atomic percent $\le x + y \le 7.5$ atomic percent; and $1.5/6 \le x/(x+y) \le 2.5/6$.

15. A Fe-based soft magnetic alloy according to claim 12, wherein the Fe-based soft magnetic alloy is represented by the following formula and has a fine crystalline texture comprising at least 50% of fine bcc-Fe crystal grains having an average crystal grain size of 100 nm or less and the balance being an amorphous phase; the bcc-Fe crystal grains being precipitated by heating to a temperature higher than the crystallization temperature and then cooling a substantially single amorphous phase which is formed by quenching an alloy melt:

$$(Fe_{1-a}Q_a)_bZr_xNb_yB_tZn_zM'_u$$

wherein Q is at least one of Co and Ni; M' is at least one selected from the group consisting of Cr, Ru, Rh and Ir; the subscripts satisfy the relationships $0 \le a \le 0.05$, 80 atomic percent $\le b$; 1.5 atomic percent $\le x \le 2.5$ atomic percent; 3.5 atomic percent $\le y \le 5.0$ atomic percent; 5 atomic percent $\le t \le 12.5$ atomic percent, 0.025 atomic percent $\le z \le 0.2$ atomic percent; $u \le 5$ atomic percent; 5.0 atomic percent $\le x + y \le 7.5$ atomic percent; and $1.5/6 \le x/(x+y) \le 2.5/6$.

16. A Fe-based soft magnetic alloy according to claim 12, wherein the fracture strain is 1.0×10^{-2} or more.

17. A low-iron-loss magnetic core comprising a Fe-based soft magnetic alloy represented by the following formula, the Fe-based soft magnetic alloy having a texture comprising at least 50% of a fine bcc-Fe crystalline phase having an average crystal grain size of 100 nm or less formed by annealing an alloy substantially comprising an amorphous phase:

$$Fe_aZr_xNb_yB_z$$

wherein the subscripts satisfy the relationships 80 atomic percent ≤ a; 5 atomic percent ≤ x+y ≤ 7.5 atomic percent; 1.5/6 ≤ x/(x+y) ≤ 2.5/6; and 5 atomic percent ≤ z ≤ 12.5 atomic percent.

18. A low-iron-loss magnetic core according to claim 17, wherein the subscripts satisfy the relationships; 83 atomic percent ≤ a; 5.7 atomic percent ≤ x+y ≤ 6.5 atomic percent; 1.5/6 ≤ x/(x+y) ≤ 2.5/6; and 6 atomic percent ≤ z ≤ 9.5 atomic percent.

19. A low-iron-loss magnetic core according to claim 17, wherein the crystallization temperature T_{X1} of the bcc-Fe phase, the crystallization temperature T_{X2} of a compound phase which is crystallized at a temperature higher than T_{X1}, and the difference $\Delta T_X = T_{X2} - T_{X1}$ of the crystallization temperatures satisfy the relationship 200°C ≤ ΔT_X.

20. A low-iron-loss magnetic core according to claim 17, wherein the saturation magnetic flux density of the Fe-based soft magnetic alloy is at least 1.5 T, the iron loss, when a magnetic flux of 1.4 T at a frequency of 50 Hz is applied, is 0.15 W/kg or less, and the change in iron loss after aging at 200°C for 500 hours is 10% or less.

21. A low-iron-loss magnetic core according to claim 17, comprising a ribbon of the Fe-based soft magnetic alloy having a fracture strain of the 1.0×10^{-2} or more.

22. A low-iron-loss magnetic core according to claim 17, comprising at least one ring formed of a ribbon of the Fe-based soft magnetic alloy.

23. A low-iron-loss magnetic core according to claim 17, comprising an annular ring formed by winding a ribbon of the Fe-based soft magnetic alloy.

24. A low-iron-loss magnetic core comprising a Fe-based soft magnetic alloy represented by the following formula and having a fine crystalline texture comprising at least 50% of fine bcc-Fe crystal grains having an average crystal grain size of 100 nm or less and the balance being an amorphous phase; the bcc-Fe crystal grains being precipitated by heating to a temperature higher than the crystallization temperature and then cooling a substantially single amorphous phase which is formed by quenching an alloy melt:

$$(Fe_{1-a}Q_a)_bB_xM_yZn_z$$

wherein Q is at least one of Co and Ni; M is at least one selected from the group consisting of Ti, Zr, Hf, V, Nb, Ta, Mo and W; the subscripts satisfy the relationships 0 ≤ a ≤ 0.05, 80 atomic percent ≤ b; 5 atomic percent ≤ x ≤ 12.5 atomic percent; 5 atomic percent ≤ y ≤ 7.5 atomic percent; and 0.025 atomic percent ≤ z ≤ 0.2 atomic percent.

25. A low-iron-loss magnetic core according to claim 24, wherein the change in iron loss of the Fe-based soft magnetic alloy after heating at 200°C for 500 hours is 10% or less, the saturation magnetic flux density is 1.5 T or more, and the iron loss, when a magnetic flux of 1.4 T is applied at a frequency of 50 Hz, is 0.15 W/kg or less.

26. A low-iron-loss magnetic core according to claim 24, wherein the fracture strain is 1.0×10^{-2} or more.

27. A low-iron-loss magnetic core according to claim 24, comprising at least one ring formed of a ribbon of the Fe-based soft magnetic alloy.

28. A low-iron-loss magnetic core according to claim 24, comprising an annular ring formed by winding a ribbon of the Fe-based soft magnetic alloy.

29. A low-iron-loss magnetic core comprising a Fe-based soft magnetic alloy, having high saturation magnetic flux density and low iron loss, represented by the following formula and having a fine crystalline texture comprising at least 50% of fine bcc-Fe crystal grains having an average crystal grain size of 100 nm or less and the balance being an amorphous phase; the bcc-Fe crystal grains being precipitated by heating to a temperature higher than the crystallization temperature and then cooling a substantially single amorphous phase which is formed by quenching an alloy melt:

$$(Fe_{1-a}Q_a)_bB_xM_yZn_zM'_u$$

wherein Q is at least one of Co and Ni; M is at least one selected from the group consisting of Ti, Zr, Hf, V, Nb, Ta, Mo and W; M' is at least one selected from the group consisting of Cr, Ru, Rh and Ir; the subscripts satisfy the relationships $0 \leq a \leq 0.05$, 80 atomic percent $\leq b$; 5 atomic percent $\leq x \leq 12.5$ atomic percent; 5 atomic percent $\leq y \leq 7.5$ atomic percent; 0.025 atomic percent $\leq z \leq 0.2$ atomic percent; and $u \leq 5$ atomic percent.

30. A low-iron-loss magnetic core according to claim 29, wherein the change in iron loss of the Fe-based soft magnetic alloy after heating at 200°C for 500 hours is 10% or less; the saturation magnetic flux density is at least 1.5 T, and the iron loss, when a magnetic flux of 1.4 T at a frequency of 50 Hz is applied, is 0.15 W/kg or less.

31. A low-iron-loss magnetic core according to claim 29, comprising a ribbon of the Fe-based soft magnetic alloy having a fracture strain of the 1.0×10^{-2} or more.

32. A low-iron-loss magnetic core according to claim 29, comprising at least one ring formed of a ribbon of the Fe-based soft magnetic alloy.

33. A low-iron-loss magnetic core according to claim 29, comprising an annular ring formed by winding a ribbon of the Fe-based soft magnetic alloy.

34. A low-iron-loss magnetic core comprising a Fe-based soft magnetic alloy comprising Fe, Zr, Nb, B, and Zn, and having a texture comprising at least 50% of bcc-Fe fine crystal grains having an average crystal grain size of 100 nm or less and the balance being an amorphous phase.

35. A low-iron-loss magnetic core according to claim 34, wherein the Fe-based soft magnetic alloy is represented by the following formula and has a fine crystalline texture comprising at least 50% of fine bcc-Fe crystal grains having an average crystal grain size of 100 nm or less and the balance being an amorphous phase; the bcc-Fe crystal grains being precipitated by heating to a temperature higher than the crystallization temperature and then cooling a substantially single amorphous phase which is formed by quenching an alloy melt:

$$(Fe_{1-a}Q_a)_bZr_cNb_dB_xZn_z$$

wherein Q is at least one of Co and Ni; the subscripts satisfy the relationships $0 \leq a \leq 0.05$, 80 atomic percent $\leq b$; 1.5 atomic percent $\leq c \leq 2.5$ atomic percent; 3.5 atomic percent $\leq d \leq 5.0$ atomic percent; 5 atomic percent $\leq x \leq 12.5$ atomic percent, 0.025 atomic percent $\leq z \leq 0.2$ atomic percent; 5.0 atomic percent $\leq c + d \leq 7.5$ atomic percent; and $1.5/6 \leq c/(c+d) \leq 2.5/6$.

36. A low-iron-loss magnetic core according to claim 34, wherein the Fe-based soft magnetic alloy is represented by the following formula and has a fine crystalline texture comprising at least 50% of fine bcc-Fe crystal grains having an average crystal grain size of 100 nm or less and the balance being an amorphous phase; the bcc-Fe crystal grains being precipitated by heating to a temperature higher than the crystallization temperature and then cooling a substantially single amorphous phase which is formed by quenching an alloy melt:

$$(Fe_{1-a}Q_a)_bZr_cNb_dB_xZn_zM'_u$$

wherein Q is at least one of Co and Ni; M' is at least one selected from the group consisting of Cr, Ru, Rh and Ir; the subscripts satisfy the relationships $0 \leq a \leq 0.05$, 80 atomic percent $\leq b$; 1.5 atomic percent $\leq c \leq 2.5$ atomic percent; 3.5 atomic percent $\leq d \leq 5.0$ atomic percent; 5 atomic percent $\leq x \leq 12.5$ atomic percent, 0.025 atomic percent $\leq z \leq 0.2$ atomic percent; $u \leq 5$ atomic percent; 5.0 atomic percent $\leq c + d \leq 7.5$ atomic percent; and $1.5/6 \leq c/(c+d) \leq 2.5/6$.

37. A low-iron-loss magnetic core according to claim 37, wherein the change in iron loss of the Fe-based soft magnetic alloy after heating at 200°C for 500 hours is 10% or less; the saturation magnetic flux density is at least 1.5 T, and the iron loss, when a magnetic flux of 1.4 T at a frequency of 50 Hz is applied, is 0.15 W/kg or less.

38. A low-iron-loss magnetic core according to claim 34, comprising a ribbon of the Fe-based soft magnetic alloy having a fracture strain of the 1.0×10^{-2} or more.

39. A low-iron-loss magnetic core according to claim 34, comprising at least one ring formed of a ribbon of the Fe-based soft magnetic alloy.

40. A low-iron-loss magnetic core according to claim 34, comprising an annular ring formed by winding a ribbon of the Fe-based soft magnetic alloy.

41. A method for making a Fe-based soft magnetic alloy comprising the steps of:

quenching an alloy melt comprising Fe as the major component, B, and at least one metal M selected from the group consisting of Ti, Zr, Hf, V, Nb, Ta, Mo, W and Mn to form a substantially amorphous phase; and
heating the alloy to a predetermined annealing temperature at a heating rate of 10°C/min to 200°C/min to form a texture comprising at least 50% of fine bcc-Fe crystal grains having an average crystal grain size of 100 nm or less and the balance being an amorphous phase.

42. A method for making a Fe-based soft magnetic alloy according to claim 41, wherein the predetermined annealing temperature is in a range of 490°C to 670°C.

43. A method for making a Fe-based soft magnetic alloy according to claim 41, wherein the predetermined annealing temperature is in a range of 500°C to 560°C.

44. A method for making a Fe-based soft magnetic alloy comprising the steps of:

melting an alloy melt comprising Fe as the major component, B, and at least one metal M selected from the group consisting of Ti, Zr, Hf, V, Nb, Ta, Mo, W and Mn, in a crucible;
ejecting the melt at less than 1,350°C onto a cooling roller through a nozzle to quench and solidify the melt on the roller to form an alloy ribbon substantially composed of an amorphous phase; and
annealing the alloy ribbon at an annealing temperature which is higher than the crystallization temperature so as to form a texture comprising at least 50% of fine bcc-Fe crystal grains having an average crystal grain size of 100 nm or less and the balance being an amorphous phase.

45. A method for making a Fe-based soft magnetic alloy according to claim 44, wherein the melt is ejected at a temperature of 1,240°C or more.

46. A method for making a Fe-based soft magnetic alloy comprising:

a first annealing step for annealing an amorphous alloy comprising Fe as the major component, B, and at least one metal M selected from the group consisting of Ti, Zr, Hf, V, Nb, Ta, Mo, W and Mn to form a fine crystalline alloy composed of fine bcc-Fe crystal grains having an average crystal grin size of 30 nm or less and containing an amorphous phase; and
a second annealing step for annealing the fine crystalline alloy at an annealing temperature which is 100°C or more and lower than the annealing temperature at the first annealing step.

47. A method for making a Fe-based soft magnetic alloy according to claim 46, wherein the annealing temperature at the second annealing step is in a range of 200°C to 400°C.

48. A method for making a Fe-based soft magnetic alloy according to claim 46, wherein the second annealing step is performed for 0.5 to 100 hours.

49. A method for making a Fe-based soft magnetic alloy according to claim 48, wherein the second annealing step is performed for 1 to 30 hours.

50. A method for making a Fe-based soft magnetic alloy according to claim 46, wherein the first annealing step is performed at a heating rate of 10 to 200°C/min.

51. A method for making a Fe-based soft magnetic alloy according to claim 46, wherein the annealing temperature at the first annealing step is in a range of 500 to 800°C.

FIG. 1

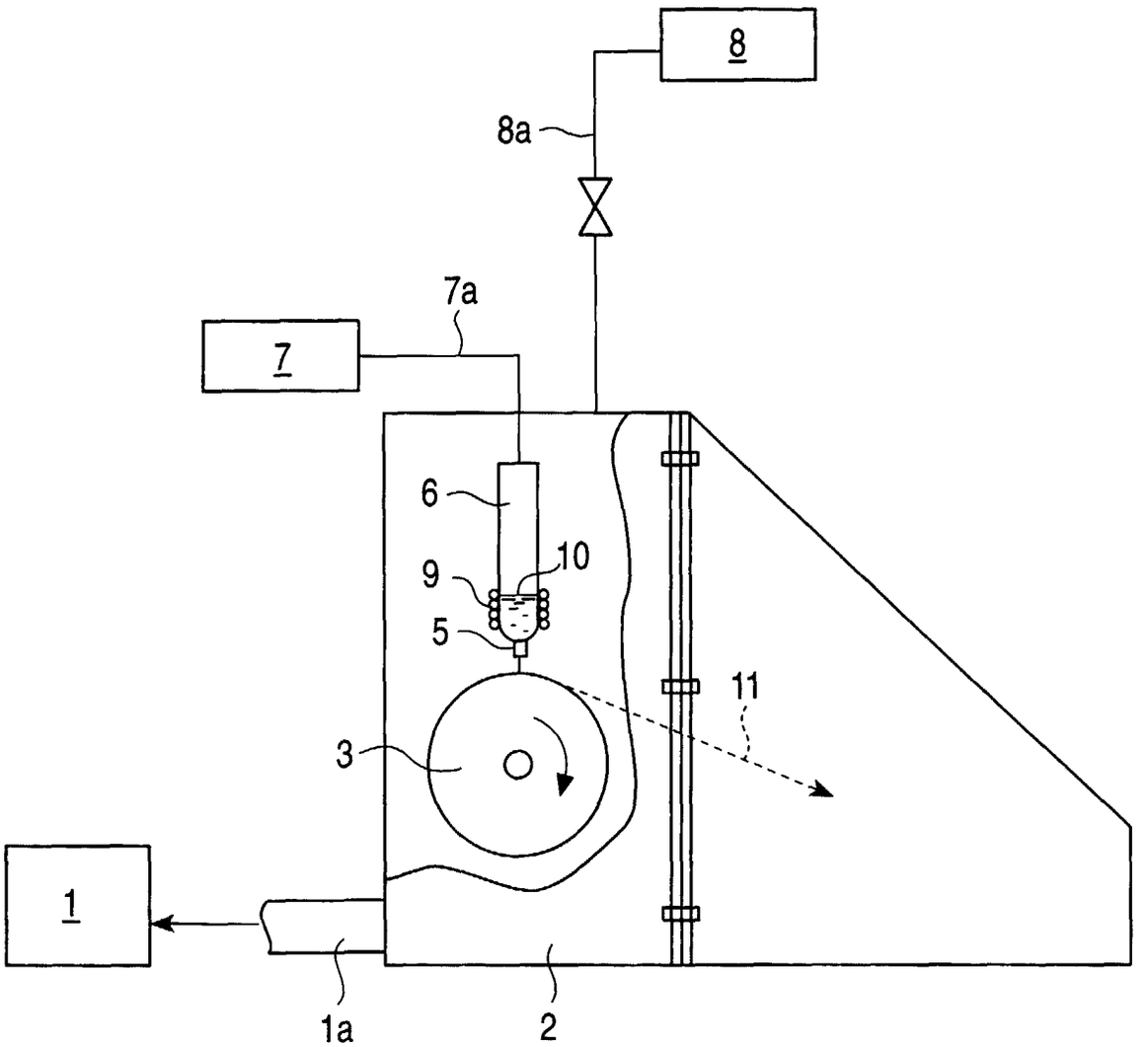

FIG. 2

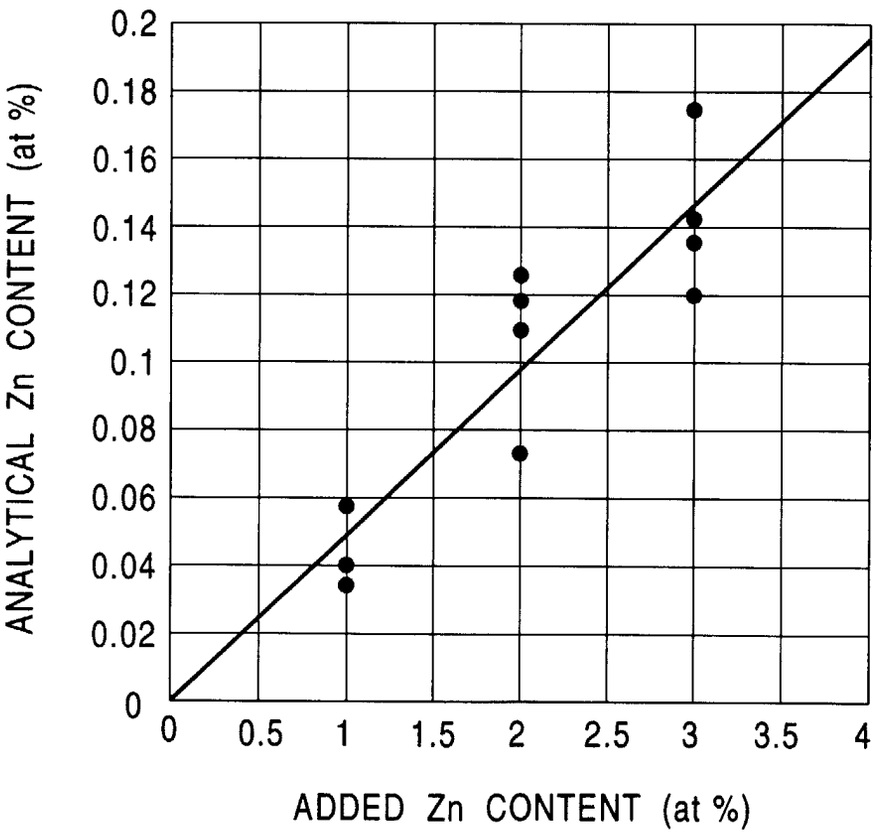
ANALYTICAL Zn CONTENT (at %)
0.2
0.18
0.16
0.14
0.12
0.1
0.08
0.06
0.04
0.02
0
0
0.5
1
1.5
2
2.5
3
3.5
4
ADDED Zn CONTENT (at %)

FIG. 3

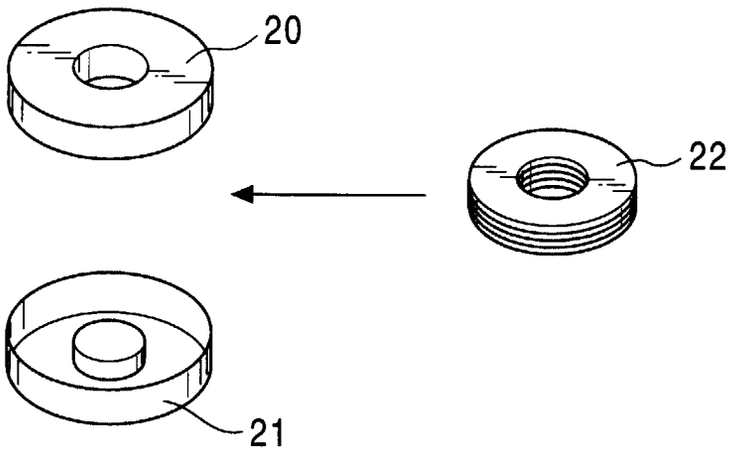

FIG. 4

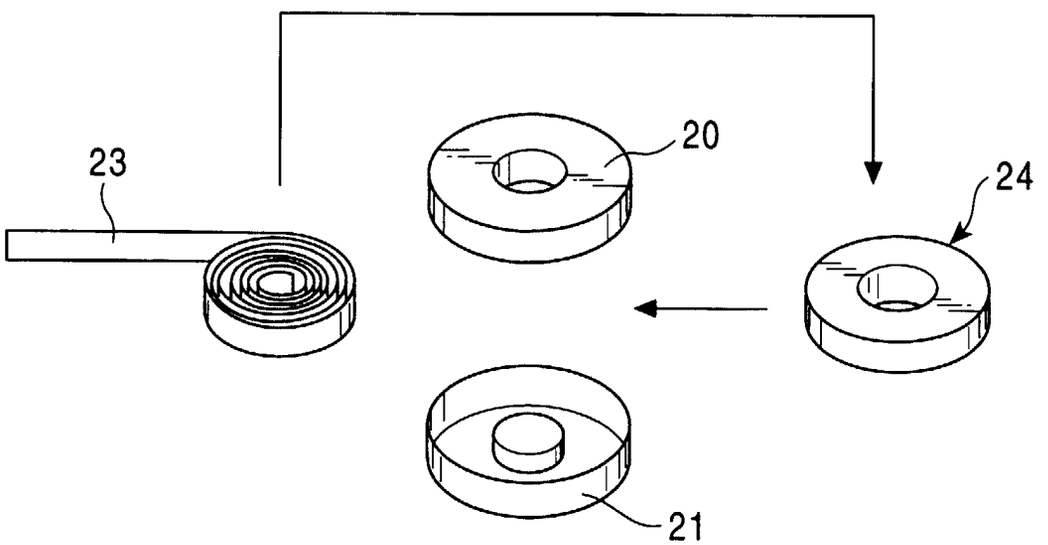

FIG. 5

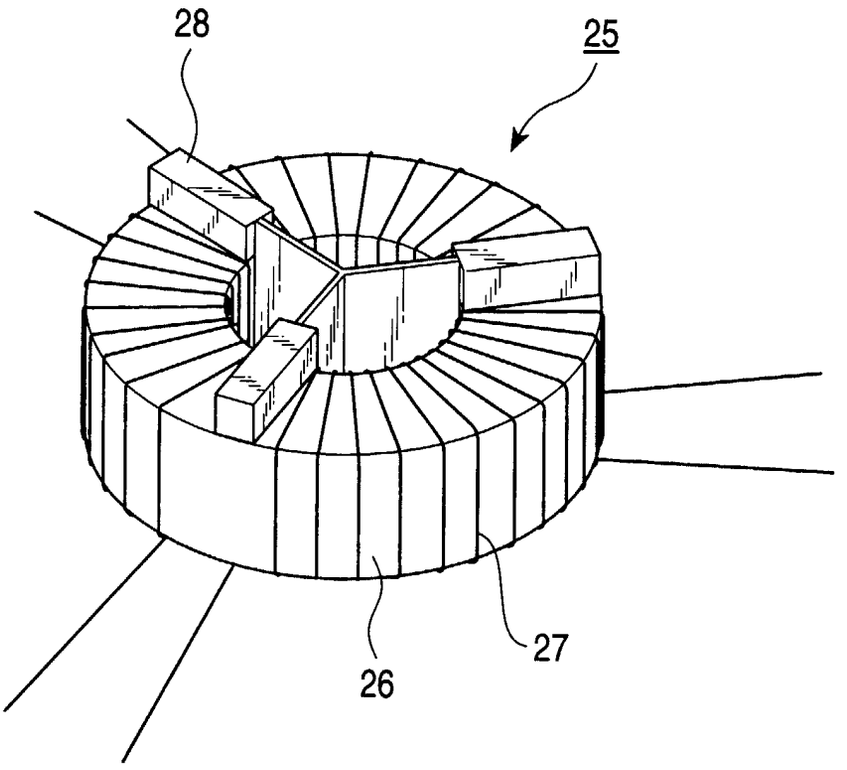

FIG. 6

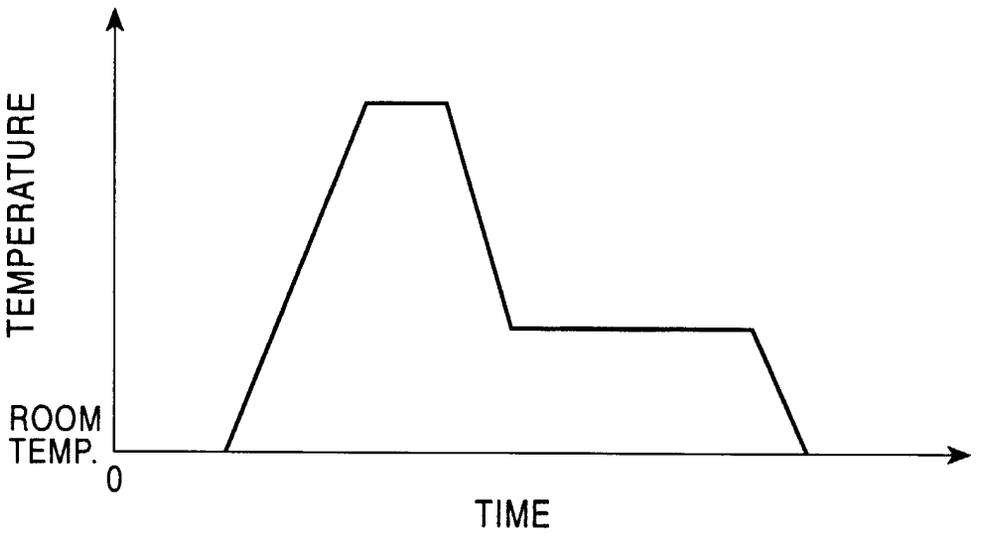

FIG. 7

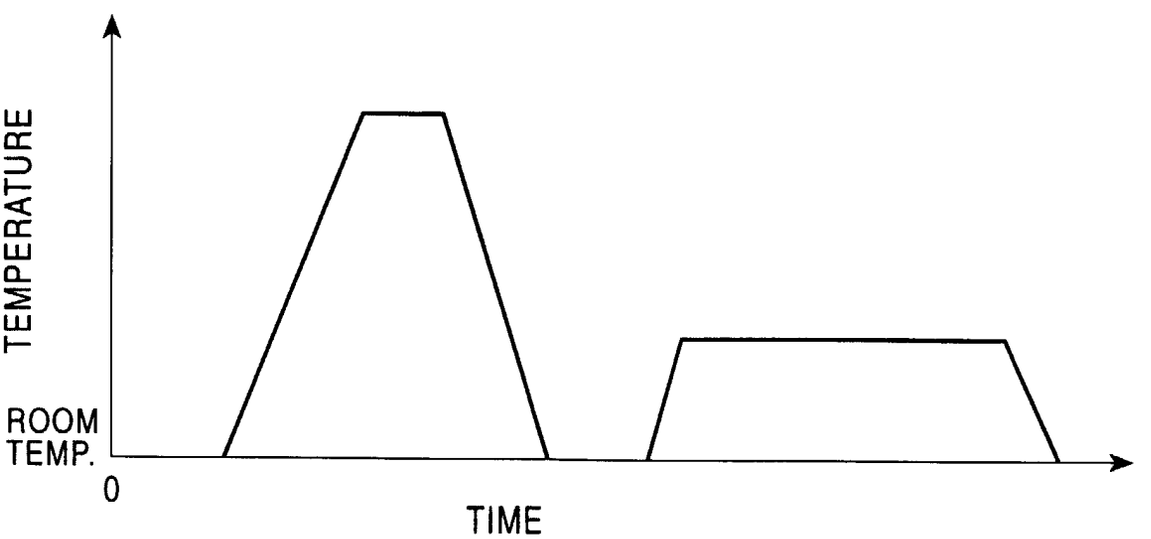

FIG. 8

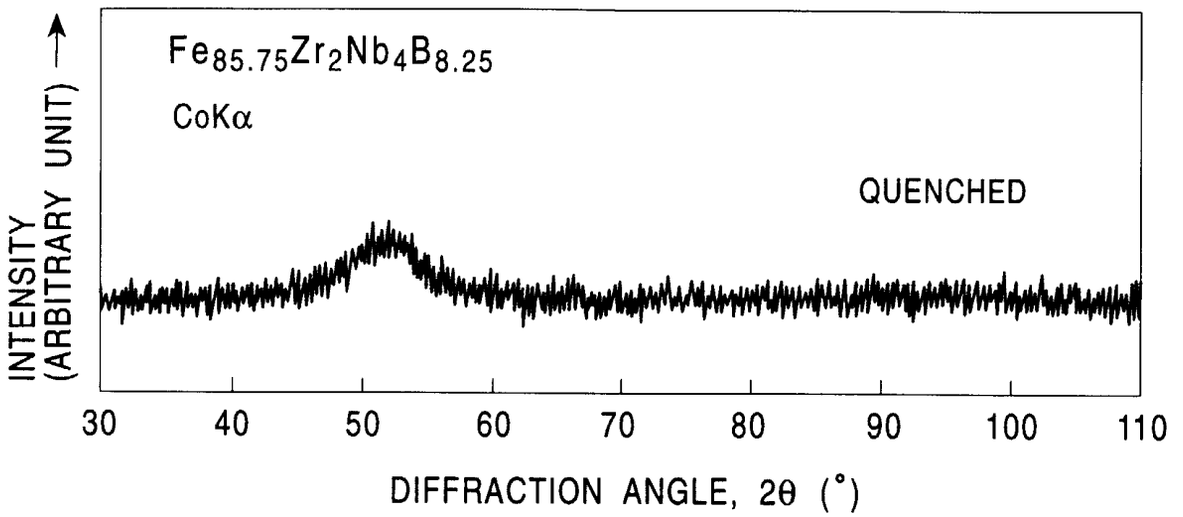
$Fe_{85.75}Zr_2Nb_4B_{8.25}$
CoKα
QUENCHED
INTENSITY (ARBITRARY UNIT)
30
40
50
60
70
80
90
100
110
DIFFRACTION ANGLE, 2θ (°)

FIG. 9

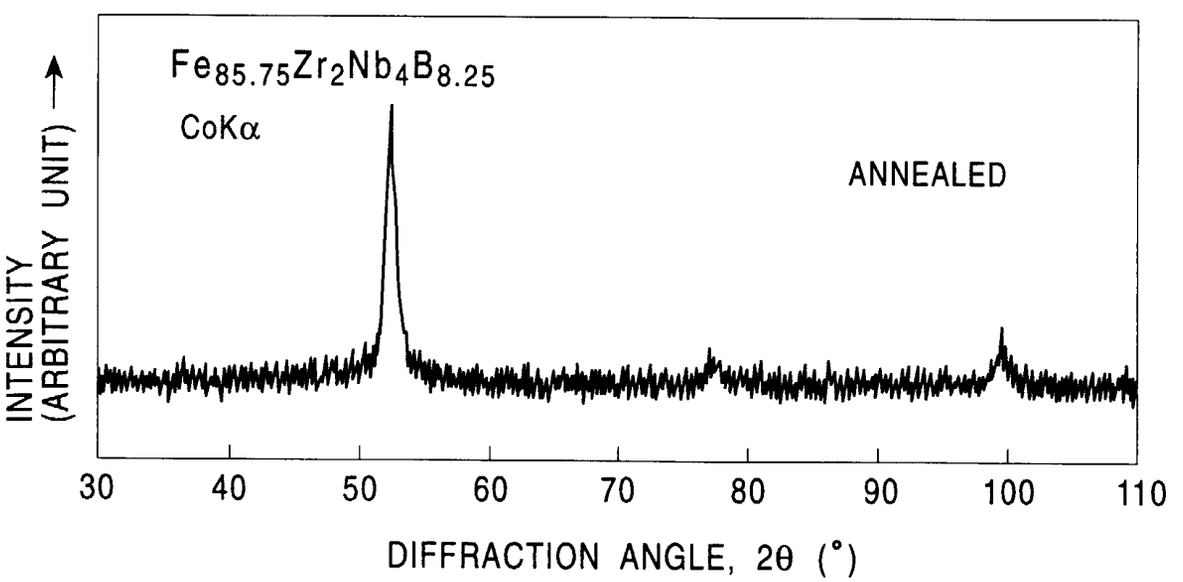
$Fe_{85.75}Zr_2Nb_4B_{8.25}$
CoKα
ANNEALED
INTENSITY (ARBITRARY UNIT)
30
40
50
60
70
80
90
100
110
DIFFRACTION ANGLE, 2θ (°)

FIG. 10

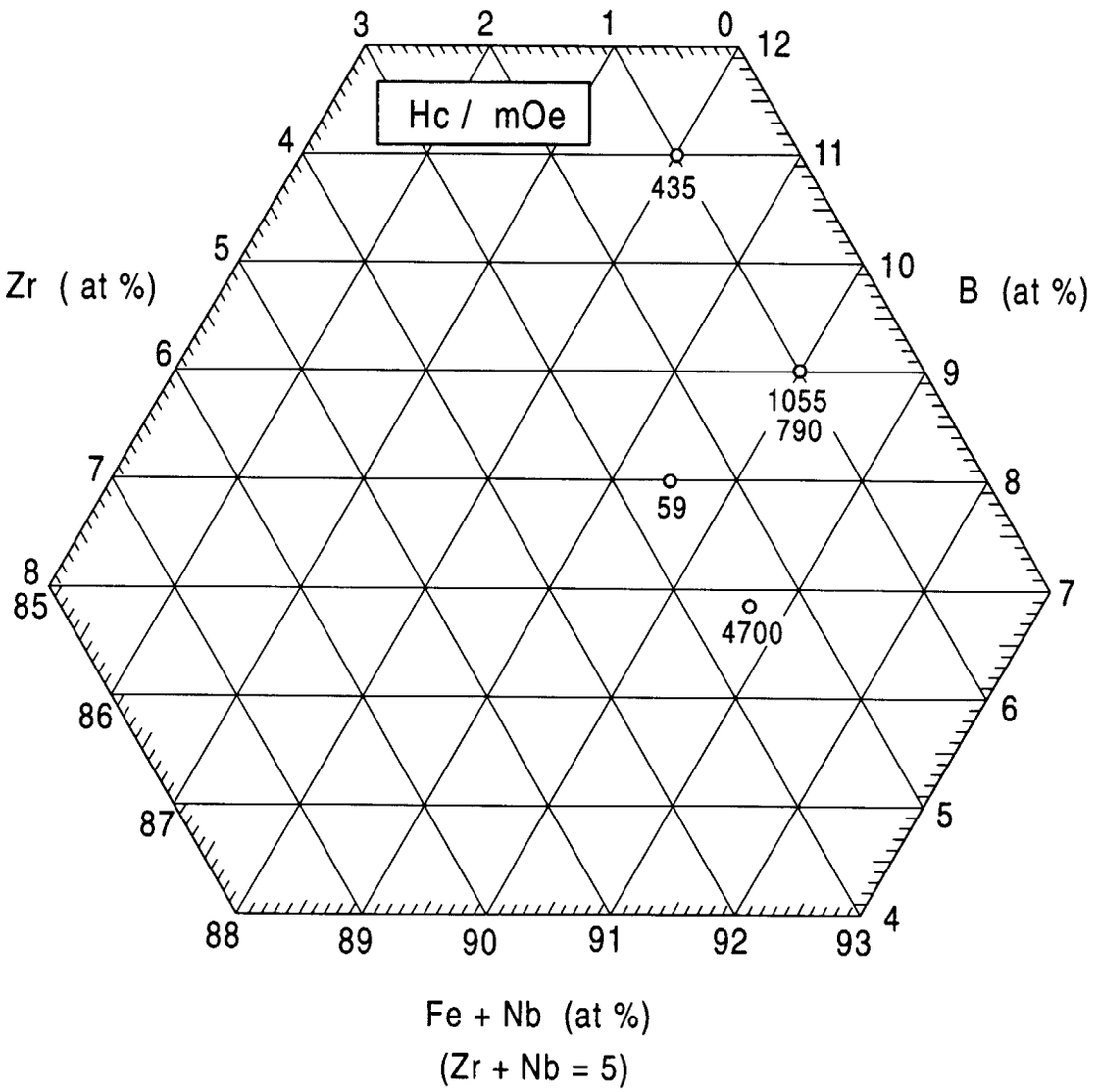
Hc / mOe
435
1055
790
59
4700
Zr (at %)
B (at %)
Fe + Nb (at %)
(Zr + Nb = 5)
3
2
1
0
12
4
11
5
10
6
9
7
8
8
85
7
86
6
87
5
88
89
90
91
92
93
4

FIG. 11

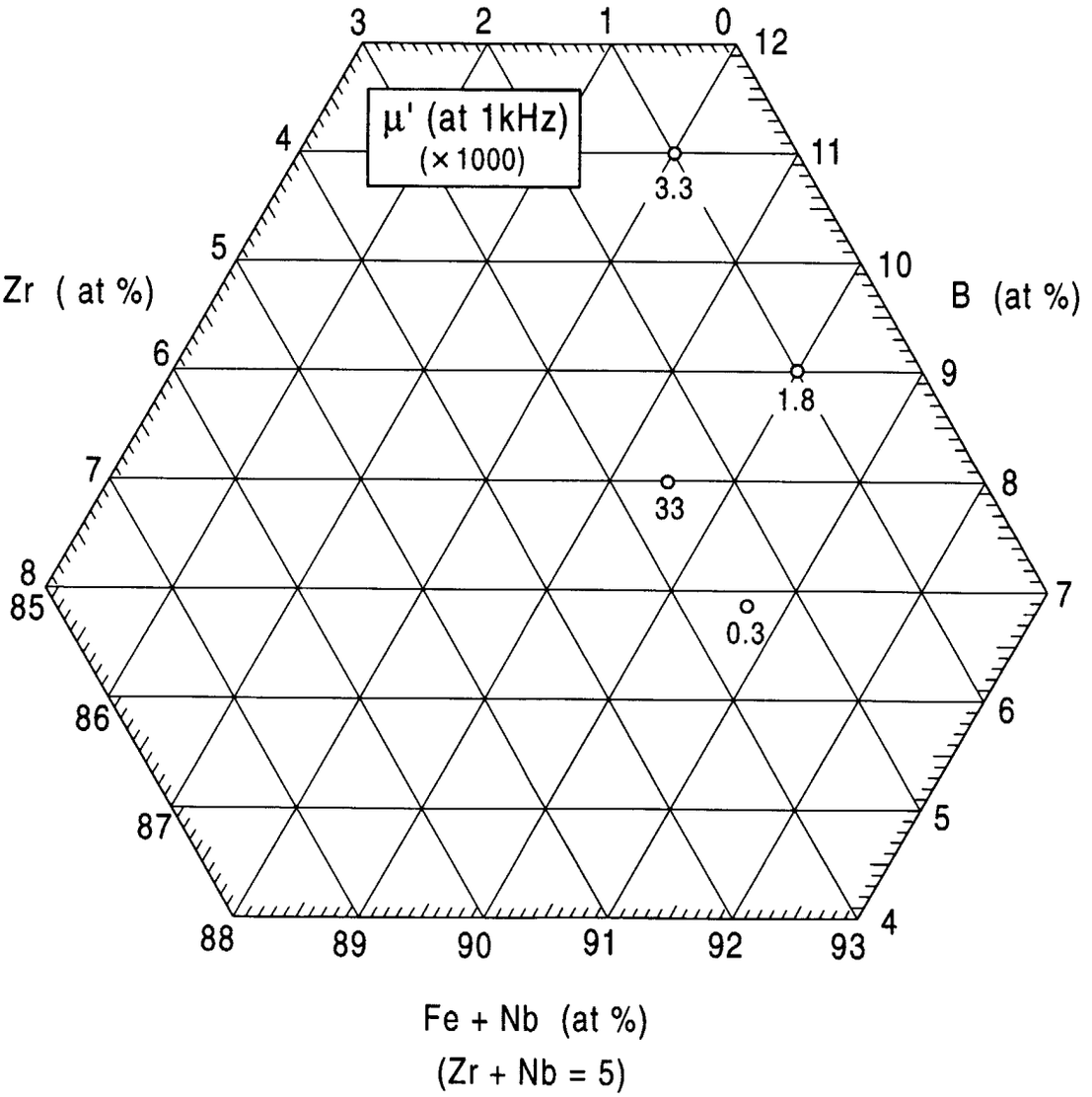
μ' (at 1kHz)
(×1000)
3.3
1.8
33
0.3
Zr (at %)
B (at %)
Fe + Nb (at %)
(Zr + Nb = 5)
3
2
1
0
12
11
10
9
8
7
6
5
4
85
86
87
88
89
90
91
92
93

FIG. 12

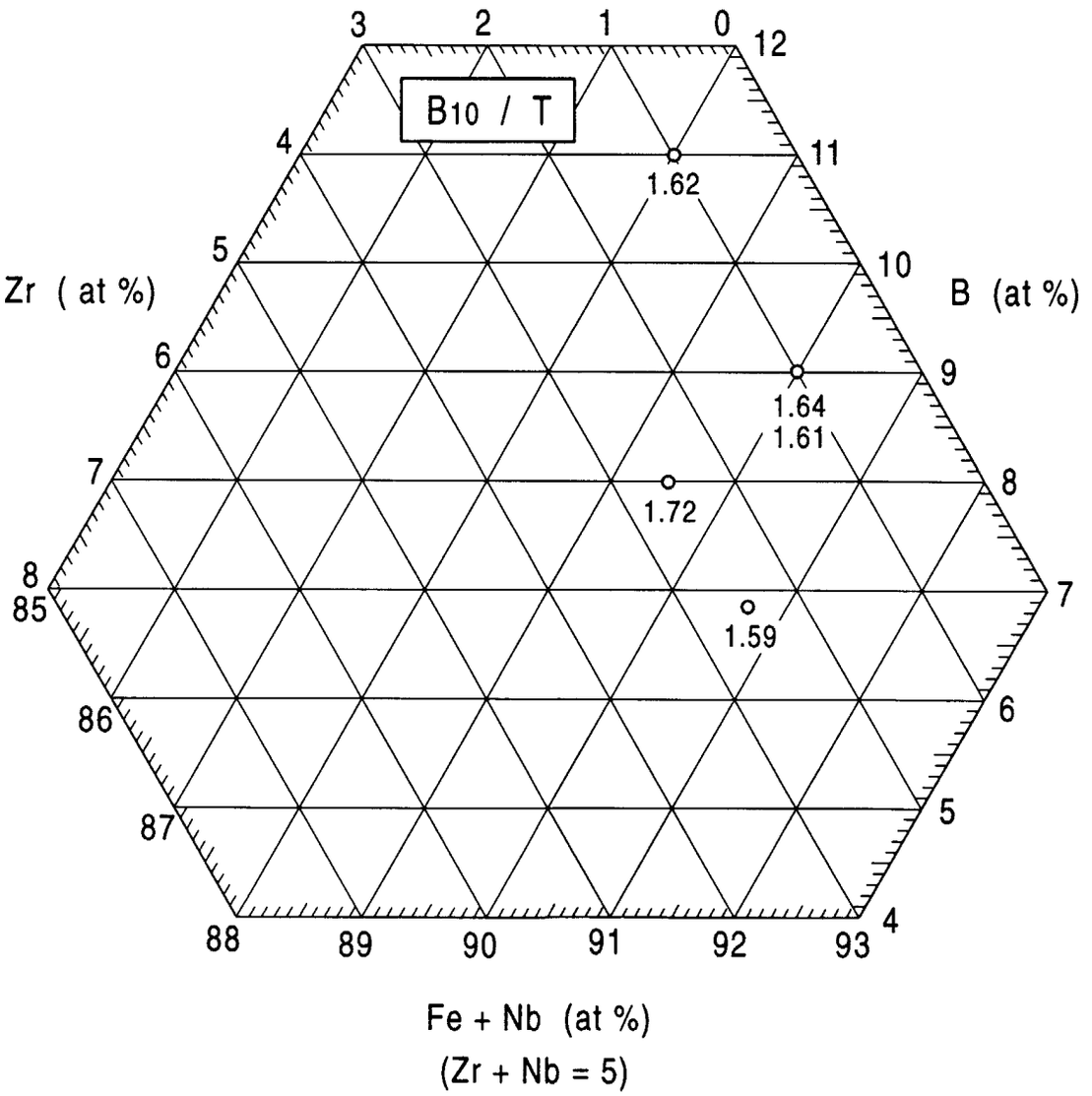
B10 / T
1.62
1.64
1.61
1.72
1.59
Zr (at %)
B (at %)
Fe + Nb (at %)
(Zr + Nb = 5)
3
2
1
0
12
4
11
5
10
6
9
7
8
8
85
7
86
6
87
5
88
89
90
91
92
93
4

FIG. 13

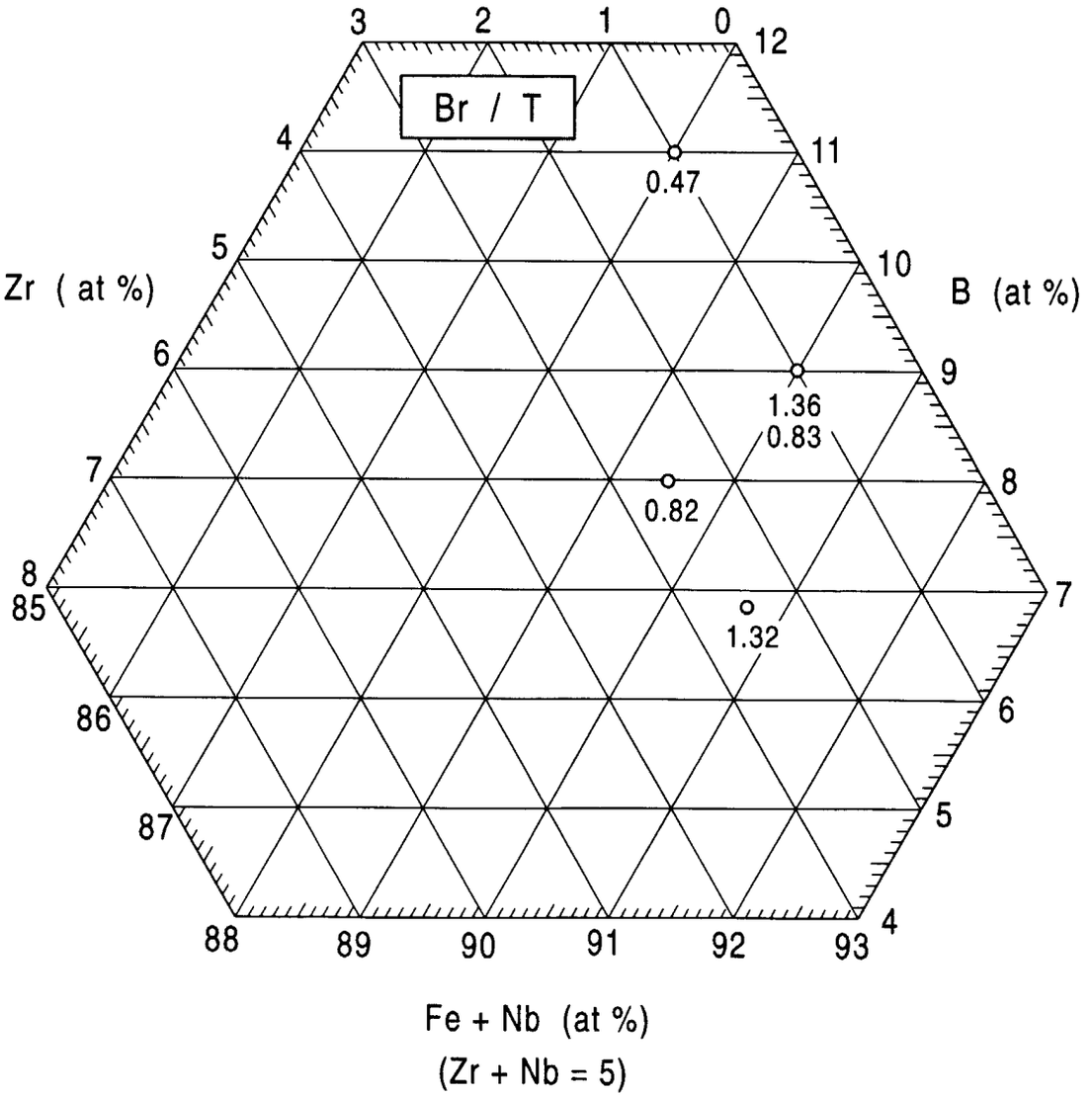
Br / T
0.47
1.36
0.83
0.82
1.32
Zr (at %)
B (at %)
Fe + Nb (at %)
(Zr + Nb = 5)
3
2
1
0
12
4
11
5
10
6
9
7
8
8
85
7
86
6
87
5
88
89
90
91
92
93
4

FIG. 14

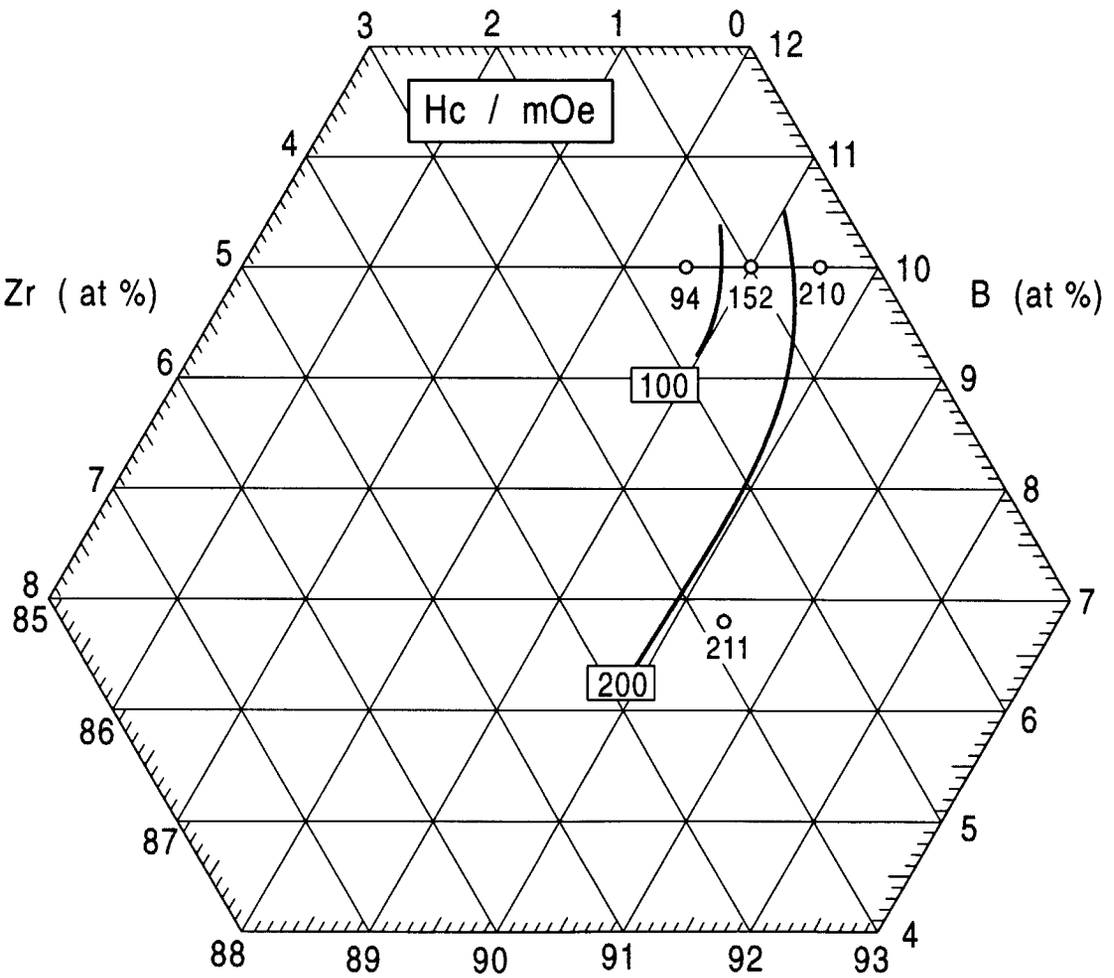
Hc / mOe
Zr (at %)
B (at %)
Fe + Nb (at %)
(Zr + Nb = 5.5)
94
152
210
211
100
200
3
2
1
0
12
4
11
5
10
6
9
7
8
8
7
85
6
86
5
87
4
88
89
90
91
92
93

FIG. 15

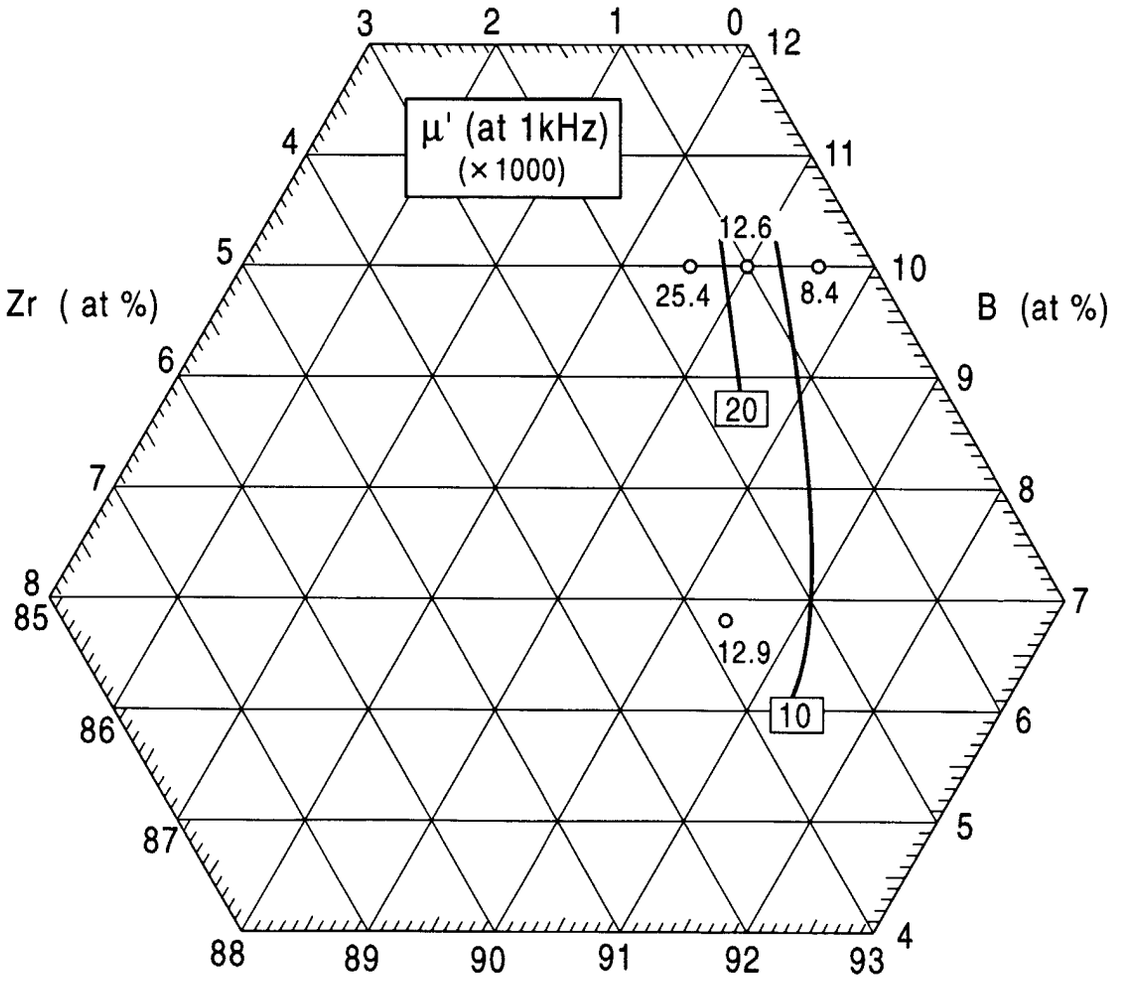

FIG. 16

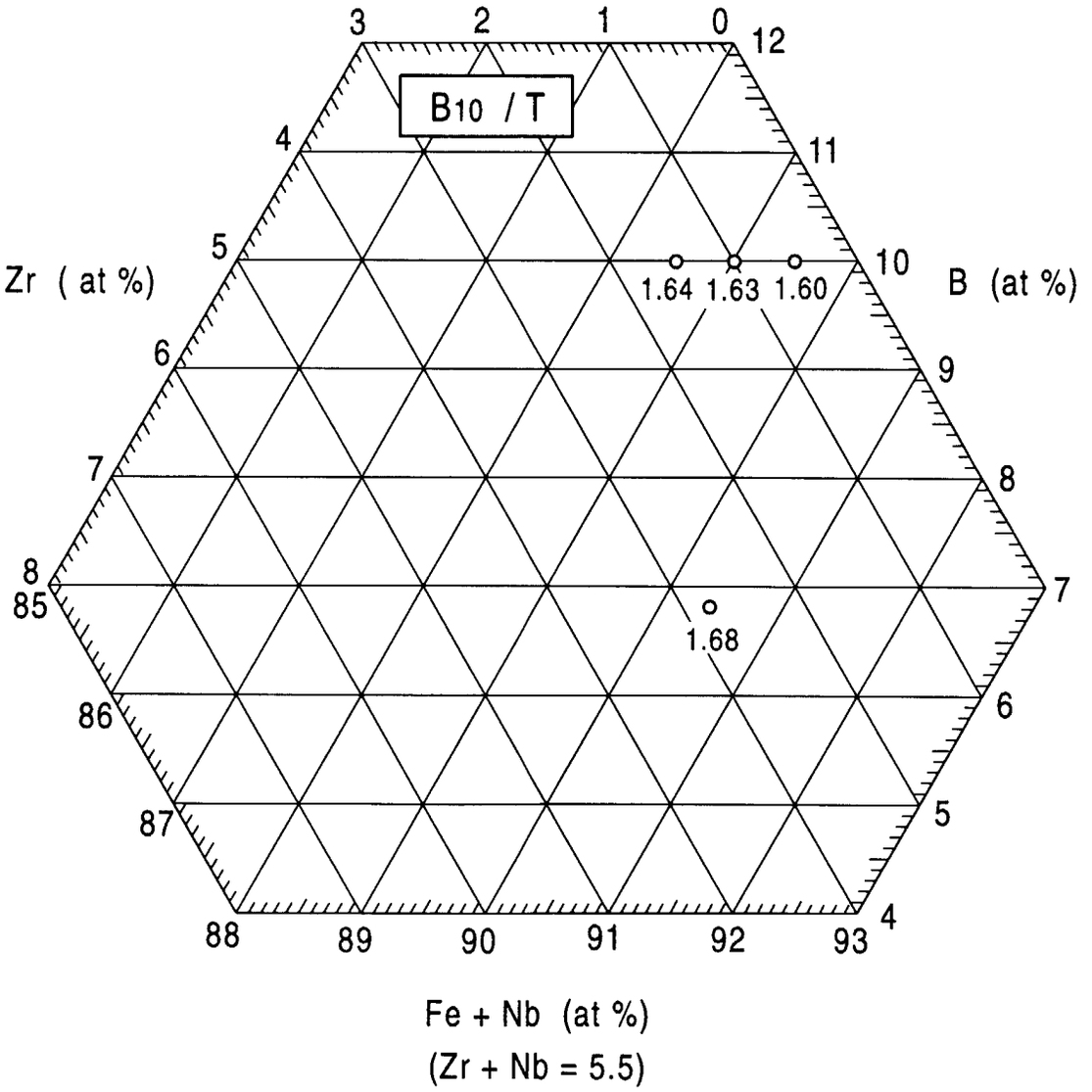
B10 / T
Zr (at %)
B (at %)
Fe + Nb (at %)
(Zr + Nb = 5.5)
1.64
1.63
1.60
1.68
3
2
1
0
12
4
11
5
10
6
9
7
8
8
7
85
6
86
5
87
4
88
89
90
91
92
93

FIG. 17

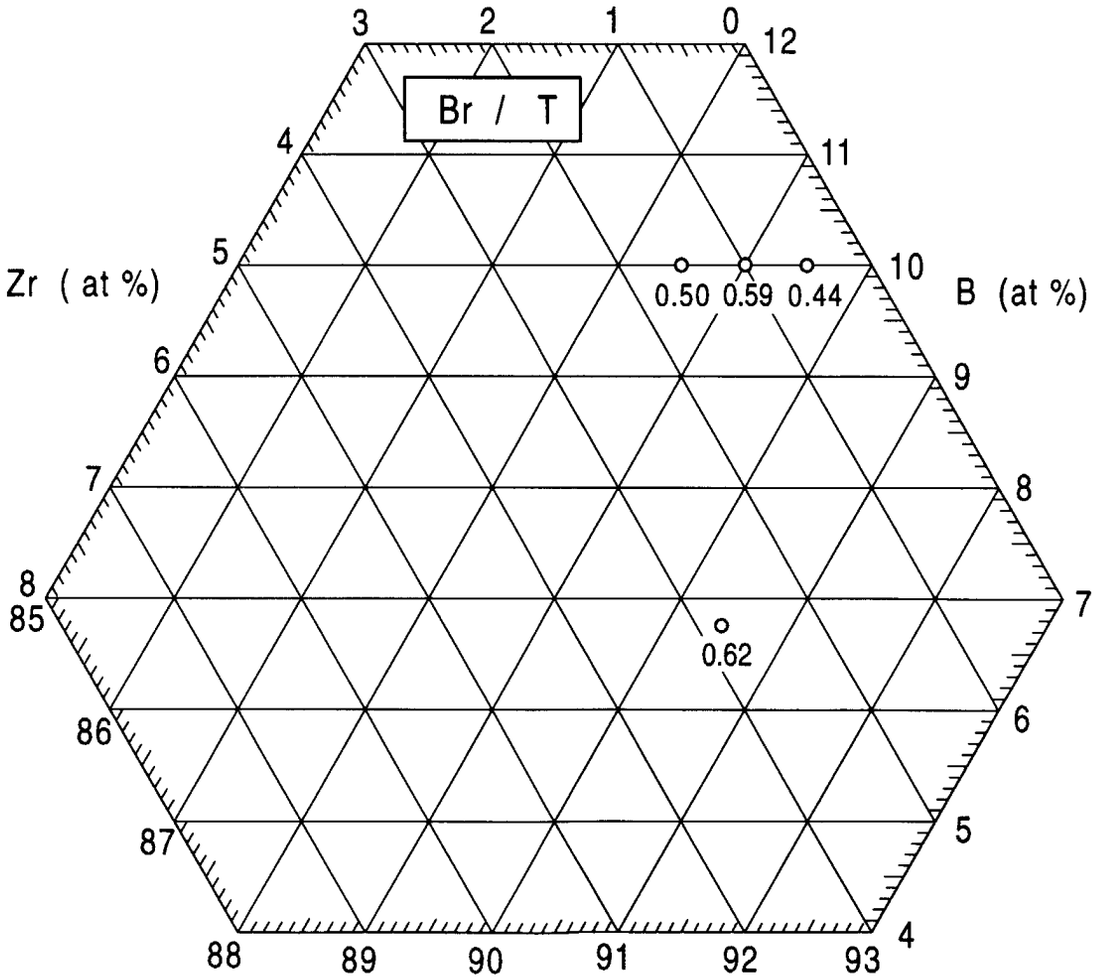
Br / T
3
2
1
0
12
4
11
5
10
6
9
7
8
8
7
85
86
87
88
89
90
91
92
93
6
5
4
0.50
0.59
0.44
0.62
Zr (at %)
B (at %)
Fe + Nb (at %)
(Zr + Nb = 5.5)

FIG. 18

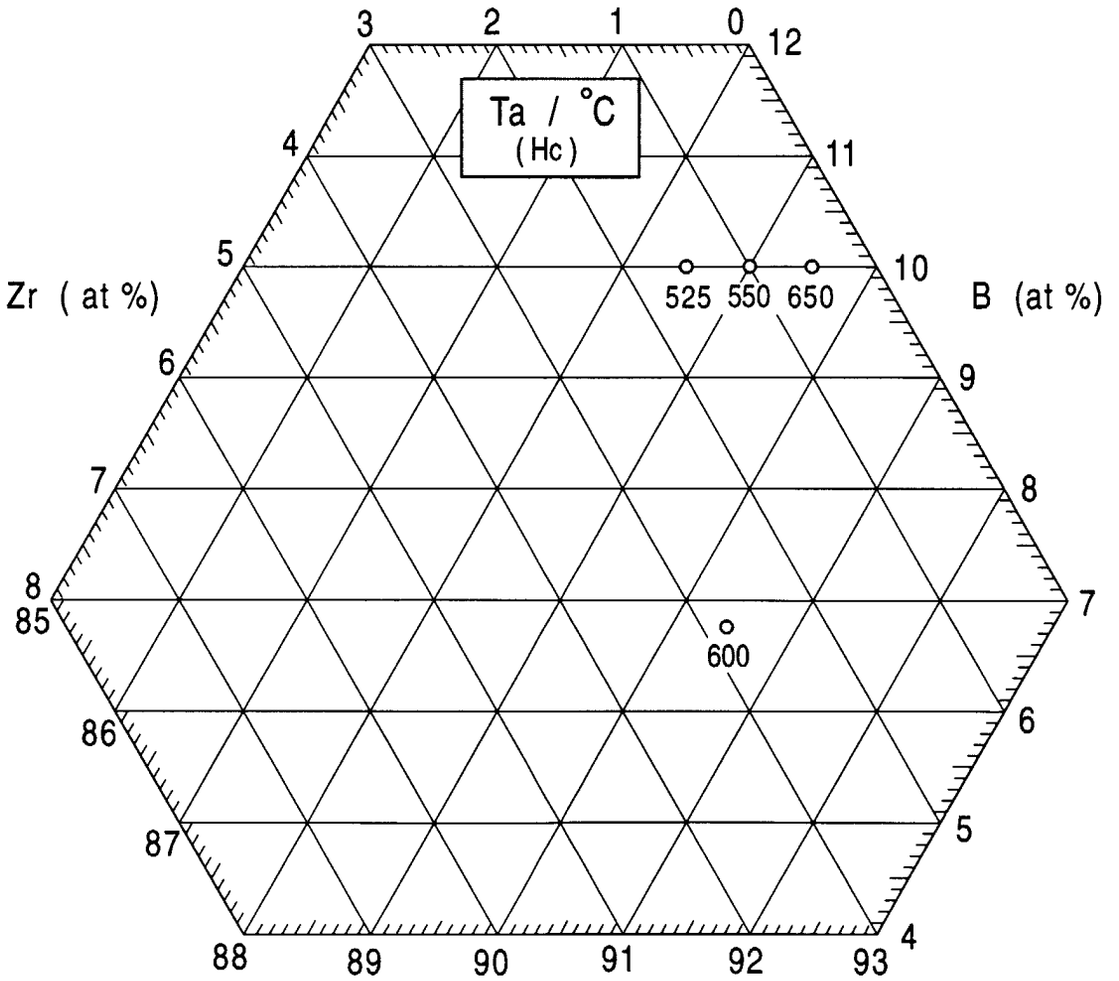

FIG. 19

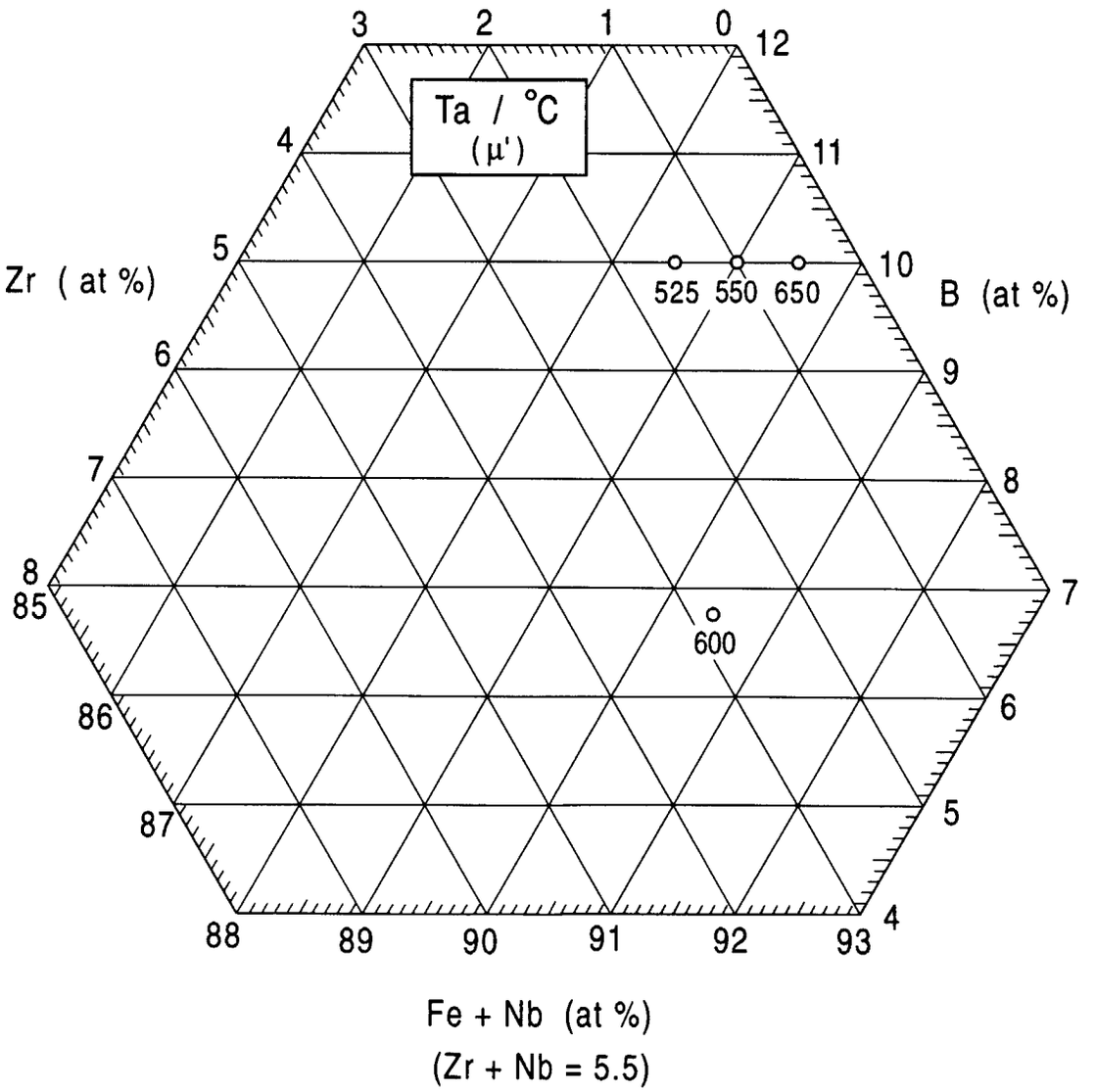

FIG. 20

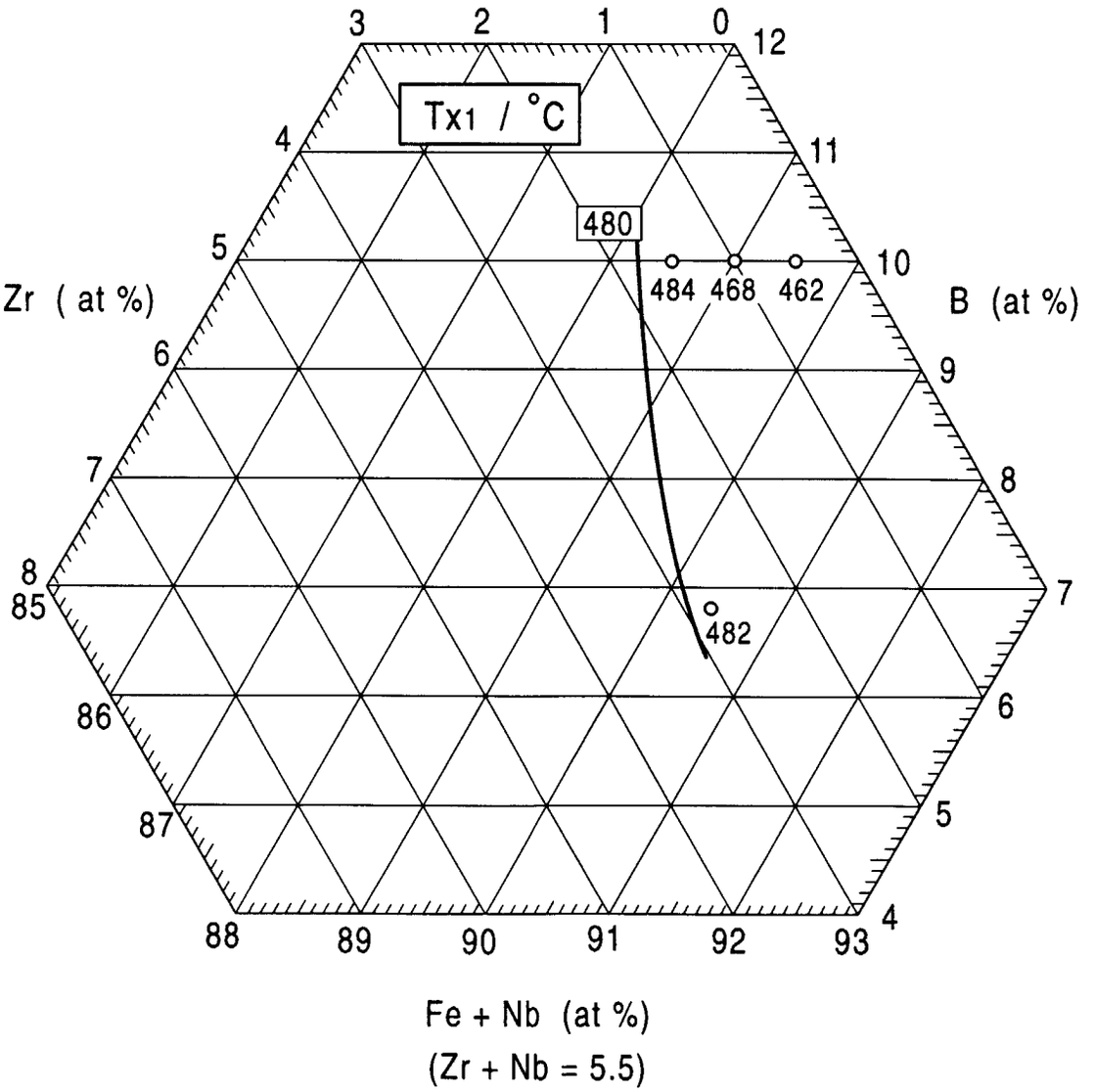
Tx1 / °C
480
484
468
462
482
Zr (at %)
B (at %)
Fe + Nb (at %)
(Zr + Nb = 5.5)
3
2
1
0
12
4
11
5
10
6
9
7
8
8
7
85
86
6
87
5
88
89
90
91
92
93
4

FIG. 21

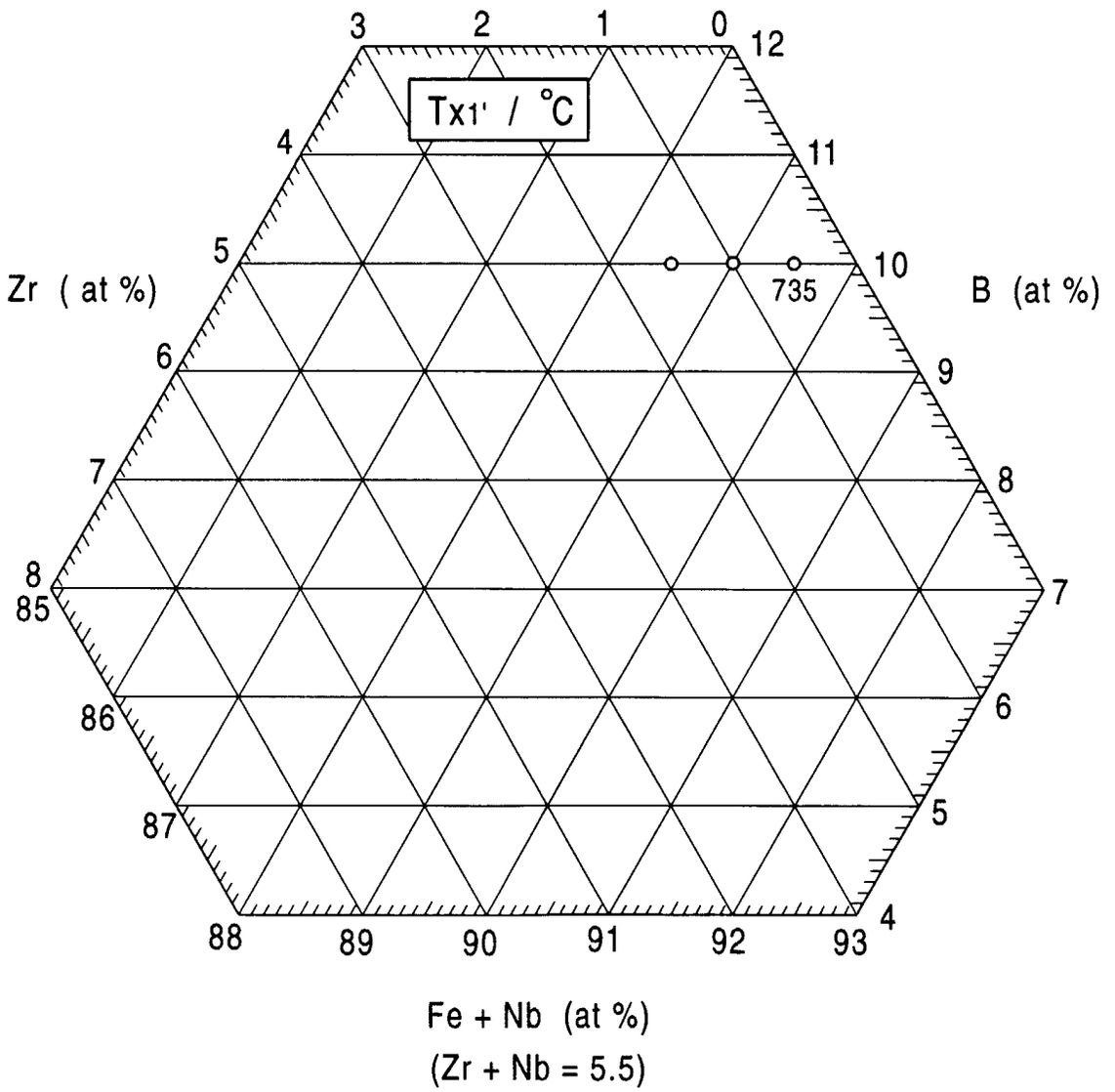
Tx1' / °C
735
Zr (at %)
B (at %)
Fe + Nb (at %)
(Zr + Nb = 5.5)
3
2
1
0
12
4
11
5
10
6
9
7
8
8
85
86
87
88
89
90
91
92
93
7
6
5
4

FIG. 22

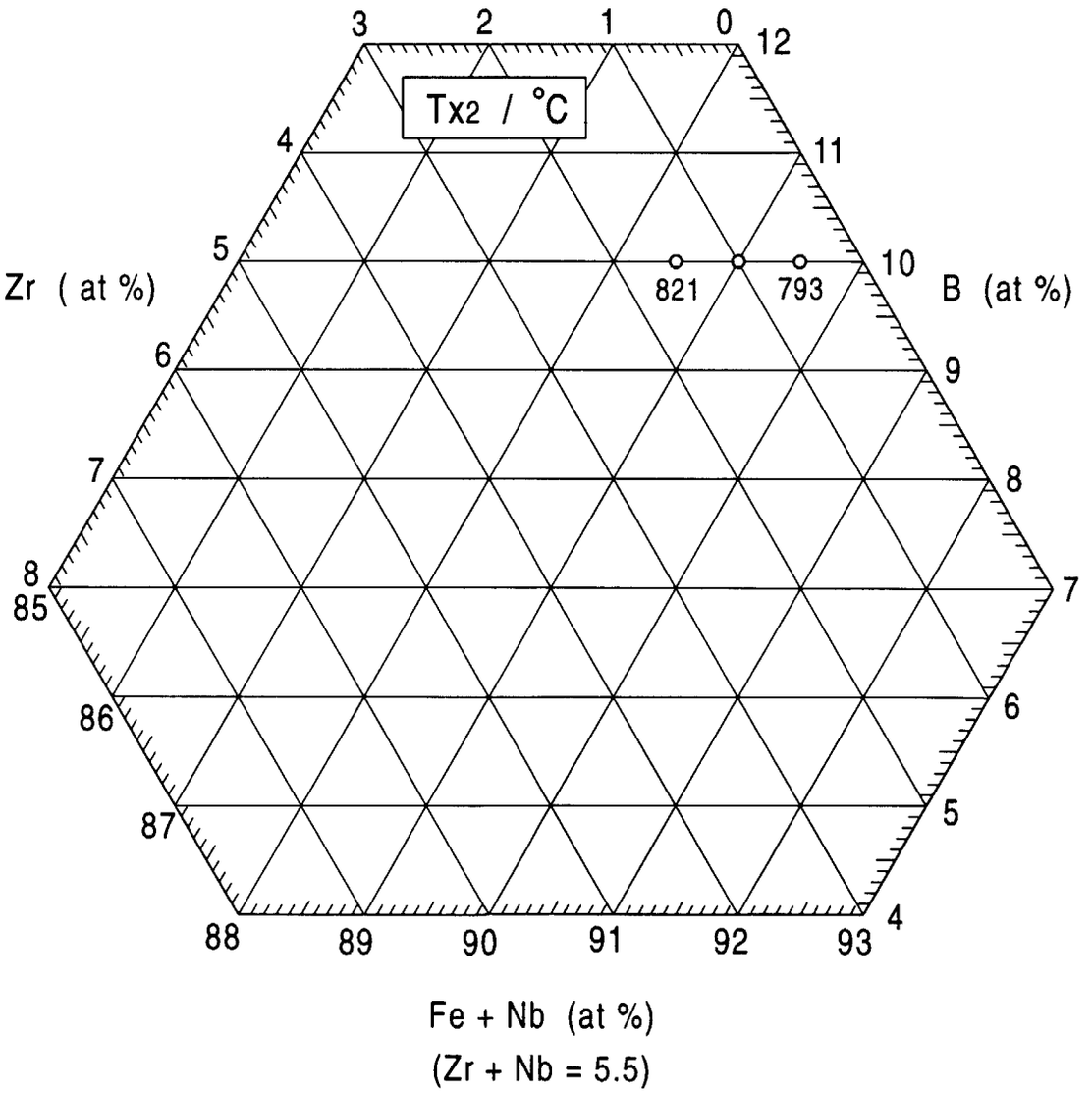

FIG. 23

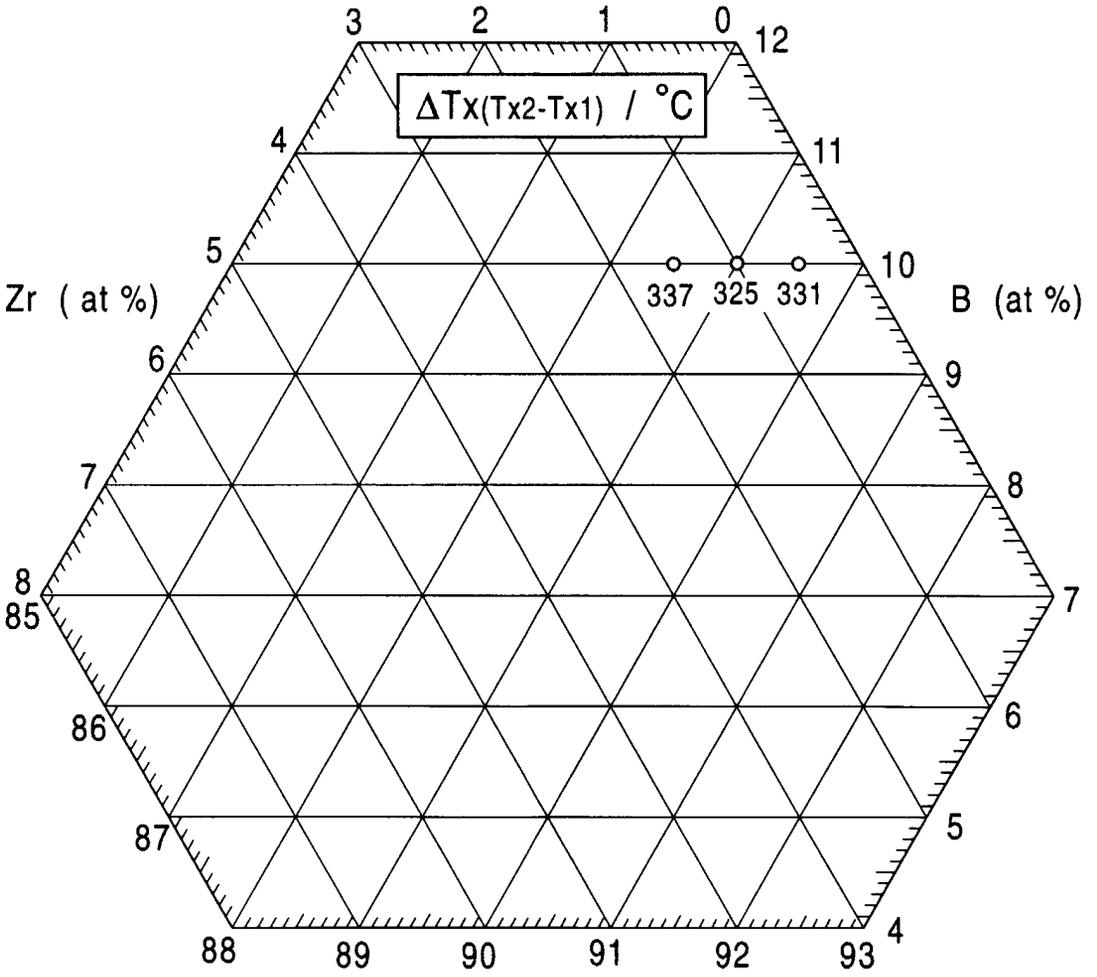
ΔTx(Tx2-Tx1) / °C
3
2
1
0
12
4
11
5
10
337
325
331
Zr (at %)
B (at %)
6
9
7
8
8
85
7
86
6
87
5
4
88
89
90
91
92
93
Fe + Nb (at %)
(Zr + Nb = 5.5)

FIG. 24

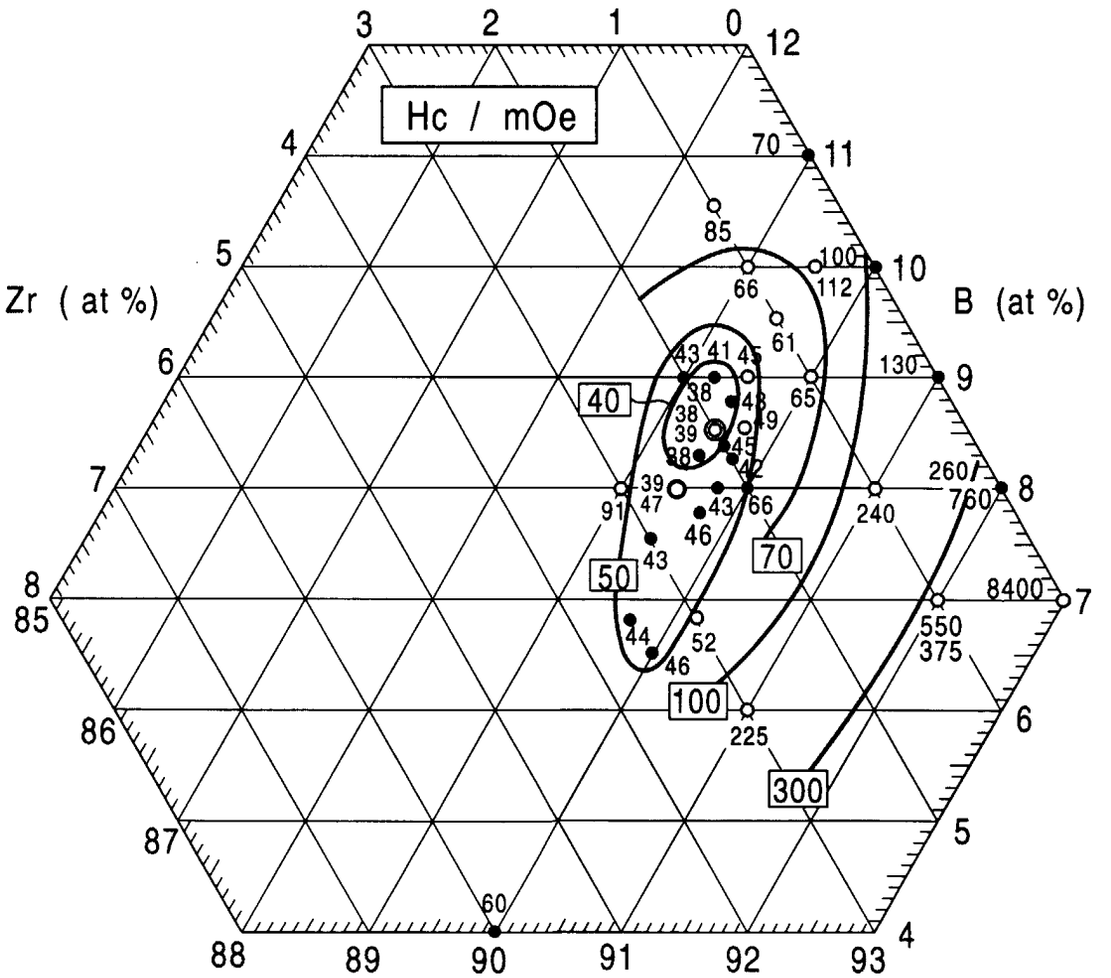
Hc / mOe
Zr (at %)
B (at %)
Fe + Nb (at %)
(Zr + Nb = 6)
40
50
70
100
300
3
2
1
0
12
11
10
9
8
7
6
5
4
85
86
87
88
89
90
91
92
93
70
85
100
112
66
61
130
65
43
41
45
38
48
39
49
45
38
42
39
91
47
43
66
46
240
260/
760
43
8400
44
52
46
550
375
225
60

FIG. 25

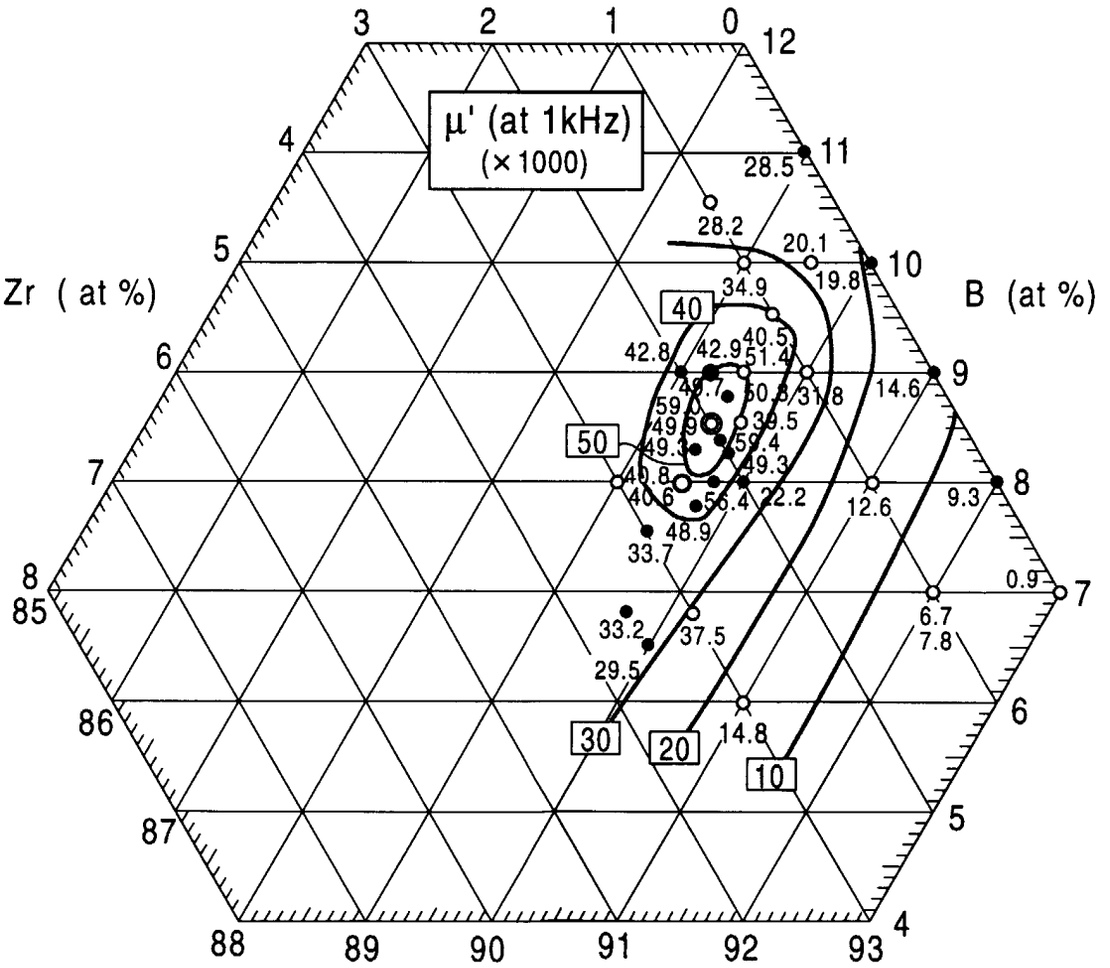
μ' (at 1kHz)
(×1000)
Zr (at %)
B (at %)
Fe + Nb (at %)
(Zr + Nb = 6)
40
50
30
20
10
28.5
28.2
20.1
19.8
34.9
42.8
42.9
40.5
51.4
14.6
39.5
49.3
40.8
40.6
56.4
22.2
12.6
9.3
48.9
33.7
0.9
33.2
37.5
6.7
7.8
29.5
14.8

FIG. 26

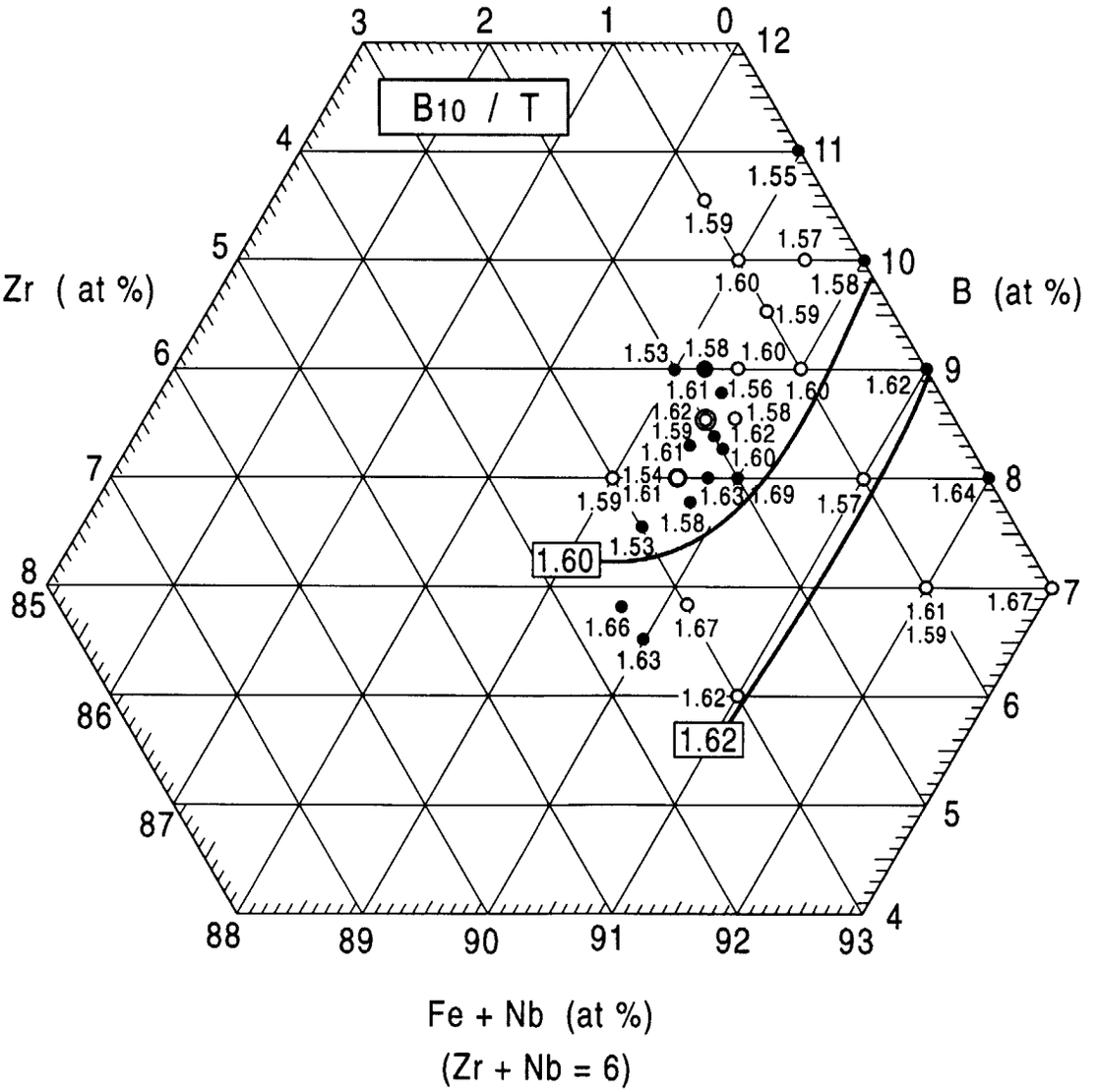

FIG. 27

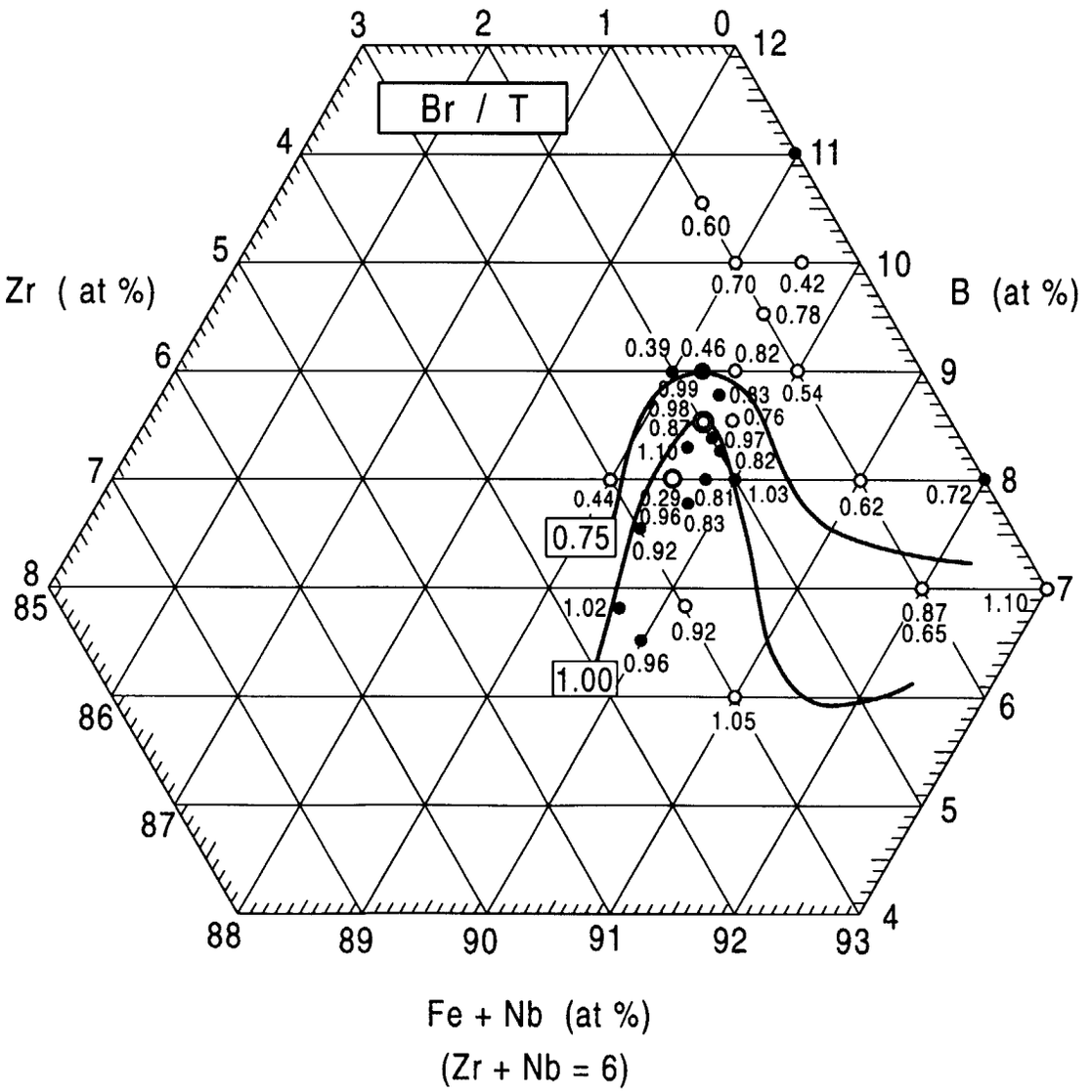
Br / T
Zr (at %)
B (at %)
Fe + Nb (at %)
(Zr + Nb = 6)
0.75
1.00
0.60
0.70
0.42
0.78
0.39
0.46
0.82
0.99
0.83
0.54
0.98
0.76
0.87
0.97
1.10
0.82
0.44
0.29
0.81
1.03
0.62
0.72
0.96
0.83
0.92
1.02
0.92
0.87
1.10
0.65
0.96
1.05

FIG. 28

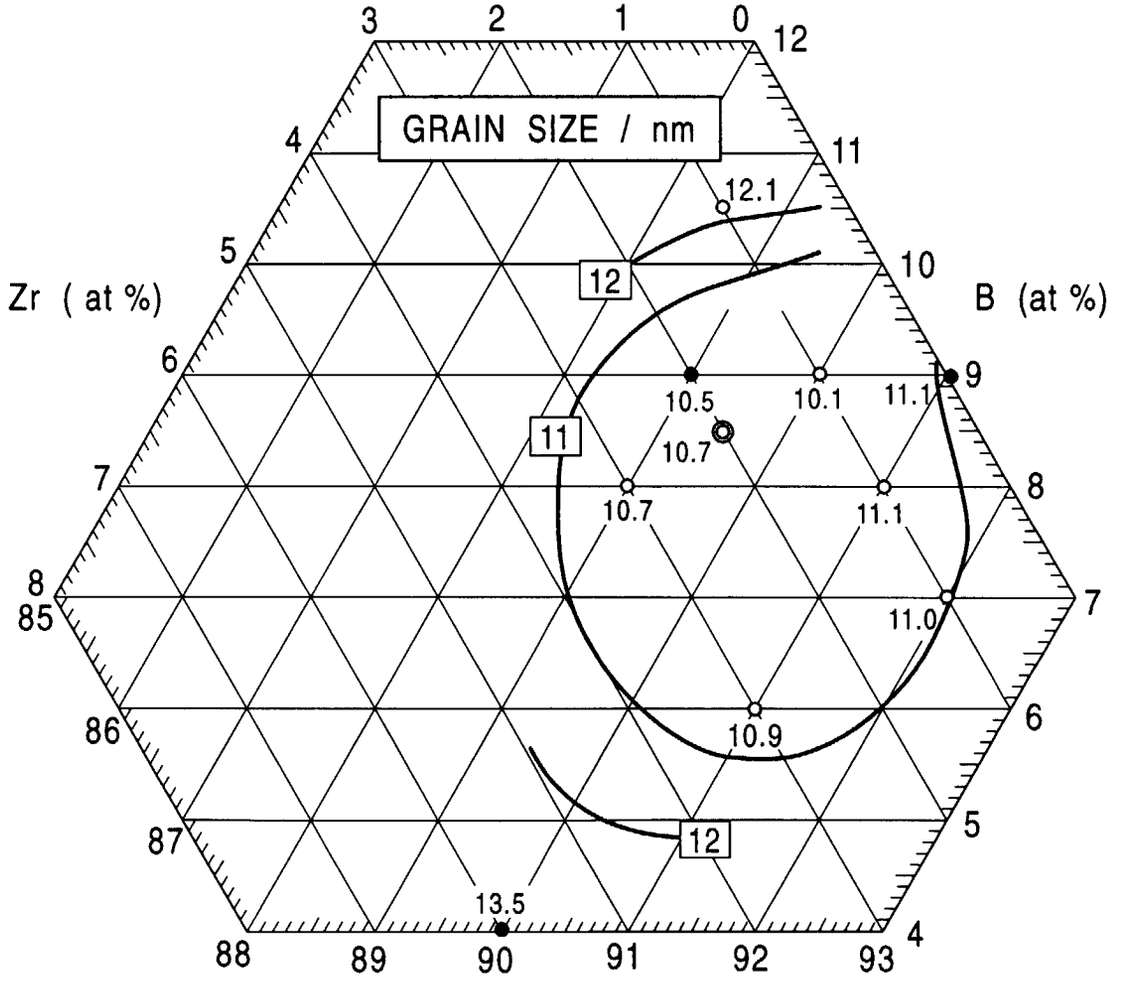
GRAIN SIZE / nm
Zr (at %)
B (at %)
Fe + Nb (at %)
(Zr + Nb = 6)
12
11
12
12.1
10.5
10.1
11.1
10.7
10.7
11.1
11.0
10.9
13.5
3
2
1
0
12
4
11
5
10
6
9
7
8
8
85
7
86
6
87
5
88
89
90
91
92
93
4

FIG. 29

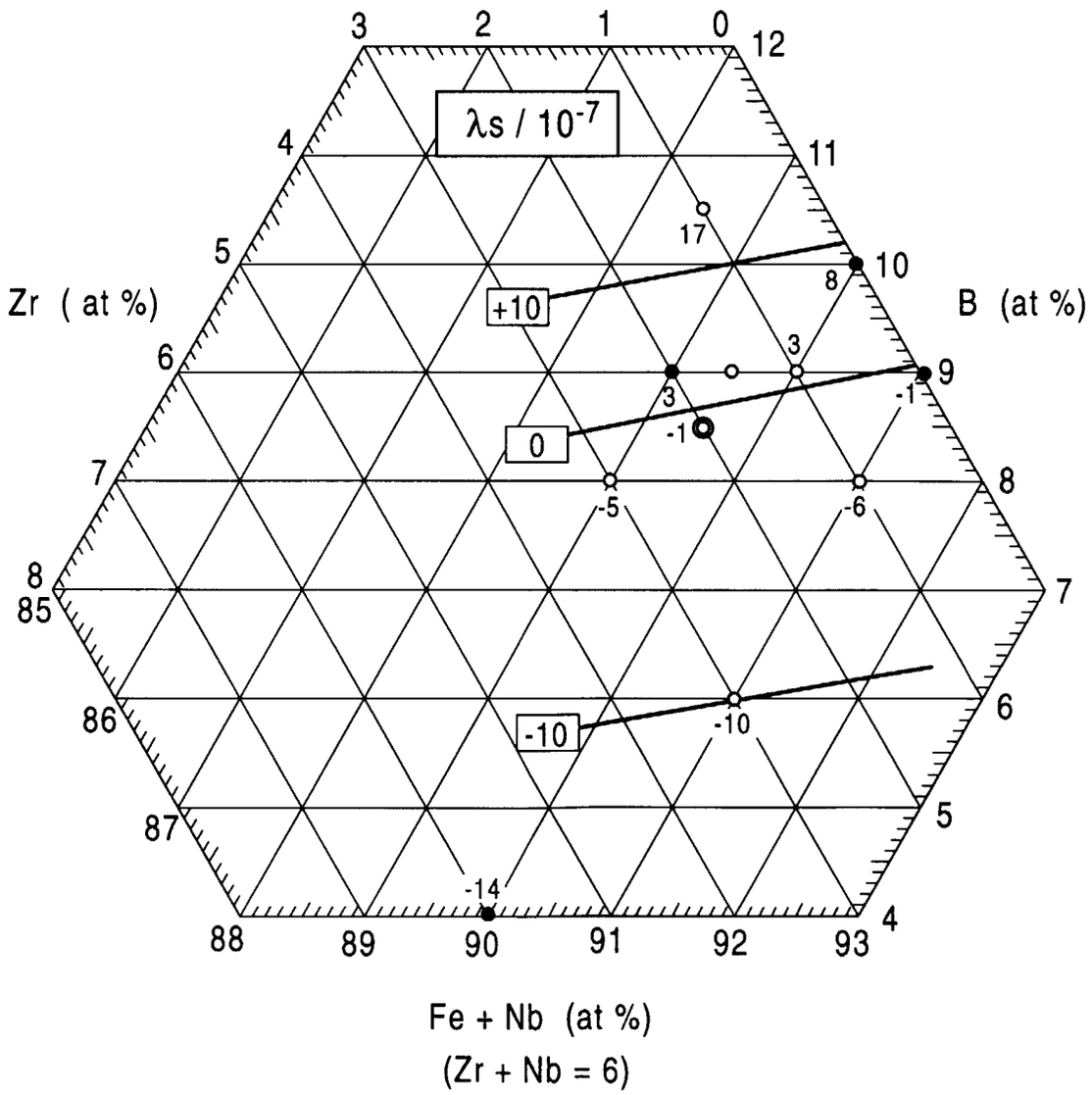
λs / 10^-7
+10
0
-10
17
8
3
3
-1
-1
-5
-6
-10
-14
Zr (at %)
B (at %)
Fe + Nb (at %)
(Zr + Nb = 6)
3
2
1
0
12
4
11
5
10
6
9
7
8
8
85
7
86
6
87
5
88
89
90
91
92
93
4

FIG. 30

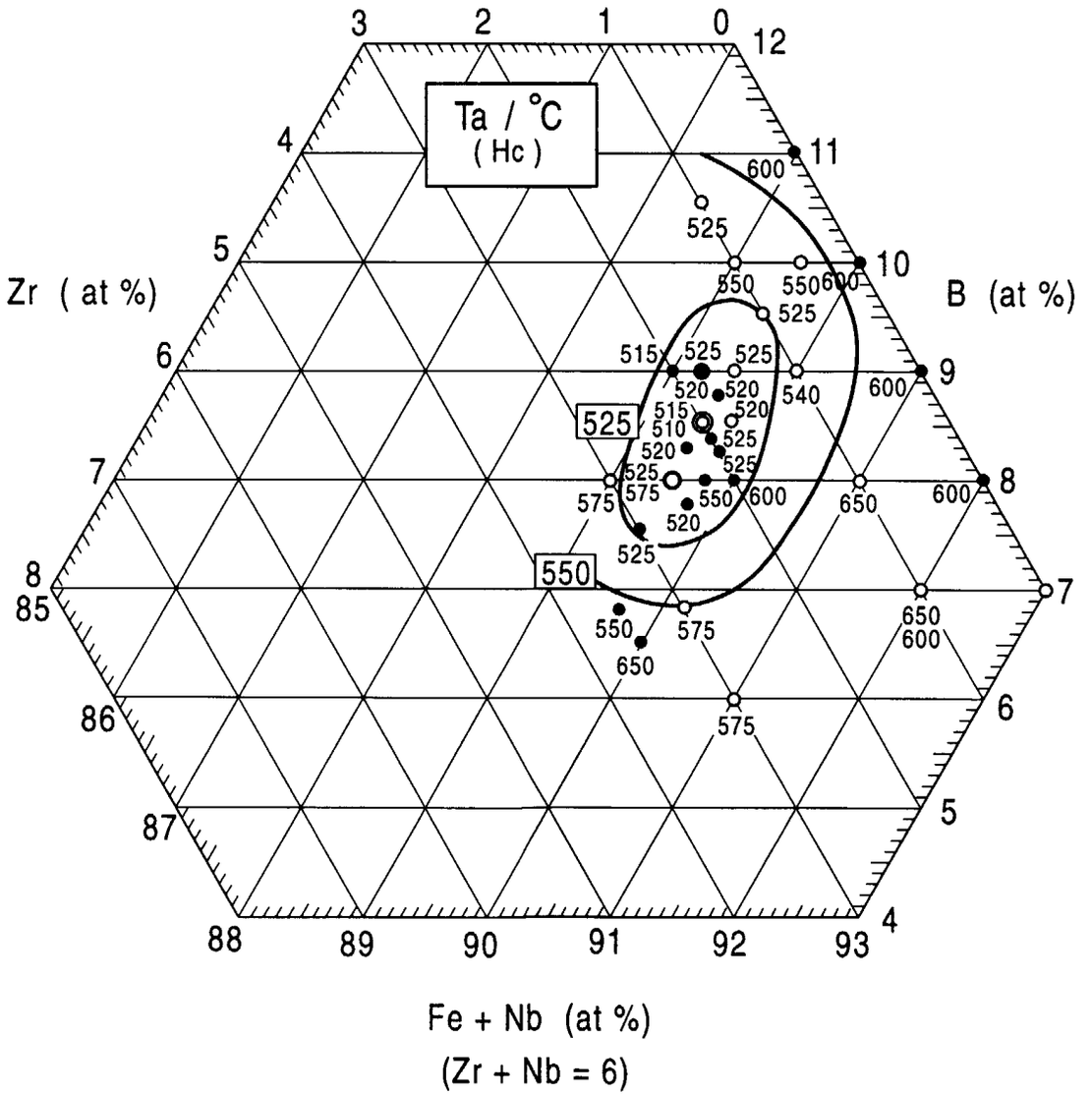
Ta / °C
(Hc)
525
550
Zr (at %)
B (at %)
Fe + Nb (at %)
(Zr + Nb = 6)
3
2
1
0
12
11
10
9
8
7
6
5
4
85
86
87
88
89
90
91
92
93

FIG. 31

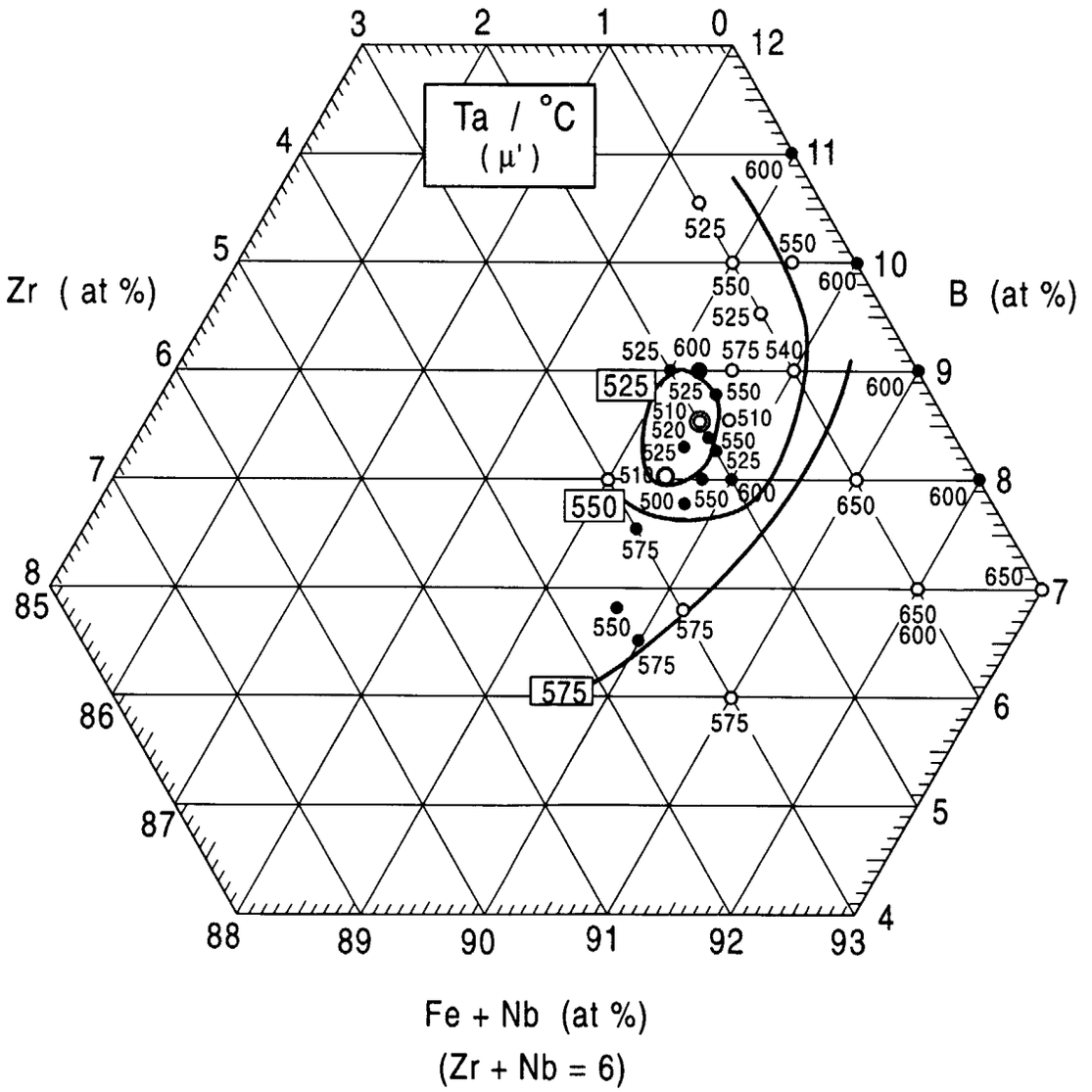

FIG. 32

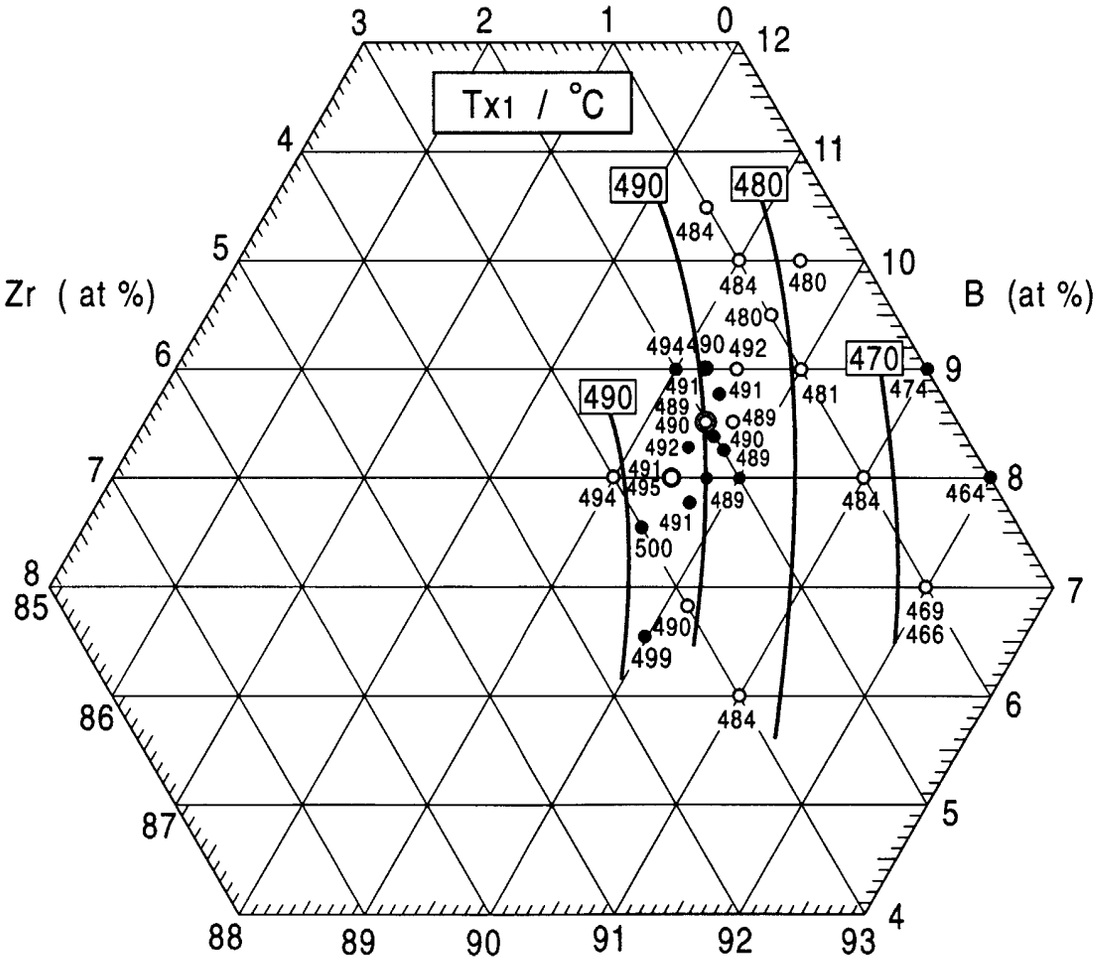
Tx1 / °C
490
480
470
490
Zr (at %)
B (at %)
Fe + Nb (at %)
(Zr + Nb = 6)
3
2
1
0
12
11
10
9
8
7
6
5
4
85
86
87
88
89
90
91
92
93
484
480
494
490
492
491
489
481
474
495
500
499
469
466
464

FIG. 33

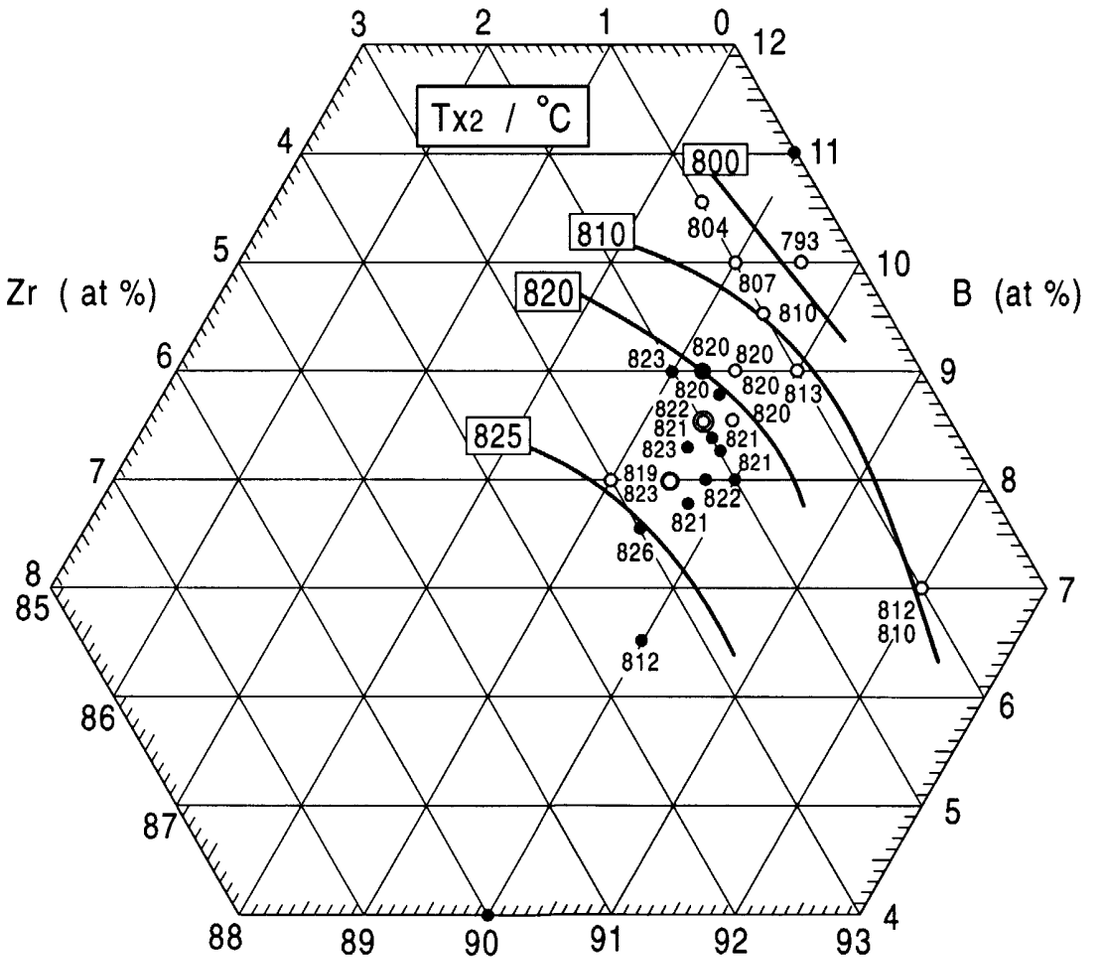
Tx2 / °C
800
810
820
825
804
793
807
810
823
820
820
820
820
813
822
821
821
820
823
821
819
823
822
821
826
812
812
810
Zr (at %)
B (at %)
Fe + Nb (at %)
(Zr + Nb = 6)

FIG. 34

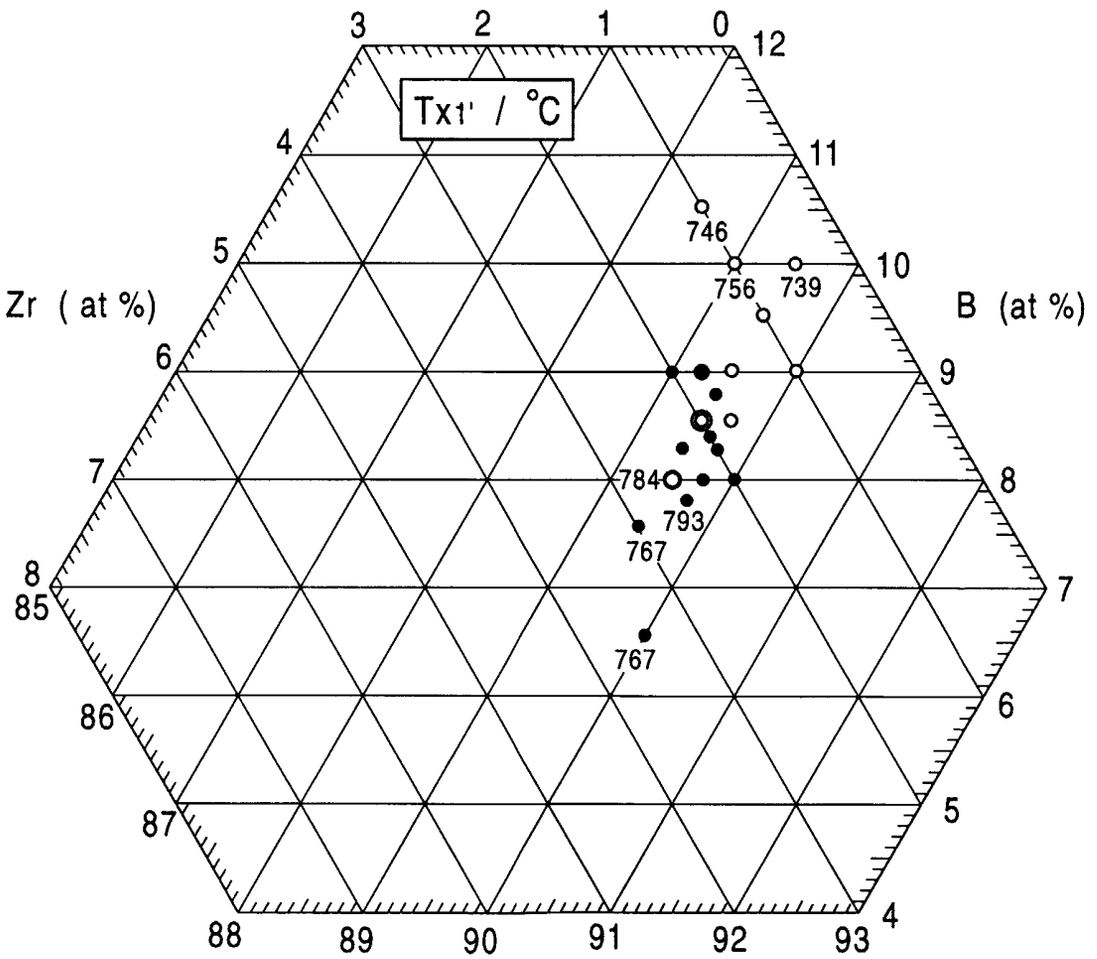

FIG. 35

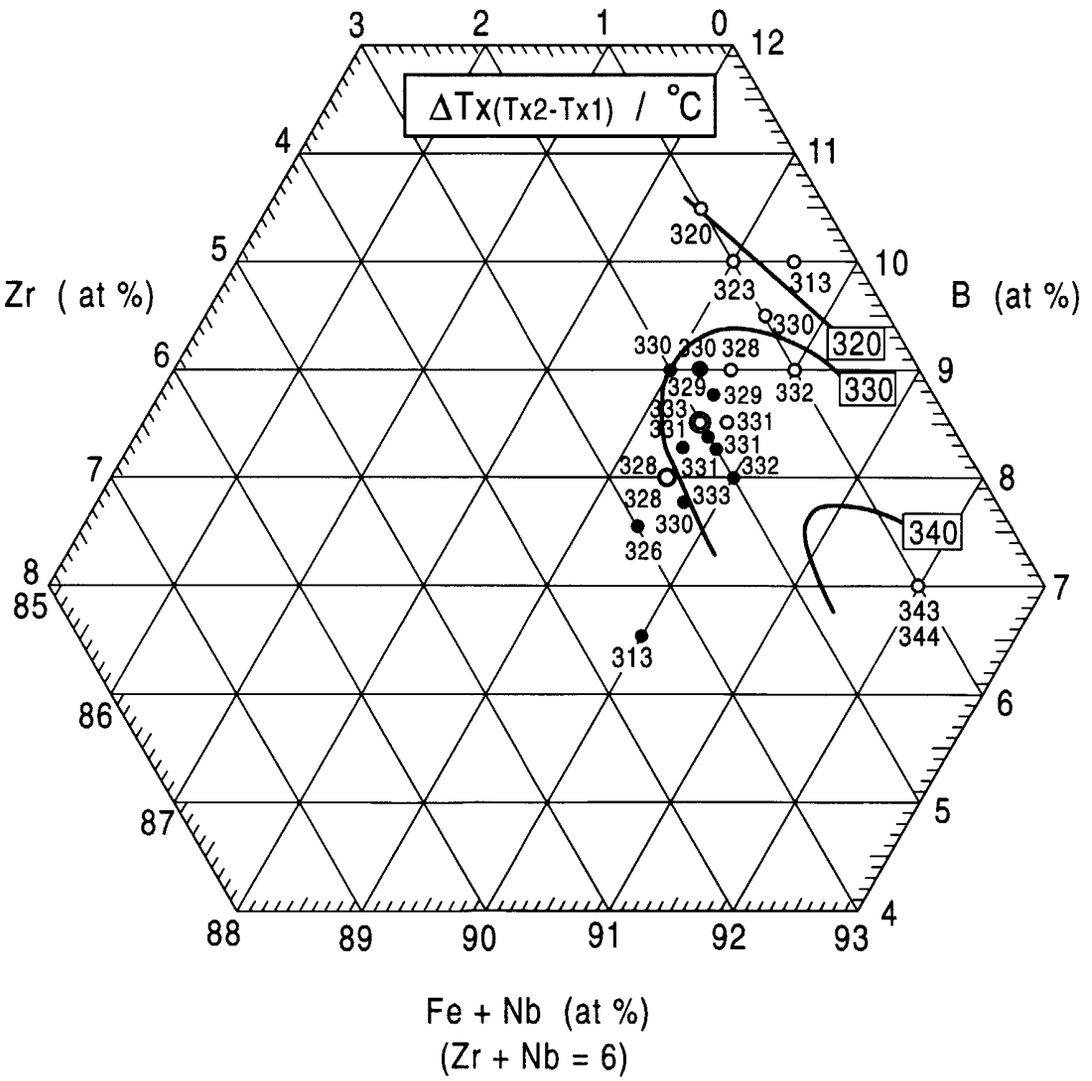
ΔTx(Tx2-Tx1) / °C
Zr (at %)
B (at %)
Fe + Nb (at %)
(Zr + Nb = 6)
320
330
340
3
2
1
0
12
4
11
5
10
6
9
7
8
85
86
87
88
89
90
91
92
93
4
5
6
7
8

FIG. 36

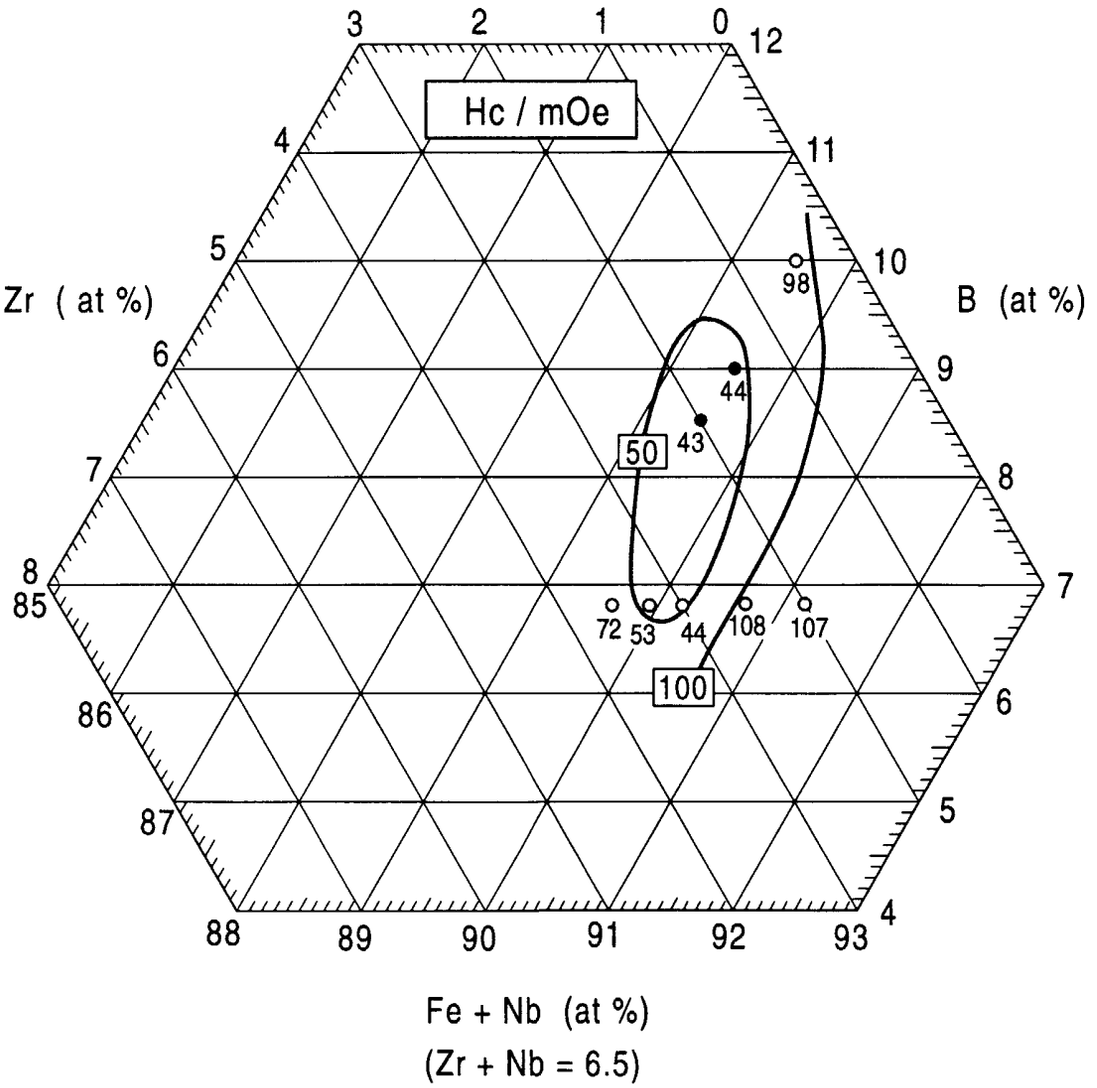

FIG. 37

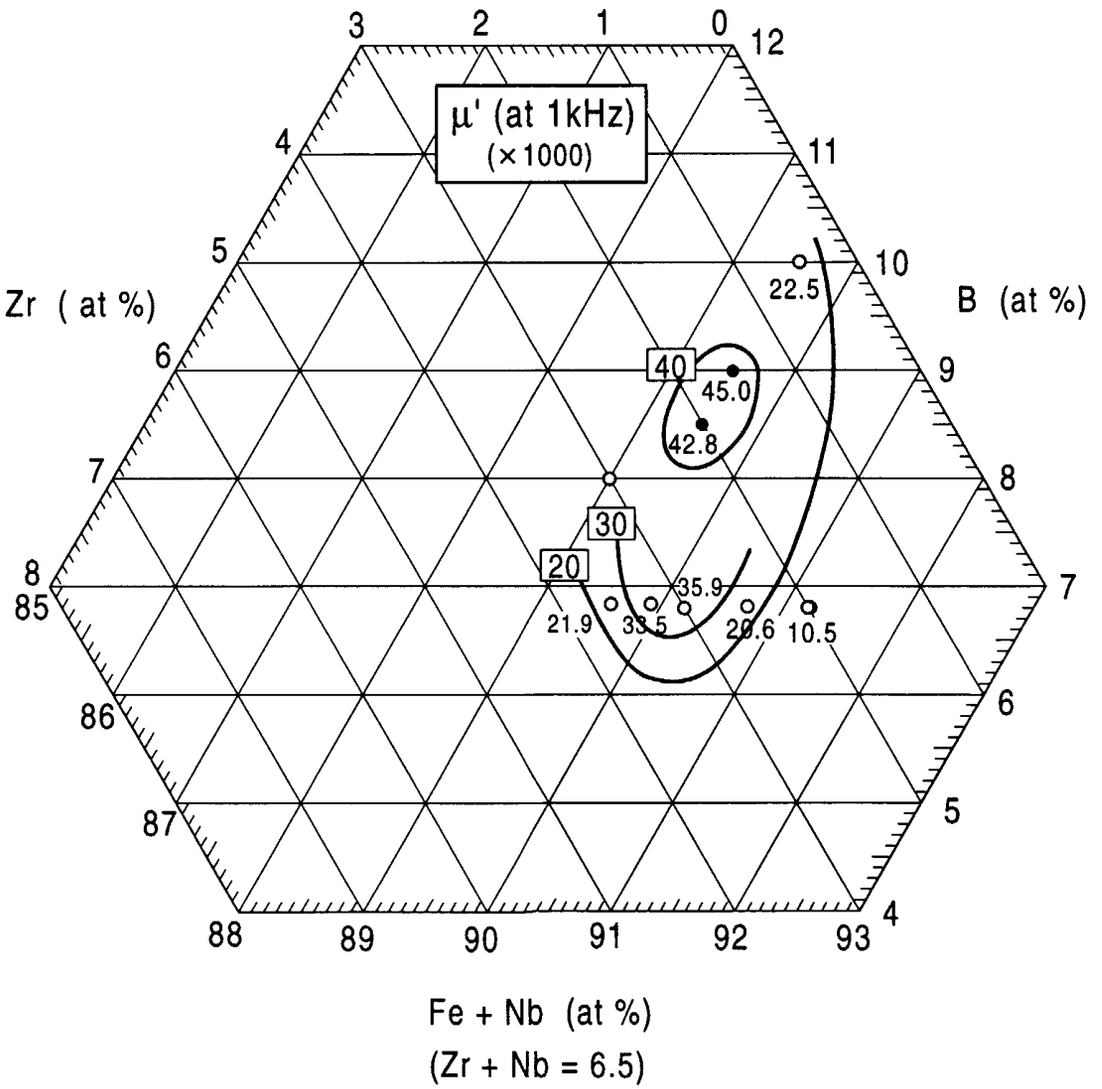
μ' (at 1kHz)
(×1000)
40
30
20
45.0
42.8
22.5
35.9
33.5
21.9
28.6
10.5
Zr (at %)
B (at %)
Fe + Nb (at %)
(Zr + Nb = 6.5)
3
2
1
0
12
11
10
9
8
7
6
5
4
85
86
87
88
89
90
91
92
93

FIG. 38

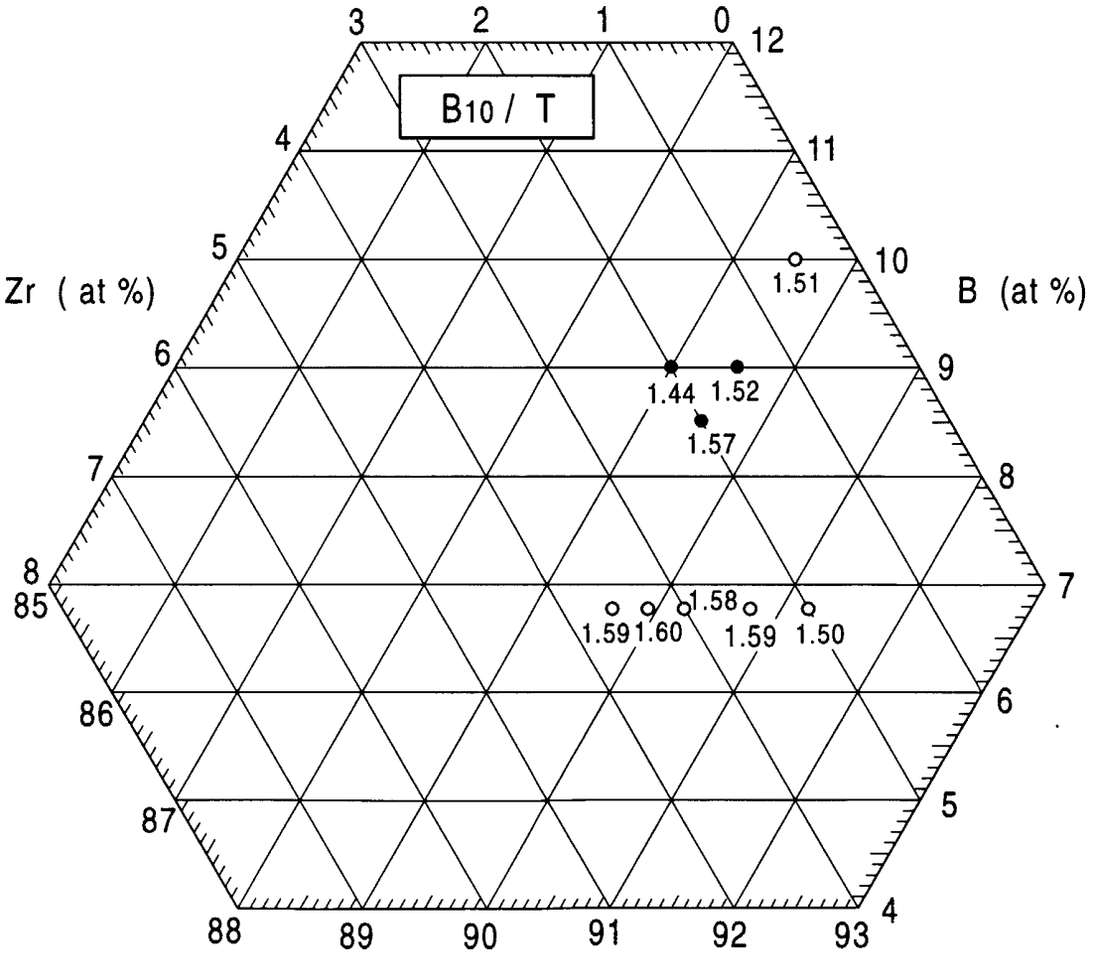
B10 / T
Zr (at %)
B (at %)
Fe + Nb (at %)
(Zr + Nb = 6.5)
1.51
1.44
1.52
1.57
1.59
1.60
1.58
1.59
1.50

FIG. 39

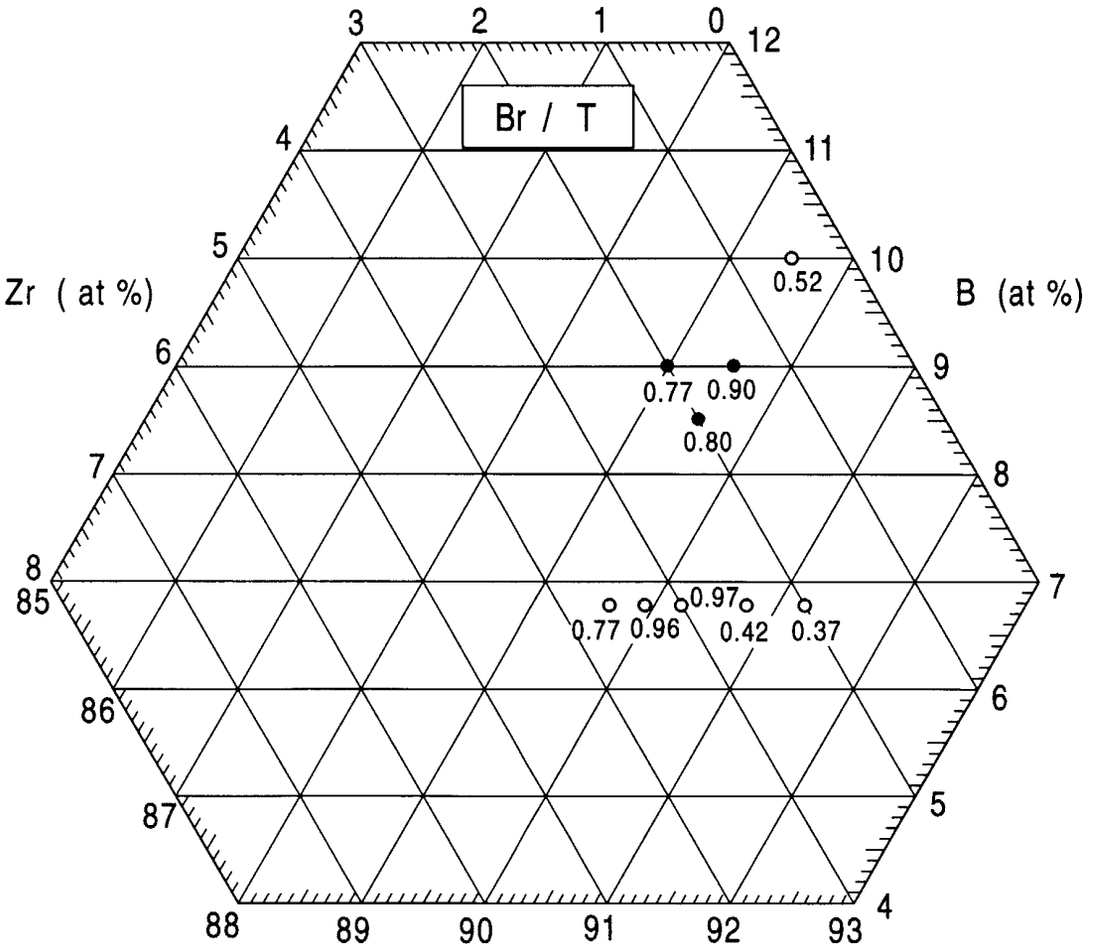

FIG. 40

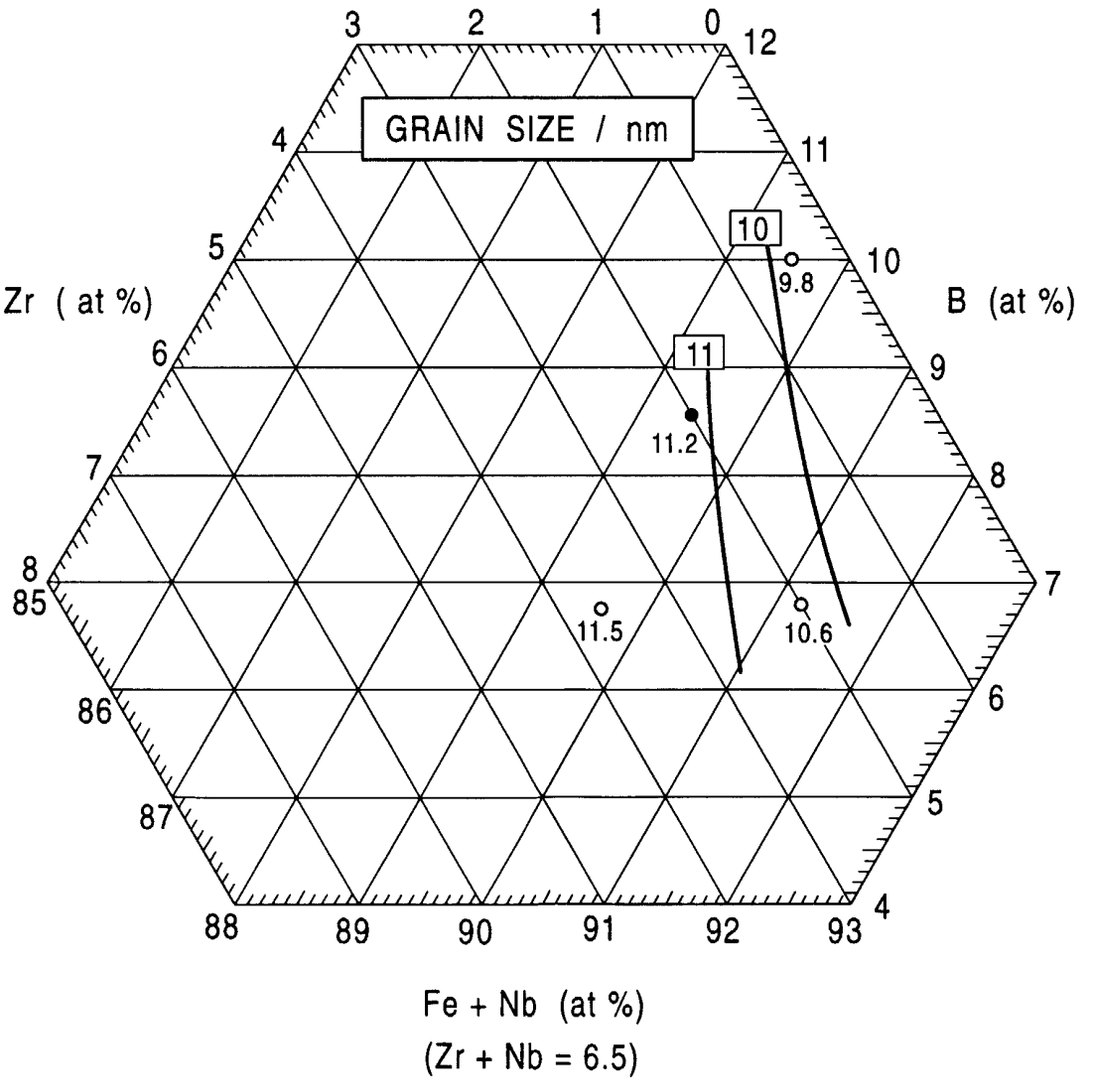
GRAIN SIZE / nm
10
11
9.8
11.2
11.5
10.6
Zr (at %)
B (at %)
Fe + Nb (at %)
(Zr + Nb = 6.5)
3
2
1
0
12
4
11
5
10
6
9
7
8
8
85
7
86
6
87
5
88
89
90
91
92
93
4

FIG. 41

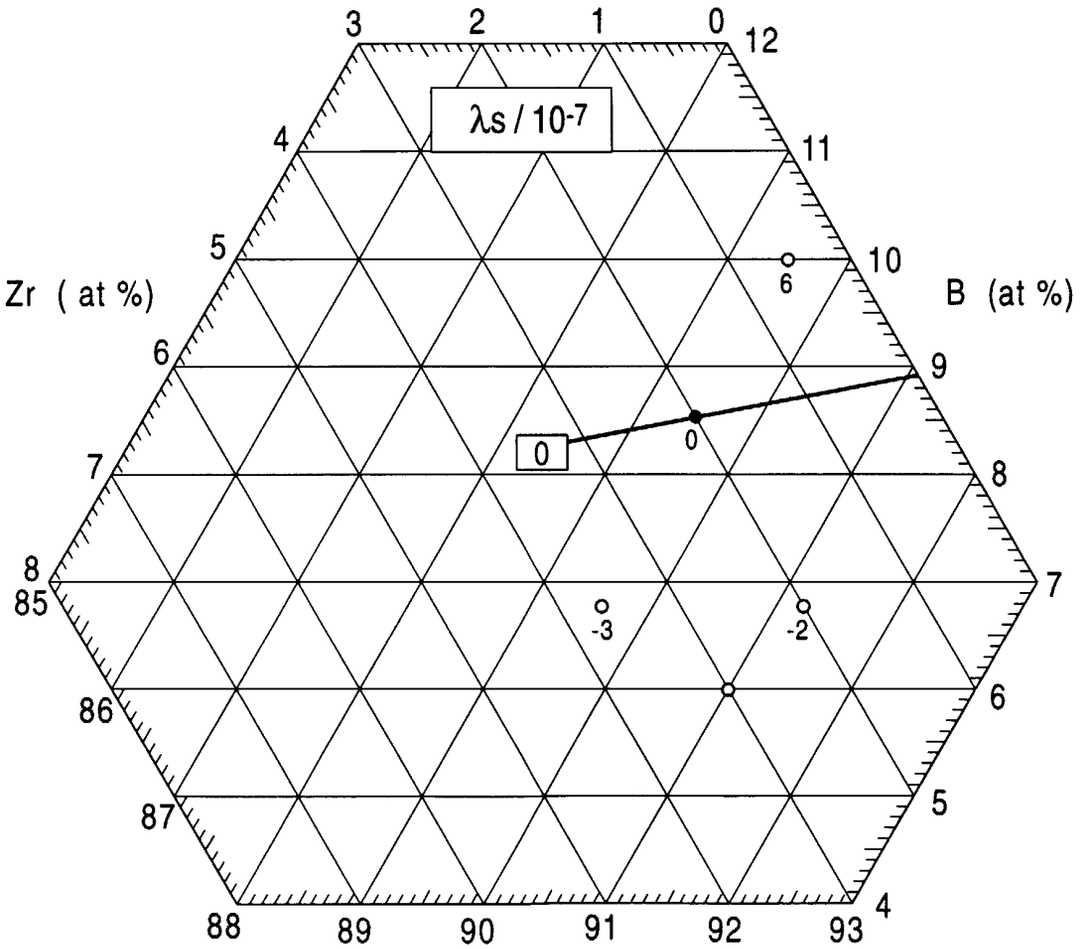

FIG. 42

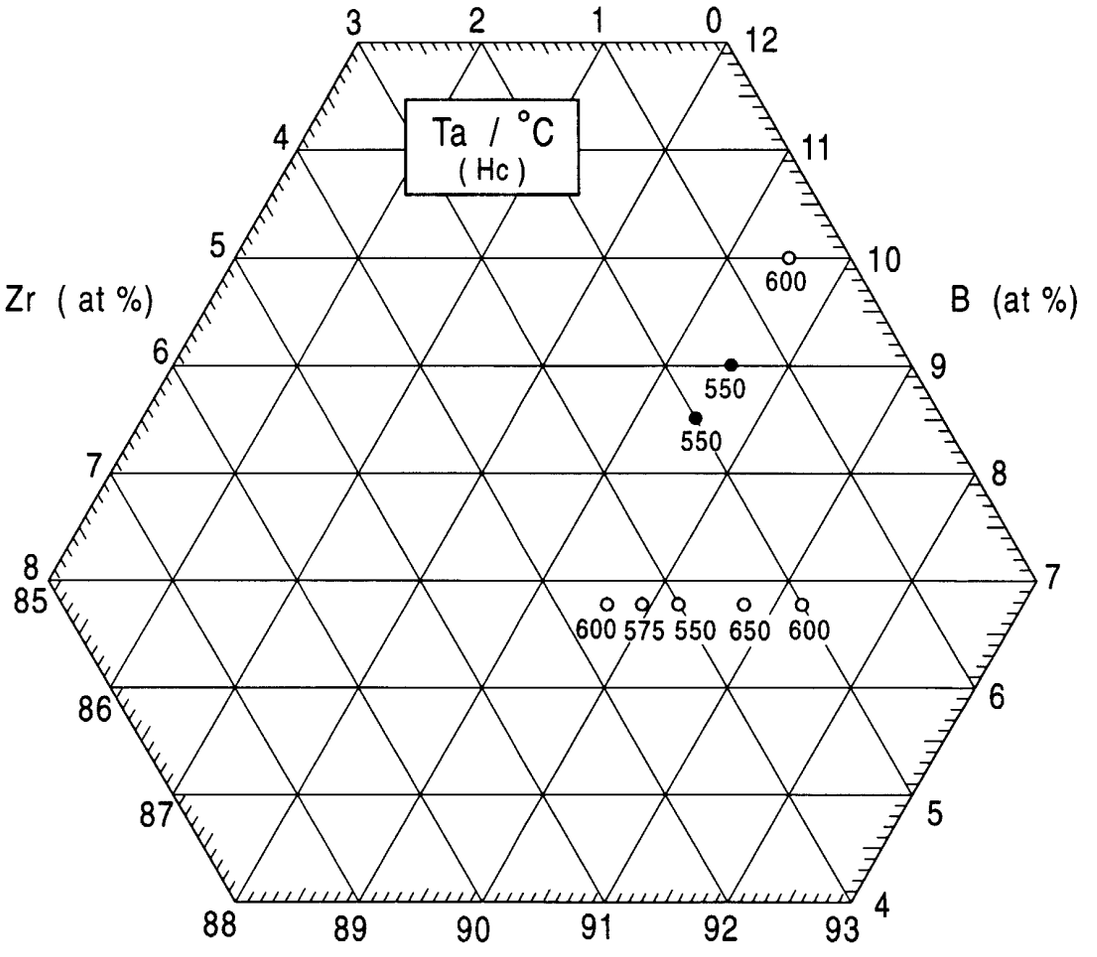

FIG. 43

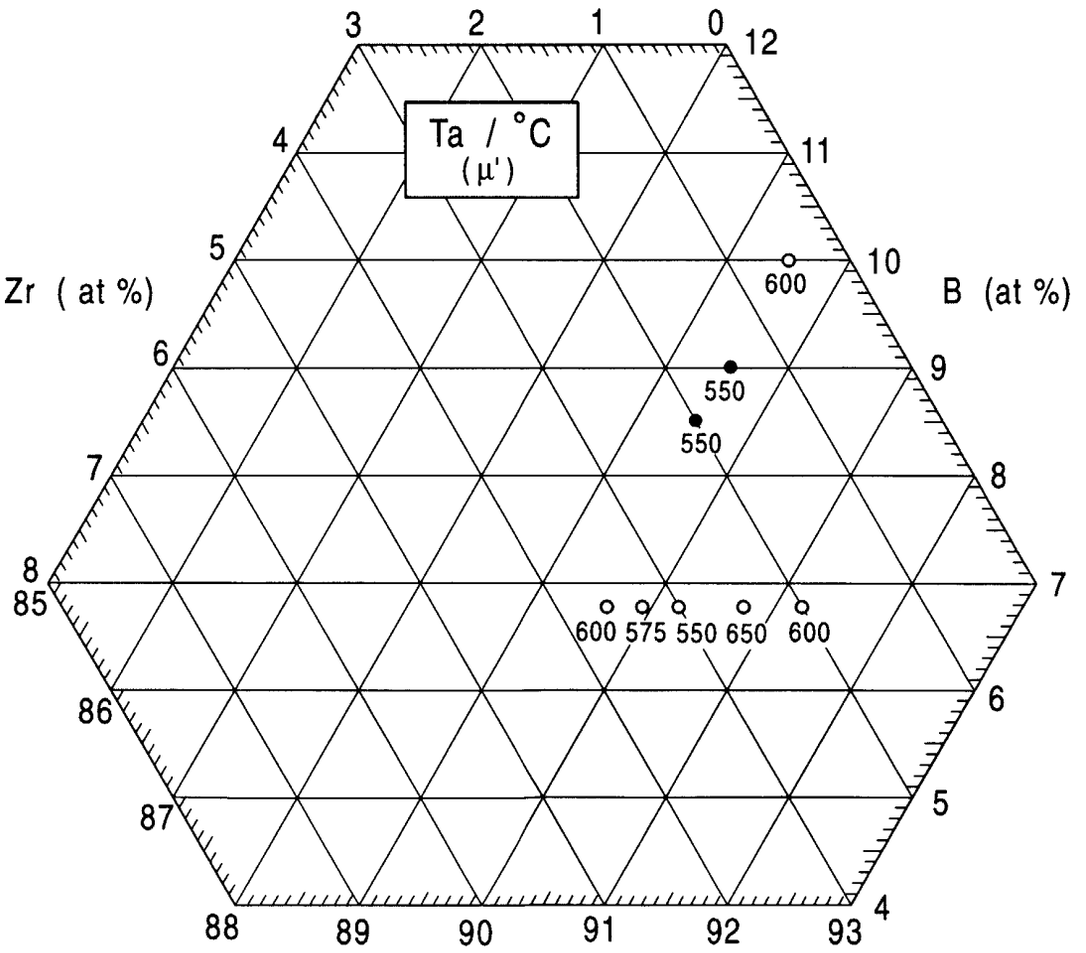

FIG. 44

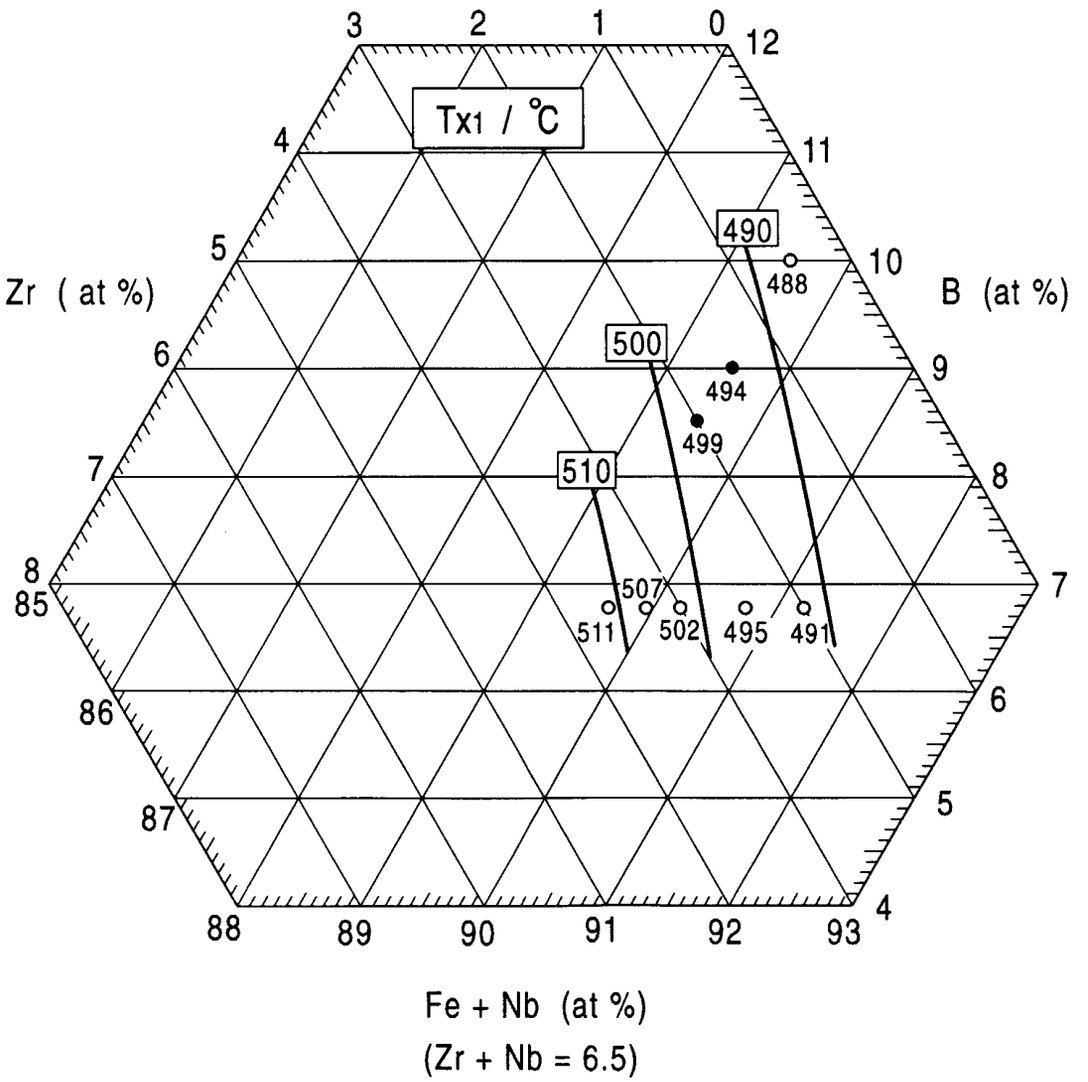
Tx1 / ℃
490
488
500
494
499
510
507
511
502
495
491
Zr (at %)
B (at %)
Fe + Nb (at %)
(Zr + Nb = 6.5)

FIG. 45

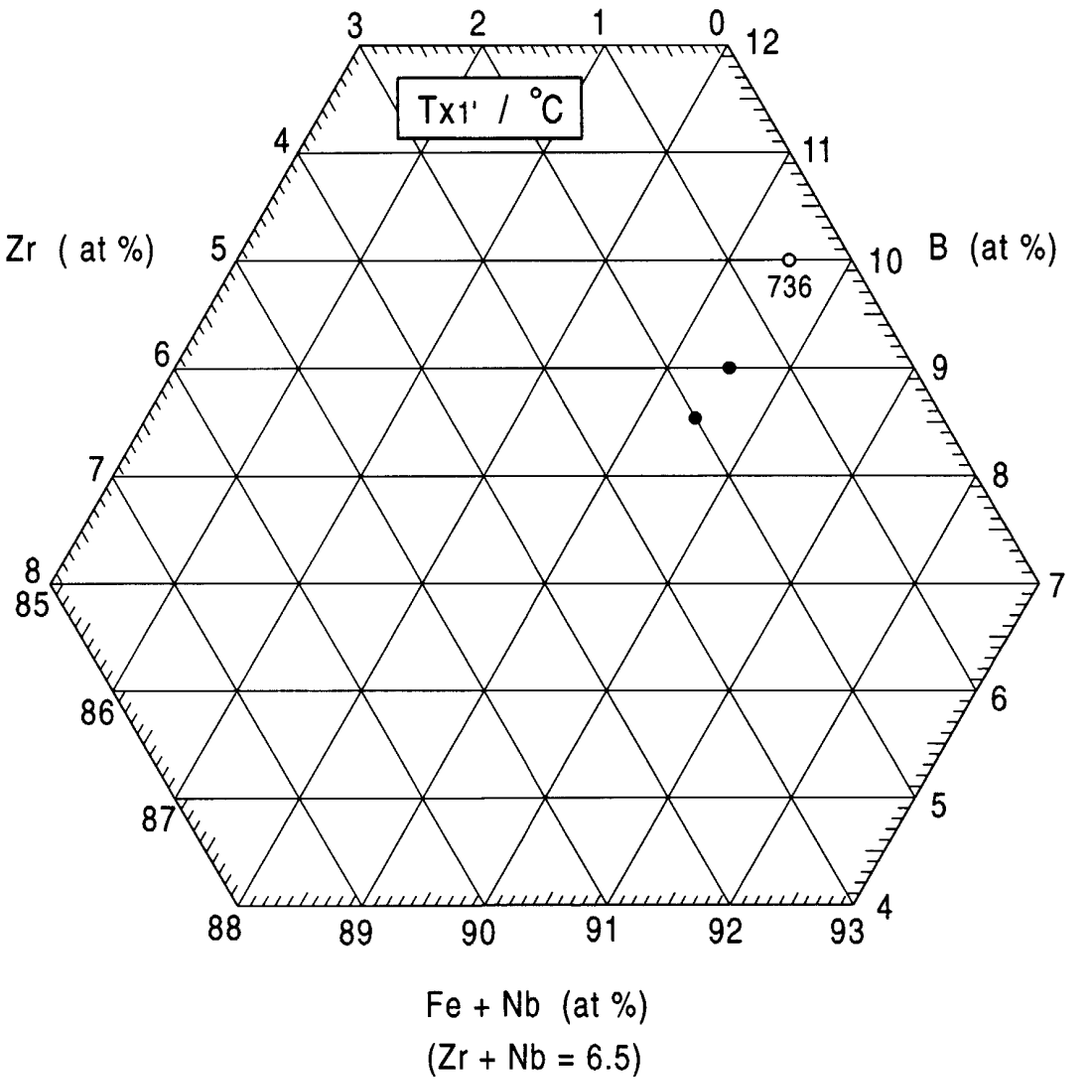
Tx1' / °C
Zr (at %)
B (at %)
Fe + Nb (at %)
(Zr + Nb = 6.5)
736
3
2
1
0
12
4
11
5
10
6
9
7
8
8
85
7
86
6
87
5
88
89
90
91
92
93
4

FIG. 46

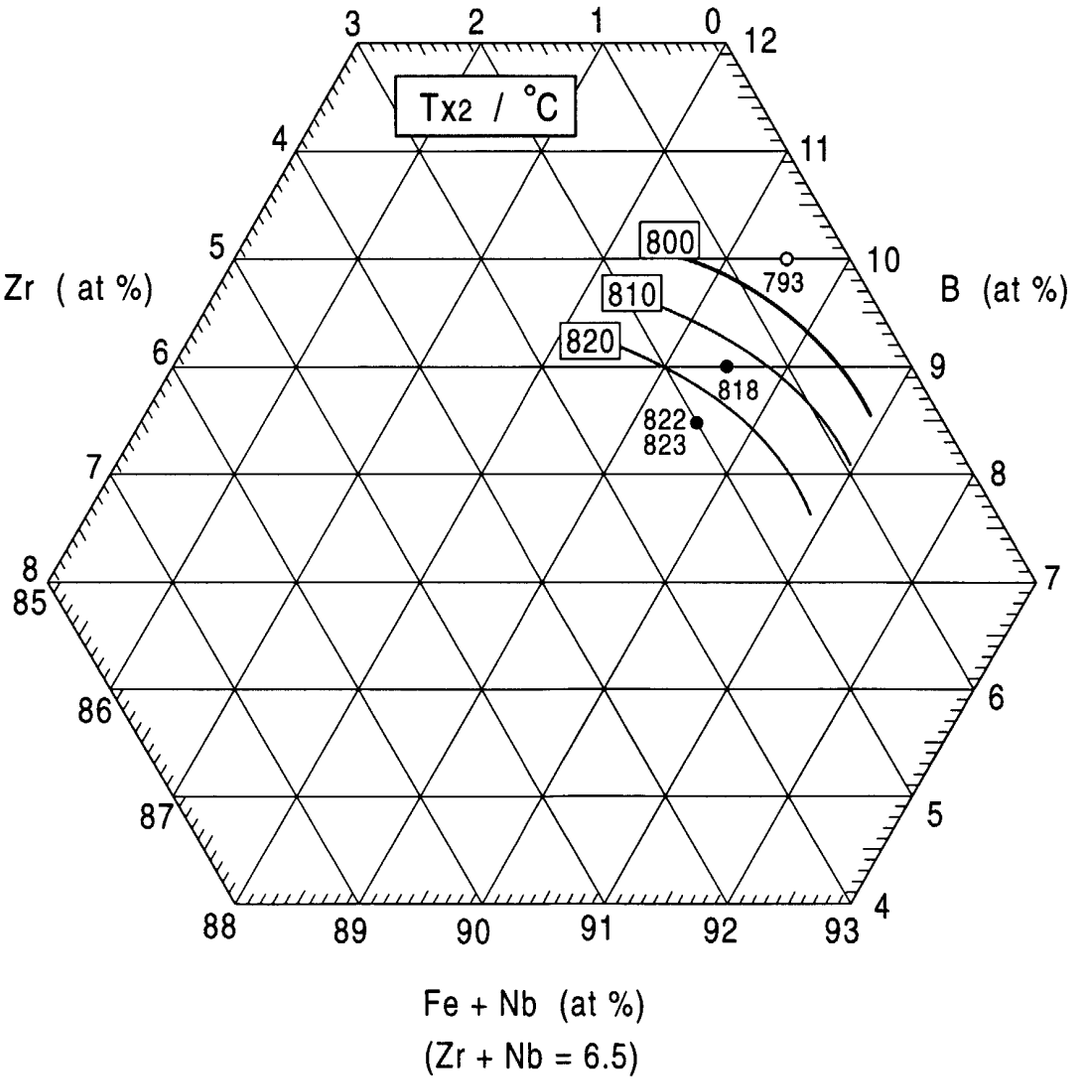

FIG. 47

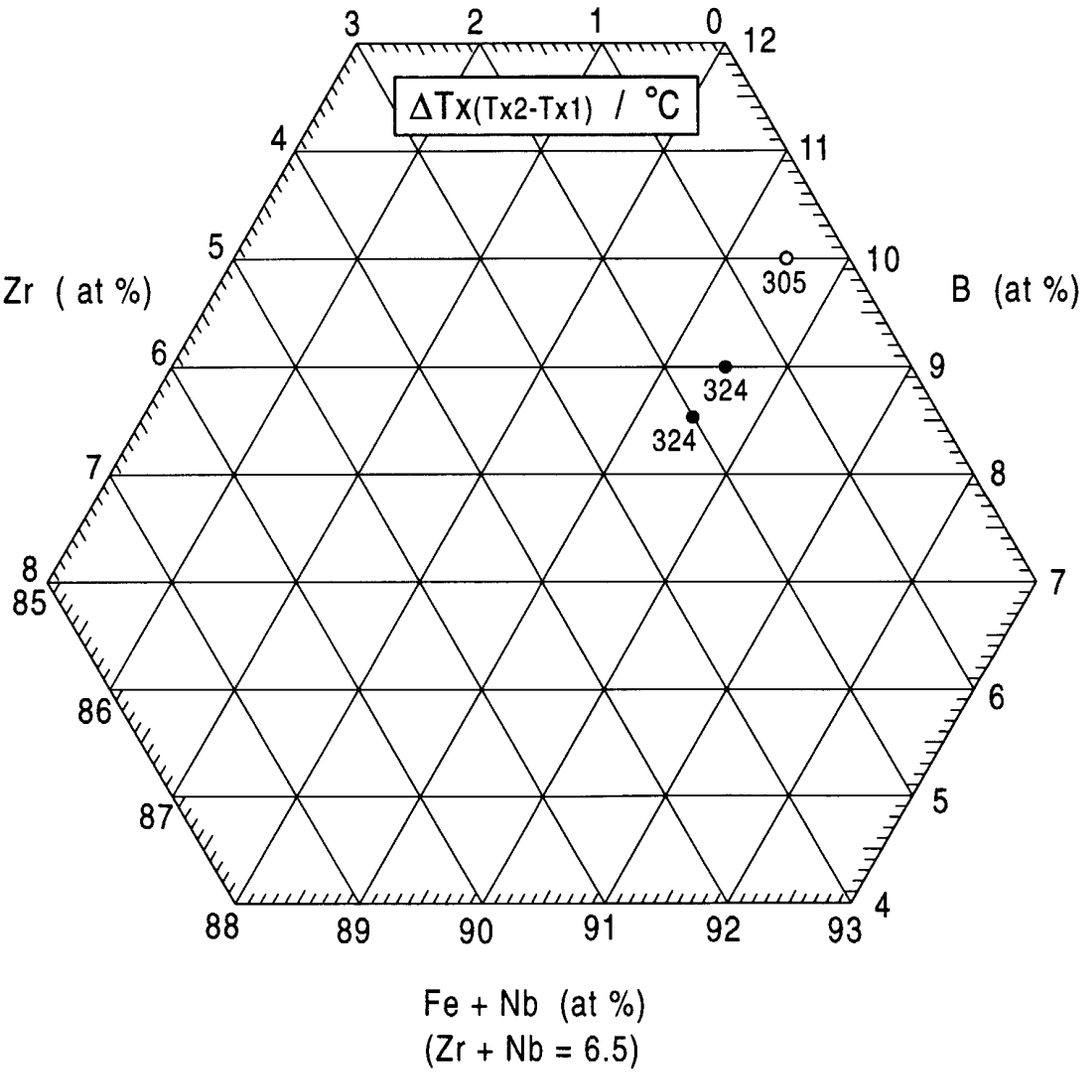
ΔTx(Tx2-Tx1) / °C
Zr (at %)
B (at %)
Fe + Nb (at %)
(Zr + Nb = 6.5)
305
324
324
3
2
1
0
12
11
10
9
8
7
6
5
4
85
86
87
88
89
90
91
92
93

FIG. 48

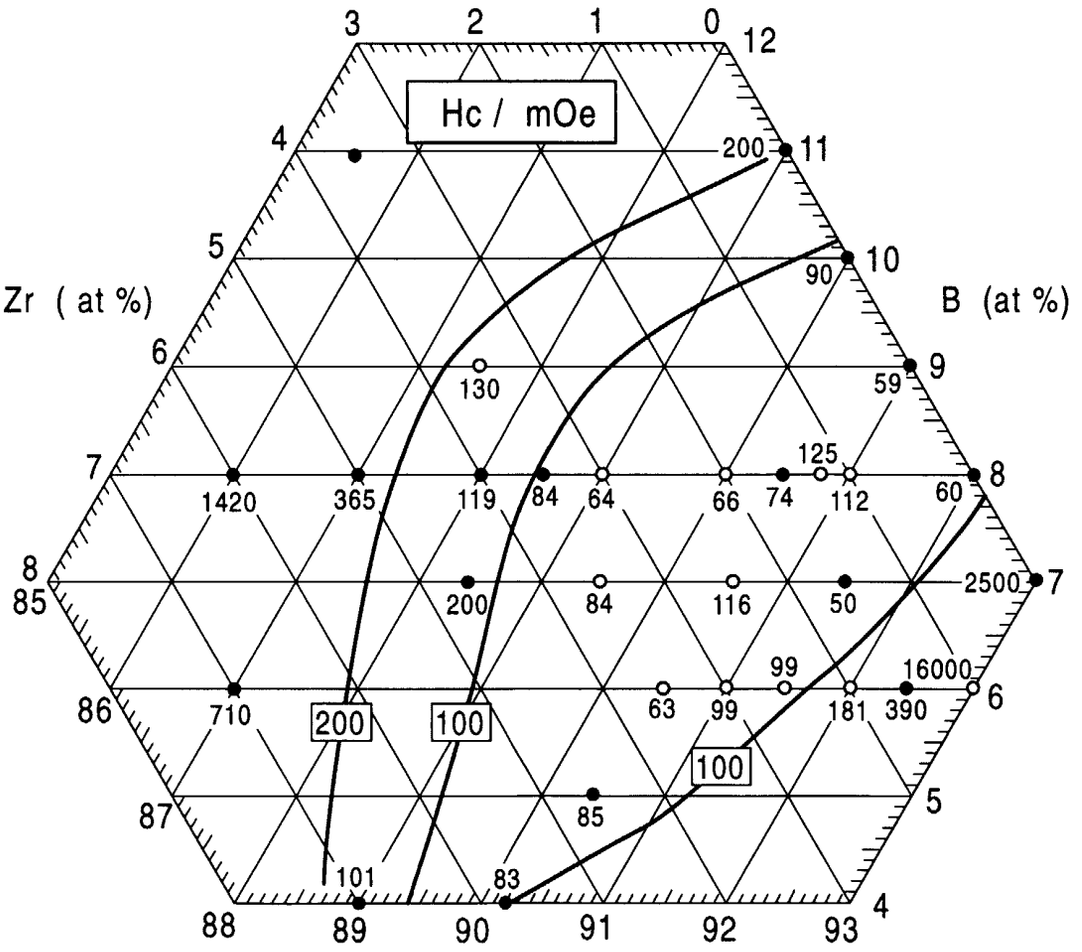
Hc / mOe
Zr (at %)
B (at %)
Fe + Nb (at %)
(Zr + Nb = 7)
3
2
1
0
12
4
11
5
10
6
9
7
8
8
85
7
86
6
87
5
88
89
90
91
92
93
4
200
90
130
59
125
1420
365
119
84
64
66
74
112
60
200
84
116
50
2500
99
16000
710
200
100
63
99
181
390
100
85
101
83

FIG. 49

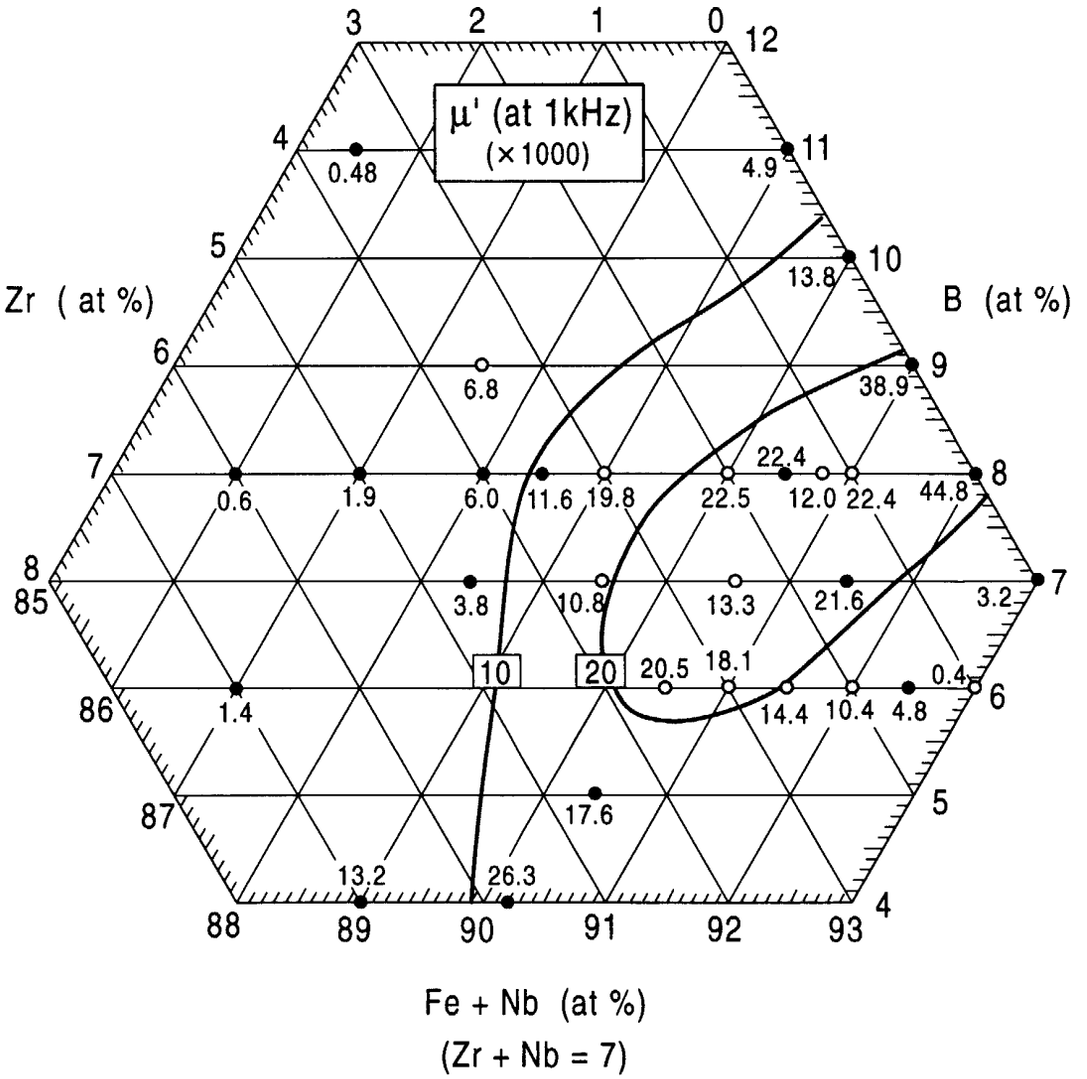
μ' (at 1kHz)
(×1000)
Zr (at %)
B (at %)
Fe + Nb (at %)
(Zr + Nb = 7)
0.48
4.9
13.8
6.8
38.9
22.4
0.6
1.9
6.0
11.6
19.8
22.5
12.0
22.4
44.8
3.8
10.8
13.3
21.6
3.2
10
20
20.5
18.1
0.4
1.4
14.4
10.4
4.8
17.6
13.2
26.3

FIG. 50

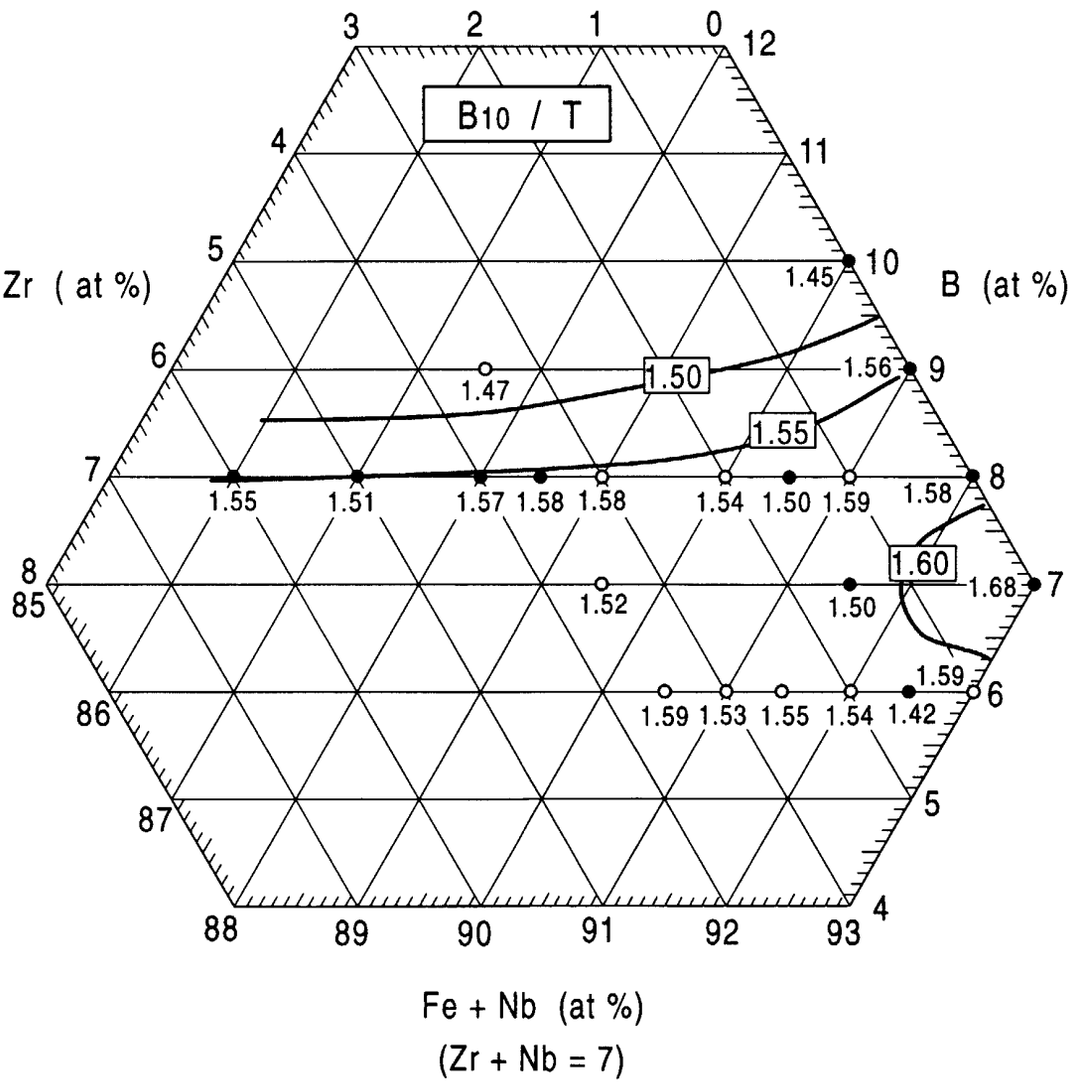
B10 / T
Zr (at %)
B (at %)
Fe + Nb (at %)
(Zr + Nb = 7)
3
2
1
0
12
4
11
5
10
6
9
7
8
8
85
7
86
6
87
5
88
89
90
91
92
93
4
1.45
1.47
1.50
1.56
1.55
1.55
1.51
1.57
1.58
1.58
1.54
1.50
1.59
1.58
1.60
1.68
1.52
1.50
1.59
1.59
1.53
1.55
1.54
1.42

FIG. 51

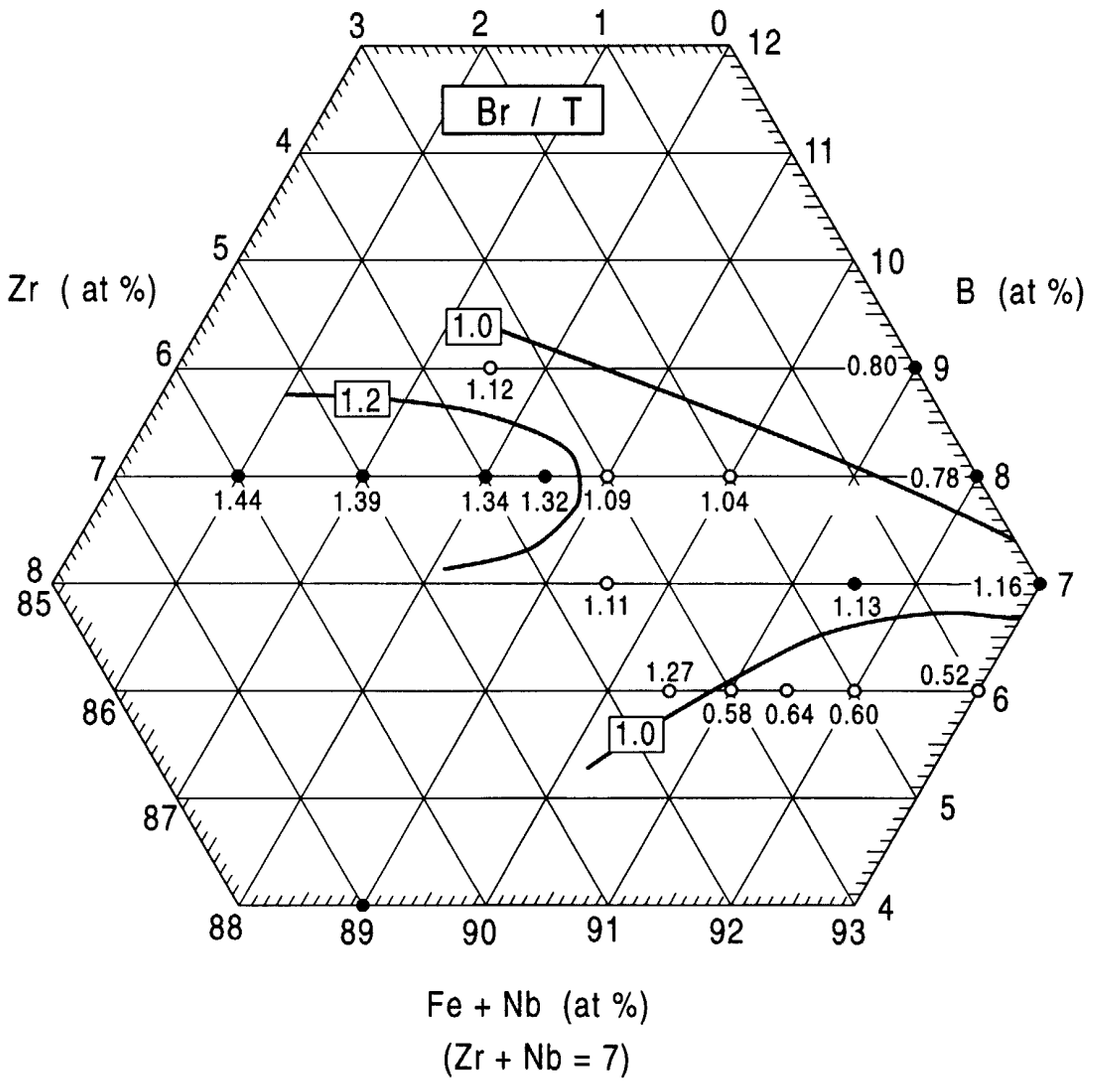
Br / T
Zr (at %)
B (at %)
Fe + Nb (at %)
(Zr + Nb = 7)
1.0
1.2
1.0
1.12
1.44
1.39
1.34
1.32
1.09
1.04
0.80
0.78
1.11
1.13
1.16
1.27
0.58
0.64
0.60
0.52

FIG. 52

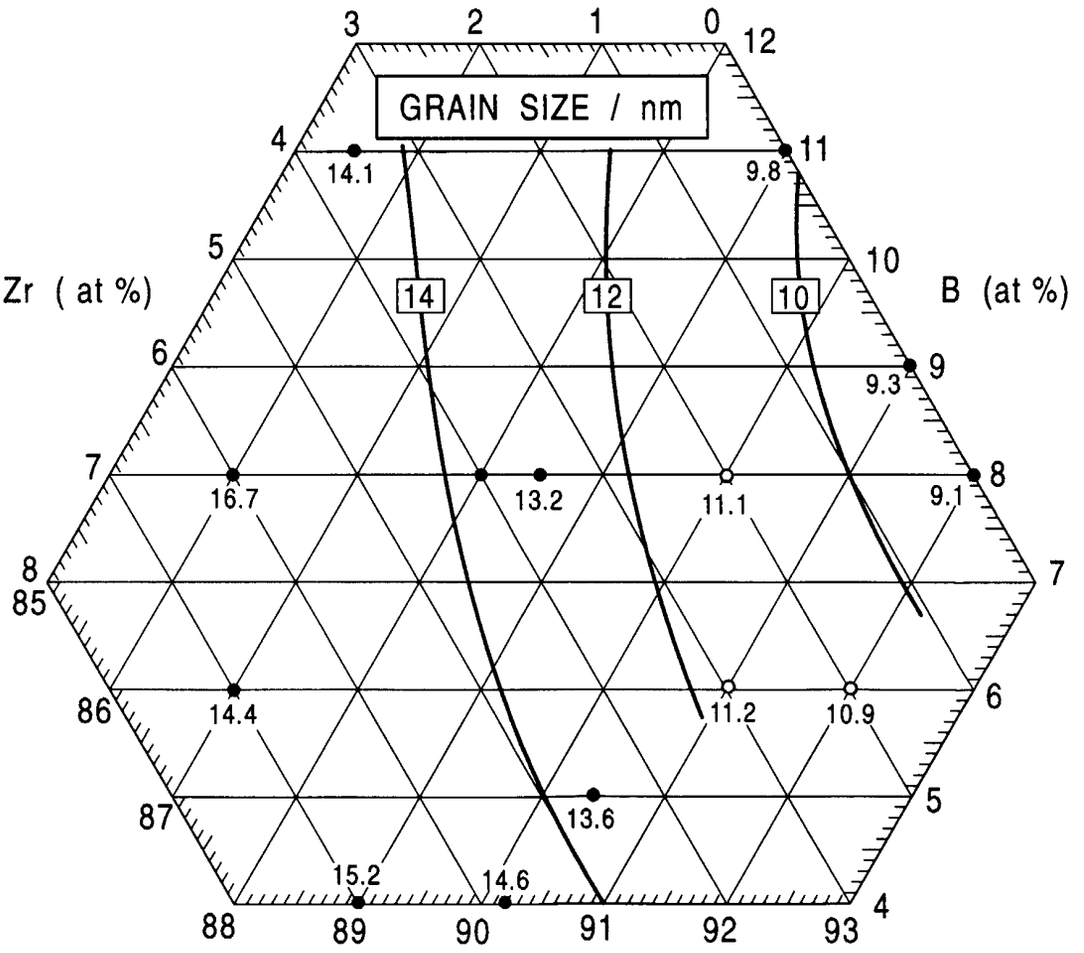
GRAIN SIZE / nm
14
12
10
14.1
9.8
9.3
16.7
13.2
11.1
9.1
14.4
11.2
10.9
13.6
15.2
14.6
Zr (at %)
B (at %)
Fe + Nb (at %)
(Zr + Nb = 7)

FIG. 53

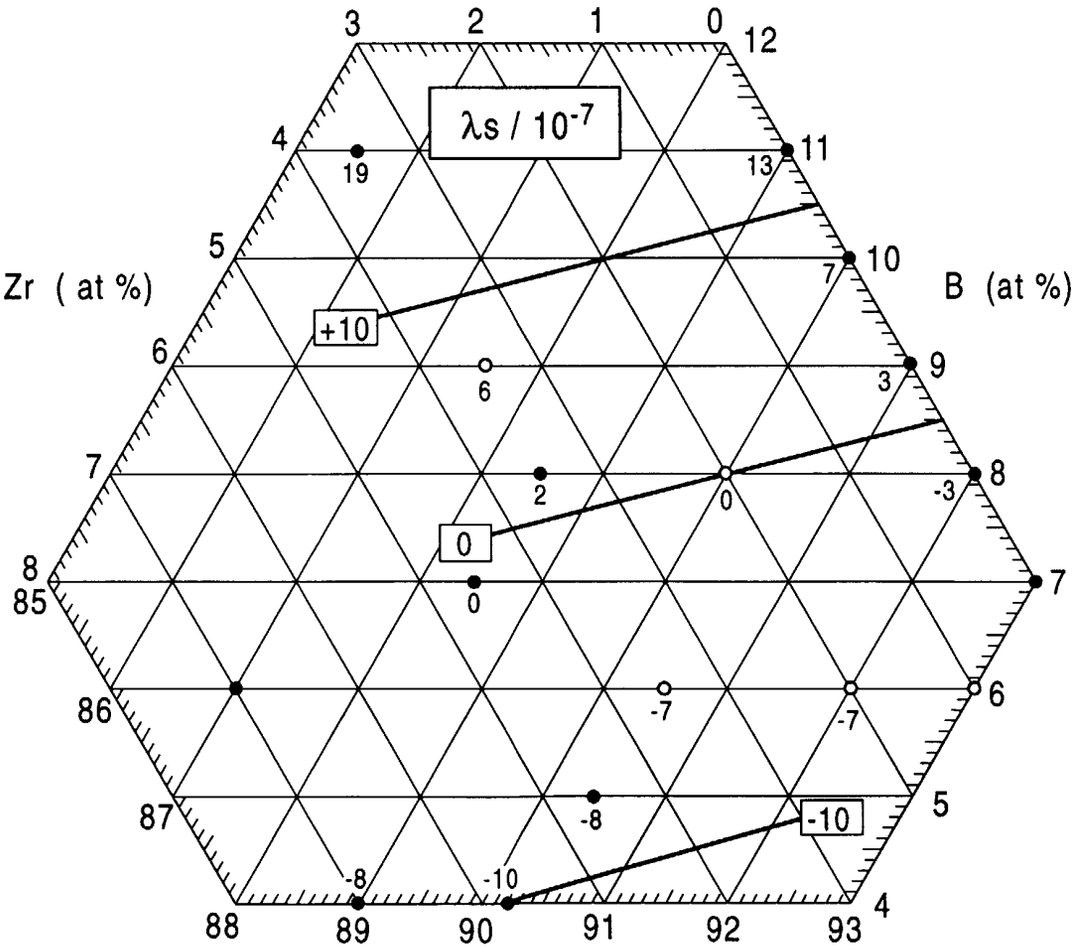
λs / 10-7
Zr (at %)
B (at %)
Fe + Nb (at %)
(Zr + Nb = 7)
+10
0
-10
19
13
7
6
3
2
0
-3
0
-7
-7
-8
-8
-10
3
2
1
0
12
11
10
9
8
7
6
5
4
85
86
87
88
89
90
91
92
93

FIG. 54

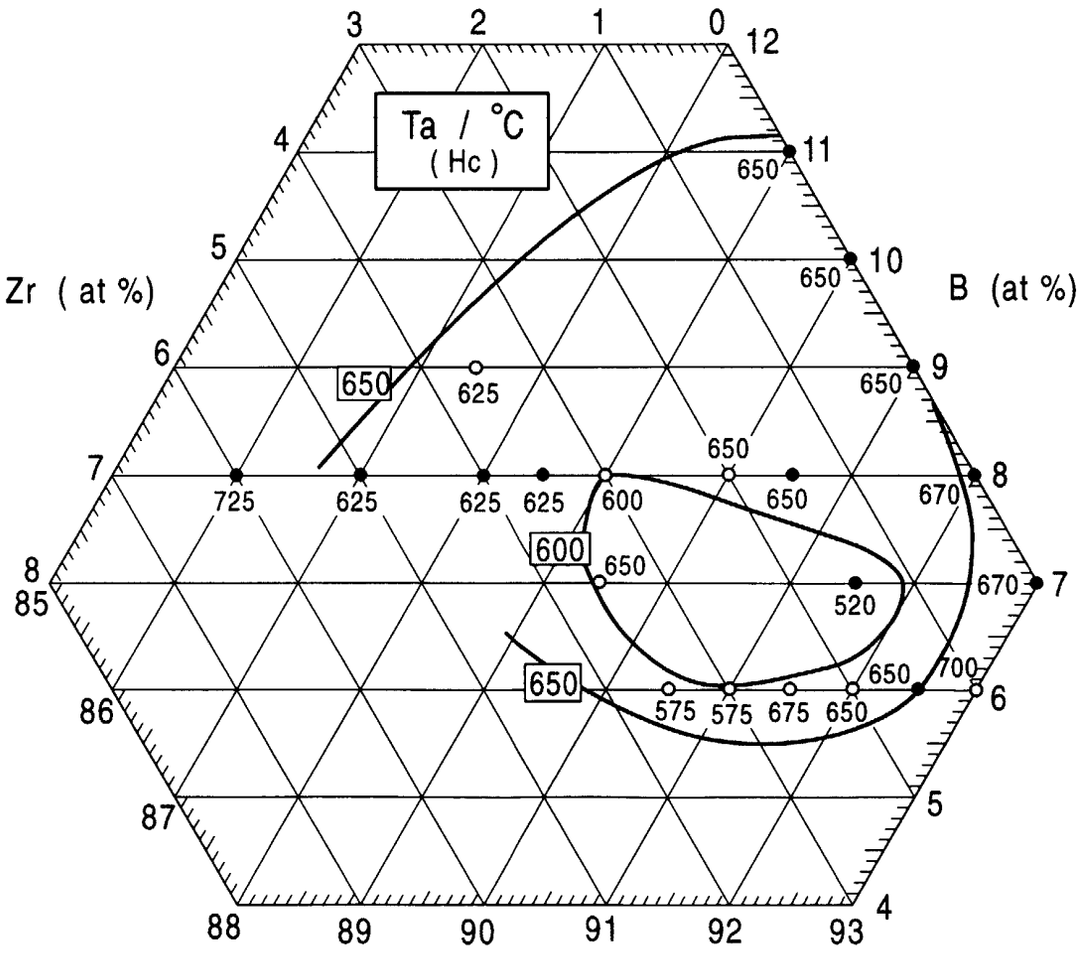
Ta / °C
(Hc)
Zr (at %)
B (at %)
Fe + Nb (at %)
(Zr + Nb = 7)
650
625
725
625
625
625
600
650
650
650
650
650
600
650
520
650
700
575
575
675
650

FIG. 55

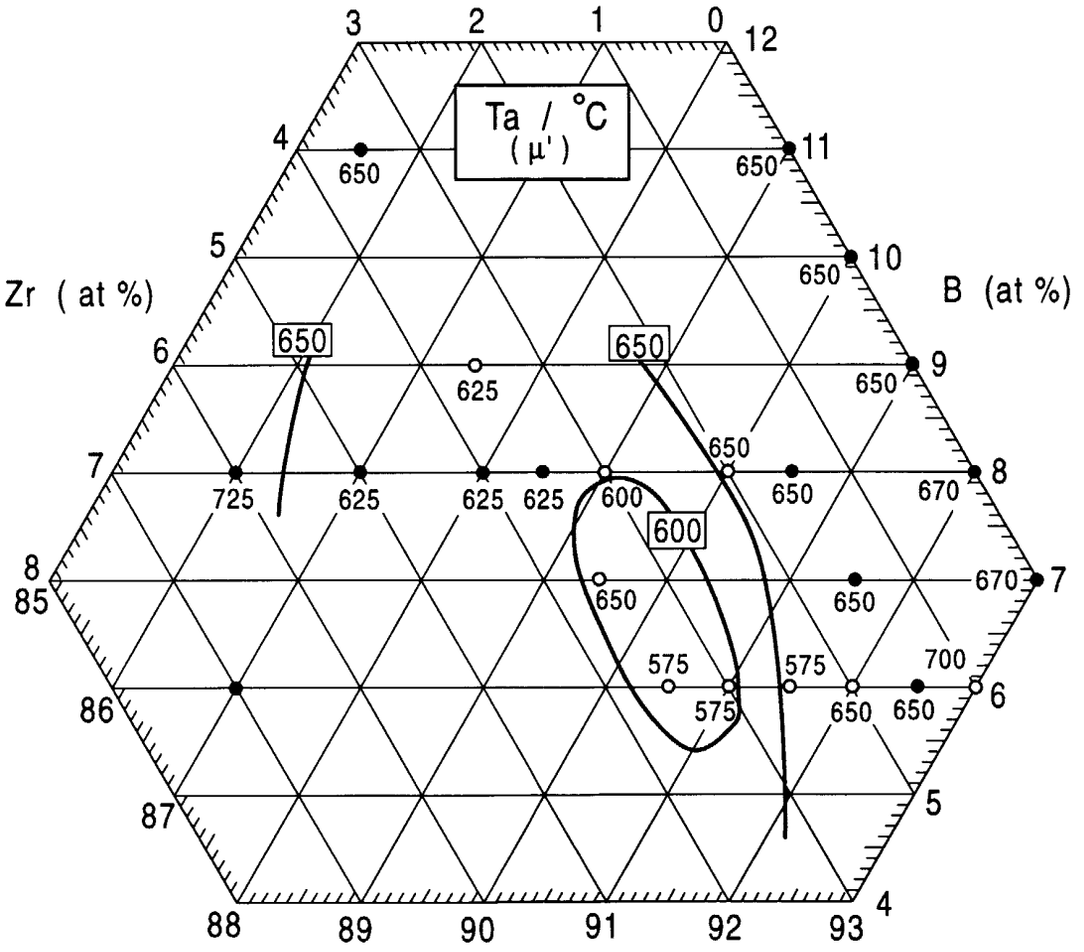

FIG. 56

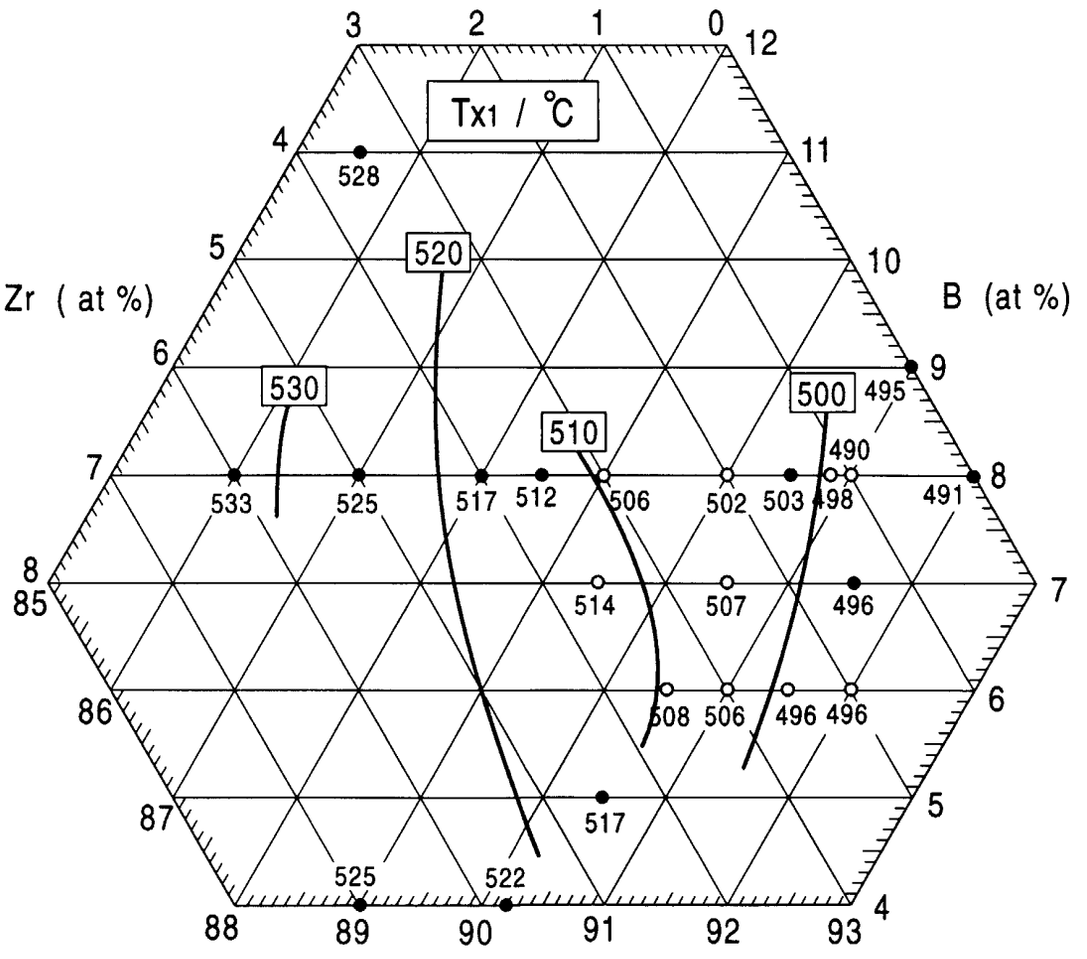
Tx1 / °C
520
530
500
510
528
533
525
517
512
506
502
503
498
495
490
491
514
507
496
508
506
496
496
517
525
522
Zr (at %)
B (at %)
Fe + Nb (at %)
(Zr + Nb = 7)

FIG. 57

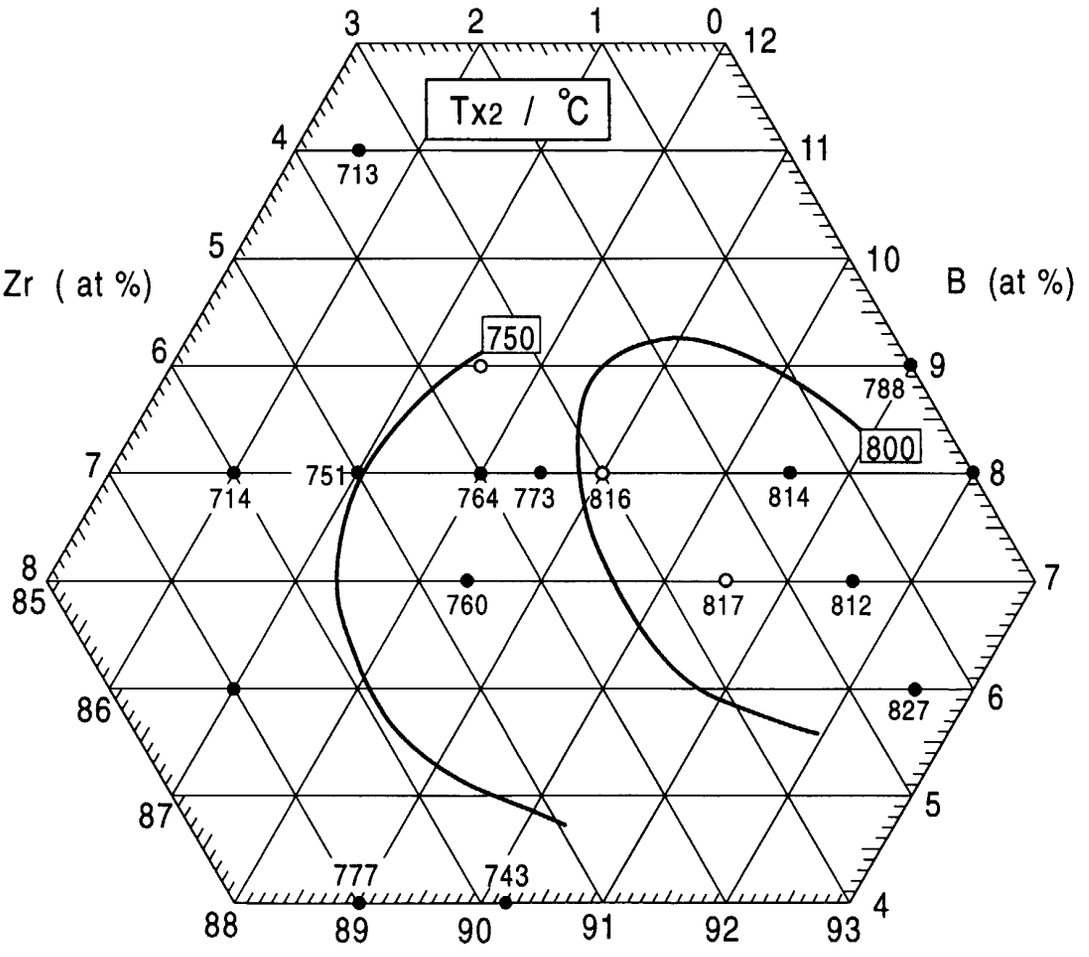
Tx2 / °C
713
750
788
800
751
714
764
773
816
814
760
817
812
827
777
743
Zr (at %)
B (at %)
Fe + Nb (at %)
(Zr + Nb = 7)

FIG. 58

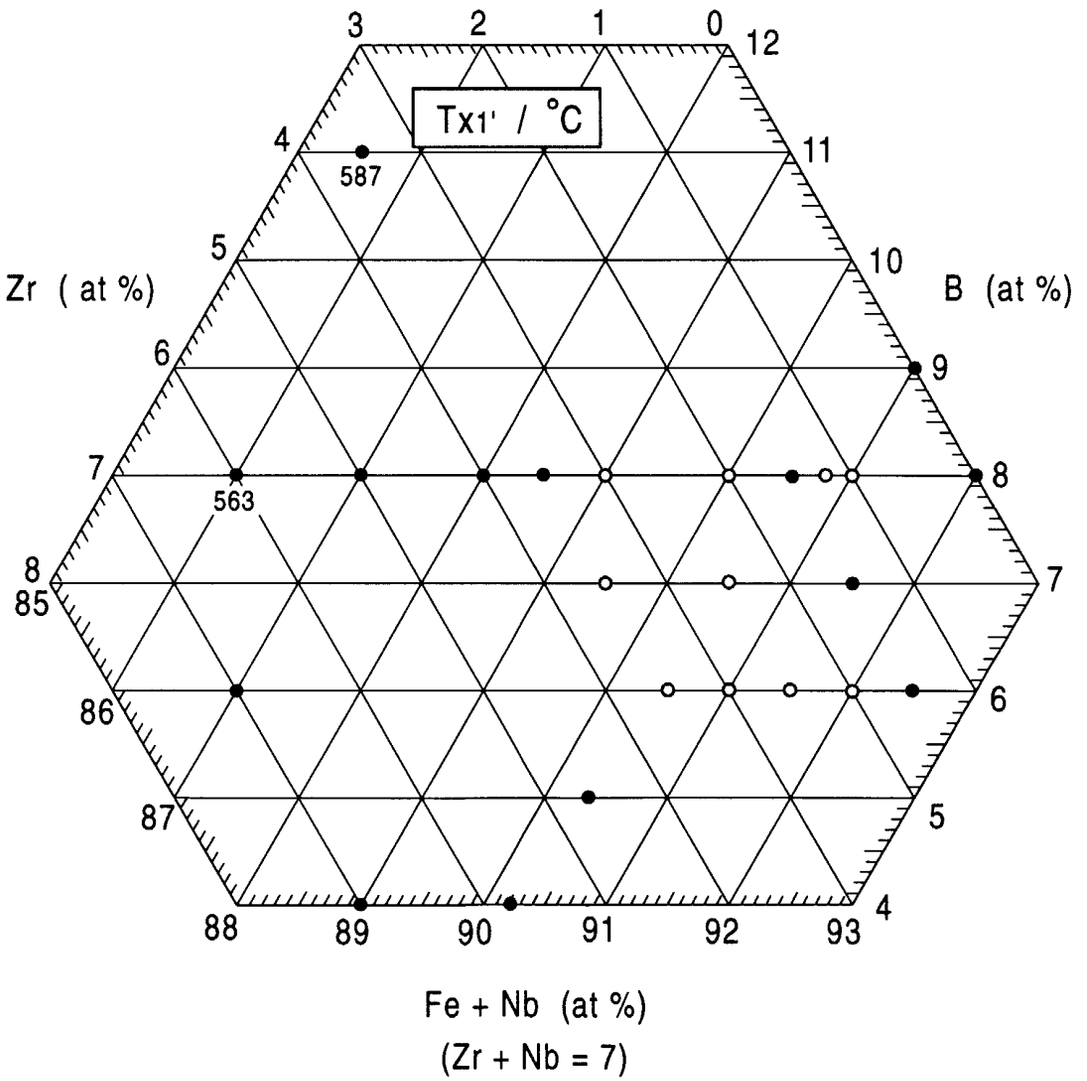
Tx1' / °C
587
563
Zr (at %)
B (at %)
Fe + Nb (at %)
(Zr + Nb = 7)
3
2
1
0
12
4
11
5
10
6
9
7
8
8
7
85
6
86
5
87
4
88
89
90
91
92
93

FIG. 59

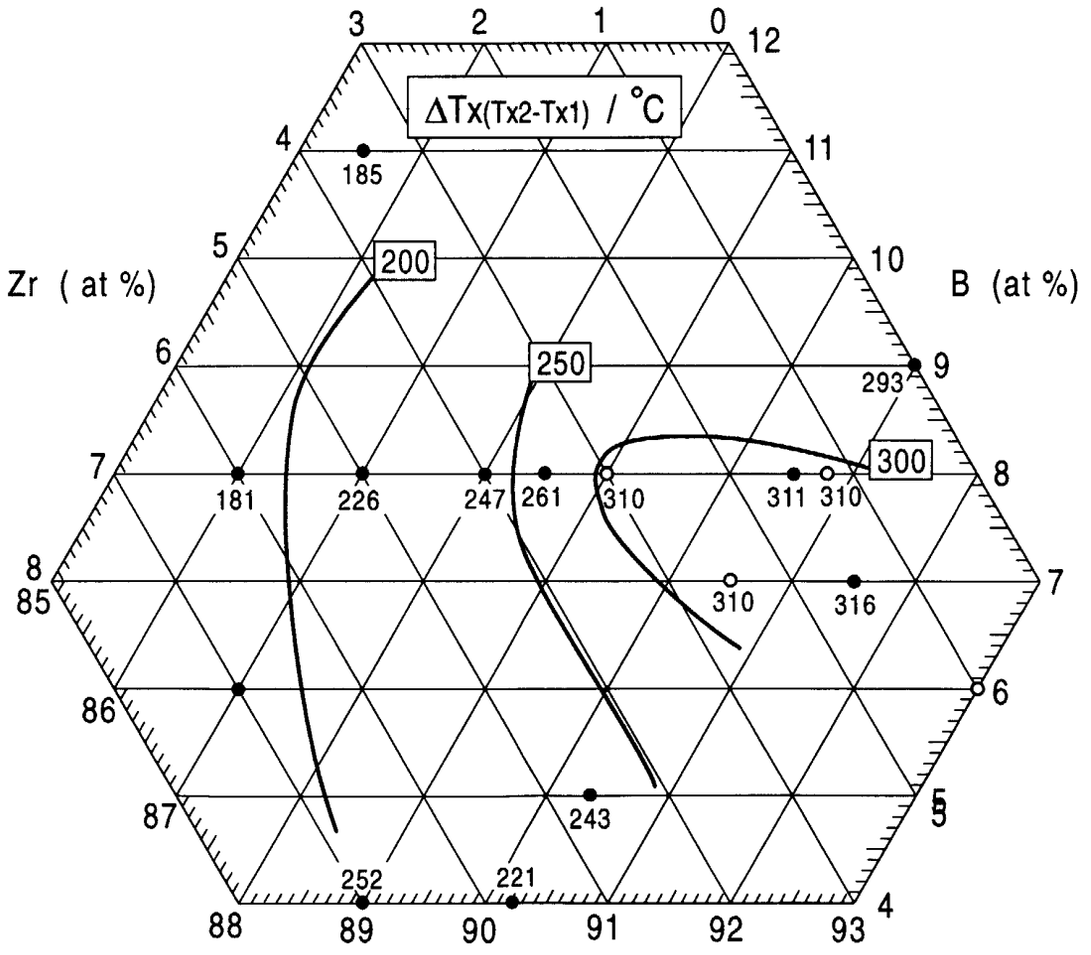
ΔTx(Tx2-Tx1) / °C
Zr (at %)
B (at %)
Fe + Nb (at %)
(Zr + Nb = 7)
200
250
300
185
181
226
247
261
310
311
310
293
310
316
243
252
221
3
2
1
0
12
11
10
9
8
7
6
5
4
85
86
87
88
89
90
91
92
93

FIG. 60

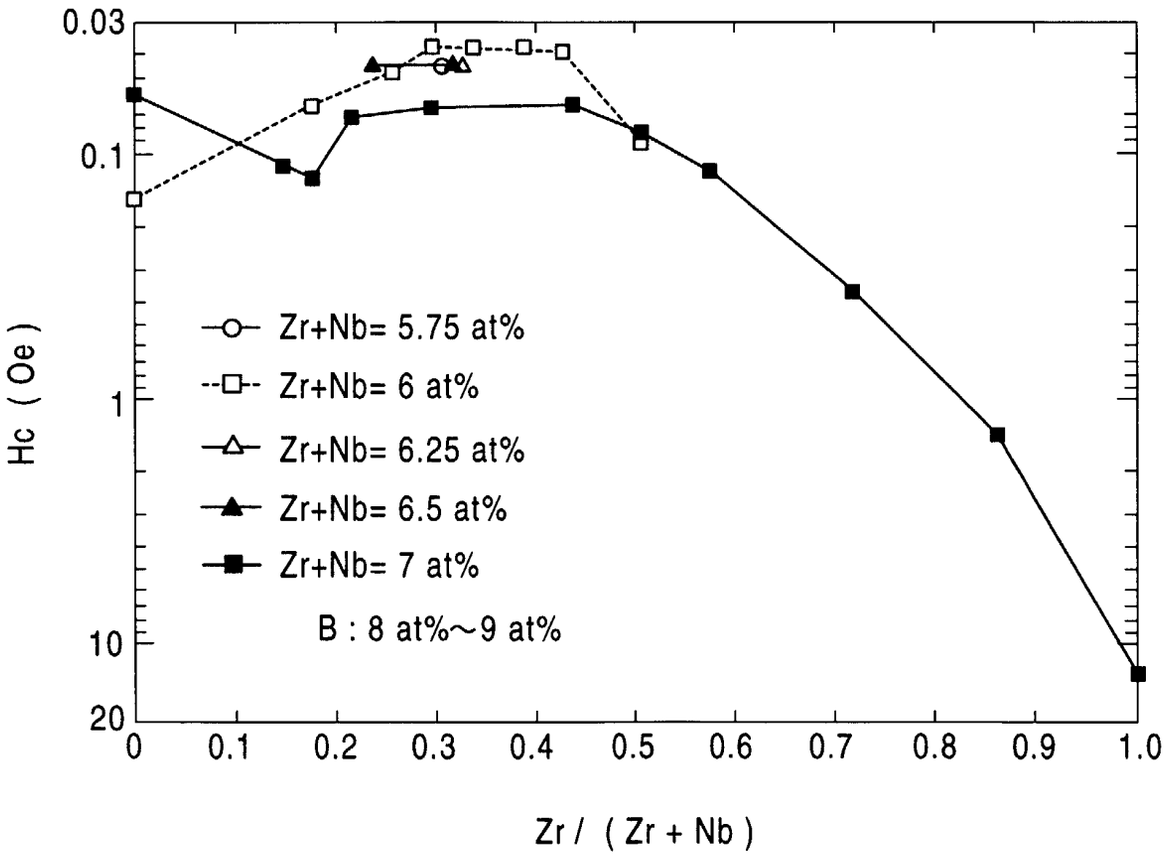
0.03
0.1
1
10
20
Hc (Oe)
0
0.1
0.2
0.3
0.4
0.5
0.6
0.7
0.8
0.9
1.0
Zr / (Zr + Nb)
Zr+Nb= 5.75 at%
Zr+Nb= 6 at%
Zr+Nb= 6.25 at%
Zr+Nb= 6.5 at%
Zr+Nb= 7 at%
B : 8 at%~9 at%

FIG. 61

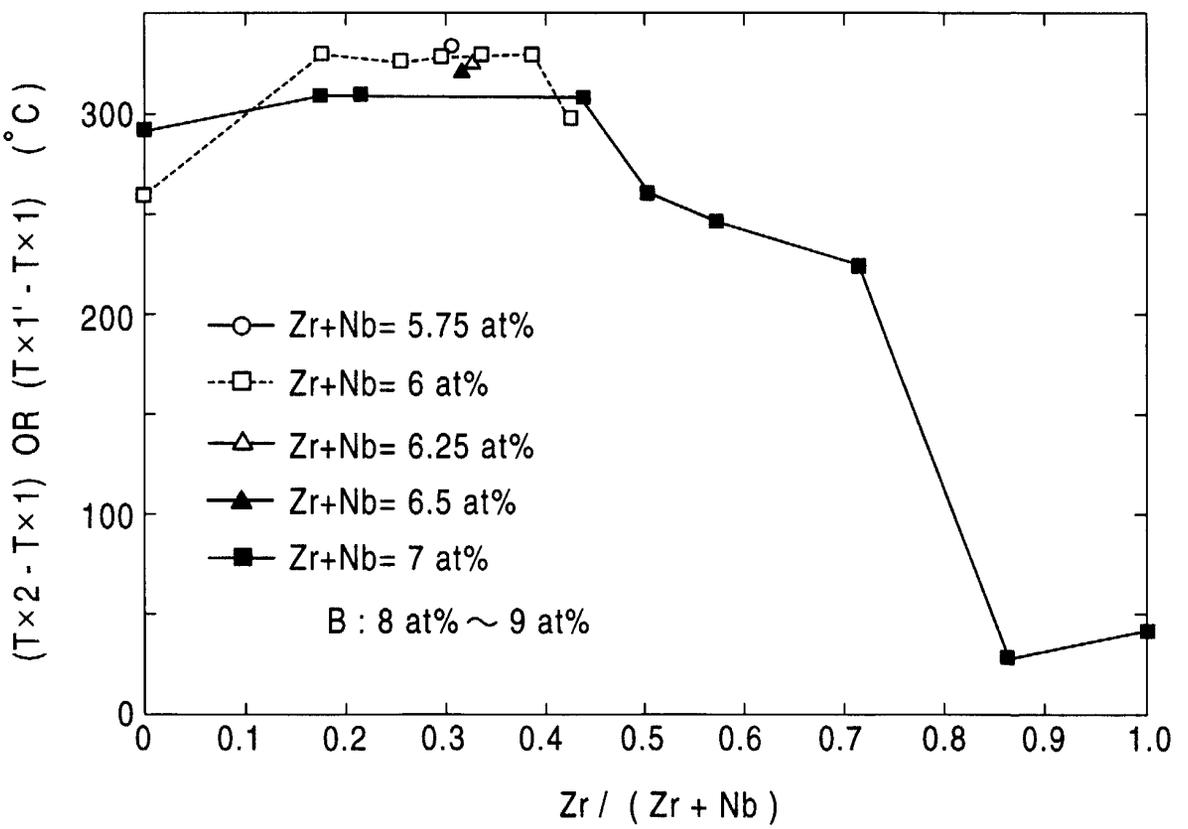
(T×2 - T×1) OR (T×1' - T×1) (°C)
300
200
100
0
0
0.1
0.2
0.3
0.4
0.5
0.6
0.7
0.8
0.9
1.0
Zr / (Zr + Nb)
Zr+Nb= 5.75 at%
Zr+Nb= 6 at%
Zr+Nb= 6.25 at%
Zr+Nb= 6.5 at%
Zr+Nb= 7 at%
B : 8 at% ~ 9 at%

FIG. 62

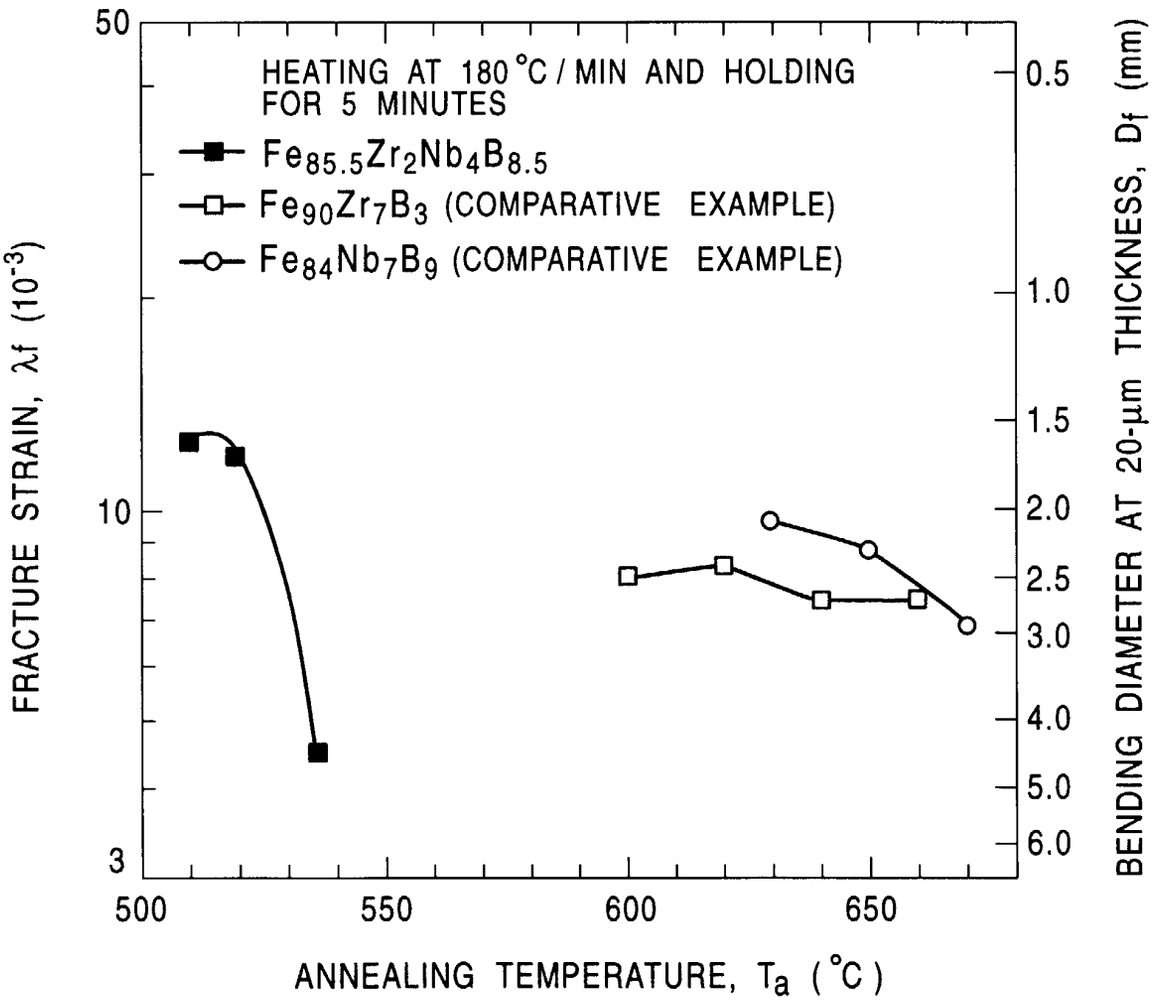
HEATING AT 180 °C / MIN AND HOLDING FOR 5 MINUTES
Fe85.5Zr2Nb4B8.5
Fe90Zr7B3 (COMPARATIVE EXAMPLE)
Fe84Nb7B9 (COMPARATIVE EXAMPLE)
FRACTURE STRAIN, λf (10-3)
BENDING DIAMETER AT 20-μm THICKNESS, Df (mm)
ANNEALING TEMPERATURE, Ta (°C)
50
10
3
500
550
600
650
0.5
1.0
1.5
2.0
2.5
3.0
4.0
5.0
6.0

FIG. 63

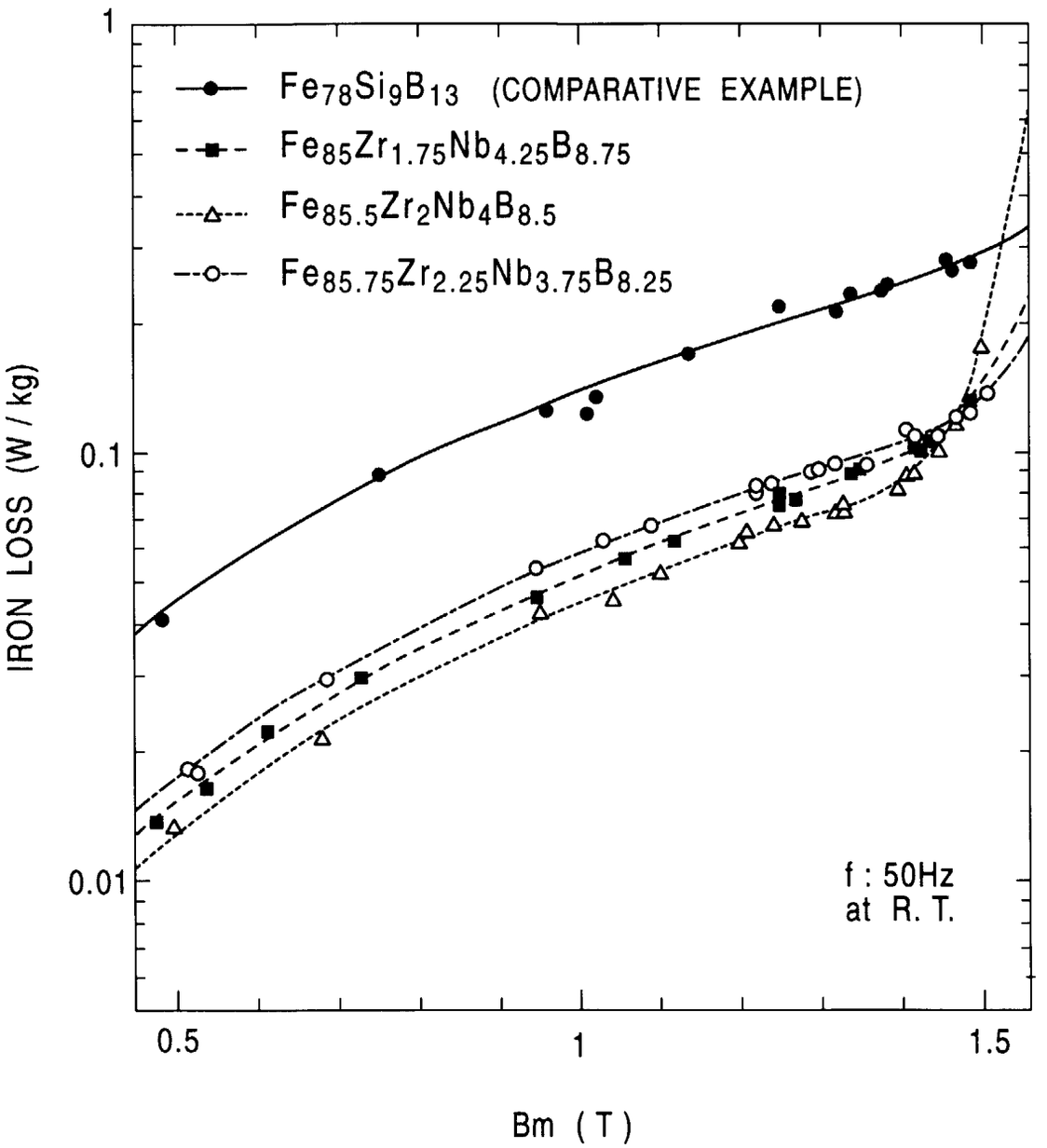
1
0.1
0.01
IRON LOSS (W / kg)
Fe78Si9B13 (COMPARATIVE EXAMPLE)
Fe85Zr1.75Nb4.25B8.75
Fe85.5Zr2Nb4B8.5
Fe85.75Zr2.25Nb3.75B8.25
f : 50Hz
at R. T.
0.5
1
1.5
Bm (T)

FIG. 64

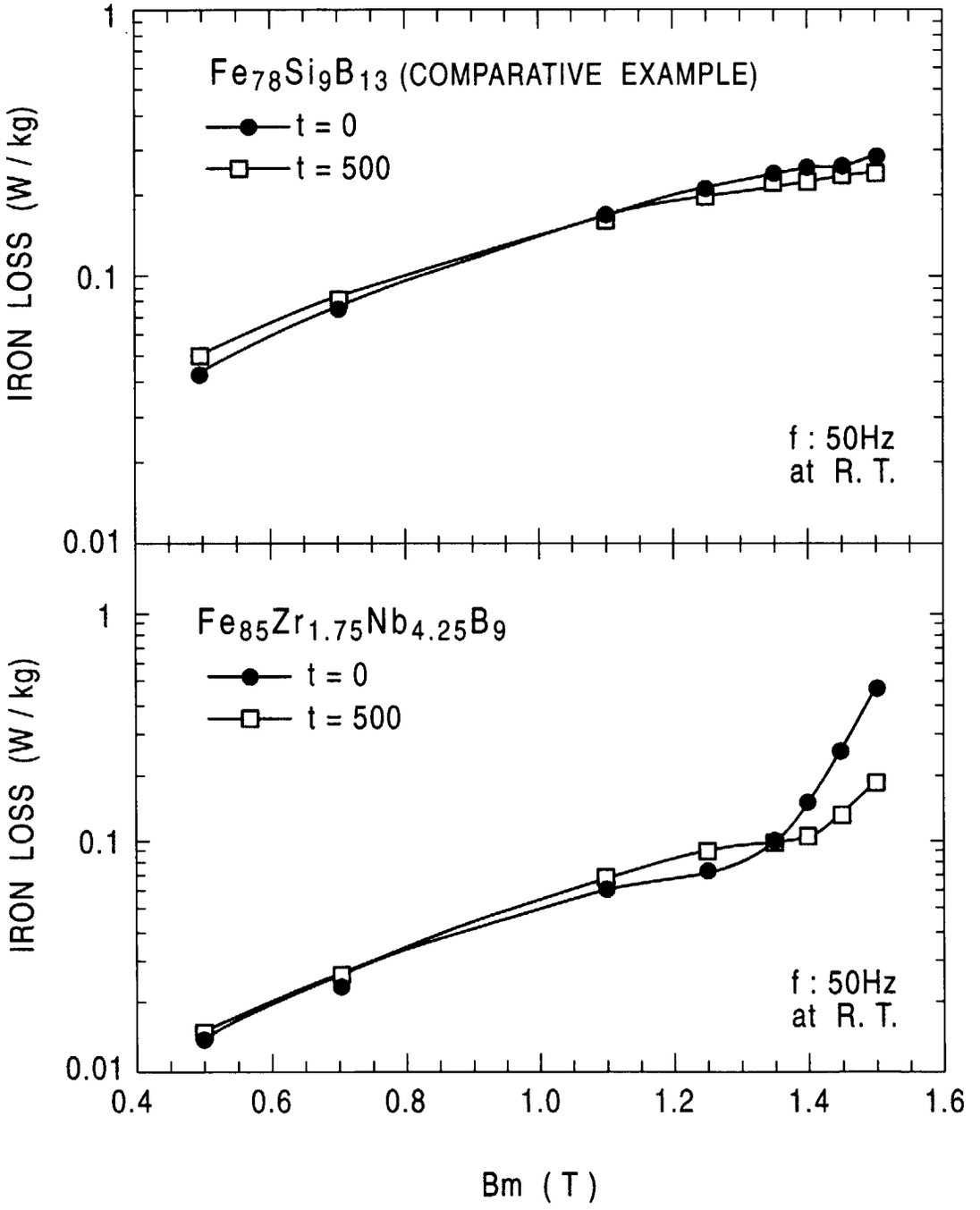
1
0.1
0.01
IRON LOSS (W / kg)
$Fe_{78}Si_9B_{13}$ (COMPARATIVE EXAMPLE)
t = 0
t = 500
f : 50Hz
at R. T.
1
0.1
0.01
IRON LOSS (W / kg)
$Fe_{85}Zr_{1.75}Nb_{4.25}B_9$
t = 0
t = 500
f : 50Hz
at R. T.
0.4
0.6
0.8
1.0
1.2
1.4
1.6
Bm (T)

FIG. 65

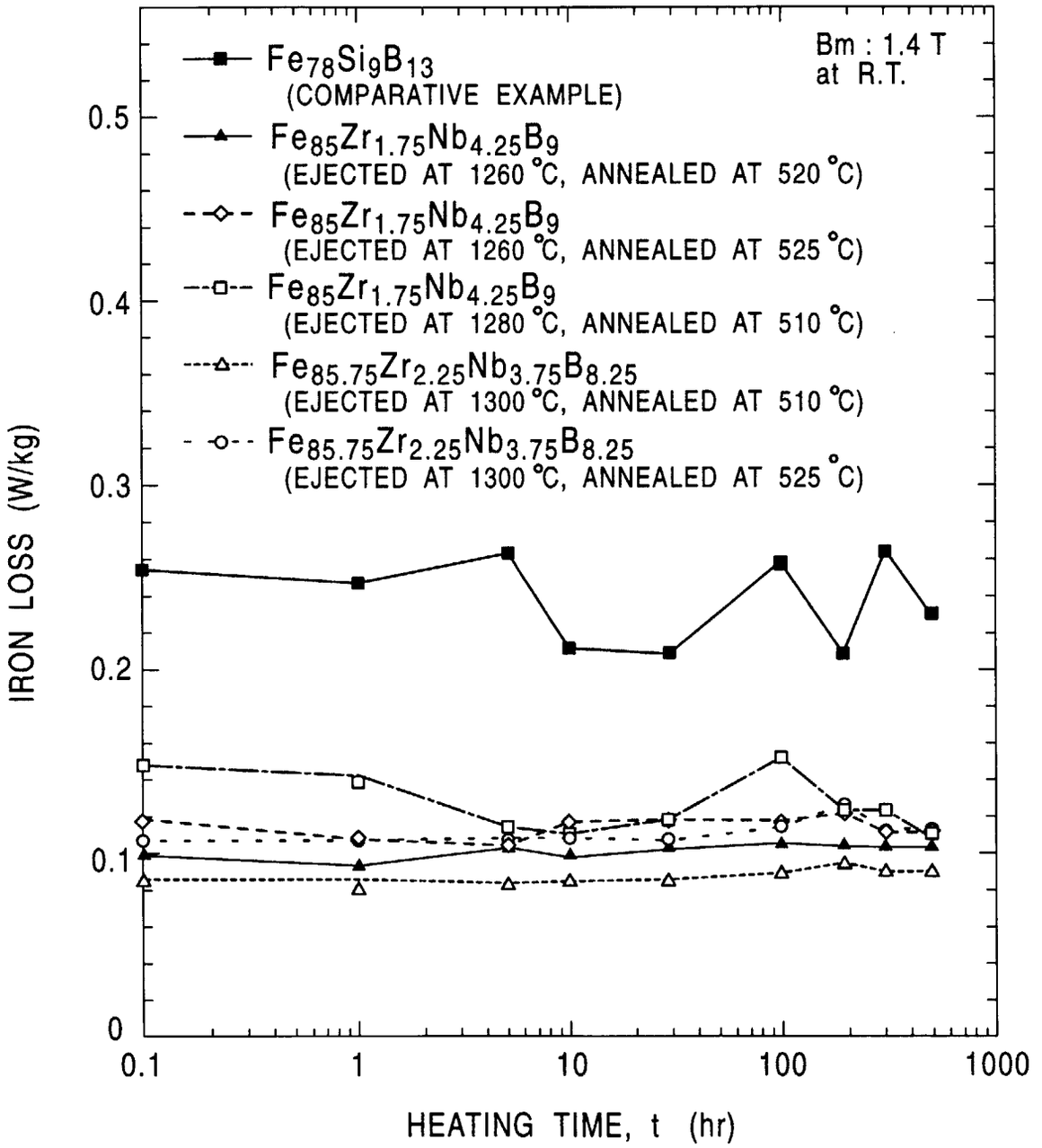
Bm : 1.4 T
at R.T.
$Fe_{78}Si_9B_{13}$
(COMPARATIVE EXAMPLE)
$Fe_{85}Zr_{1.75}Nb_{4.25}B_9$
(EJECTED AT 1260 °C, ANNEALED AT 520 °C)
$Fe_{85}Zr_{1.75}Nb_{4.25}B_9$
(EJECTED AT 1260 °C, ANNEALED AT 525 °C)
$Fe_{85}Zr_{1.75}Nb_{4.25}B_9$
(EJECTED AT 1280 °C, ANNEALED AT 510 °C)
$Fe_{85.75}Zr_{2.25}Nb_{3.75}B_{8.25}$
(EJECTED AT 1300 °C, ANNEALED AT 510 °C)
$Fe_{85.75}Zr_{2.25}Nb_{3.75}B_{8.25}$
(EJECTED AT 1300 °C, ANNEALED AT 525 °C)
IRON LOSS (W/kg)
0
0.1
0.2
0.3
0.4
0.5
0.1
1
10
100
1000
HEATING TIME, t (hr)

FIG. 66

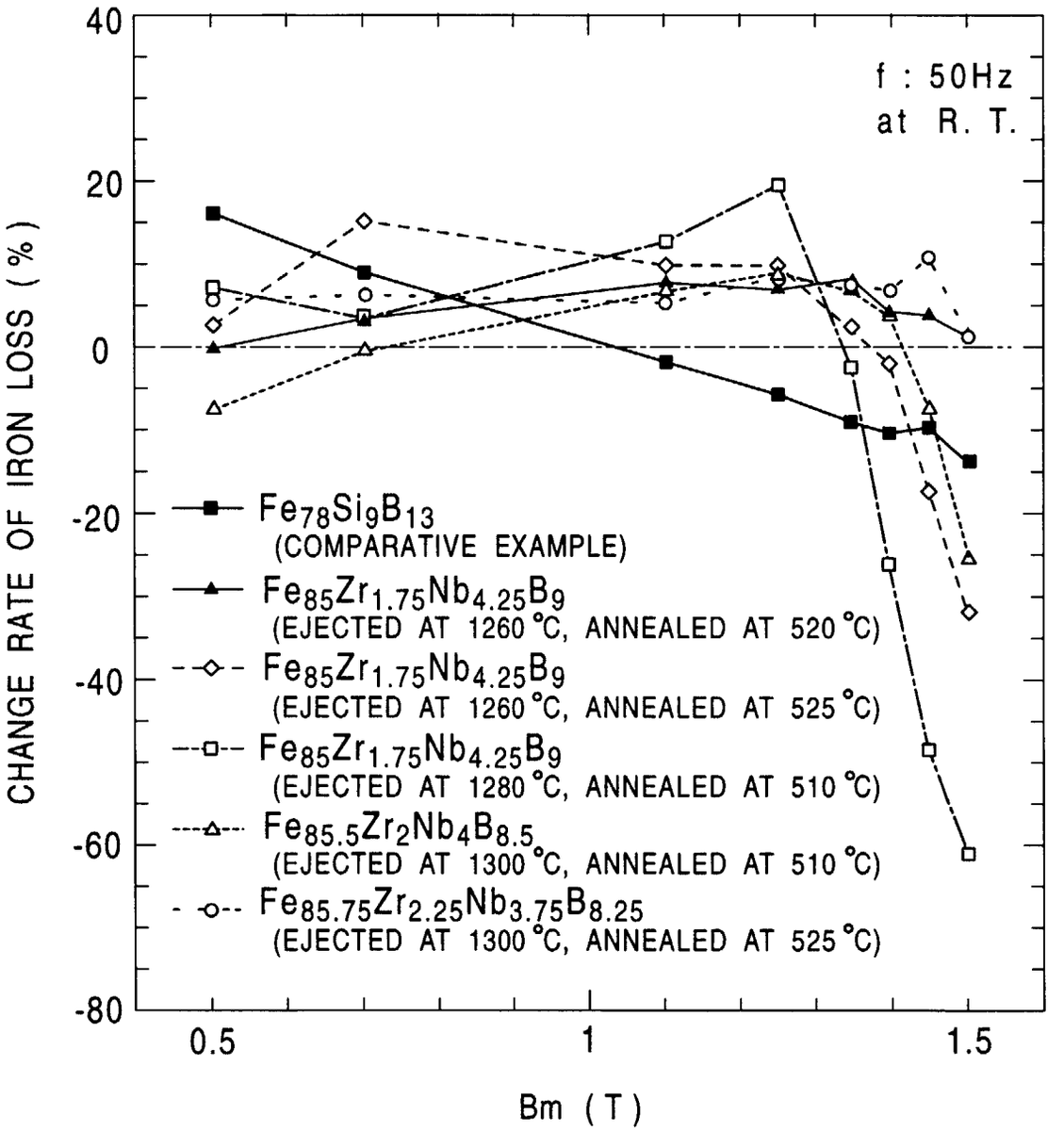
f : 50Hz
at R. T.
CHANGE RATE OF IRON LOSS (%)
40
20
0
-20
-40
-60
-80
0.5
1
1.5
Bm (T)
Fe78Si9B13
(COMPARATIVE EXAMPLE)
Fe85Zr1.75Nb4.25B9
(EJECTED AT 1260 °C, ANNEALED AT 520 °C)
Fe85Zr1.75Nb4.25B9
(EJECTED AT 1260 °C, ANNEALED AT 525 °C)
Fe85Zr1.75Nb4.25B9
(EJECTED AT 1280 °C, ANNEALED AT 510 °C)
Fe85.5Zr2Nb4B8.5
(EJECTED AT 1300 °C, ANNEALED AT 510 °C)
Fe85.75Zr2.25Nb3.75B8.25
(EJECTED AT 1300 °C, ANNEALED AT 525 °C)

FIG. 67

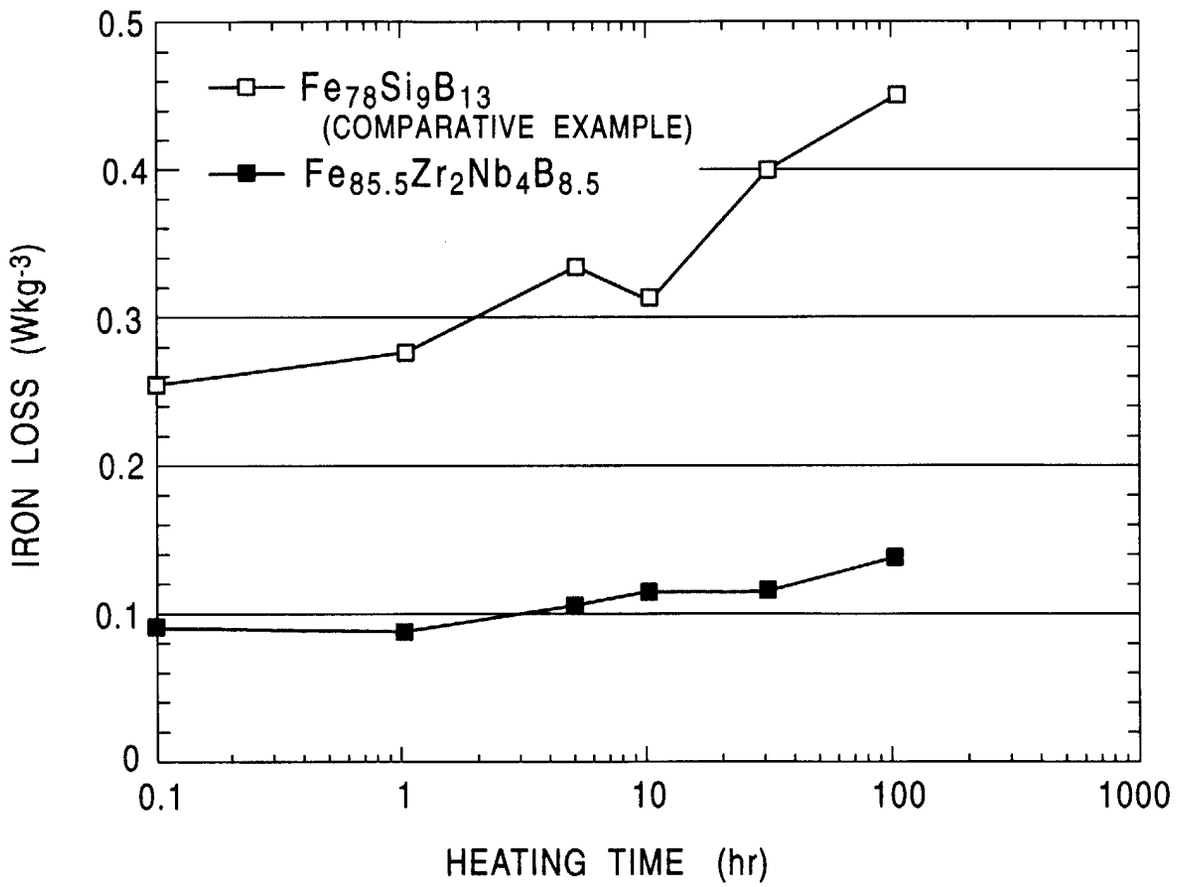
0.5
0.4
0.3
0.2
0.1
0
IRON LOSS (Wkg-3)
Fe78Si9B13
(COMPARATIVE EXAMPLE)
Fe85.5Zr2Nb4B8.5
0.1
1
10
100
1000
HEATING TIME (hr)

FIG. 68

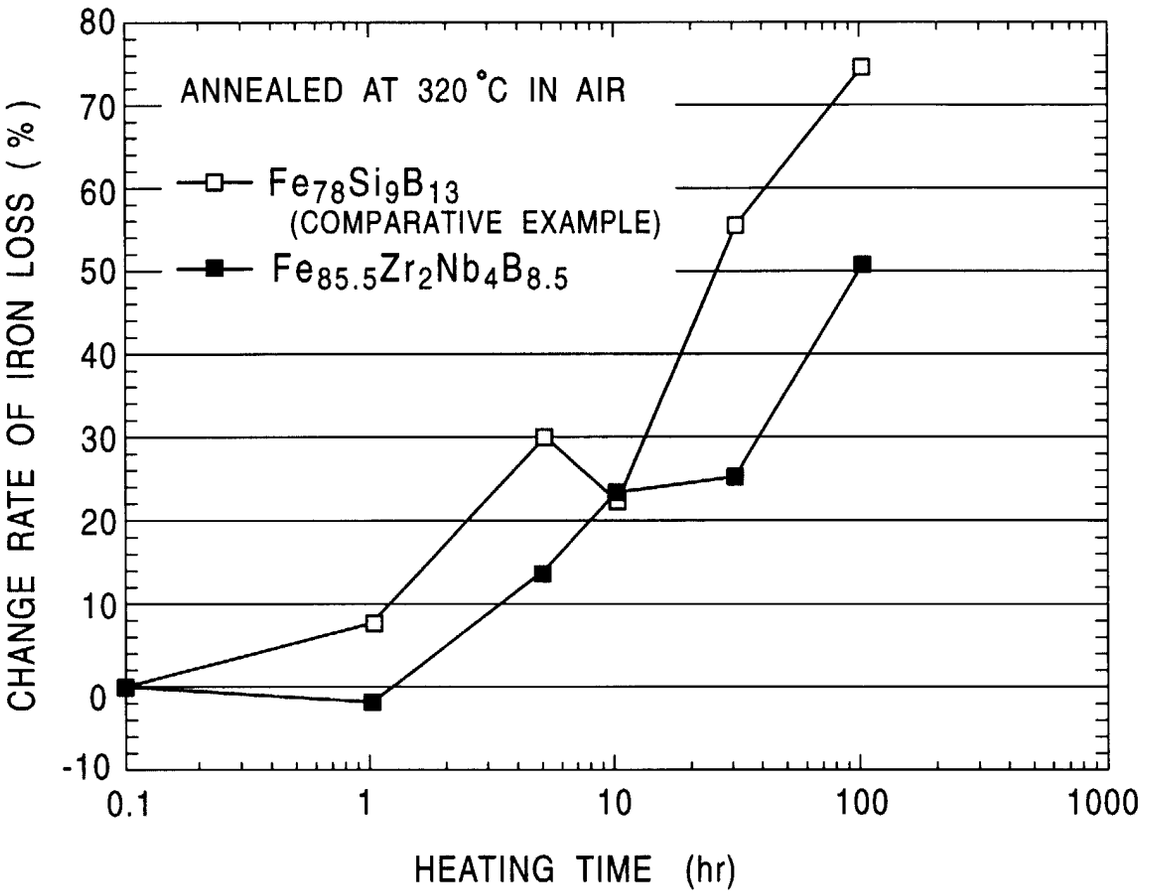
ANNEALED AT 320 °C IN AIR
$Fe_{78}Si_9B_{13}$
(COMPARATIVE EXAMPLE)
$Fe_{85.5}Zr_2Nb_4B_{8.5}$
CHANGE RATE OF IRON LOSS (%)
80
70
60
50
40
30
20
10
0
-10
0.1
1
10
100
1000
HEATING TIME (hr)

FIG. 69

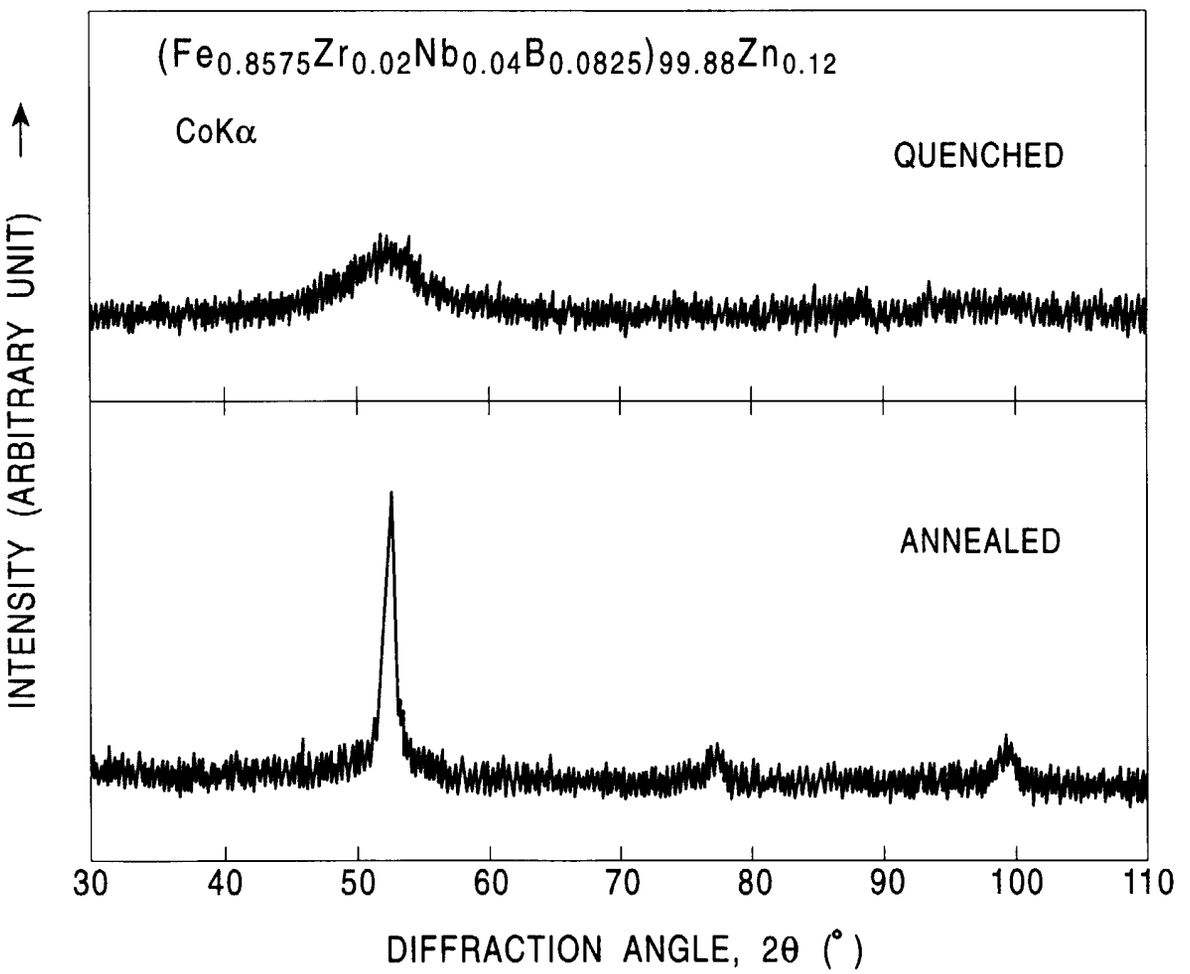
$(Fe_{0.8575}Zr_{0.02}Nb_{0.04}B_{0.0825})_{99.88}Zn_{0.12}$
CoKα
QUENCHED
ANNEALED
INTENSITY (ARBITRARY UNIT)
30
40
50
60
70
80
90
100
110
DIFFRACTION ANGLE, 2θ (°)

FIG. 70

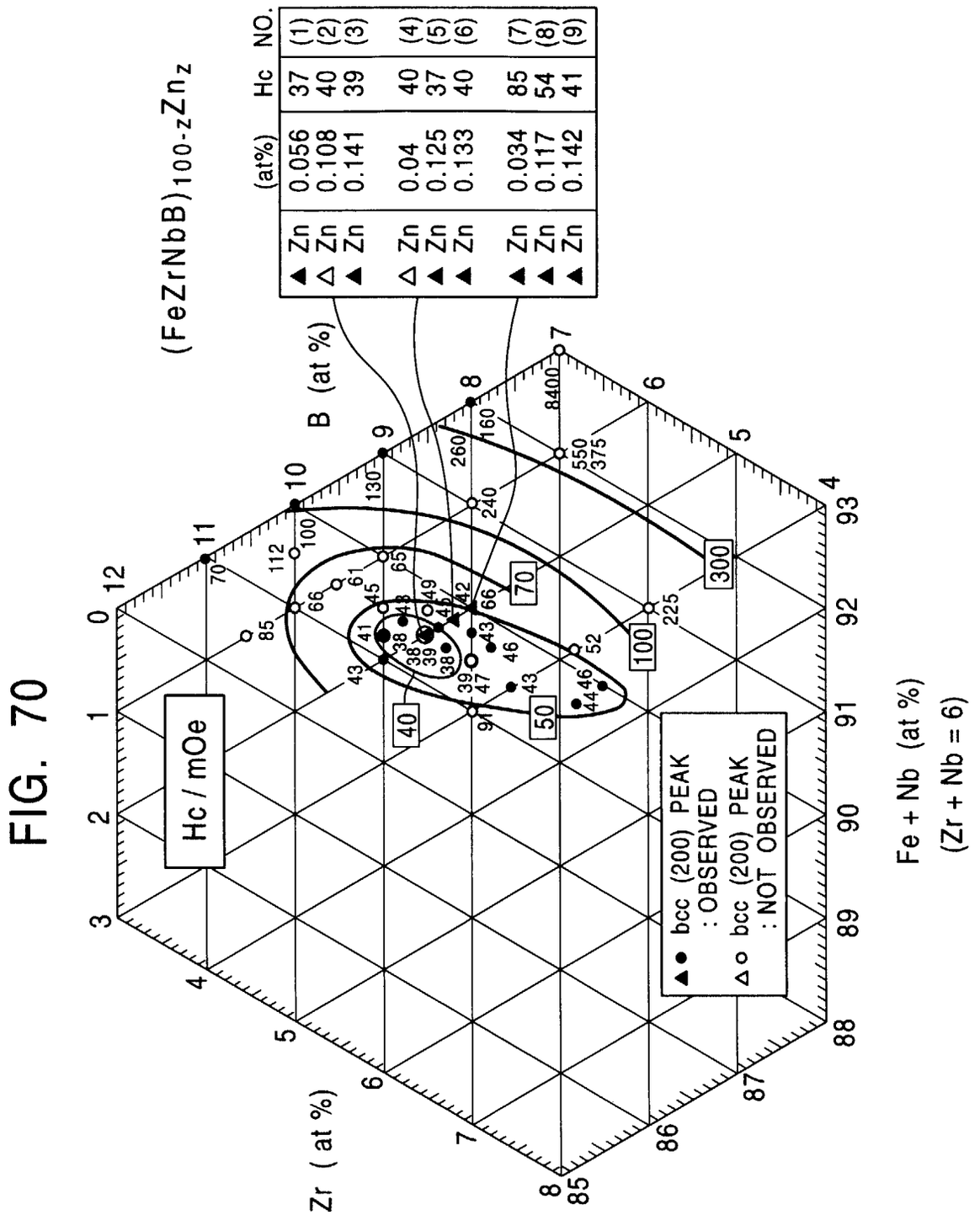
(FeZrNbB)100-zZnz
B (at %)
Zr (at %)
Fe + Nb (at %)
(Zr + Nb = 6)
Hc / mOe
40
50
70
100
300
▲● bcc (200) PEAK : OBSERVED
△○ bcc (200) PEAK : NOT OBSERVED
▲ Zn 0.056 37 (1)
△ Zn 0.108 40 (2)
▲ Zn 0.141 39 (3)
△ Zn 0.04 40 (4)
▲ Zn 0.125 37 (5)
▲ Zn 0.133 40 (6)
▲ Zn 0.034 85 (7)
▲ Zn 0.117 54 (8)
▲ Zn 0.142 41 (9)
(at%) Hc NO.

FIG. 71

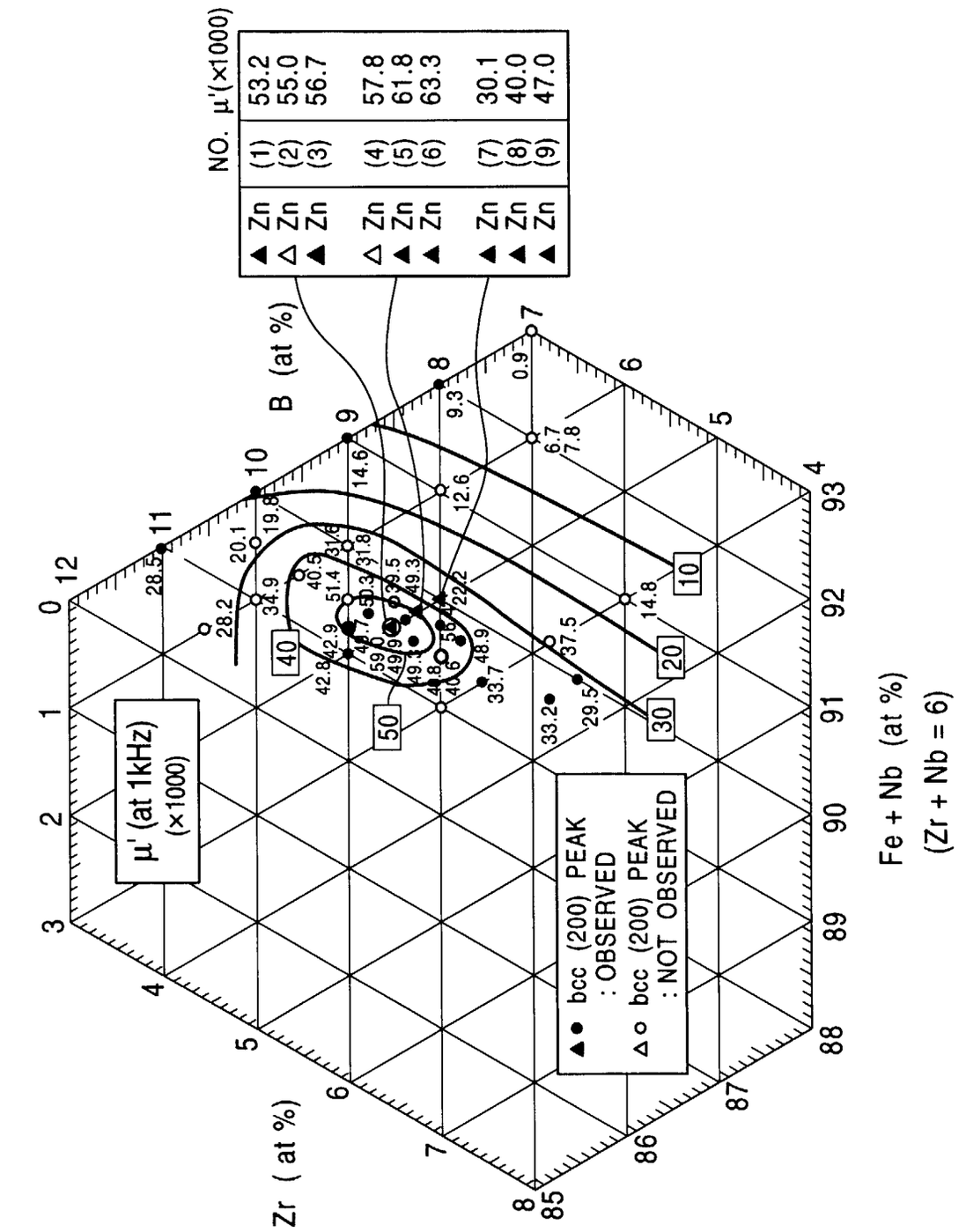
NO. μ'(×1000)
▲ Zn (1) 53.2
△ Zn (2) 55.0
▲ Zn (3) 56.7
△ Zn (4) 57.8
▲ Zn (5) 61.8
▲ Zn (6) 63.3
▲ Zn (7) 30.1
▲ Zn (8) 40.0
▲ Zn (9) 47.0
μ' (at 1kHz) (×1000)
▲● bcc (200) PEAK : OBSERVED
△○ bcc (200) PEAK : NOT OBSERVED
B (at %)
Zr (at %)
Fe + Nb (at %)
(Zr + Nb = 6)

FIG. 72

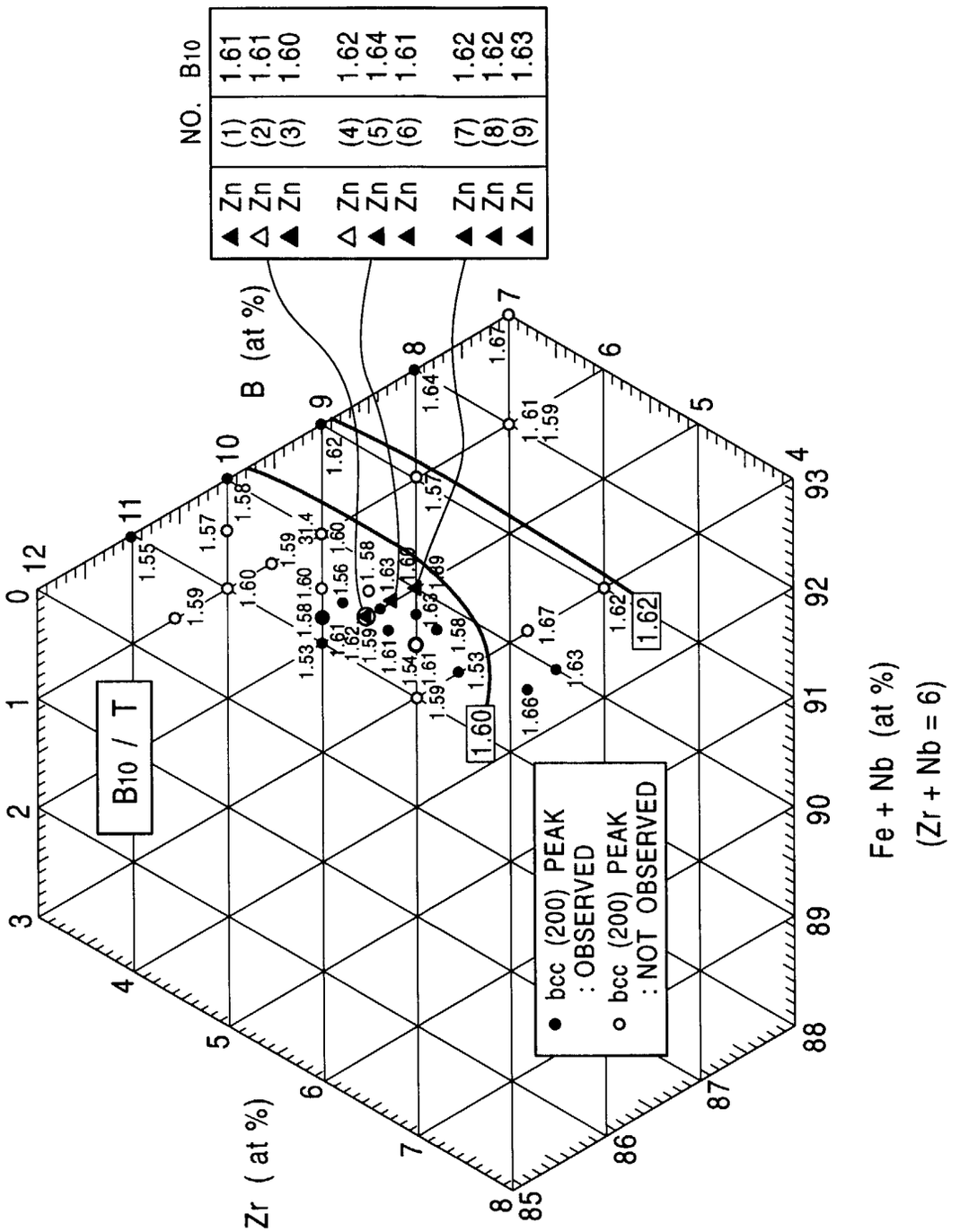
NO. B10
▲ Zn (1) 1.61
△ Zn (2) 1.61
▲ Zn (3) 1.60
△ Zn (4) 1.62
▲ Zn (5) 1.64
▲ Zn (6) 1.61
▲ Zn (7) 1.62
▲ Zn (8) 1.62
▲ Zn (9) 1.63
B10 / T
B (at %)
Zr (at %)
Fe + Nb (at %)
(Zr + Nb = 6)
● bcc (200) PEAK : OBSERVED
○ bcc (200) PEAK : NOT OBSERVED

FIG. 73

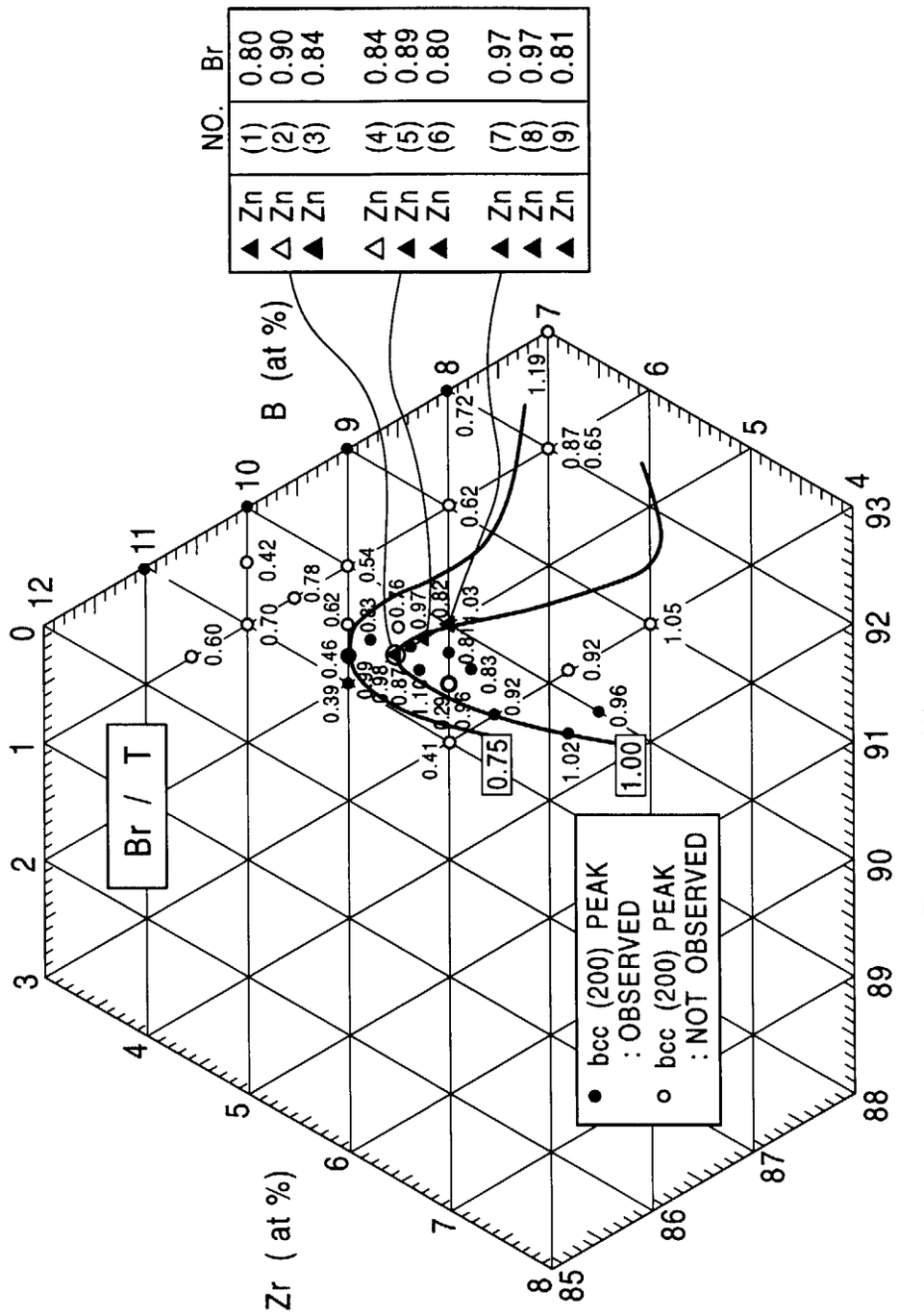
NO. Br
▲ Zn (1) 0.80
△ Zn (2) 0.90
▲ Zn (3) 0.84
△ Zn (4) 0.84
▲ Zn (5) 0.89
▲ Zn (6) 0.80
▲ Zn (7) 0.97
▲ Zn (8) 0.97
▲ Zn (9) 0.81
B (at %)
Zr (at %)
Fe + Nb (at %)
(Zr + Nb = 6)
Br / T
0.75
1.00
● bcc (200) PEAK : OBSERVED
○ bcc (200) PEAK : NOT OBSERVED

FIG. 74

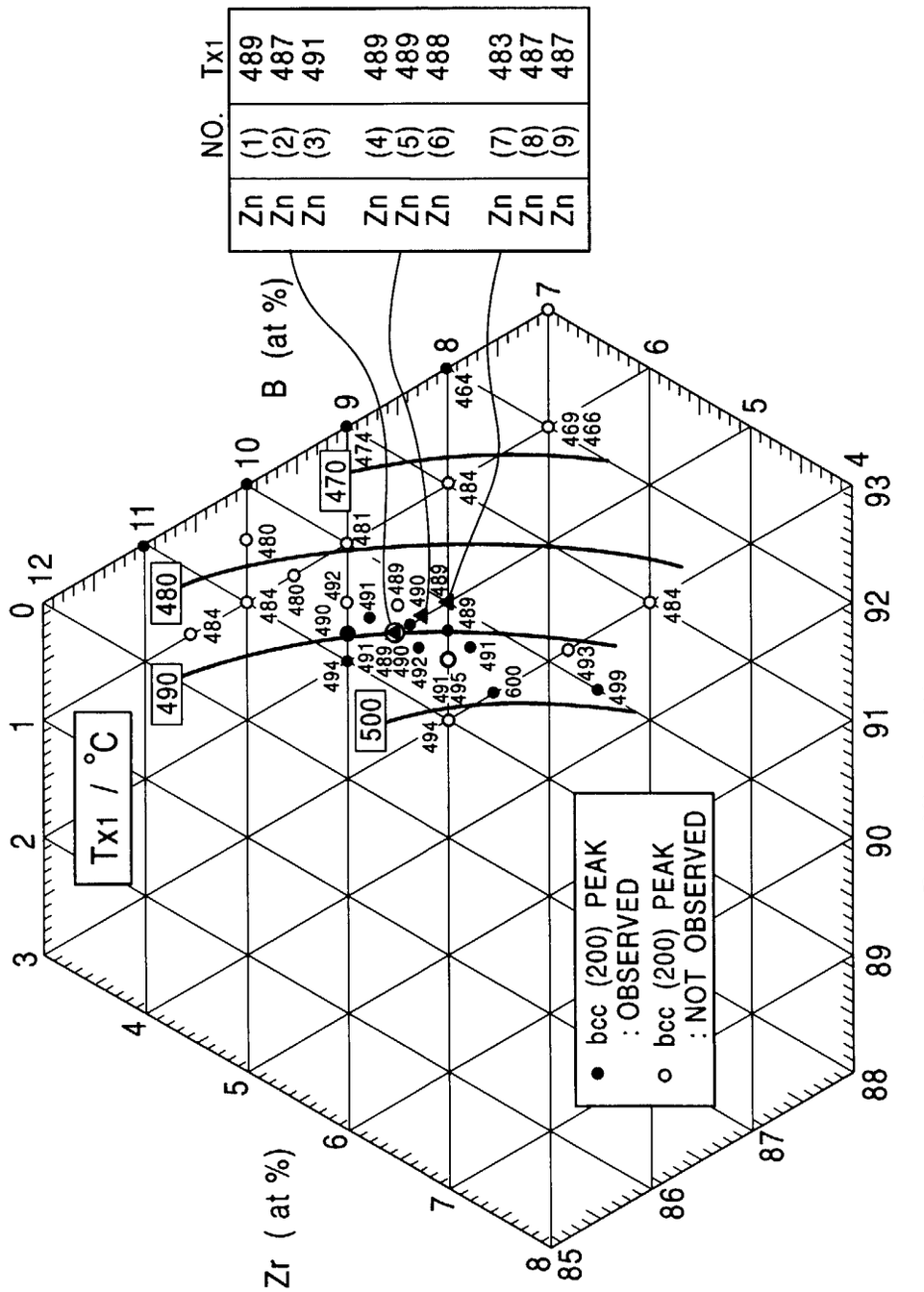
NO. Tx1
(1) 489
(2) 487
(3) 491
(4) 489
(5) 489
(6) 488
(7) 483
(8) 487
(9) 487
Zn
Tx1 / °C
480
490
500
470
B (at %)
Zr (at %)
Fe + Nb (at %)
(Zr + Nb = 6)
● bcc (200) PEAK : OBSERVED
○ bcc (200) PEAK : NOT OBSERVED

FIG. 75

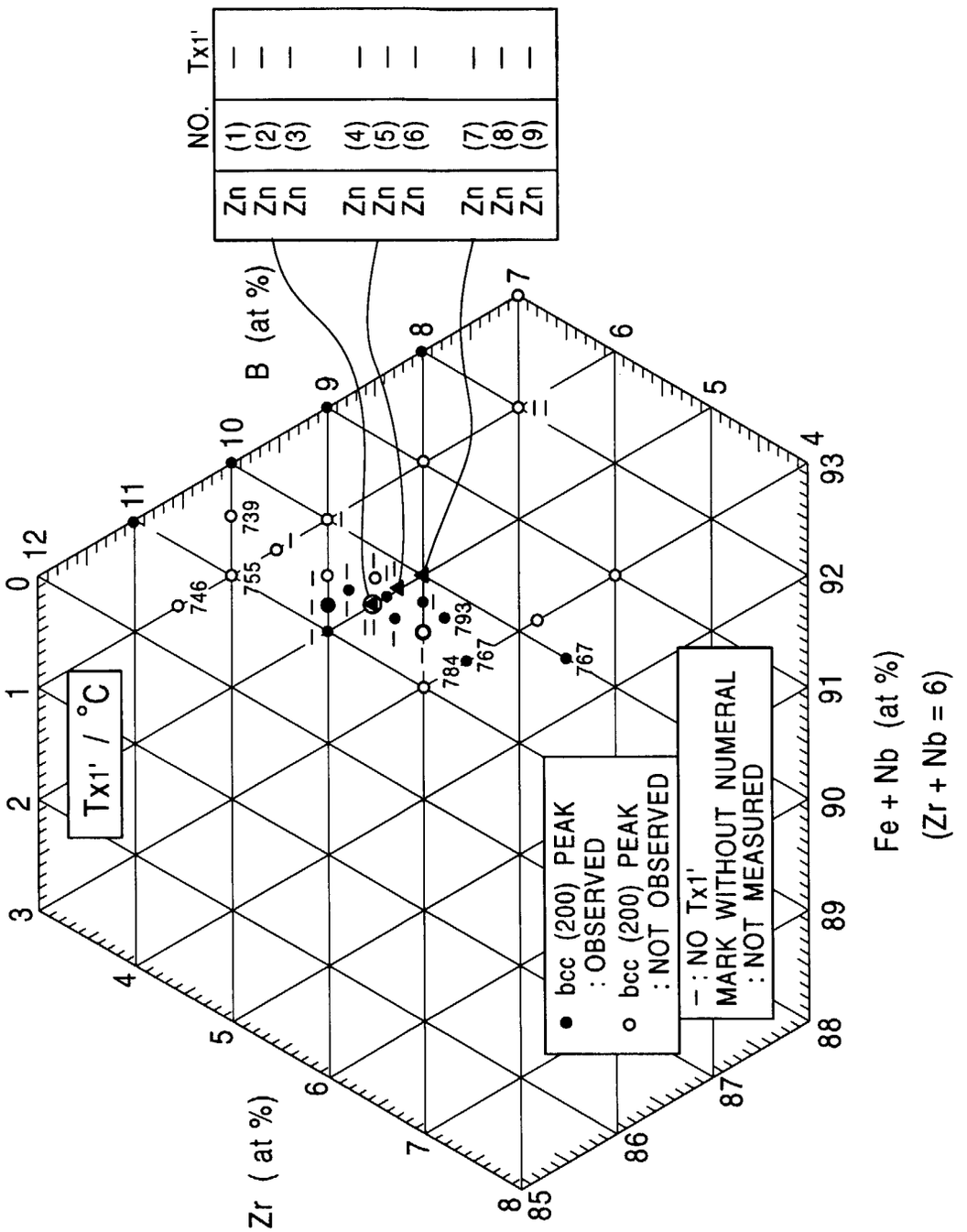
NO. Tx1'
(1) —
(2) —
(3) —
(4) —
(5) —
(6) —
(7) —
(8) —
(9) —
Zn
Tx1' / °C
B (at %)
Zr (at %)
Fe + Nb (at %)
(Zr + Nb = 6)
746
739
755
784
793
767
767
● bcc (200) PEAK : OBSERVED
o bcc (200) PEAK : NOT OBSERVED
— : NO Tx1' MARK WITHOUT NUMERAL : NOT MEASURED

FIG. 76

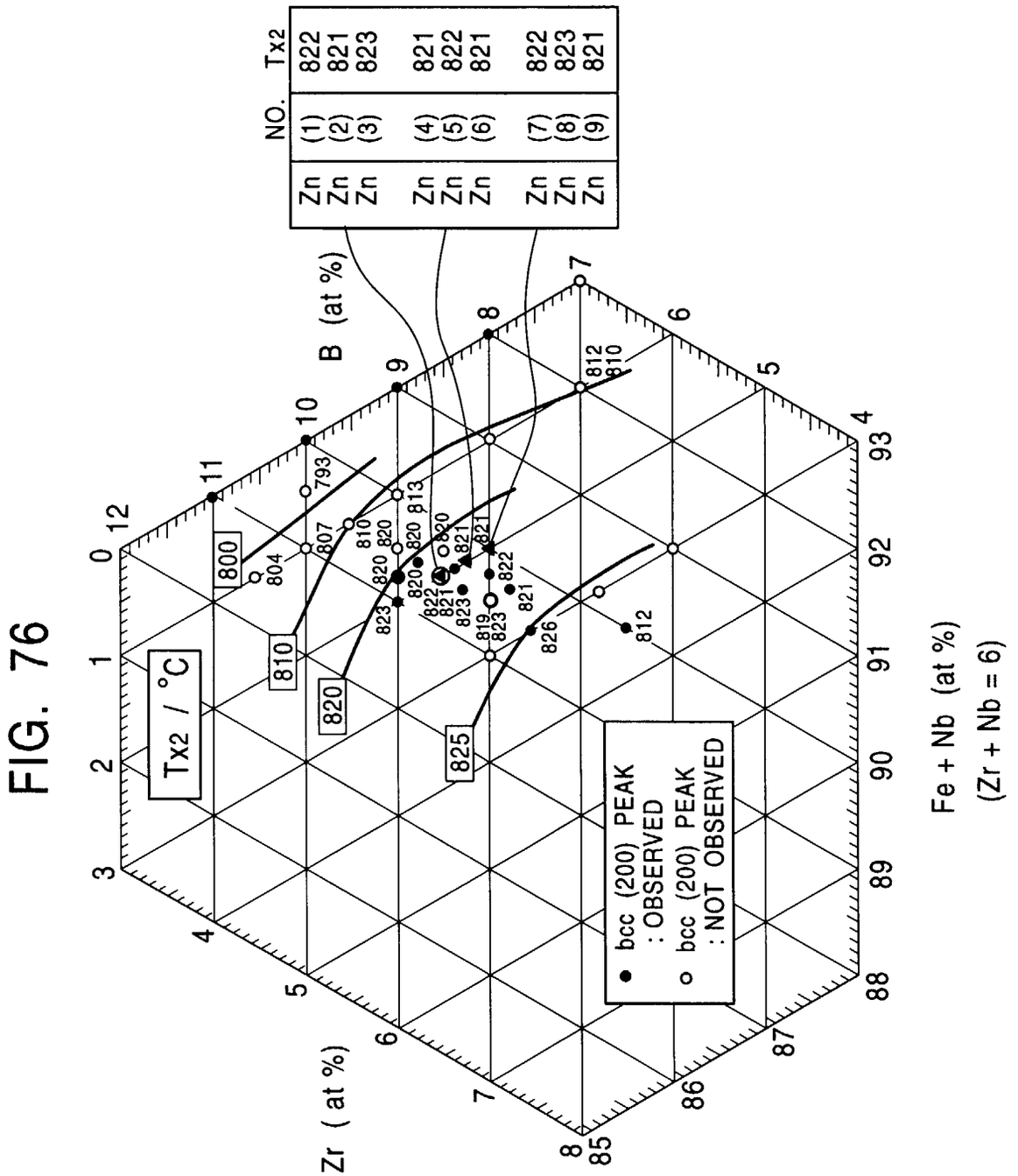
NO. Tx2
(1) Zn 822
(2) Zn 821
(3) Zn 823
(4) Zn 821
(5) Zn 822
(6) Zn 821
(7) Zn 822
(8) Zn 823
(9) Zn 821
Tx2 / °C
800
810
820
825
B (at %)
Zr (at %)
Fe + Nb (at %)
(Zr + Nb = 6)
● bcc (200) PEAK : OBSERVED
○ bcc (200) PEAK : NOT OBSERVED

FIG. 77

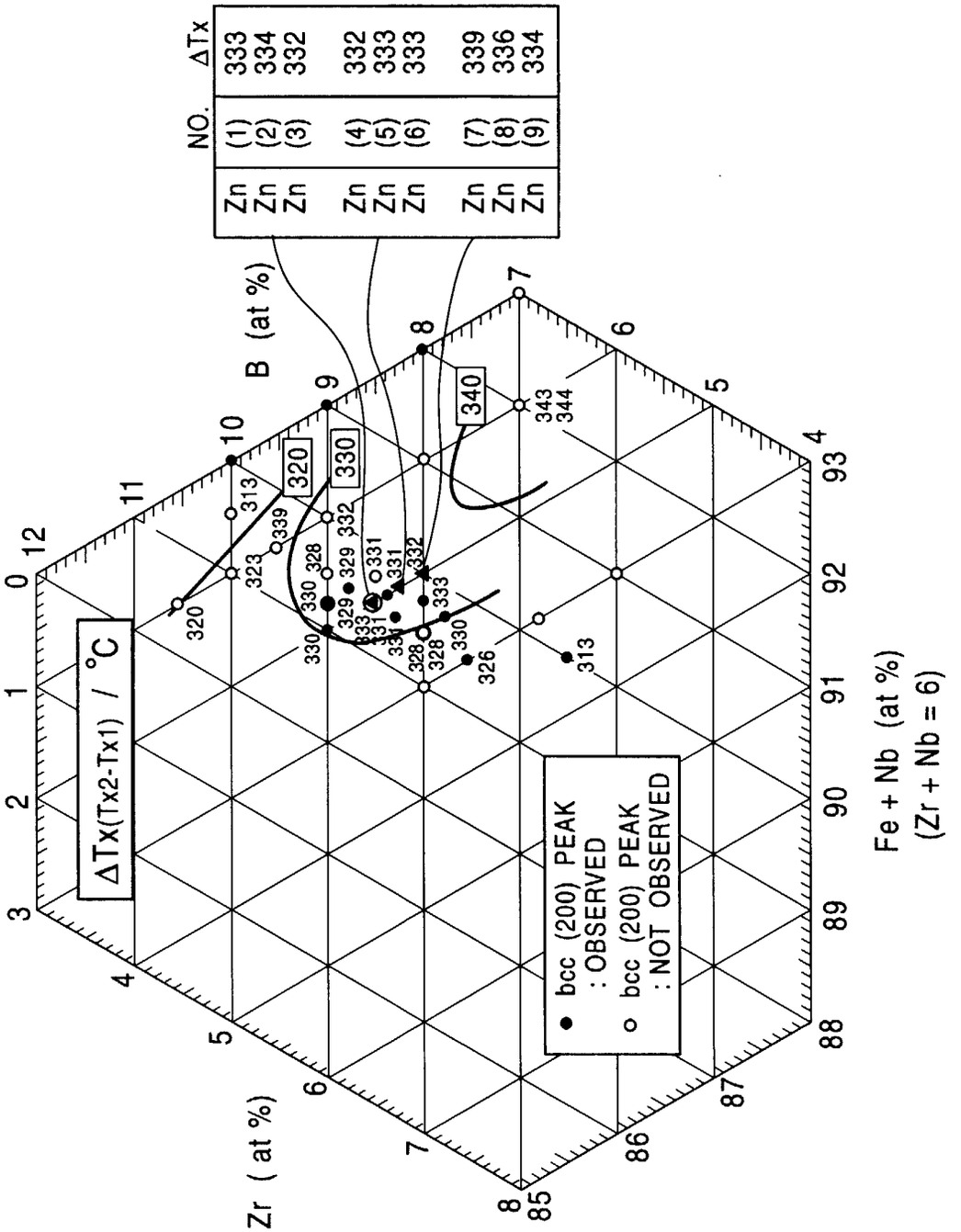
NO. ΔTx
Zn (1) 333
Zn (2) 334
Zn (3) 332
Zn (4) 332
Zn (5) 333
Zn (6) 333
Zn (7) 339
Zn (8) 336
Zn (9) 334
ΔTx(Tx2-Tx1) / °C
B (at %)
Zr (at %)
Fe + Nb (at %)
(Zr + Nb = 6)
320
330
340
● bcc (200) PEAK : OBSERVED
○ bcc (200) PEAK : NOT OBSERVED

FIG. 78

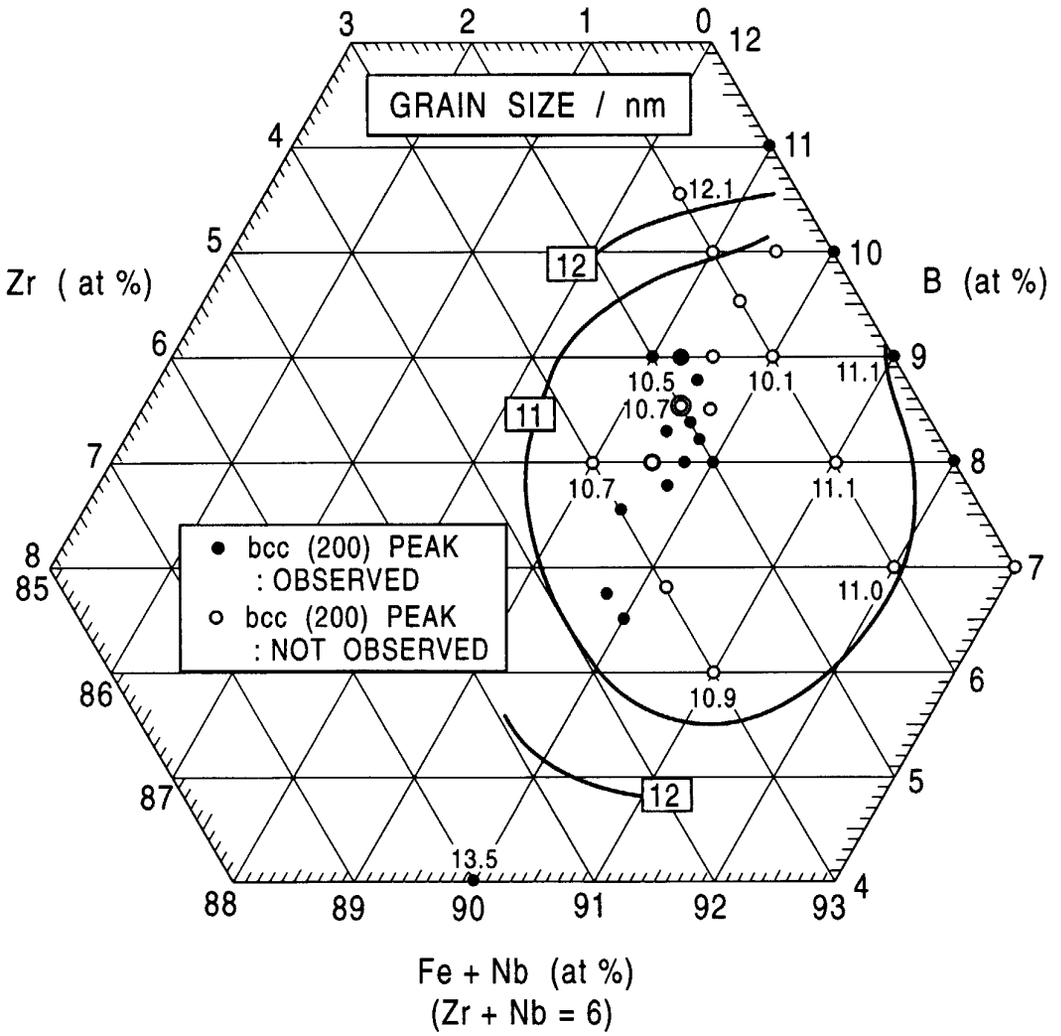
GRAIN SIZE / nm
Zr (at %)
B (at %)
Fe + Nb (at %)
(Zr + Nb = 6)
bcc (200) PEAK
: OBSERVED
bcc (200) PEAK
: NOT OBSERVED
12
11
12
12.1
10.5
10.7
10.1
11.1
10.7
11.1
11.0
10.9
13.5

FIG. 79

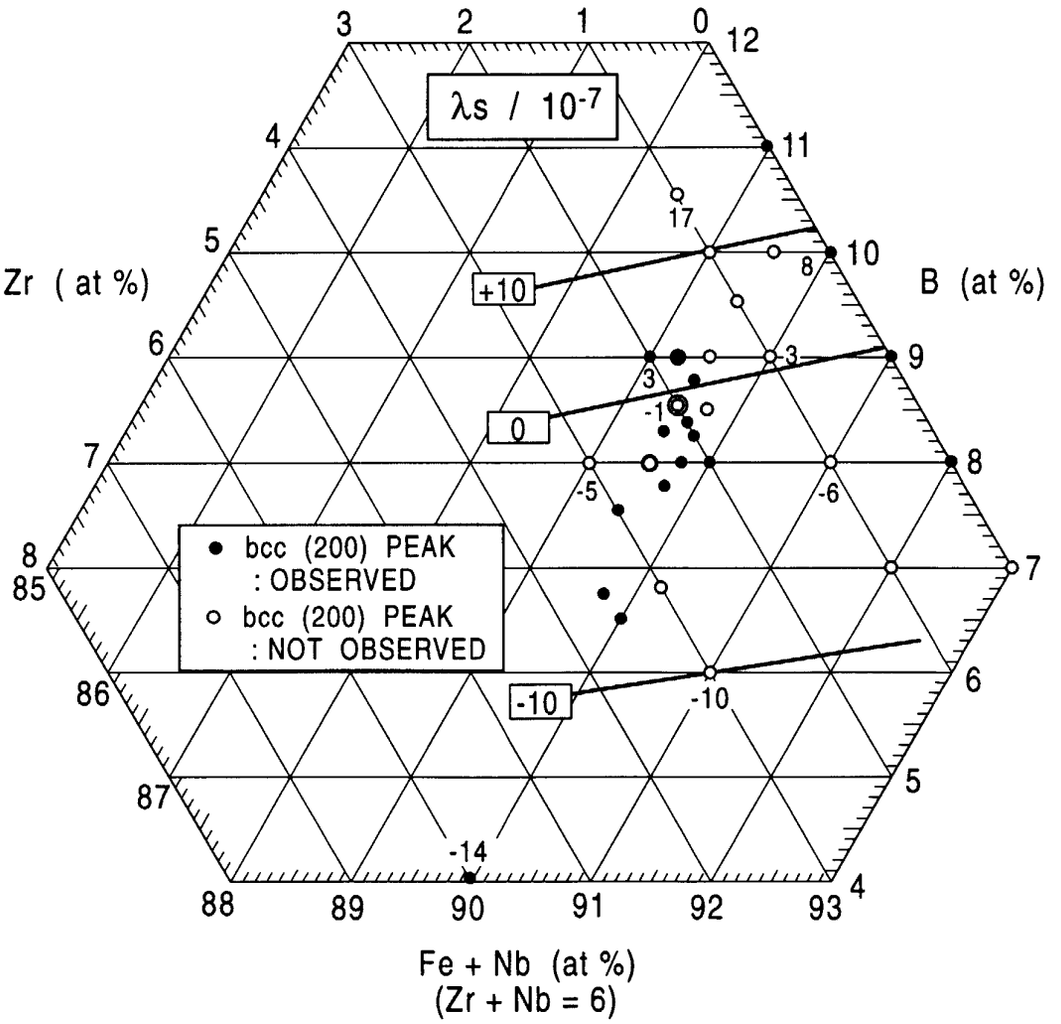
λs / 10-7
+10
0
-10
17
8
3
-1
-5
-6
-10
-14
bcc (200) PEAK
: OBSERVED
bcc (200) PEAK
: NOT OBSERVED
Zr (at %)
B (at %)
Fe + Nb (at %)
(Zr + Nb = 6)

FIG. 80

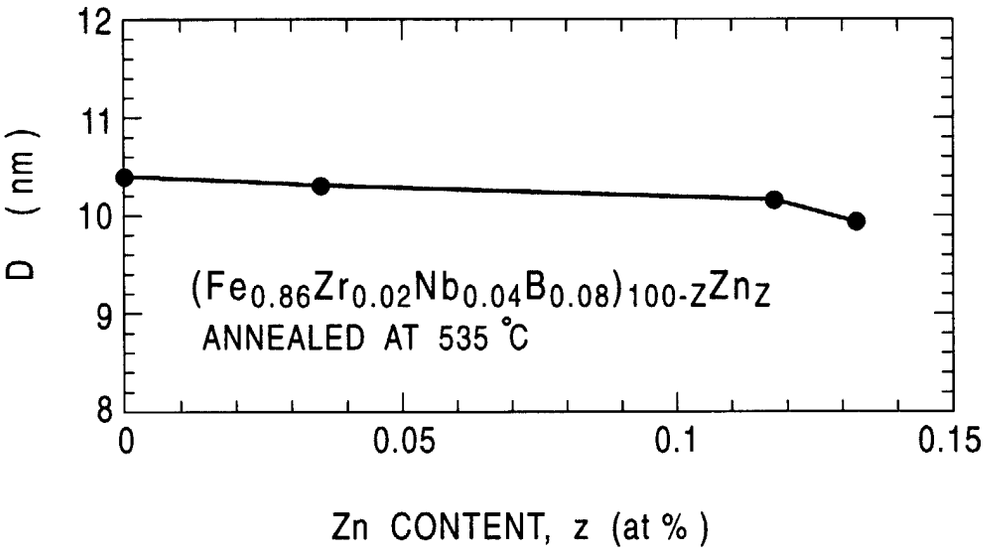
12
11
10
9
8
D (nm)
$(Fe_{0.86}Zr_{0.02}Nb_{0.04}B_{0.08})_{100-z}Zn_z$
ANNEALED AT 535 ℃
0
0.05
0.1
0.15
Zn CONTENT, z (at %)

FIG. 81

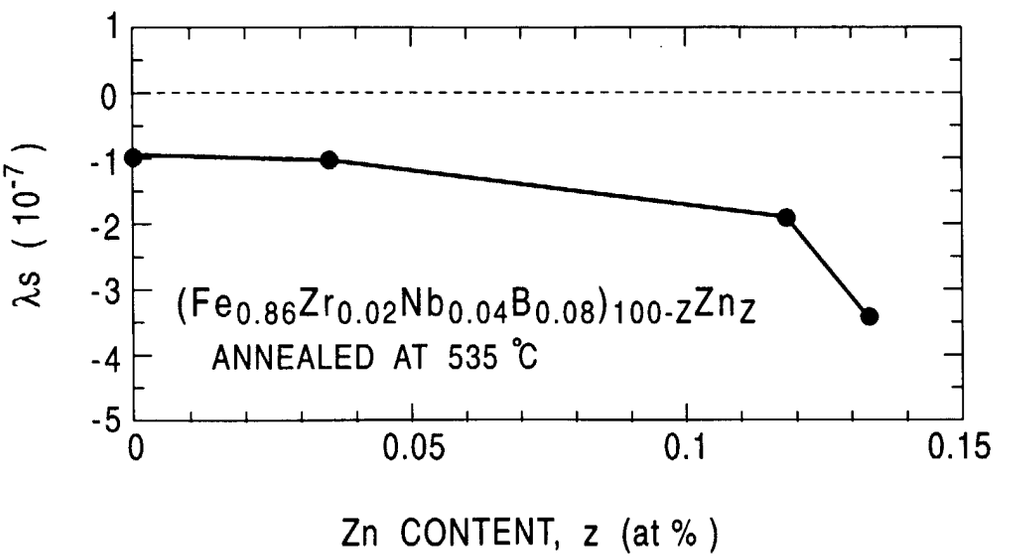
1
0
-1
-2
-3
-4
-5
λs (10^{-7})
$(Fe_{0.86}Zr_{0.02}Nb_{0.04}B_{0.08})_{100-z}Zn_z$
ANNEALED AT 535 ℃
0
0.05
0.1
0.15
Zn CONTENT, z (at %)

FIG. 82

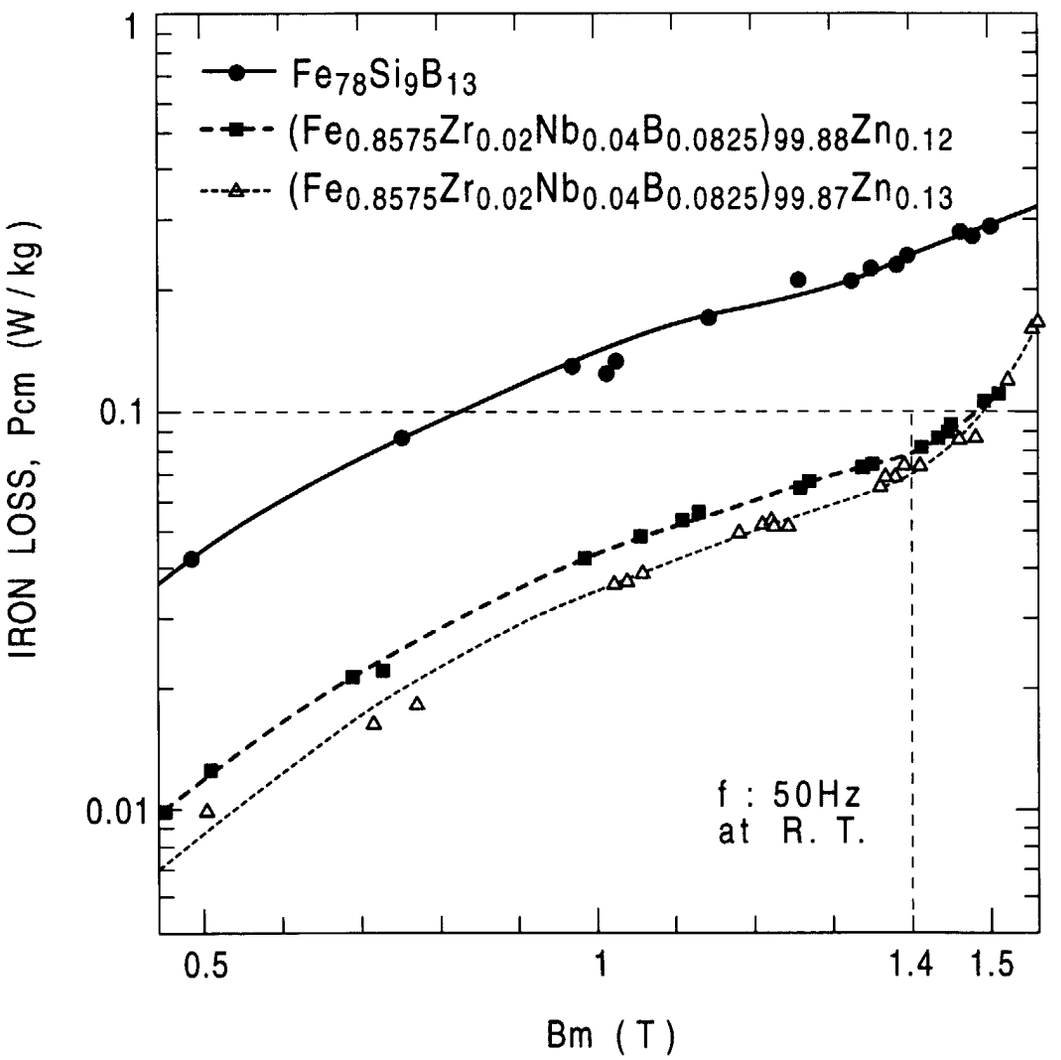
1
0.1
0.01
IRON LOSS, Pcm (W / kg)
Fe78Si9B13
(Fe0.8575Zr0.02Nb0.04B0.0825)99.88Zn0.12
(Fe0.8575Zr0.02Nb0.04B0.0825)99.87Zn0.13
f : 50Hz
at R. T.
0.5
1
1.4
1.5
Bm (T)

FIG. 83

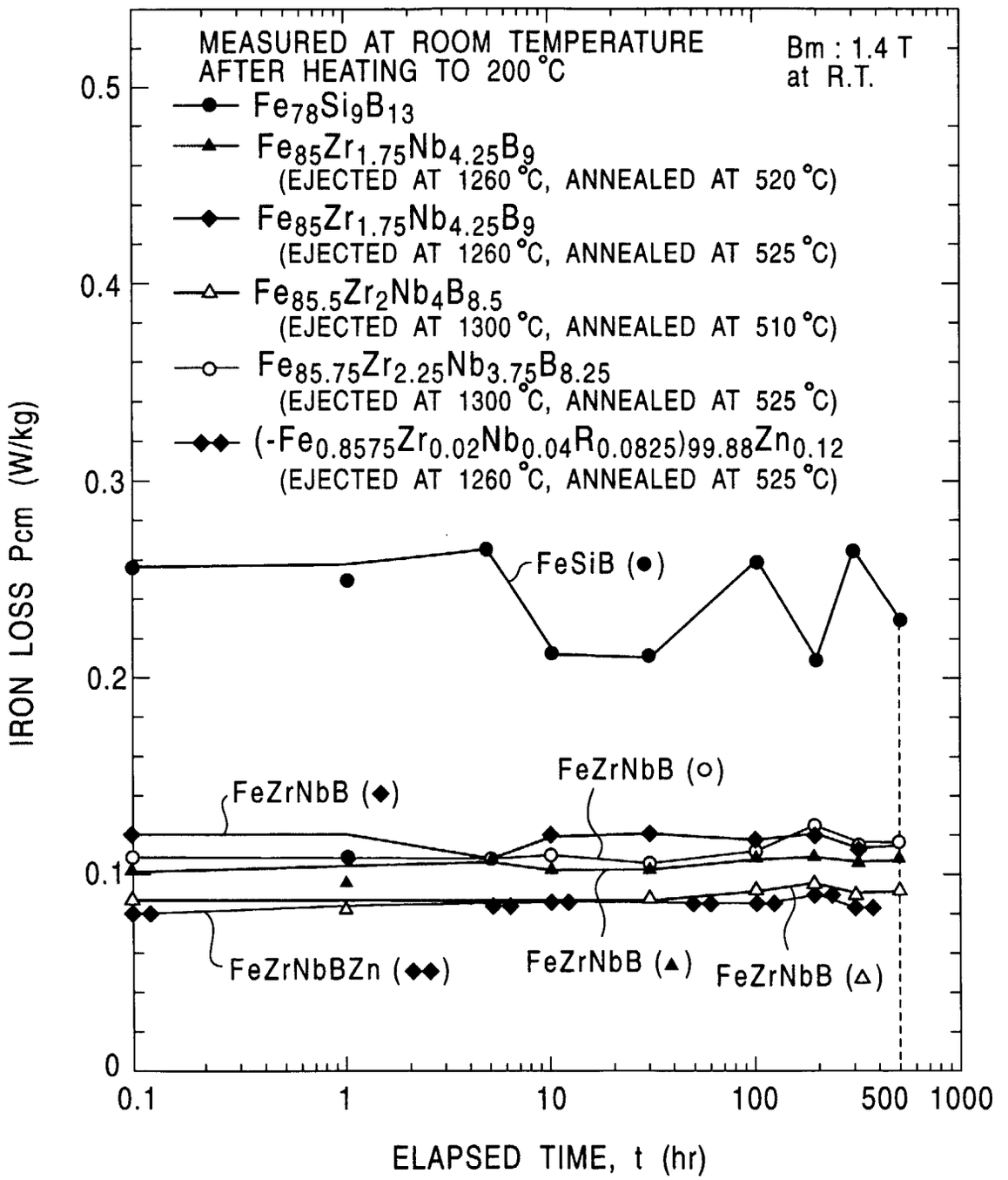
MEASURED AT ROOM TEMPERATURE
AFTER HEATING TO 200 °C
Bm : 1.4 T
at R.T.
Fe78Si9B13
Fe85Zr1.75Nb4.25B9
(EJECTED AT 1260 °C, ANNEALED AT 520 °C)
Fe85Zr1.75Nb4.25B9
(EJECTED AT 1260 °C, ANNEALED AT 525 °C)
Fe85.5Zr2Nb4B8.5
(EJECTED AT 1300 °C, ANNEALED AT 510 °C)
Fe85.75Zr2.25Nb3.75B8.25
(EJECTED AT 1300 °C, ANNEALED AT 525 °C)
(-Fe0.8575Zr0.02Nb0.04R0.0825)99.88Zn0.12
(EJECTED AT 1260 °C, ANNEALED AT 525 °C)
FeSiB (●)
FeZrNbB (◆)
FeZrNbB (○)
FeZrNbBZn (◆◆)
FeZrNbB (▲)
FeZrNbB (△)
IRON LOSS Pcm (W/kg)
0
0.1
0.2
0.3
0.4
0.5
0.1
1
10
100
500
1000
ELAPSED TIME, t (hr)

FIG. 84

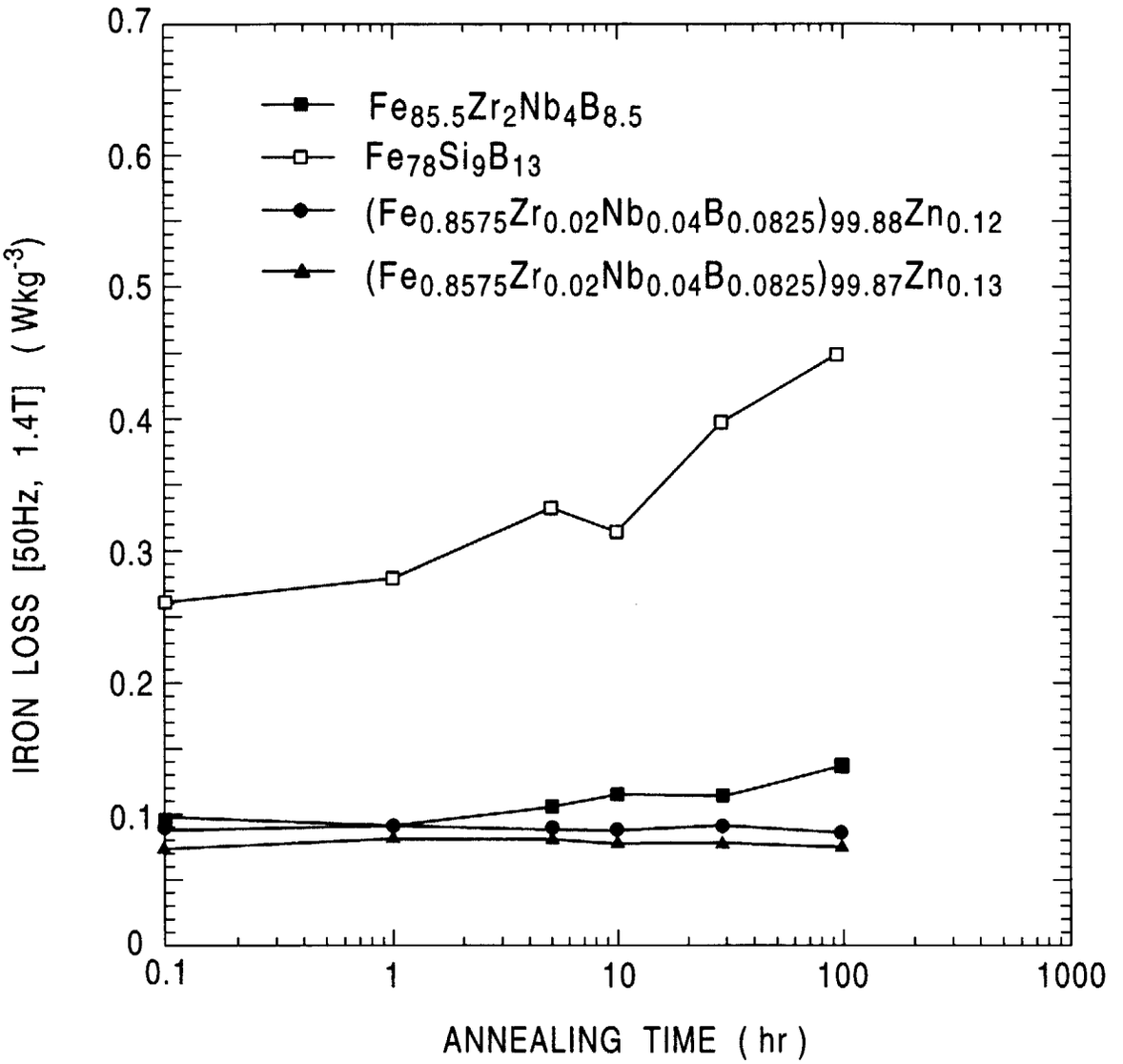
0.7
0.6
0.5
0.4
0.3
0.2
0.1
0
0.1
1
10
100
1000
IRON LOSS [50Hz, 1.4T] (Wkg-3)
ANNEALING TIME (hr)
Fe85.5Zr2Nb4B8.5
Fe78Si9B13
(Fe0.8575Zr0.02Nb0.04B0.0825)99.88Zn0.12
(Fe0.8575Zr0.02Nb0.04B0.0825)99.87Zn0.13

FIG. 85

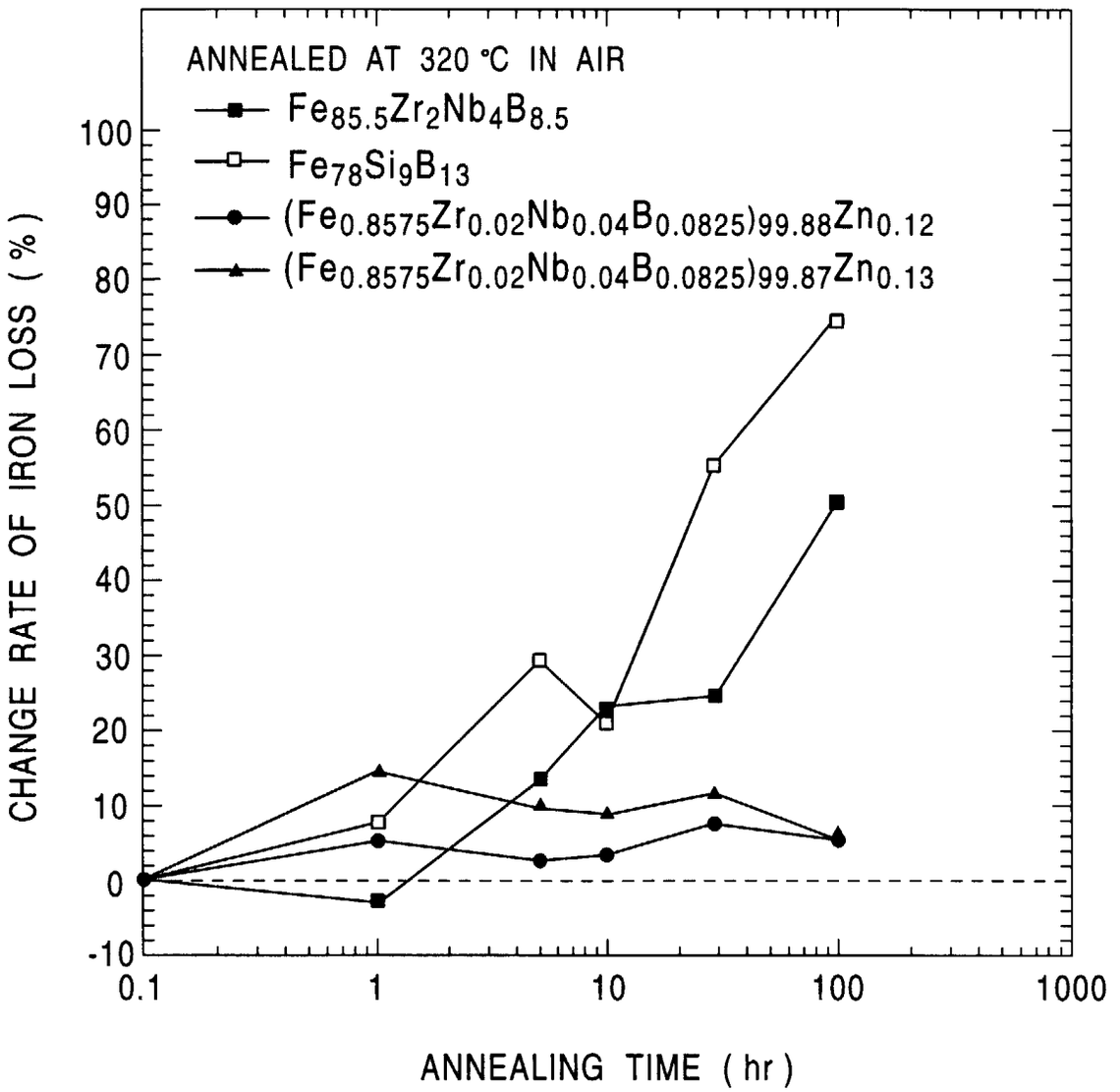
ANNEALED AT 320 °C IN AIR
$Fe_{85.5}Zr_2Nb_4B_{8.5}$
$Fe_{78}Si_9B_{13}$
$(Fe_{0.8575}Zr_{0.02}Nb_{0.04}B_{0.0825})_{99.88}Zn_{0.12}$
$(Fe_{0.8575}Zr_{0.02}Nb_{0.04}B_{0.0825})_{99.87}Zn_{0.13}$
CHANGE RATE OF IRON LOSS (%)
100
90
80
70
60
50
40
30
20
10
0
-10
0.1
1
10
100
1000
ANNEALING TIME (hr)

FIG. 86

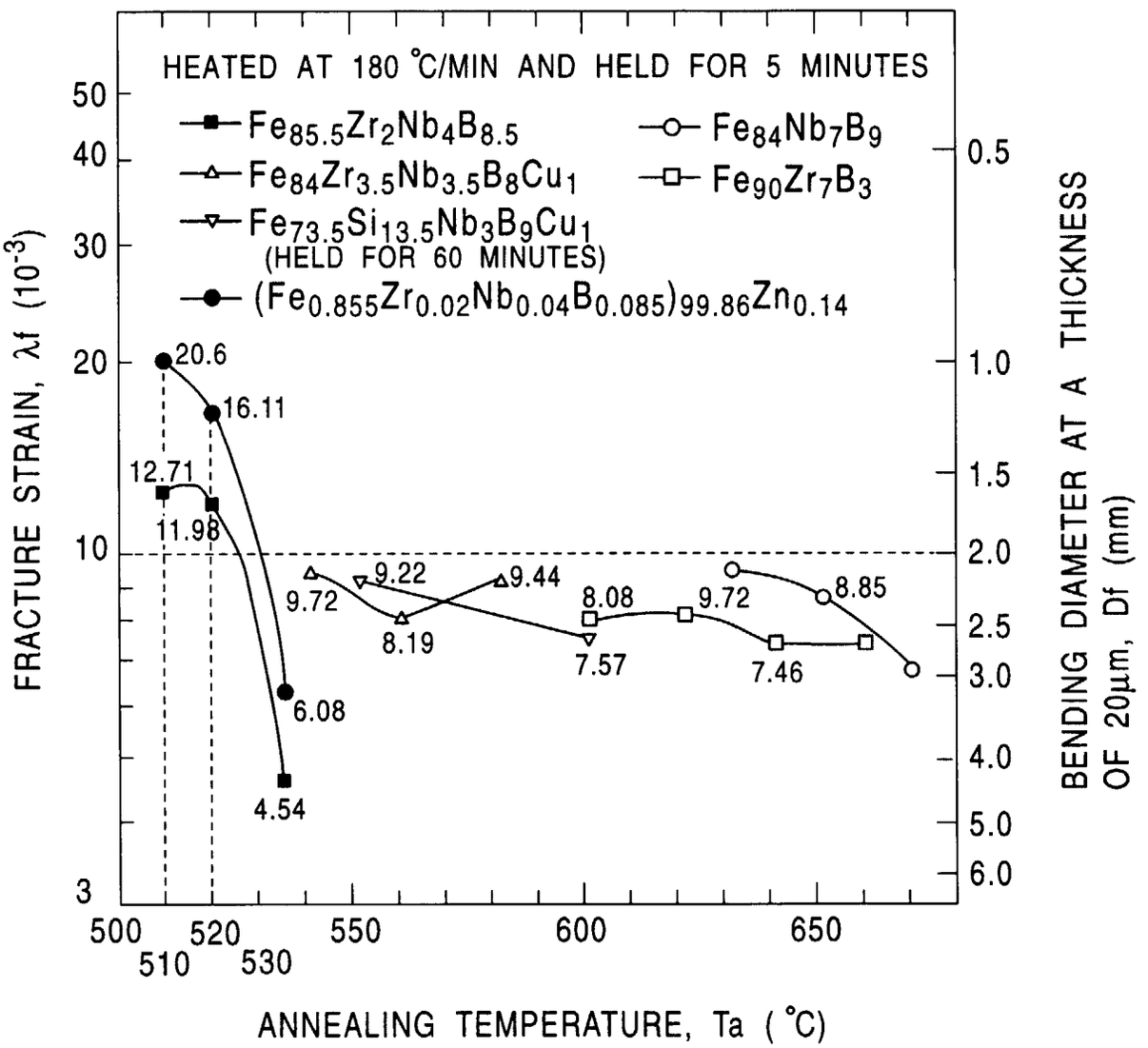
HEATED AT 180 °C/MIN AND HELD FOR 5 MINUTES
$Fe_{85.5}Zr_2Nb_4B_{8.5}$
$Fe_{84}Nb_7B_9$
$Fe_{84}Zr_{3.5}Nb_{3.5}B_8Cu_1$
$Fe_{90}Zr_7B_3$
$Fe_{73.5}Si_{13.5}Nb_3B_9Cu_1$
(HELD FOR 60 MINUTES)
$(Fe_{0.855}Zr_{0.02}Nb_{0.04}B_{0.085})_{99.86}Zn_{0.14}$
FRACTURE STRAIN, λf (10^{-3})
BENDING DIAMETER AT A THICKNESS OF 20μm, Df (mm)
ANNEALING TEMPERATURE, Ta (°C)
50
40
30
20
10
3
0.5
1.0
1.5
2.0
2.5
3.0
4.0
5.0
6.0
500
510
520
530
550
600
650
20.6
16.11
12.71
11.98
6.08
4.54
9.72
9.22
8.19
9.44
7.57
8.08
9.72
7.46
8.85

FIG. 87

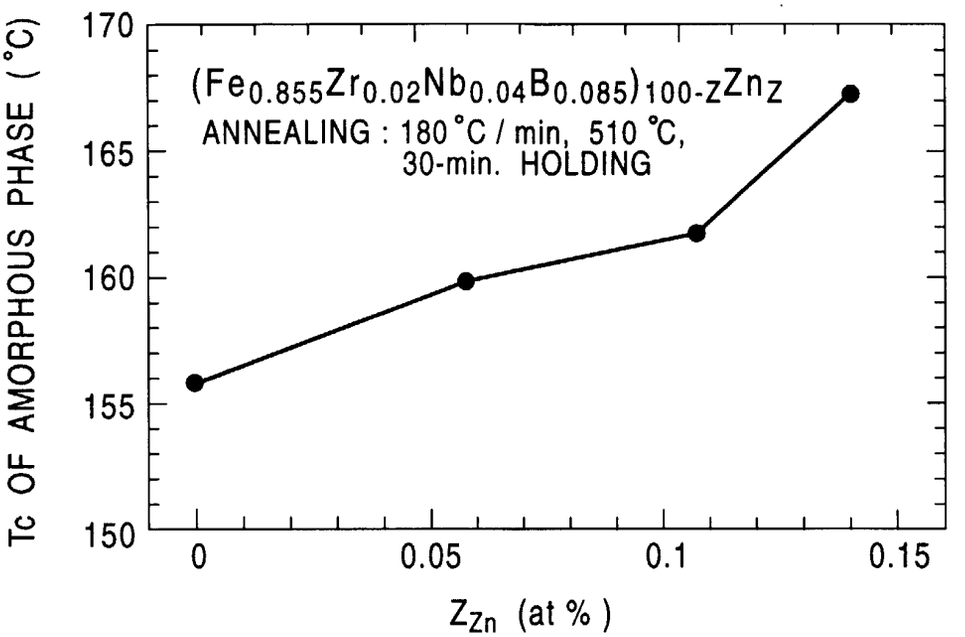
Tc OF AMORPHOUS PHASE (°C)
170
165
160
155
150
$(Fe_{0.855}Zr_{0.02}Nb_{0.04}B_{0.085})_{100-Z}Zn_Z$
ANNEALING : 180 °C / min, 510 °C,
30-min. HOLDING
0
0.05
0.1
0.15
Z_{Zn} (at %)

FIG. 88

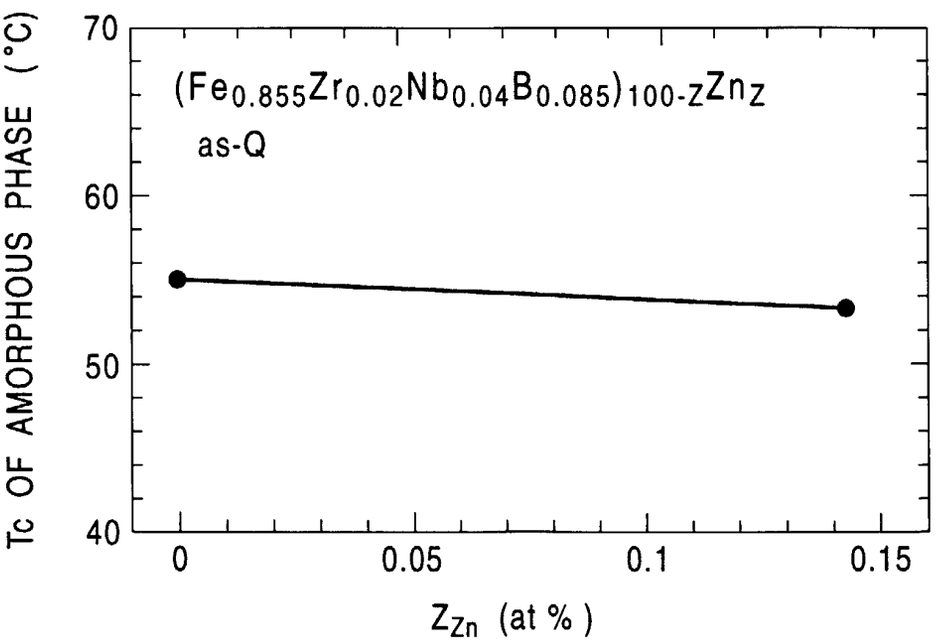
Tc OF AMORPHOUS PHASE (°C)
70
60
50
40
$(Fe_{0.855}Zr_{0.02}Nb_{0.04}B_{0.085})_{100-Z}Zn_Z$
as-Q
0
0.05
0.1
0.15
Z_{Zn} (at %)

FIG. 89

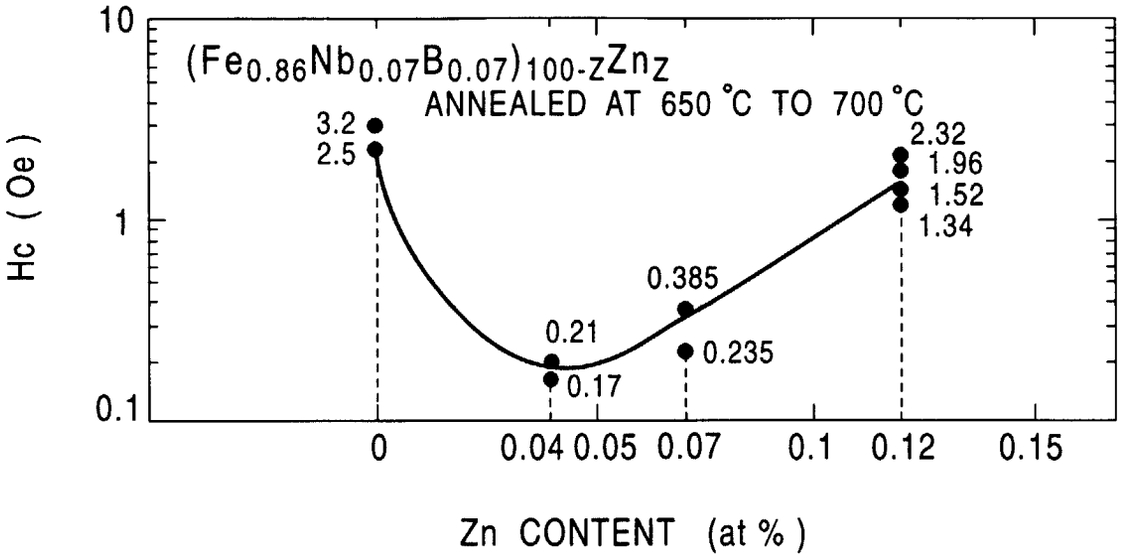
(Fe0.86Nb0.07B0.07)100-ZZnZ
ANNEALED AT 650 °C TO 700 °C
Hc (Oe)
10
1
0.1
3.2
2.5
2.32
1.96
1.52
1.34
0.385
0.21
0.17
0.235
0
0.04 0.05 0.07
0.1
0.12
0.15
Zn CONTENT (at %)

FIG. 90

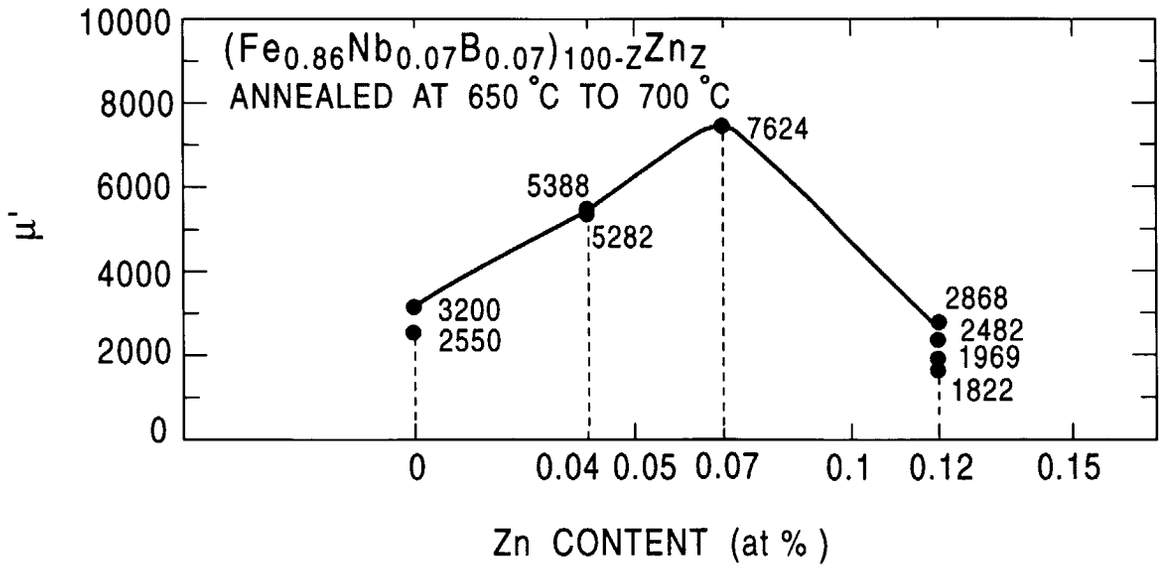
(Fe0.86Nb0.07B0.07)100-ZZnZ
ANNEALED AT 650 °C TO 700 °C
μ'
10000
8000
6000
4000
2000
0
7624
5388
5282
3200
2550
2868
2482
1969
1822
0
0.04 0.05 0.07
0.1
0.12
0.15
Zn CONTENT (at %)

FIG. 91

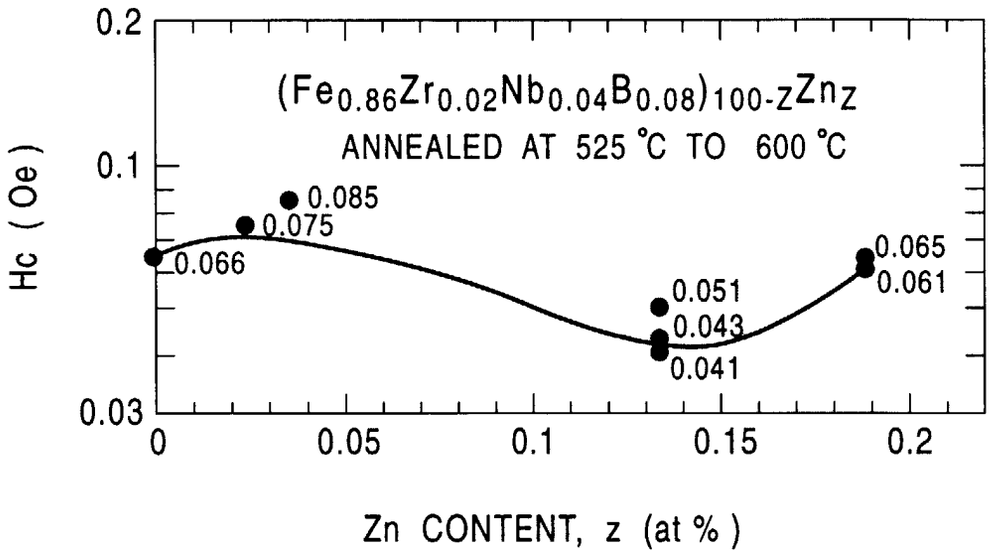
0.2
0.1
0.03
Hc (Oe)
$(Fe_{0.86}Zr_{0.02}Nb_{0.04}B_{0.08})_{100-z}Zn_z$
ANNEALED AT 525 °C TO 600 °C
0.085
0.075
0.066
0.065
0.061
0.051
0.043
0.041
0
0.05
0.1
0.15
0.2
Zn CONTENT, z (at %)

FIG. 92

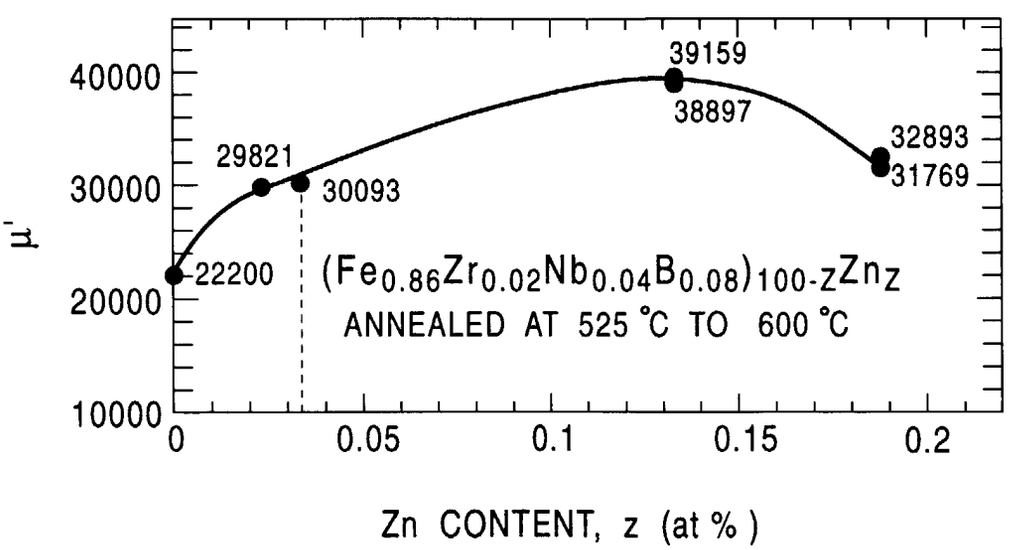
40000
30000
20000
10000
μ'
39159
38897
32893
31769
29821
30093
22200
$(Fe_{0.86}Zr_{0.02}Nb_{0.04}B_{0.08})_{100-z}Zn_z$
ANNEALED AT 525 °C TO 600 °C
0
0.05
0.1
0.15
0.2
Zn CONTENT, z (at %)

FIG. 93

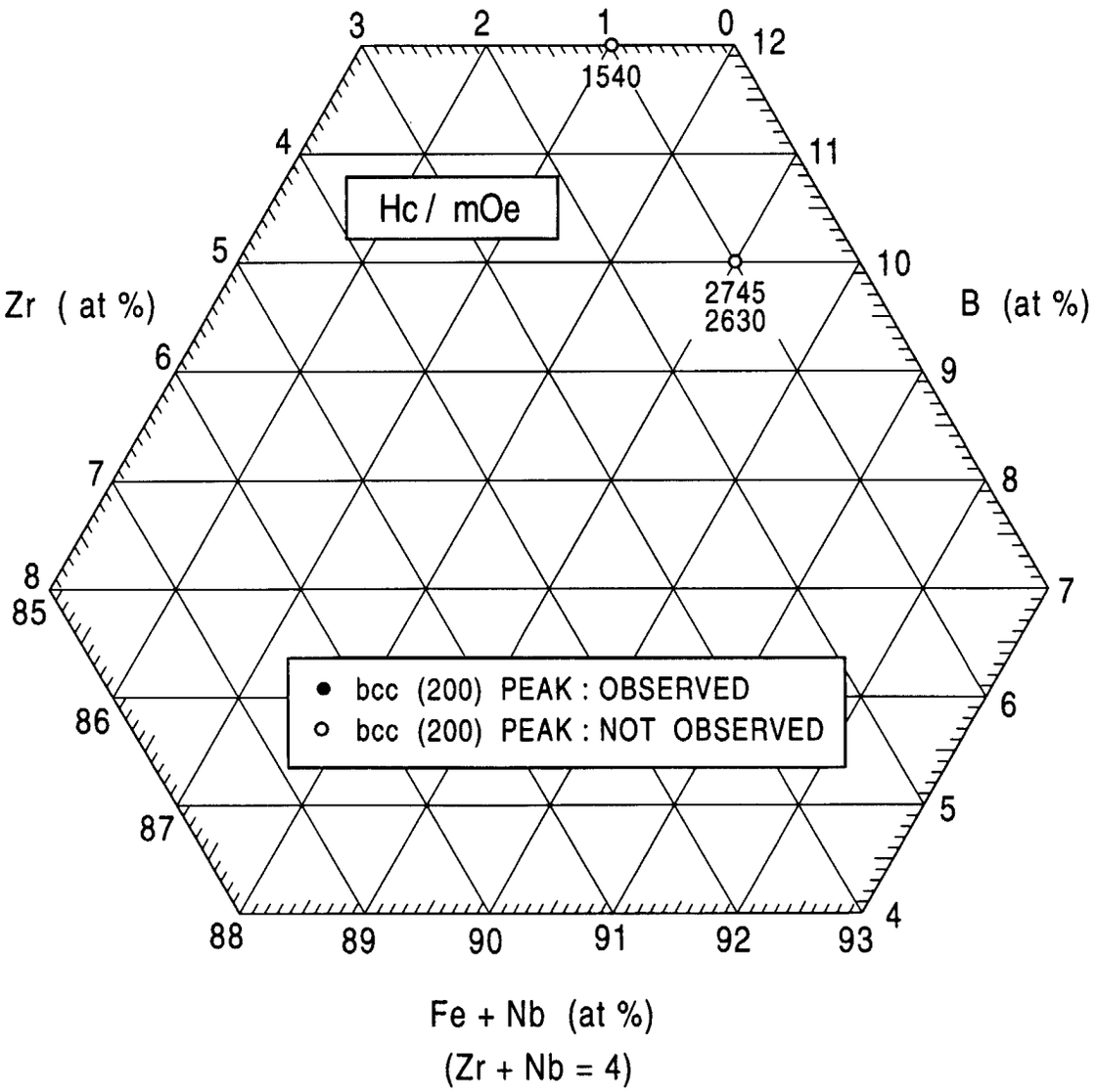
3
2
1
0
12
1540
4
11
Hc / mOe
5
10
2745
2630
Zr (at %)
B (at %)
6
9
7
8
8
7
85
● bcc (200) PEAK : OBSERVED
○ bcc (200) PEAK : NOT OBSERVED
86
6
87
5
88
89
90
91
92
93
4
Fe + Nb (at %)
(Zr + Nb = 4)

FIG. 94

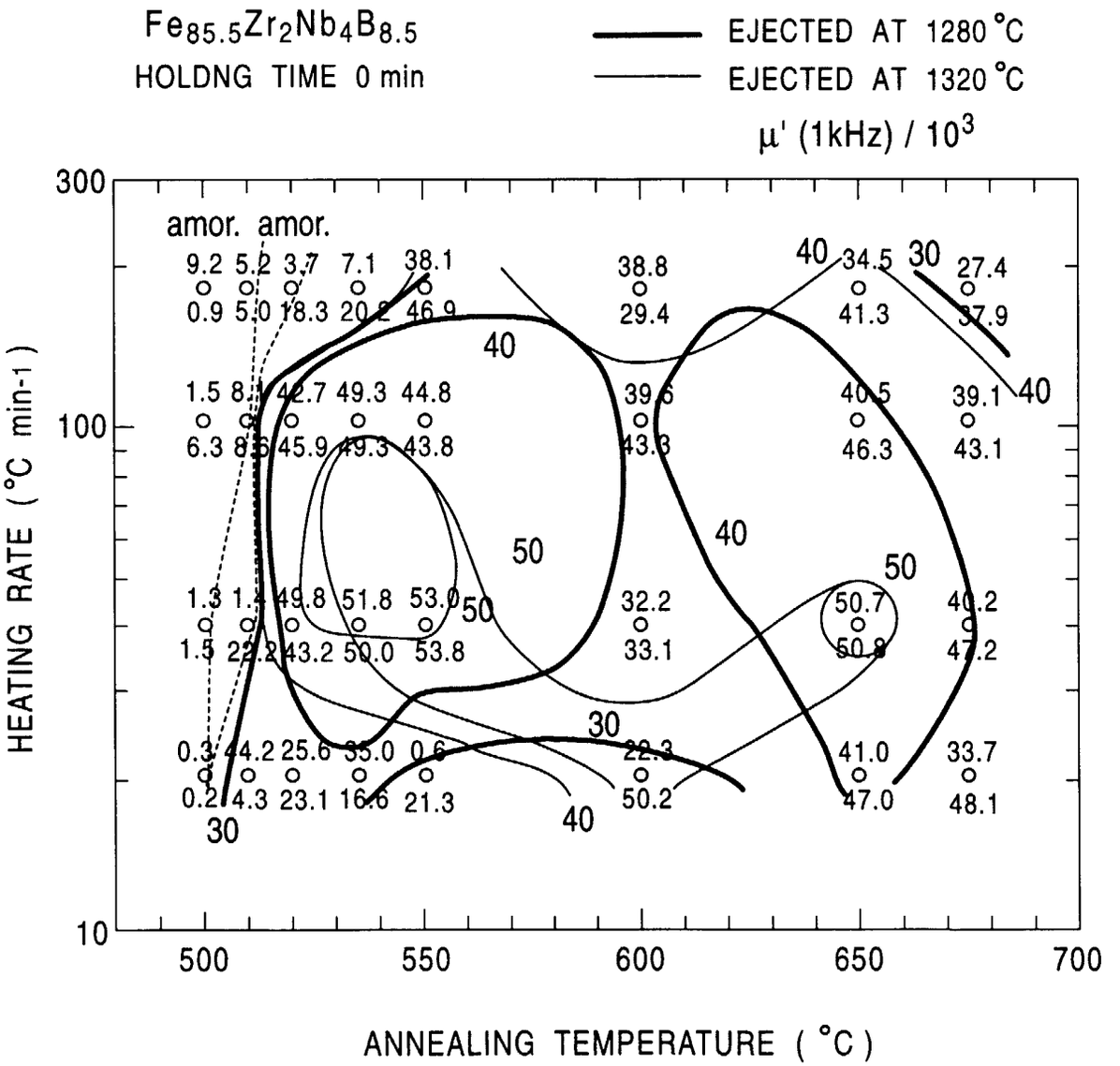
$Fe_{85.5}Zr_2Nb_4B_{8.5}$
HOLDNG TIME 0 min
EJECTED AT 1280 °C
EJECTED AT 1320 °C
μ' (1kHz) / 10^3
HEATING RATE (°C min-1)
ANNEALING TEMPERATURE (°C)
300
100
10
500
550
600
650
700
amor. amor.
9.2 5.2 3.7 7.1 38.1
0.9 5.0 18.3 20.2 46.9
38.8
29.4
40
34.5
41.3
30
27.4
37.9
40
1.5 8.1 42.7 49.3 44.8
6.3 8.6 45.9 49.3 43.8
39.6
43.3
40.5
46.3
39.1
43.1
40
50
40
50
1.3 1.4 49.8 51.8 53.0
1.5 22.2 43.2 50.0 53.8
50
32.2
33.1
50.7
50.8
40.2
47.2
30
0.3 44.2 25.6 35.0 0.6
0.2 4.3 23.1 16.6 21.3
22.3
50.2
41.0
47.0
33.7
48.1
30
40

FIG. 95

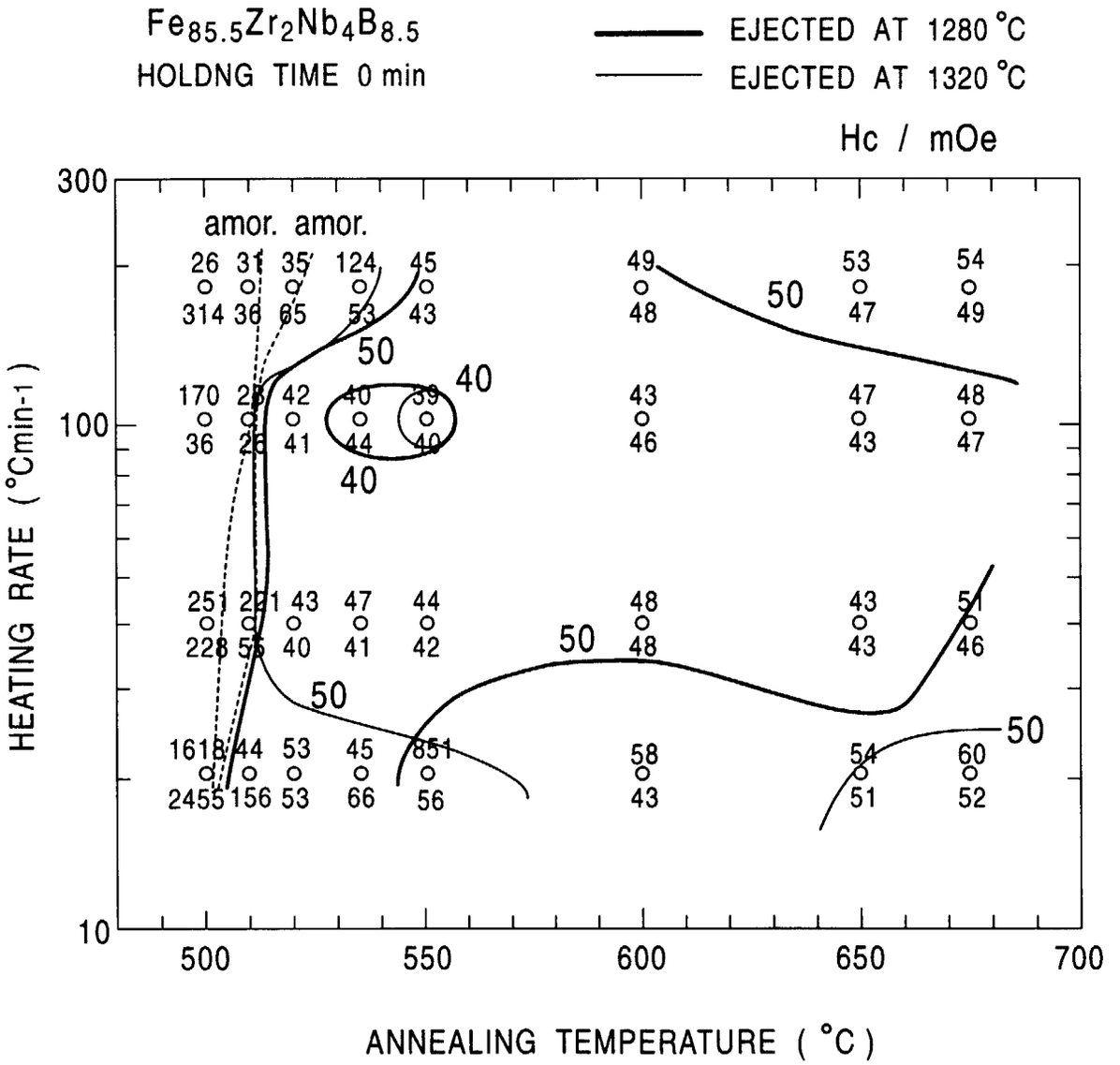
$Fe_{85.5}Zr_2Nb_4B_{8.5}$
HOLDNG TIME 0 min
EJECTED AT 1280 °C
EJECTED AT 1320 °C
Hc / mOe
HEATING RATE (°Cmin-1)
ANNEALING TEMPERATURE (°C)
300
100
10
500
550
600
650
700
amor. amor.
50
40
50
50
50

FIG. 96

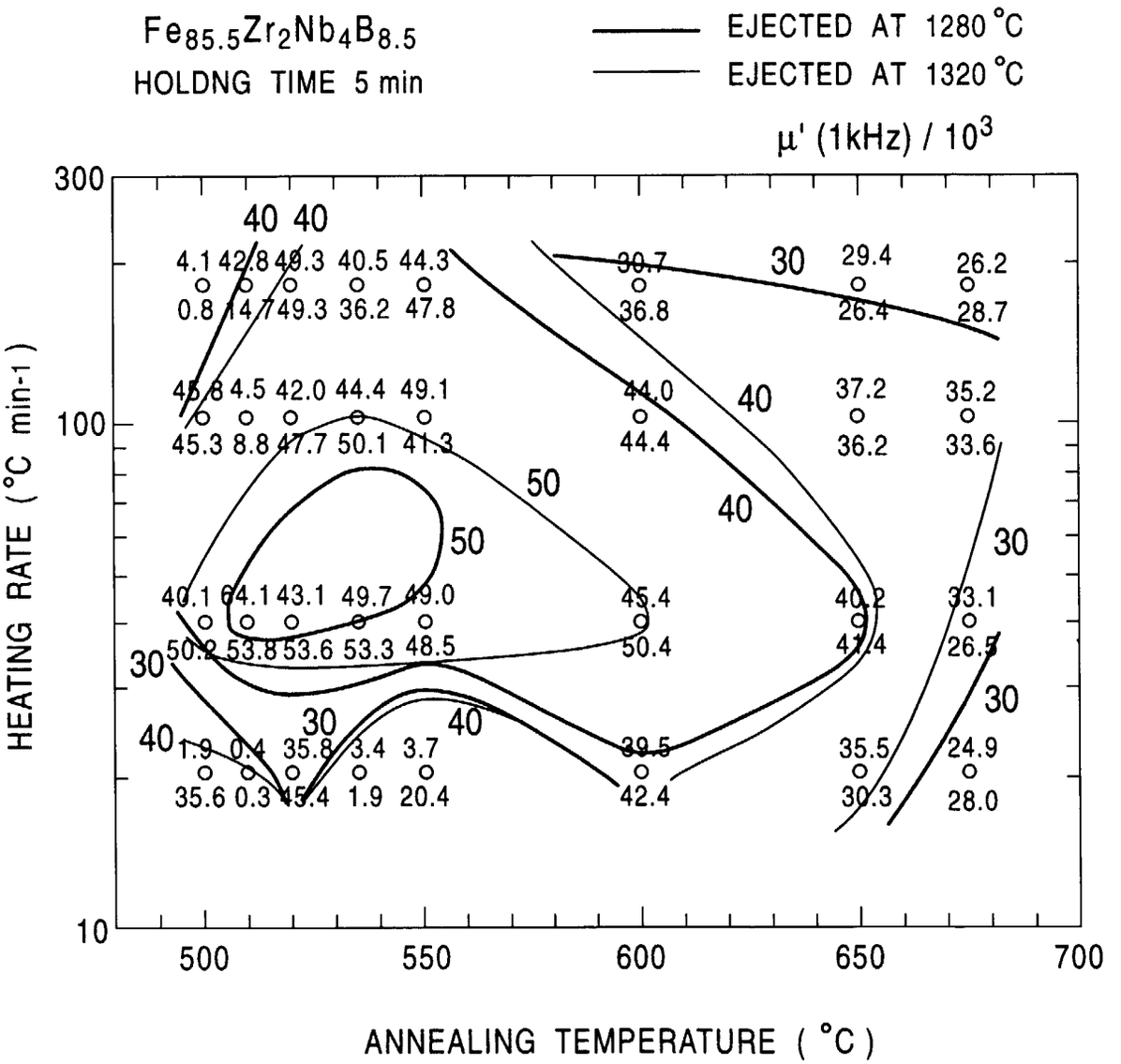
$Fe_{85.5}Zr_2Nb_4B_{8.5}$
HOLDNG TIME 5 min
EJECTED AT 1280 °C
EJECTED AT 1320 °C
μ' (1kHz) / 10^3
HEATING RATE (°C min-1)
ANNEALING TEMPERATURE (°C)
300
100
10
500
550
600
650
700
40 40
4.1 42.8 48.3 40.5 44.3
0.8 14.7 49.3 36.2 47.8
30.7
36.8
30
29.4
26.4
26.2
28.7
45.8 4.5 42.0 44.4 49.1
45.3 8.8 47.7 50.1 41.3
44.0
44.4
40
37.2
36.2
35.2
33.6
50
50
40
30
40.1 64.1 43.1 49.7 49.0
50.2 53.8 53.6 53.3 48.5
45.4
50.4
40.2
41.4
33.1
26.5
30
30
40
40
1.9 0.4 35.8 3.4 3.7
35.6 0.3 45.4 1.9 20.4
39.5
42.4
35.5
30.3
24.9
28.0
30

FIG. 97

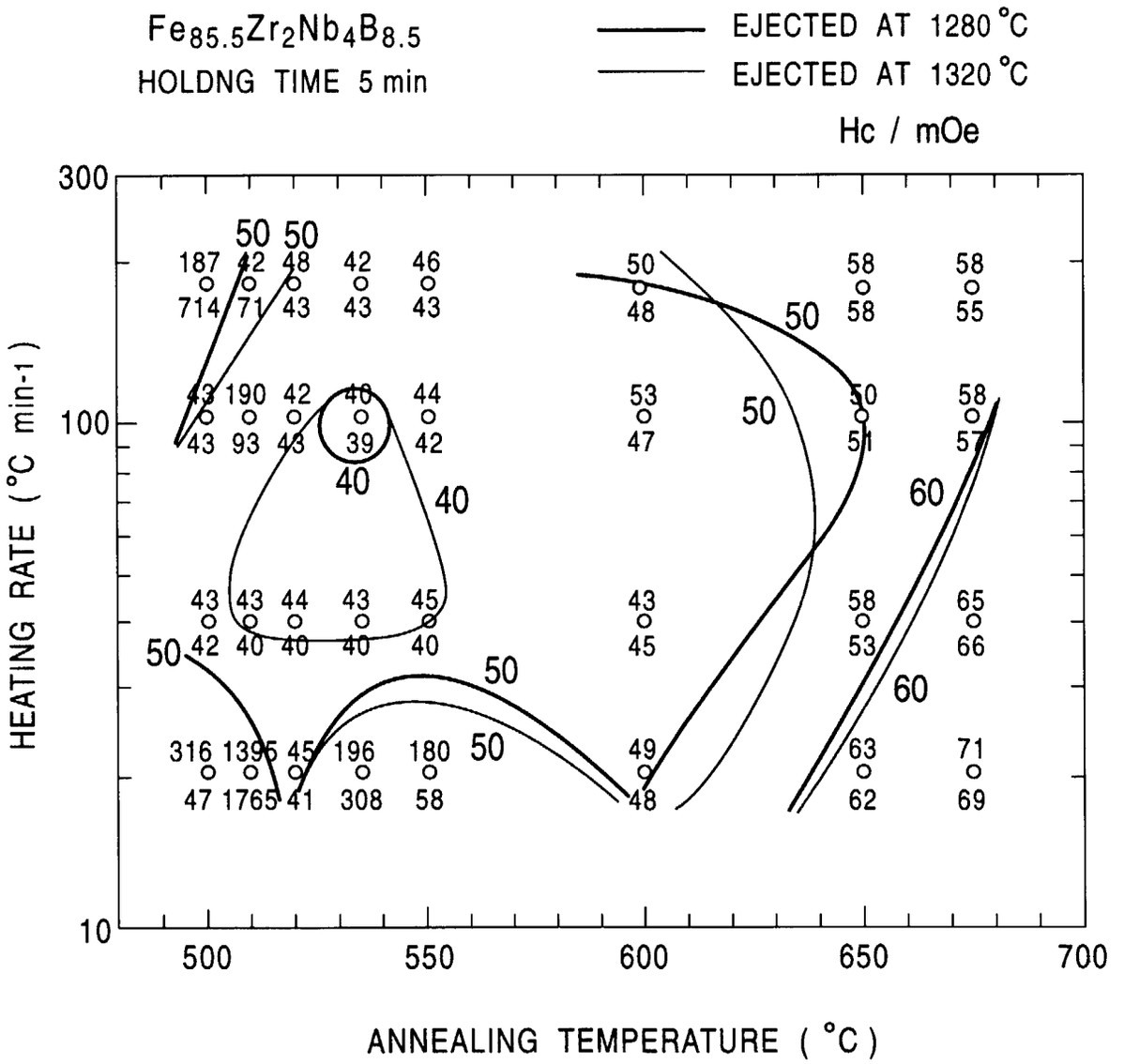
$Fe_{85.5}Zr_2Nb_4B_{8.5}$
HOLDNG TIME 5 min
EJECTED AT 1280 °C
EJECTED AT 1320 °C
Hc / mOe
HEATING RATE (°C min-1)
ANNEALING TEMPERATURE (°C)
300
100
10
500
550
600
650
700
50
40
60

FIG. 98

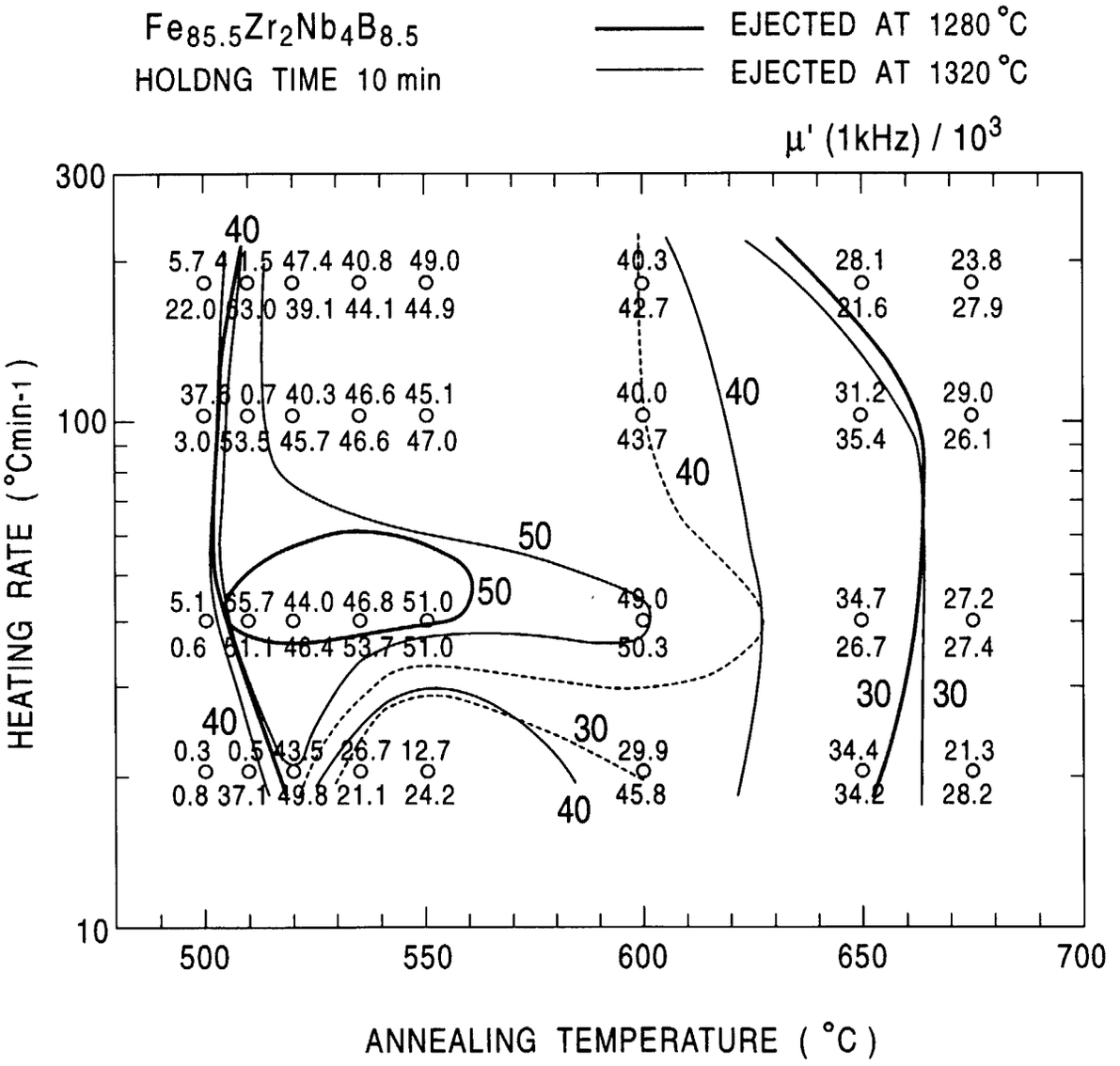
Fe85.5Zr2Nb4B8.5
HOLDNG TIME 10 min
EJECTED AT 1280 °C
EJECTED AT 1320 °C
μ' (1kHz) / 10³
HEATING RATE (°Cmin-1)
ANNEALING TEMPERATURE (°C)
300
100
10
500
550
600
650
700
40
50
30
5.7 41.5 47.4 40.8 49.0
22.0 33.0 39.1 44.1 44.9
40.3
42.7
28.1
23.8
21.6
27.9
37.8 0.7 40.3 46.6 45.1
3.0 53.5 45.7 46.6 47.0
40.0
43.7
31.2
29.0
35.4
26.1
5.1 55.7 44.0 46.8 51.0
0.6 51.1 46.4 53.7 51.0
49.0
50.3
34.7
27.2
26.7
27.4
0.3 0.5 43.5 26.7 12.7
0.8 37.1 49.8 21.1 24.2
29.9
45.8
34.4
21.3
34.2
28.2

FIG. 99

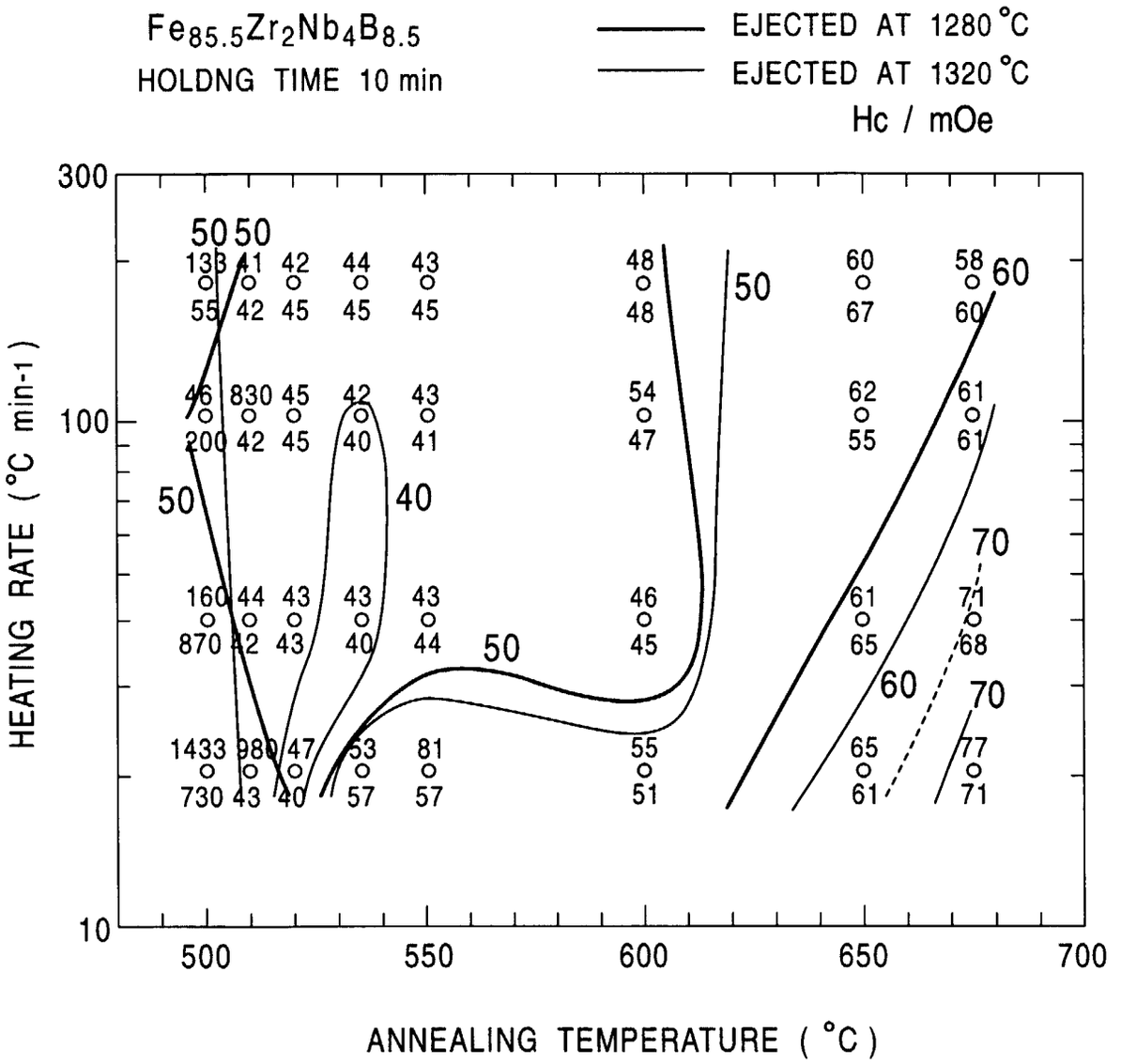
$Fe_{85.5}Zr_2Nb_4B_{8.5}$
HOLDNG TIME 10 min
EJECTED AT 1280 °C
EJECTED AT 1320 °C
Hc / mOe
HEATING RATE (°C min-1)
ANNEALING TEMPERATURE (°C)
300
100
10
500
550
600
650
700
50
40
60
70

FIG. 100

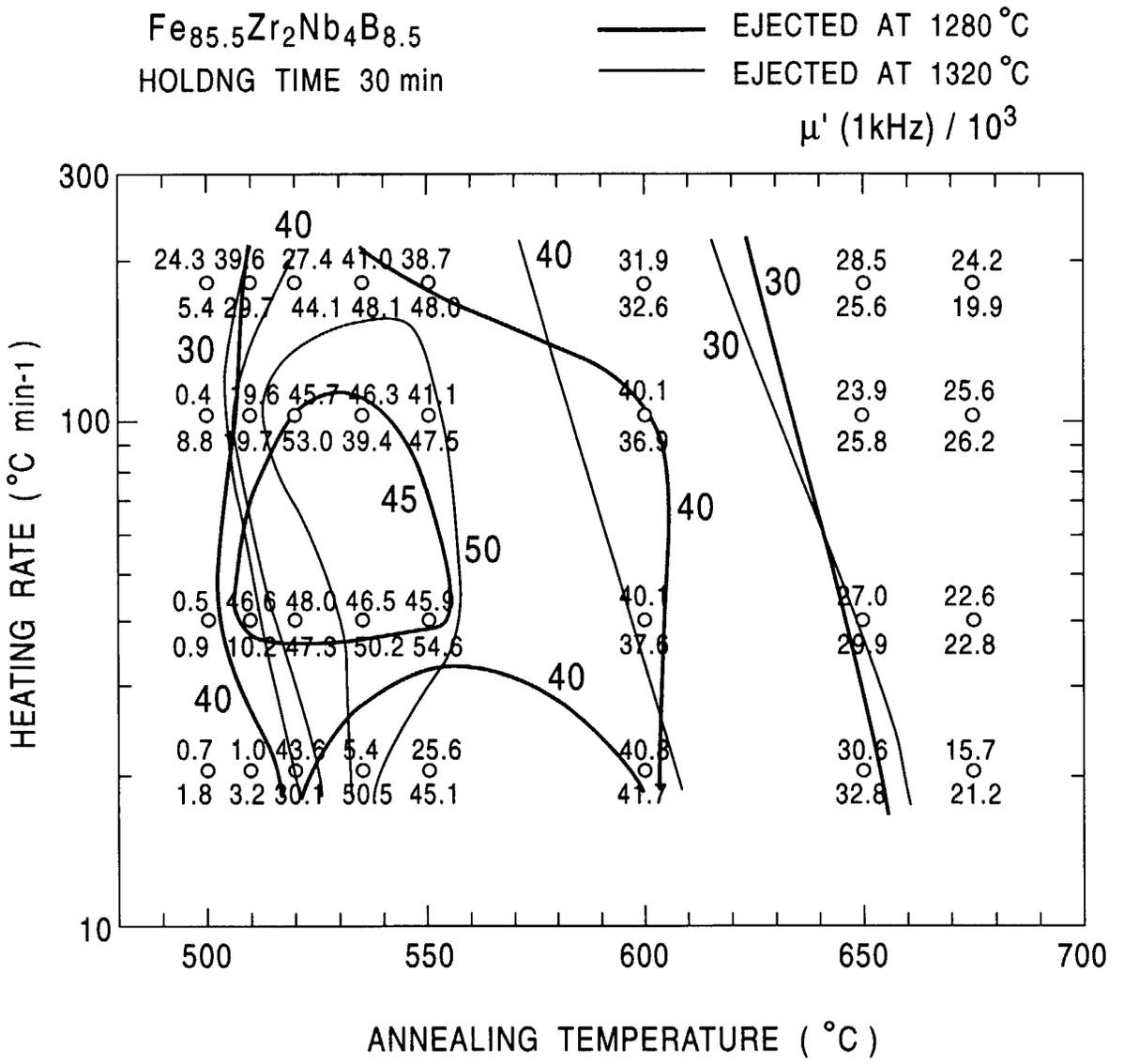
$Fe_{85.5}Zr_2Nb_4B_{8.5}$
HOLDNG TIME 30 min
EJECTED AT 1280 °C
EJECTED AT 1320 °C
μ' (1kHz) / 10^3
HEATING RATE (°C min-1)
ANNEALING TEMPERATURE (°C)
300
100
10
500
550
600
650
700
40
30
45
50
24.3 39.6 27.4 41.0 38.7
5.4 29.7 44.1 48.1 48.0
0.4 19.6 45.7 46.3 41.1
8.8 19.7 53.0 39.4 47.5
0.5 46.6 48.0 46.5 45.9
0.9 10.2 47.3 50.2 54.6
0.7 1.0 43.6 5.4 25.6
1.8 3.2 30.1 50.5 45.1
31.9
32.6
40.1
36.9
40.1
37.6
40.8
41.7
28.5
25.6
23.9
25.8
27.0
29.9
30.6
32.8
24.2
19.9
25.6
26.2
22.6
22.8
15.7
21.2

FIG. 101

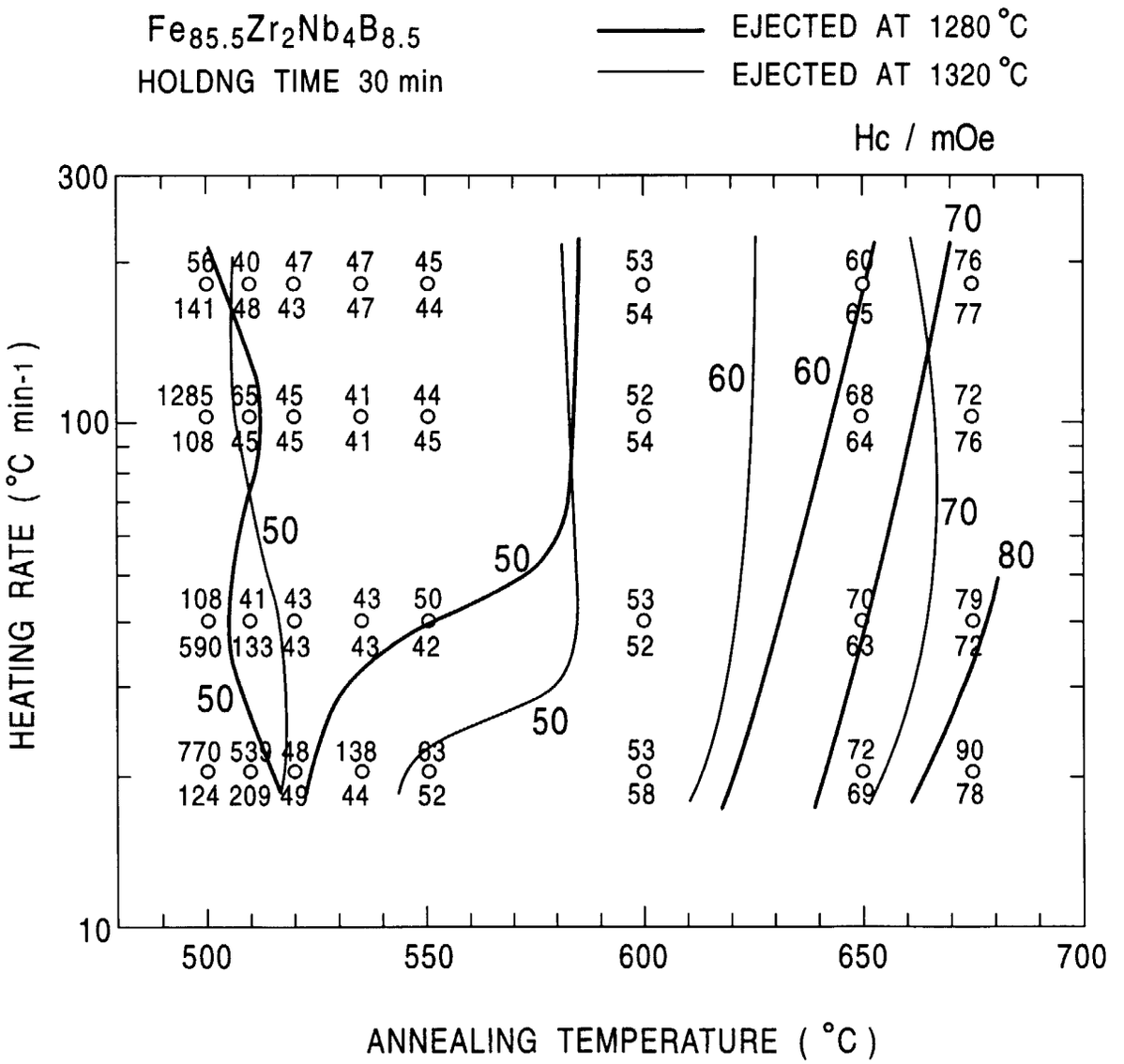
$Fe_{85.5}Zr_2Nb_4B_{8.5}$
HOLDNG TIME 30 min
EJECTED AT 1280 °C
EJECTED AT 1320 °C
Hc / mOe
HEATING RATE (°C min-1)
ANNEALING TEMPERATURE (°C)
300
100
10
500
550
600
650
700
50
60
70
80

FIG. 102

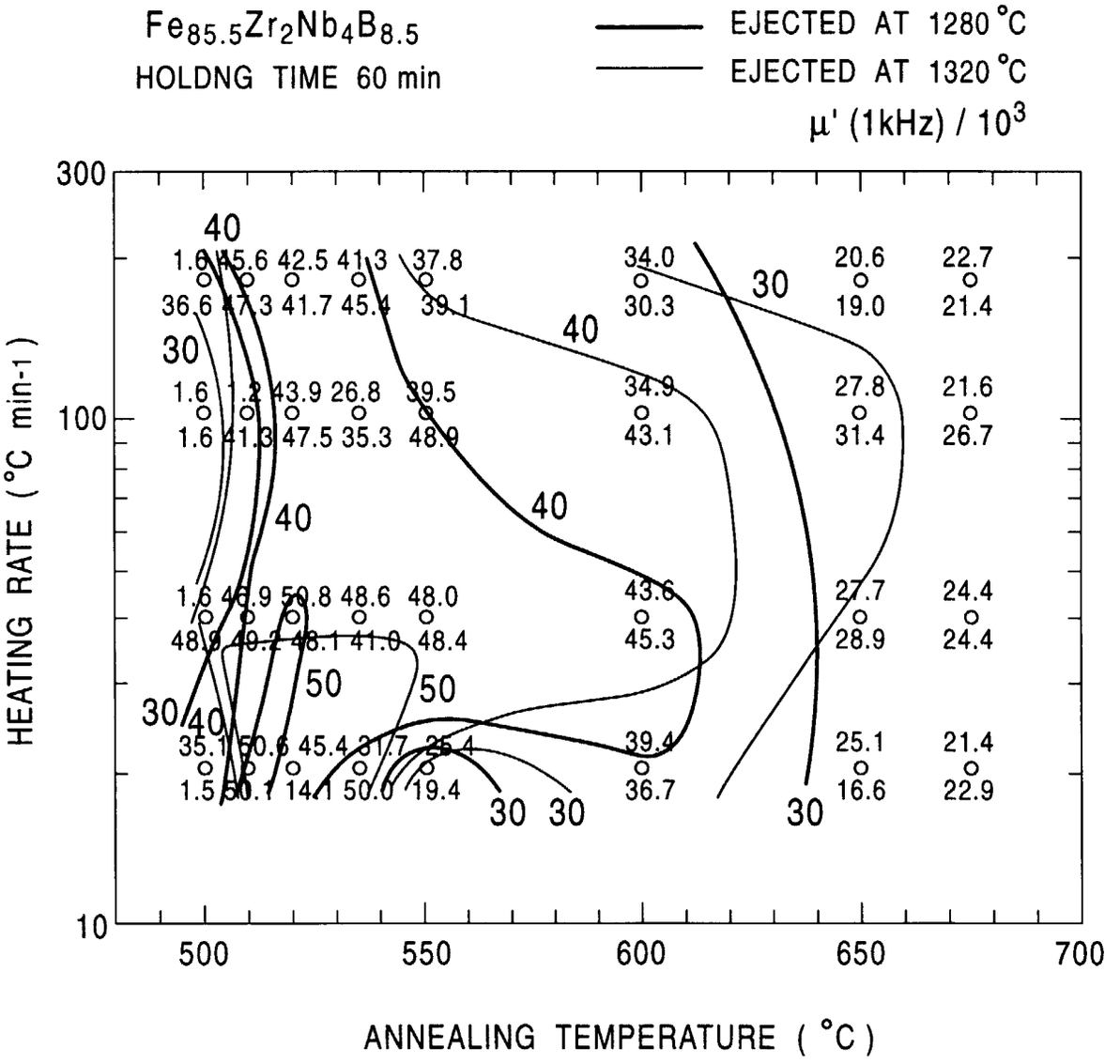
$Fe_{85.5}Zr_2Nb_4B_{8.5}$
HOLDNG TIME 60 min
EJECTED AT 1280 °C
EJECTED AT 1320 °C
μ' (1kHz) / 10^3
HEATING RATE (°C min-1)
ANNEALING TEMPERATURE (°C)
300
100
10
500
550
600
650
700
40
30
50

FIG. 103

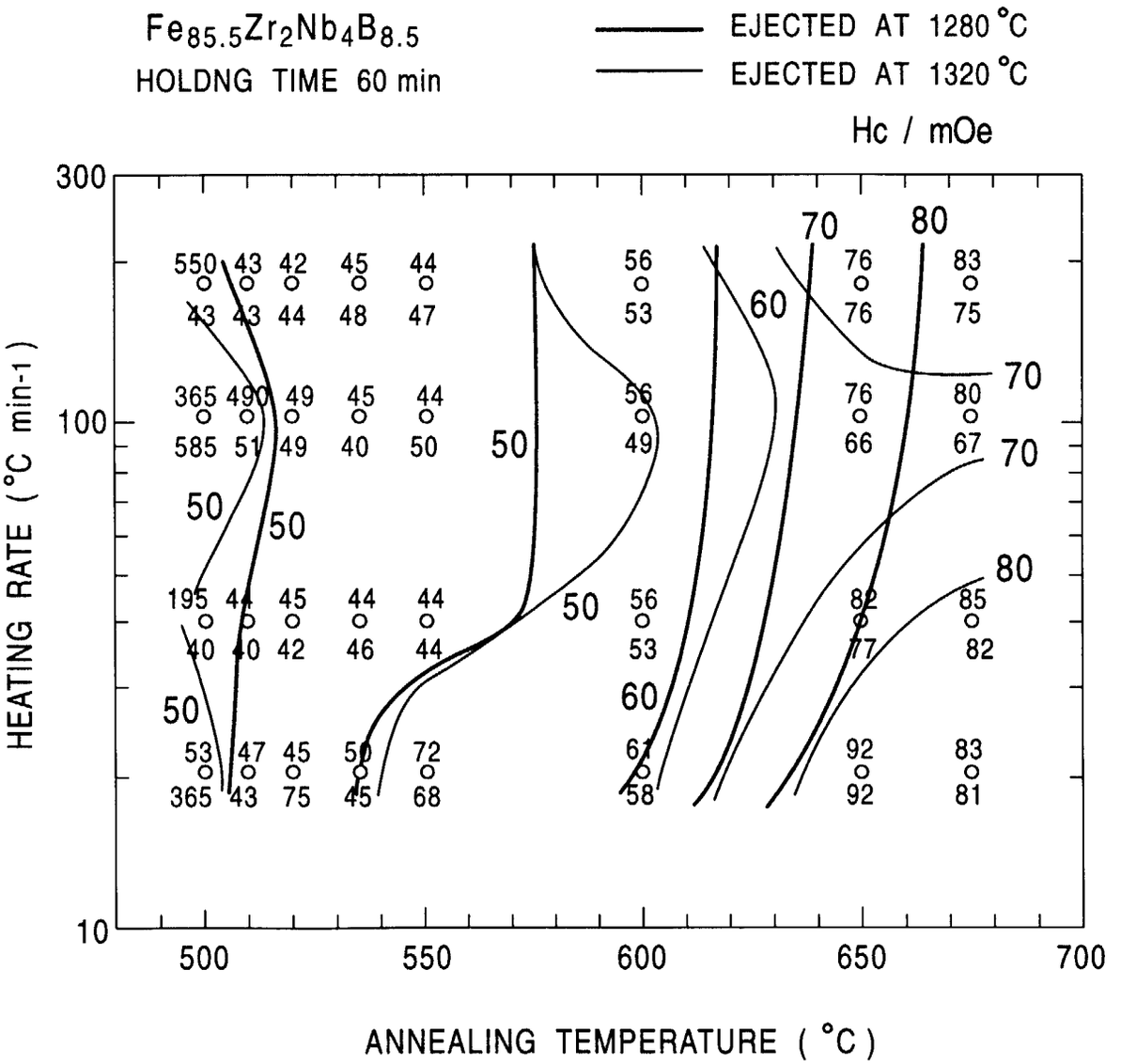
$Fe_{85.5}Zr_2Nb_4B_{8.5}$
HOLDNG TIME 60 min
EJECTED AT 1280 °C
EJECTED AT 1320 °C
Hc / mOe
HEATING RATE (°C min-1)
ANNEALING TEMPERATURE (°C)
300
100
10
500
550
600
650
700
550 43 42 45 44
43 43 44 48 47
365 490 49 45 44
585 51 49 40 50
195 44 45 44 44
40 40 42 46 44
53 47 45 50 72
365 43 75 45 68
56
53
56
49
56
53
61
58
76 83
76 75
76 80
66 67
82 85
77 82
92 83
92 81
50
50
50
50
60
60
70
70
70
80
80

FIG. 104

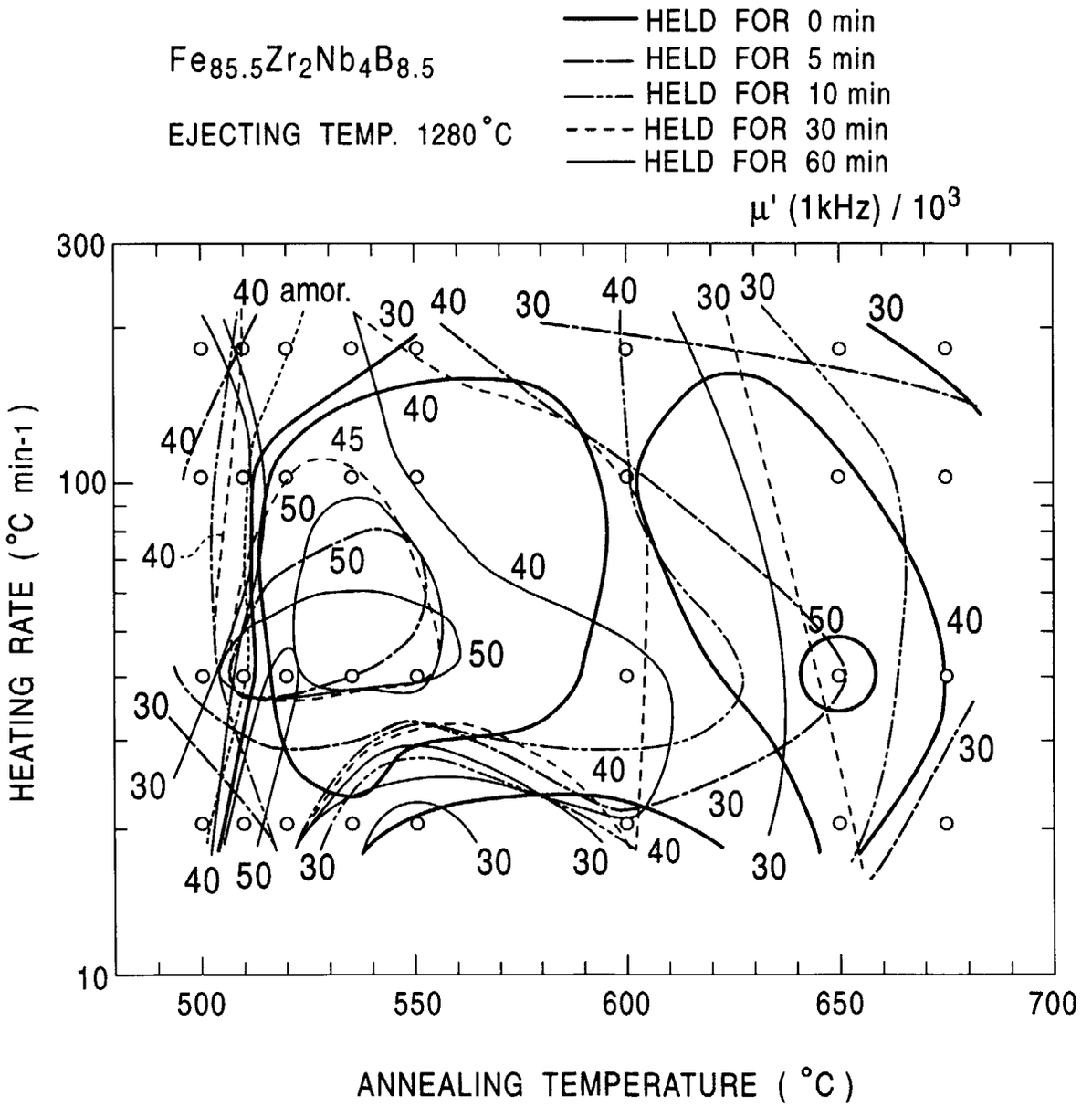
HELD FOR 0 min
HELD FOR 5 min
HELD FOR 10 min
HELD FOR 30 min
HELD FOR 60 min
$Fe_{85.5}Zr_2Nb_4B_{8.5}$
EJECTING TEMP. 1280 °C
μ' (1kHz) / 10^3
HEATING RATE (°C min-1)
ANNEALING TEMPERATURE (°C)
300
100
10
500
550
600
650
700
40 amor.
30
40
45
50

FIG. 105

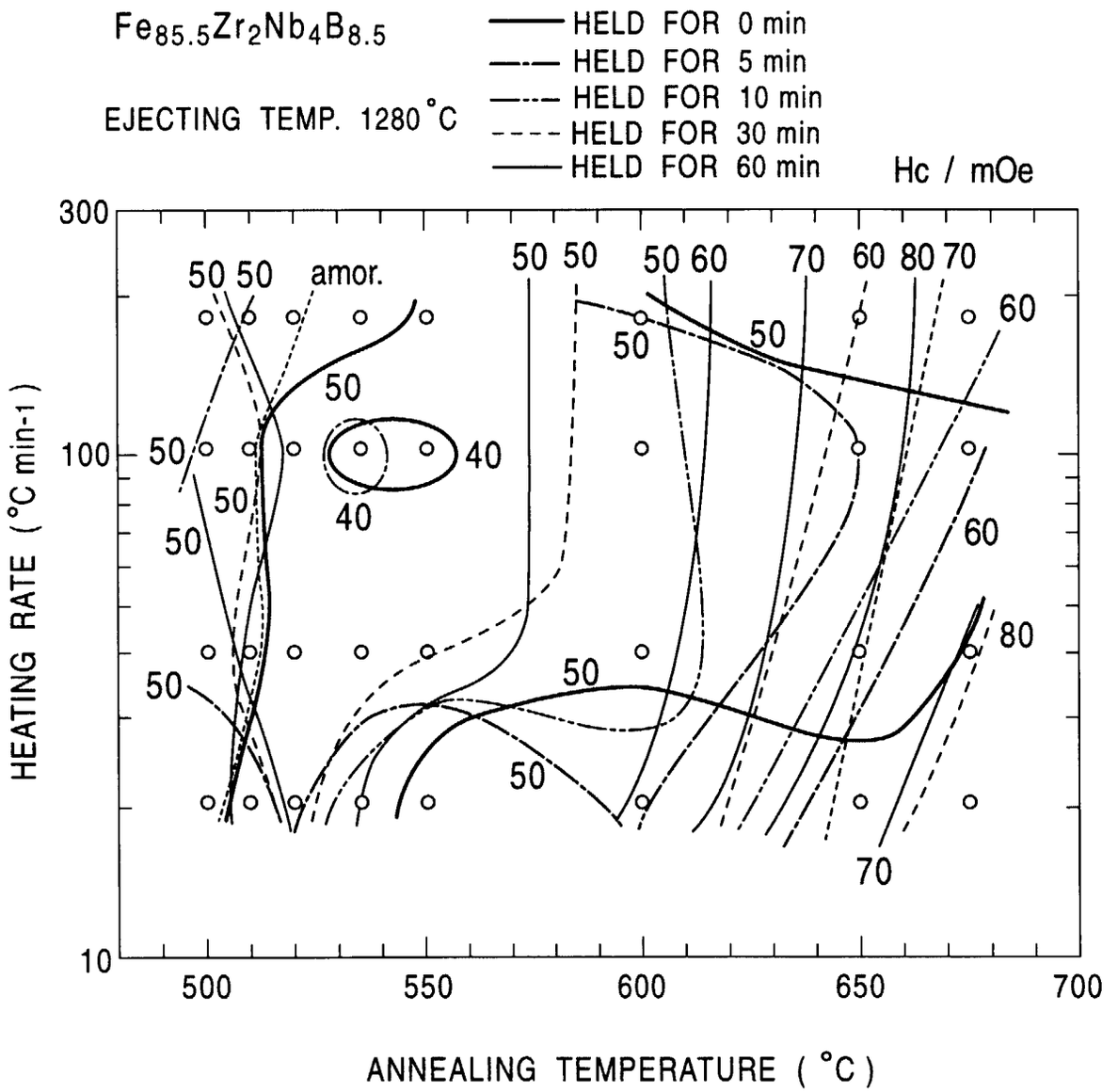
$Fe_{85.5}Zr_2Nb_4B_{8.5}$
EJECTING TEMP. 1280 °C
HELD FOR 0 min
HELD FOR 5 min
HELD FOR 10 min
HELD FOR 30 min
HELD FOR 60 min
Hc / mOe
HEATING RATE (°C min-1)
ANNEALING TEMPERATURE (°C)
300
100
10
500
550
600
650
700
amor.
50
40
60
70
80

FIG. 106

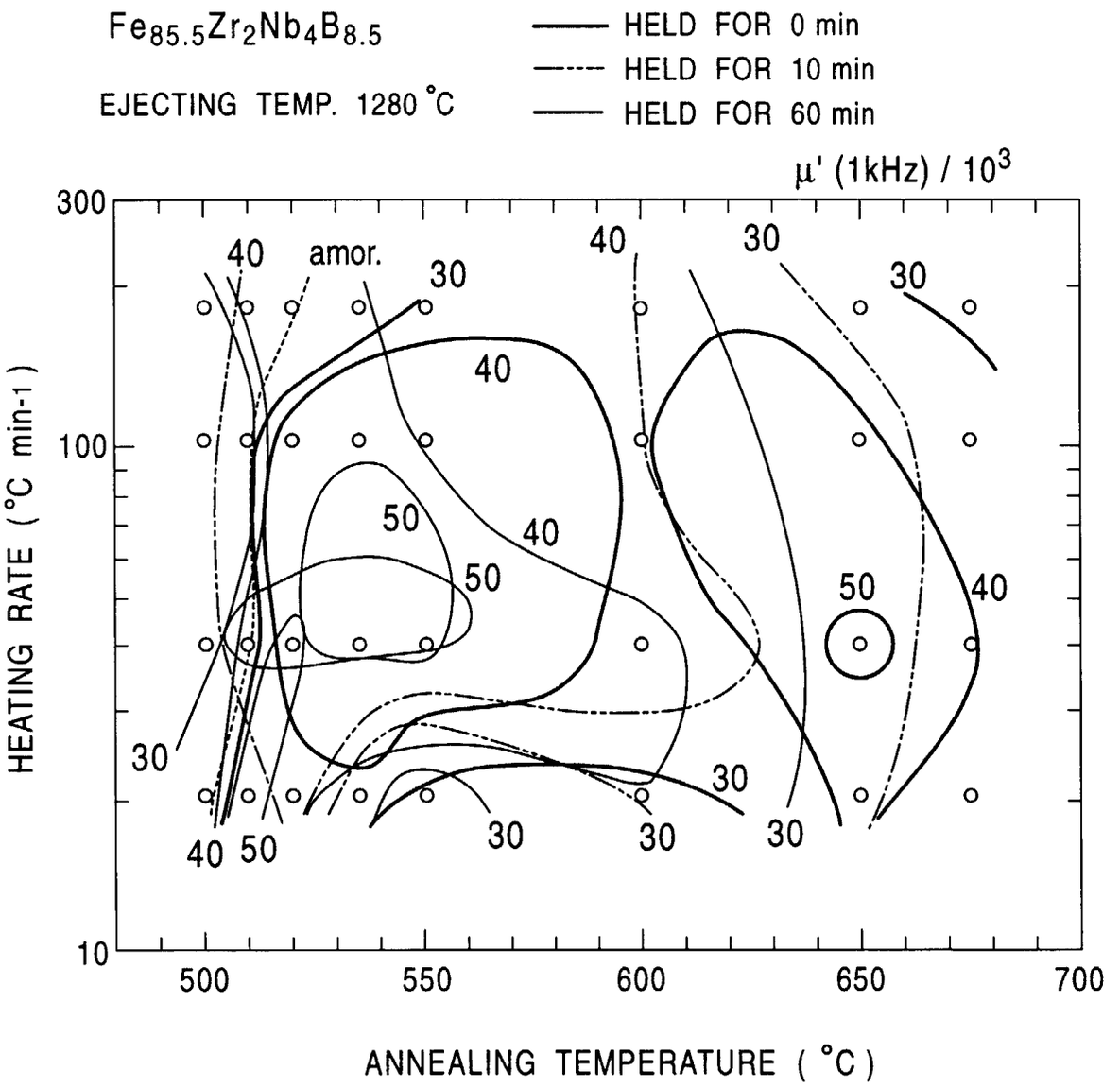
$Fe_{85.5}Zr_2Nb_4B_{8.5}$
EJECTING TEMP. 1280 °C
HELD FOR 0 min
HELD FOR 10 min
HELD FOR 60 min
μ' (1kHz) / 10^3
HEATING RATE (°C min-1)
ANNEALING TEMPERATURE (°C)
300
100
10
500
550
600
650
700
amor.
40
30
50

FIG. 107

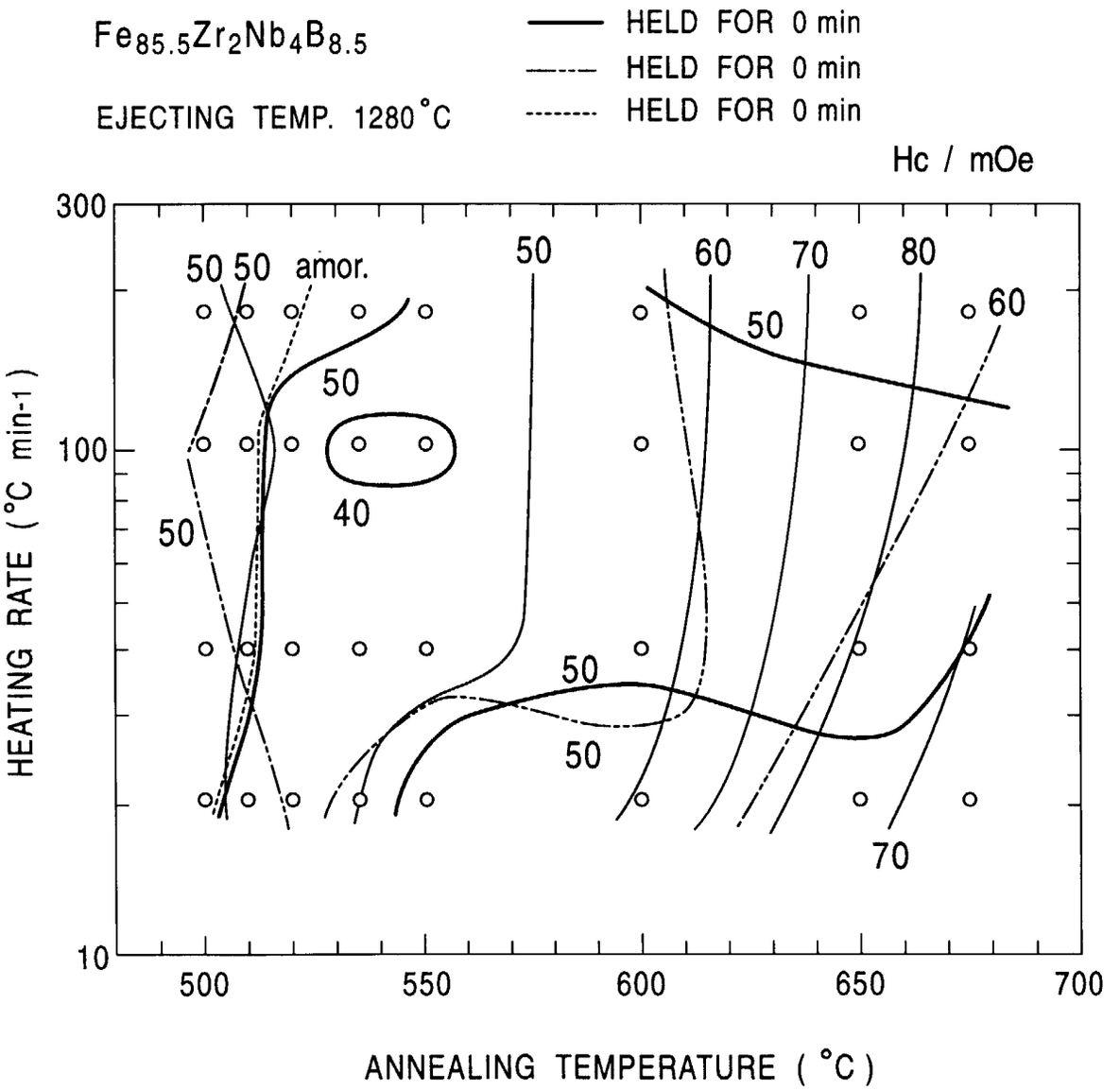
$Fe_{85.5}Zr_2Nb_4B_{8.5}$
EJECTING TEMP. 1280°C
HELD FOR 0 min
HELD FOR 0 min
HELD FOR 0 min
Hc / mOe
HEATING RATE (°C min-1)
ANNEALING TEMPERATURE (°C)
300
100
10
500
550
600
650
700
50 50 amor.
50
50
40
50
50
50
60
70
80
60
50
70

FIG. 108

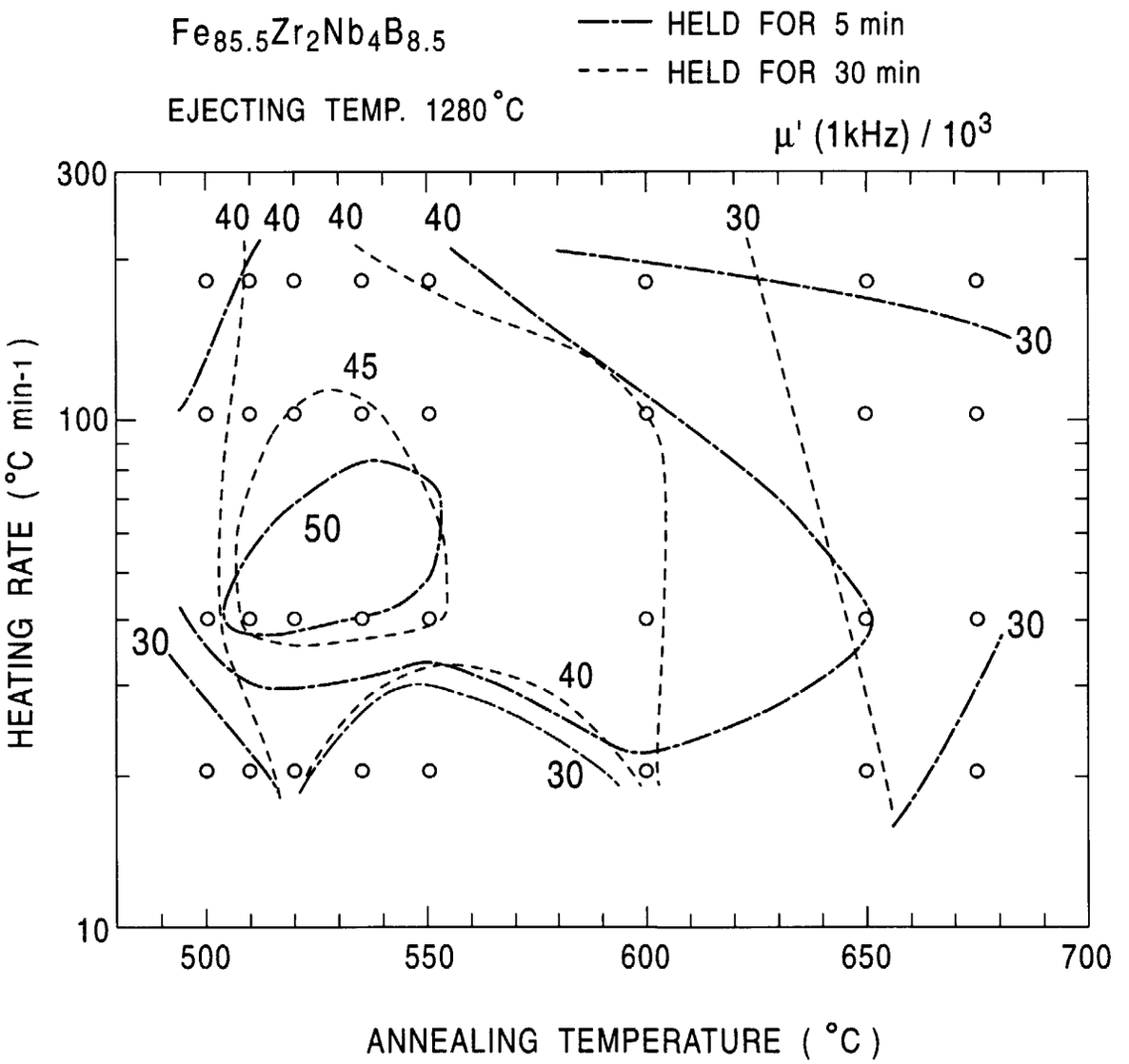
$Fe_{85.5}Zr_2Nb_4B_{8.5}$
HELD FOR 5 min
HELD FOR 30 min
EJECTING TEMP. 1280 °C
μ' (1kHz) / 10^3
HEATING RATE (°C min-1)
ANNEALING TEMPERATURE (°C)
300
100
10
500
550
600
650
700
40
40
40
40
30
30
45
50
30
40
30
30

FIG. 109

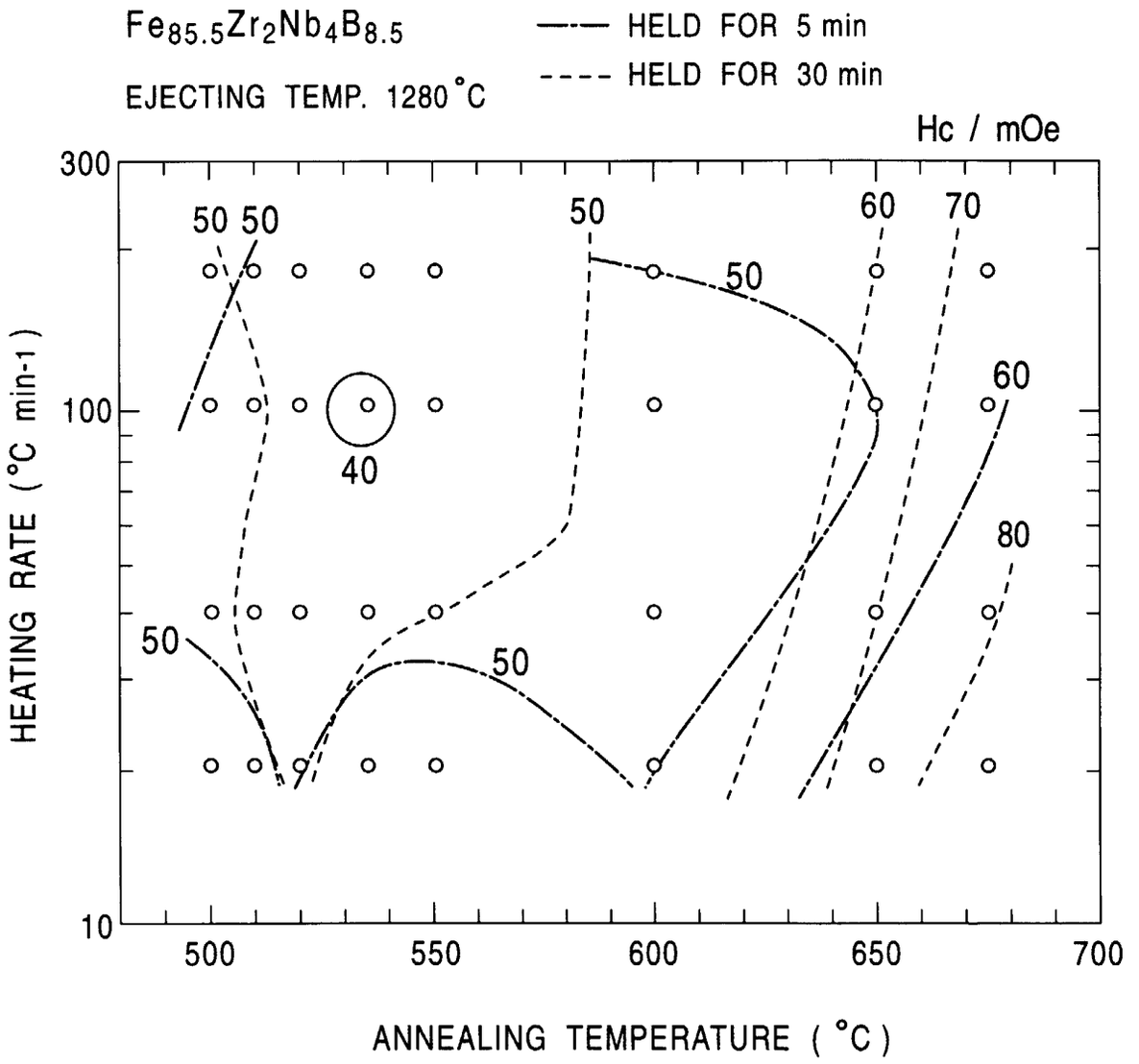
$Fe_{85.5}Zr_2Nb_4B_{8.5}$
EJECTING TEMP. 1280°C
HELD FOR 5 min
HELD FOR 30 min
Hc / mOe
HEATING RATE (°C min-1)
ANNEALING TEMPERATURE (°C)
300
100
10
500
550
600
650
700
50
50
50
50
50
60
70
60
80
40

FIG. 110

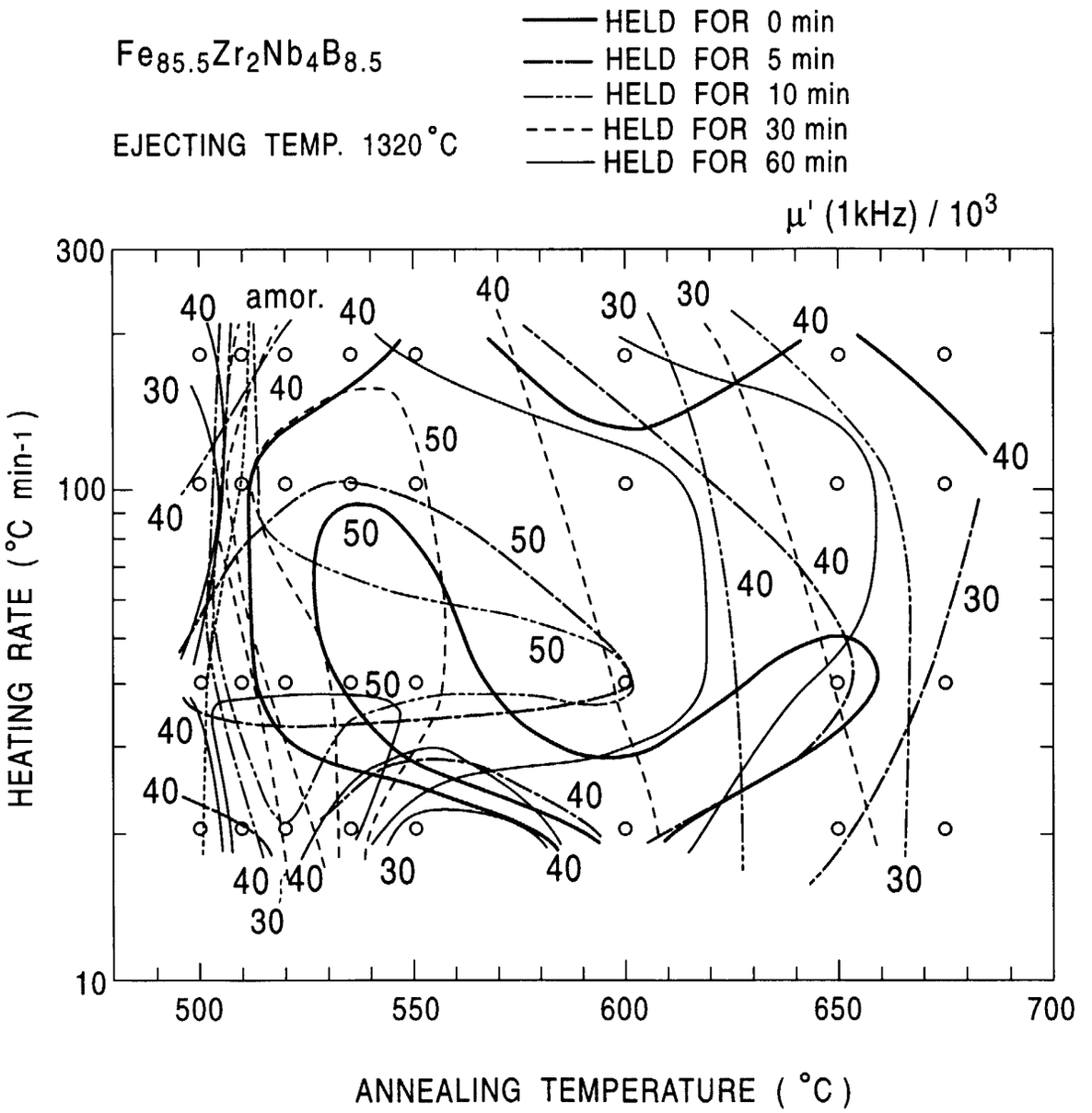
Fe85.5Zr2Nb4B8.5
EJECTING TEMP. 1320°C
HELD FOR 0 min
HELD FOR 5 min
HELD FOR 10 min
HELD FOR 30 min
HELD FOR 60 min
μ' (1kHz) / 10³
HEATING RATE (°C min-1)
ANNEALING TEMPERATURE (°C)
300
100
10
500
550
600
650
700
amor.

FIG. 111

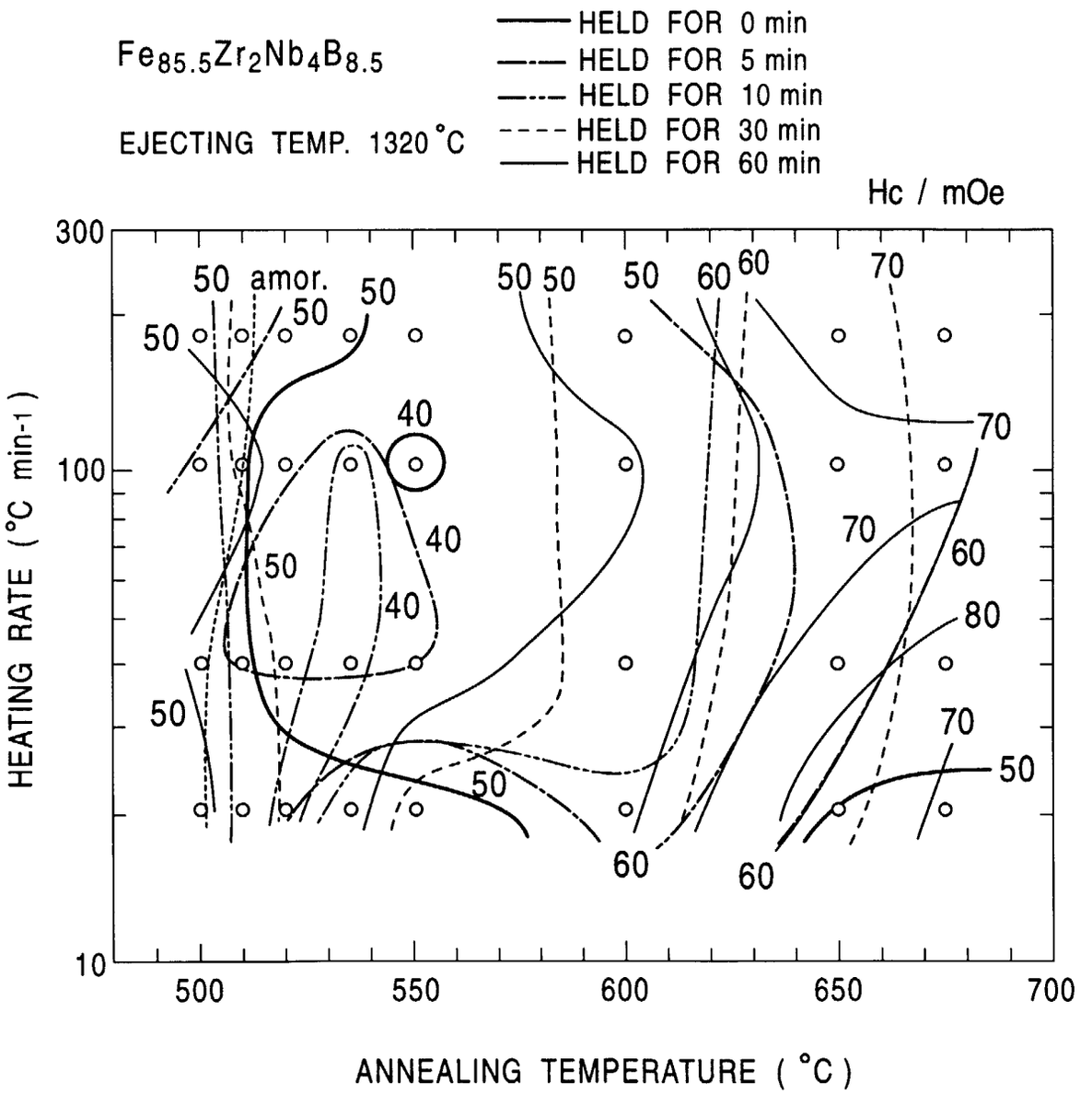
Fe85.5Zr2Nb4B8.5
EJECTING TEMP. 1320 °C
HELD FOR 0 min
HELD FOR 5 min
HELD FOR 10 min
HELD FOR 30 min
HELD FOR 60 min
Hc / mOe
HEATING RATE (°C min-1)
ANNEALING TEMPERATURE (°C)
300
100
10
500
550
600
650
700
50 amor.
50
50
50
50
50
50
50
50
40
40
40
50
50
50
50
60
60
60
60
70
70
70
70
70
80
50

FIG. 112

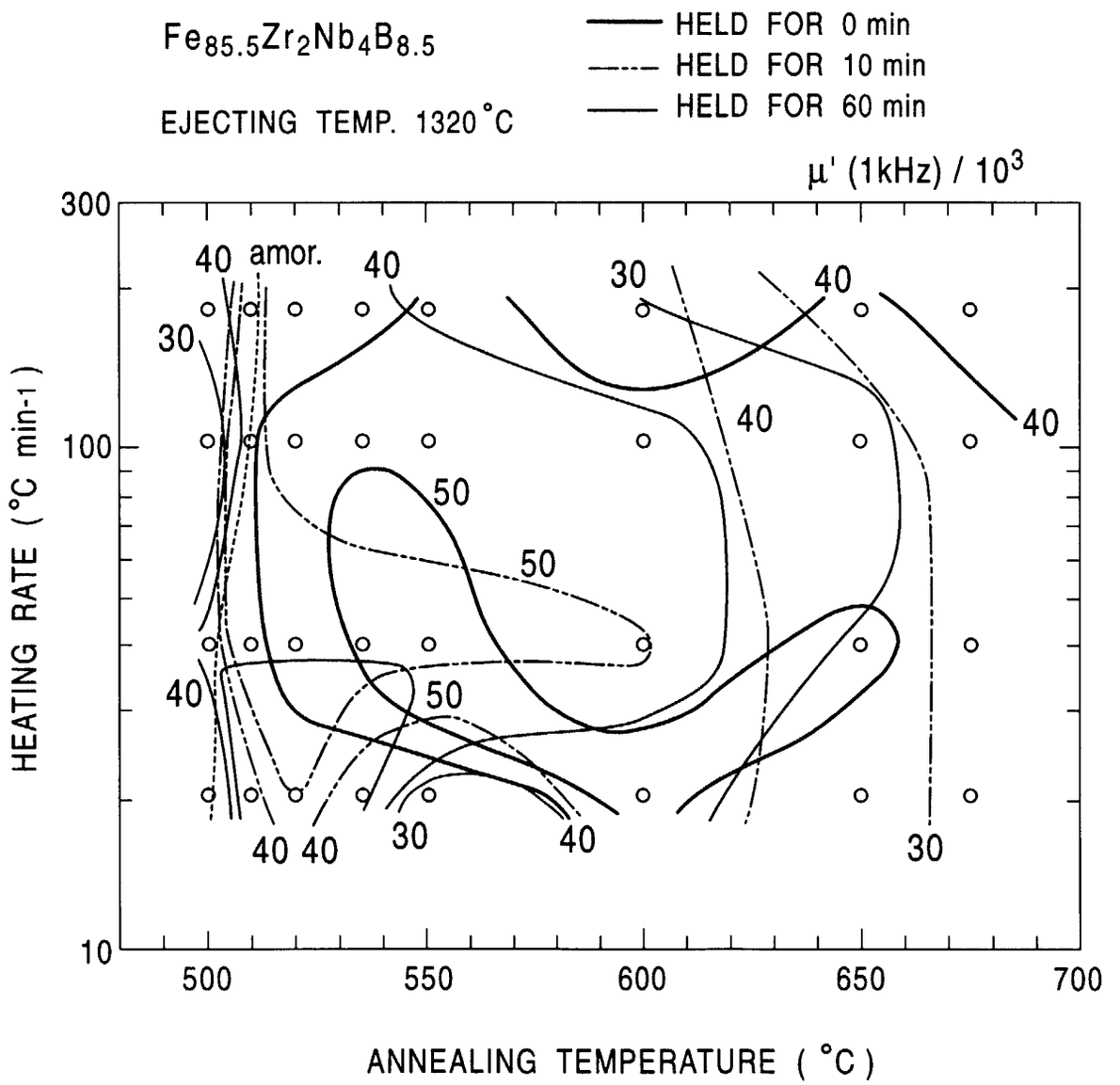
$Fe_{85.5}Zr_2Nb_4B_{8.5}$
EJECTING TEMP. 1320 °C
HELD FOR 0 min
HELD FOR 10 min
HELD FOR 60 min
μ' (1kHz) / 10^3
HEATING RATE (°C min-1)
ANNEALING TEMPERATURE (°C)
300
100
10
500
550
600
650
700
40 amor.
40
30
40
30
40
40
50
50
40
50
40 40
30
40
30

FIG. 113

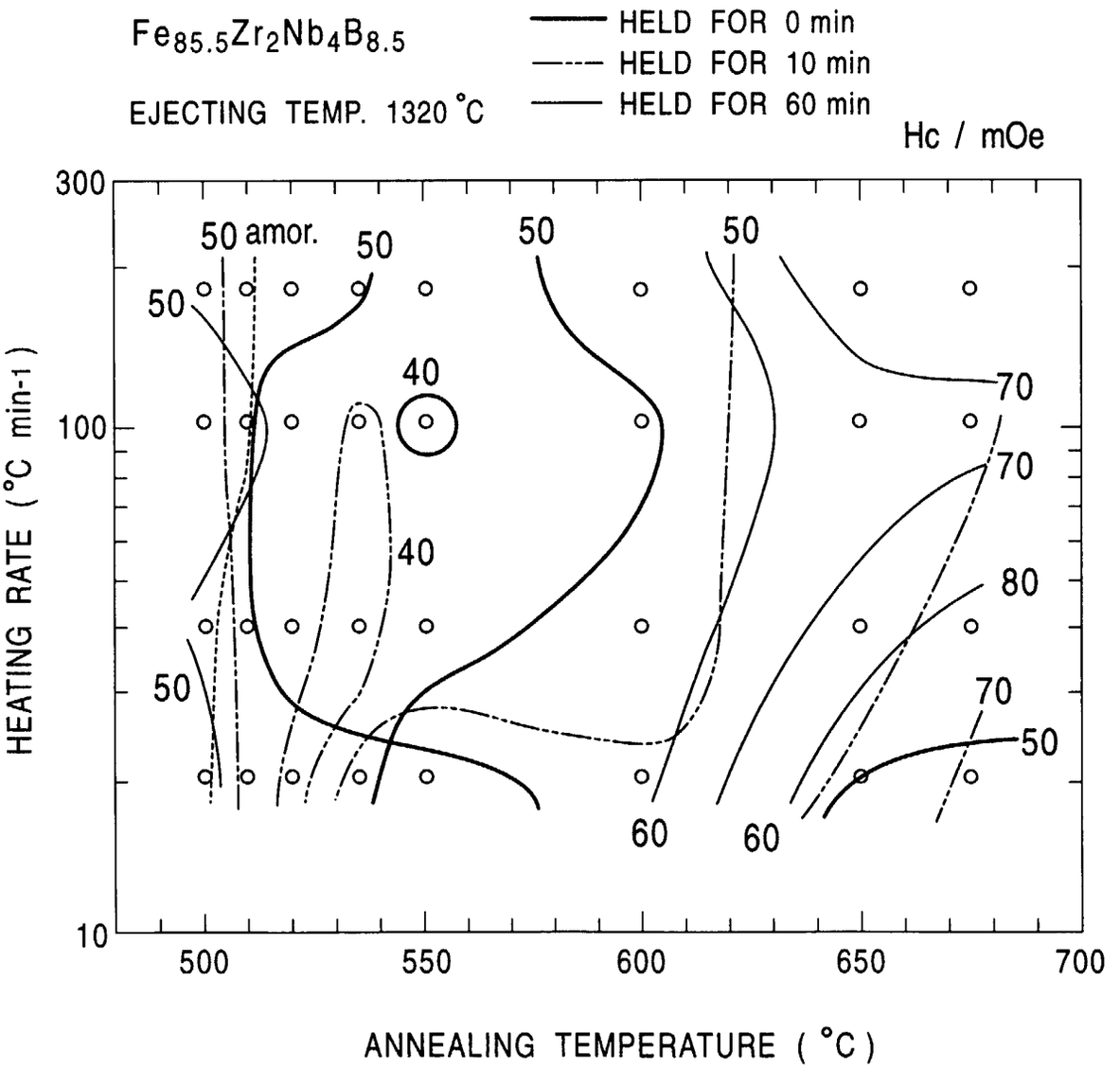
$Fe_{85.5}Zr_2Nb_4B_{8.5}$
EJECTING TEMP. 1320 °C
HELD FOR 0 min
HELD FOR 10 min
HELD FOR 60 min
Hc / mOe
HEATING RATE (°C min-1)
ANNEALING TEMPERATURE (°C)
300
100
10
500
550
600
650
700
50 amor.
50
40
60
70
80

FIG. 114

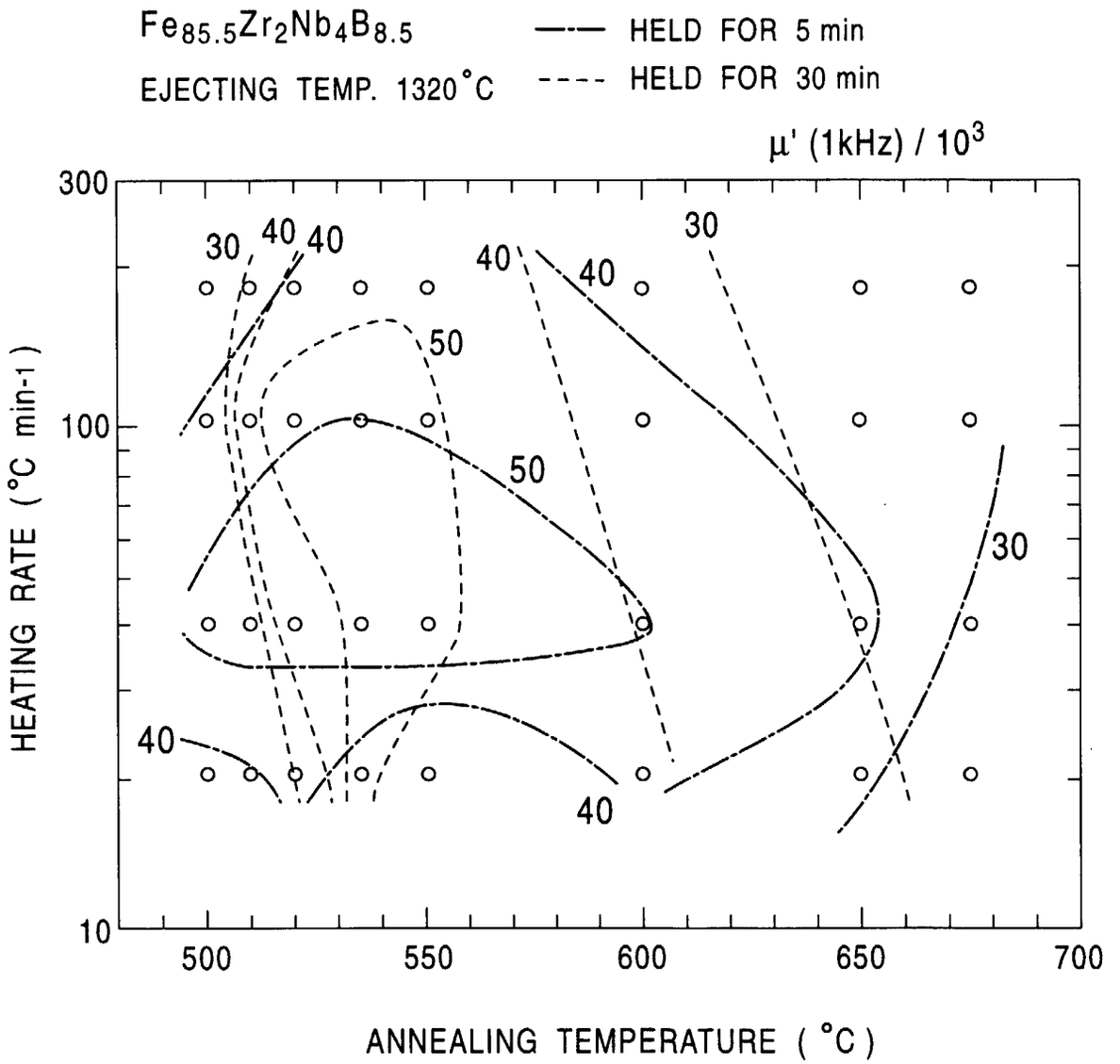
$Fe_{85.5}Zr_2Nb_4B_{8.5}$
EJECTING TEMP. 1320°C
—·— HELD FOR 5 min
---- HELD FOR 30 min
μ' (1kHz) / 10^3
HEATING RATE (°C min-1)
ANNEALING TEMPERATURE (°C)
300
100
10
500
550
600
650
700
30
40
50

FIG. 115

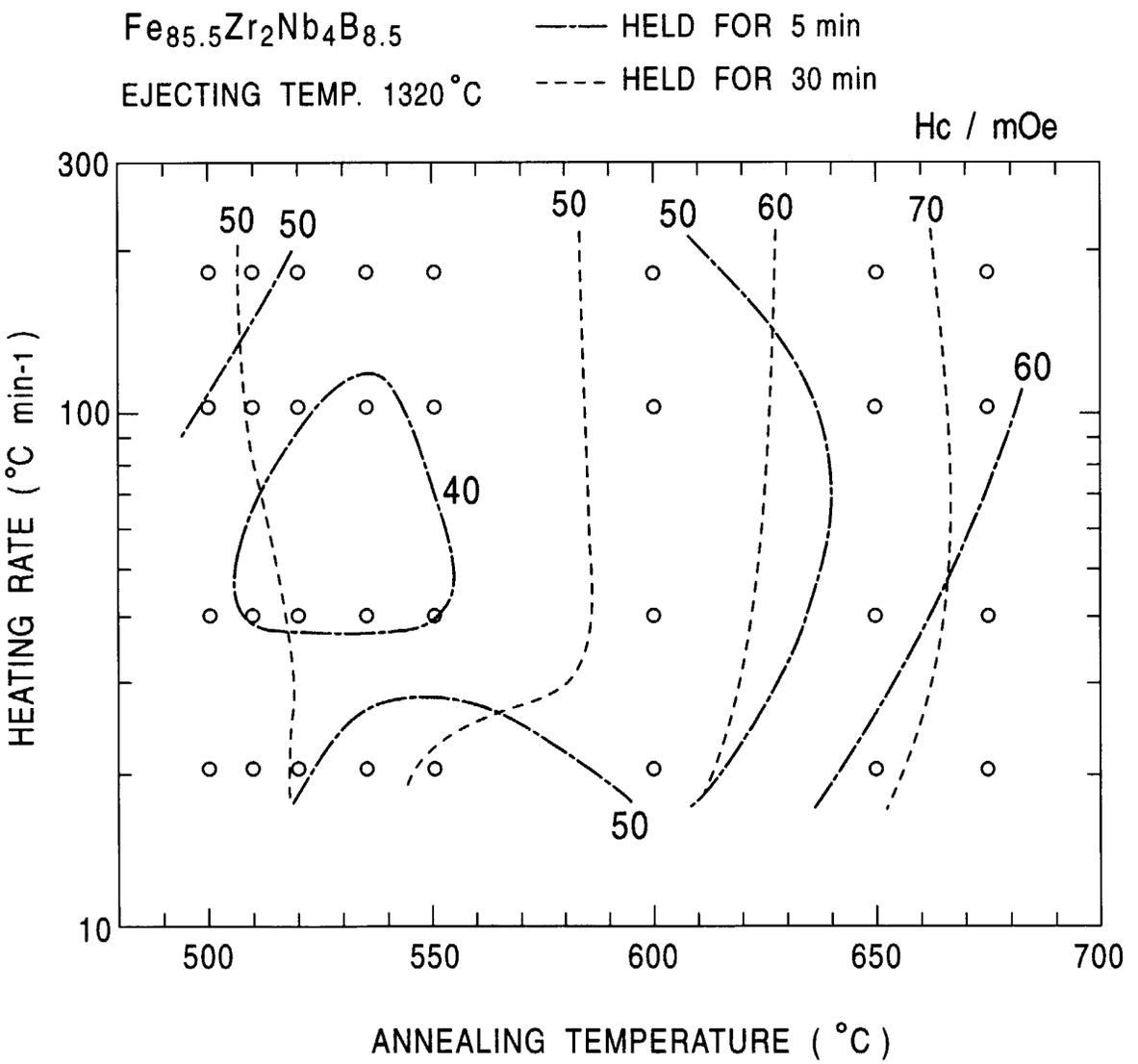
$Fe_{85.5}Zr_2Nb_4B_{8.5}$
EJECTING TEMP. 1320 °C
HELD FOR 5 min
HELD FOR 30 min
Hc / mOe
HEATING RATE (°C min-1)
ANNEALING TEMPERATURE (°C)
300
100
10
500
550
600
650
700
50
50
50
50
60
70
60
40
50

FIG. 116

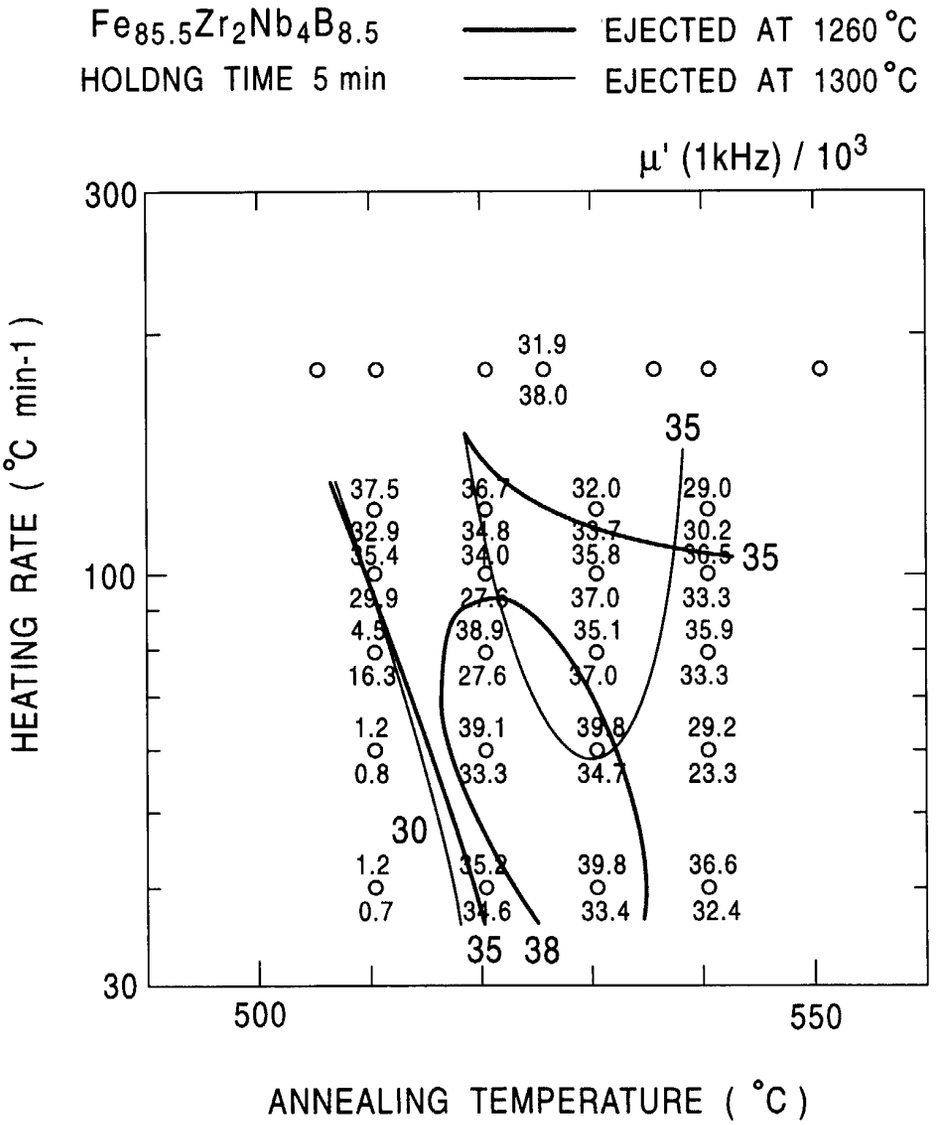
$Fe_{85.5}Zr_2Nb_4B_{8.5}$
HOLDNG TIME 5 min
EJECTED AT 1260 °C
EJECTED AT 1300 °C
μ' (1kHz) / 10^3
HEATING RATE (°C min-1)
ANNEALING TEMPERATURE (°C)
300
100
30
500
550
31.9
38.0
35
37.5
32.9
29.9
4.5
16.3
1.2
0.8
36.7
34.8
34.0
27.6
38.9
27.6
39.1
33.3
32.0
33.7
35.8
37.0
35.1
37.0
39.8
34.7
29.0
30.2
33.3
35.9
33.3
29.2
23.3
35
30
1.2
0.7
35.2
34.6
39.8
33.4
36.6
32.4
35 38

FIG. 117

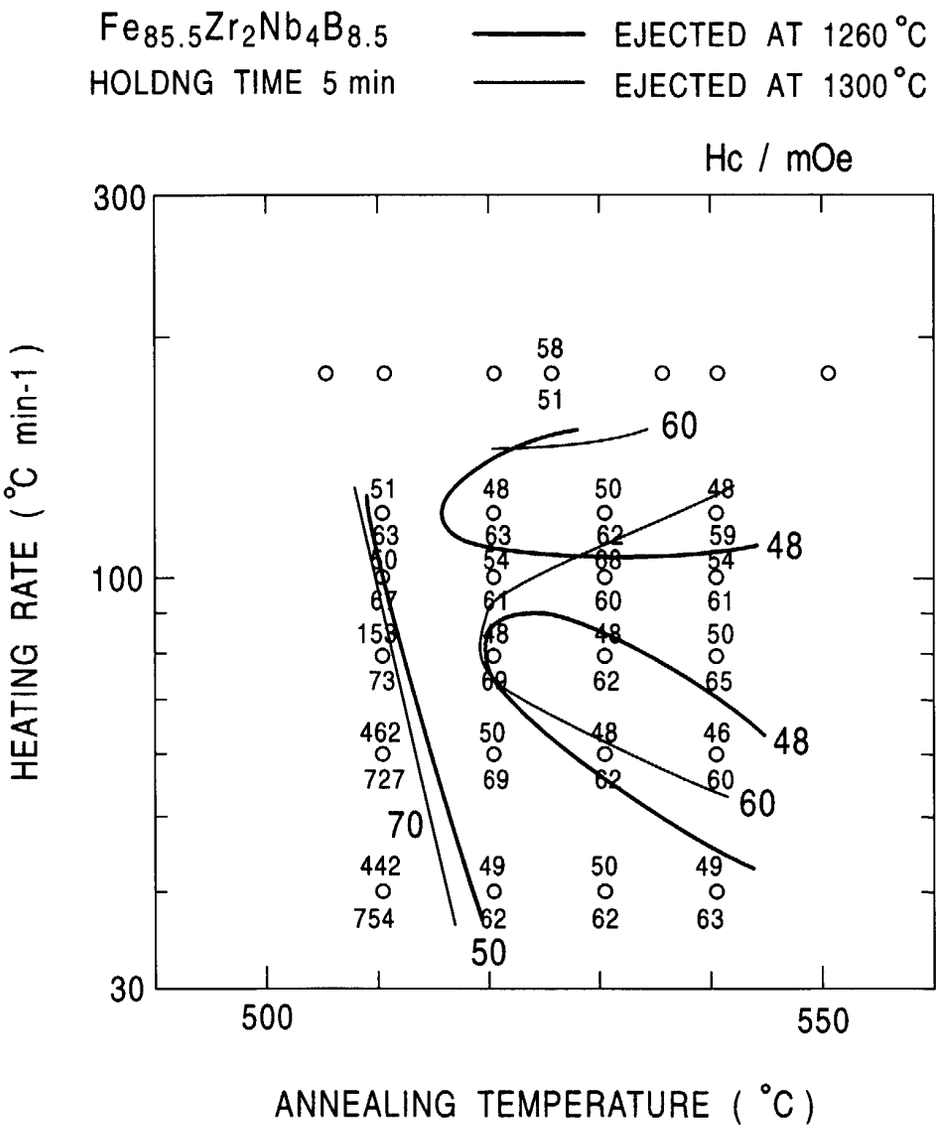
$Fe_{85.5}Zr_2Nb_4B_{8.5}$
HOLDNG TIME 5 min
EJECTED AT 1260 °C
EJECTED AT 1300 °C
Hc / mOe
300
100
30
500
550
HEATING RATE (°C min-1)
ANNEALING TEMPERATURE (°C)
60
48
48
60
70
50

FIG. 118

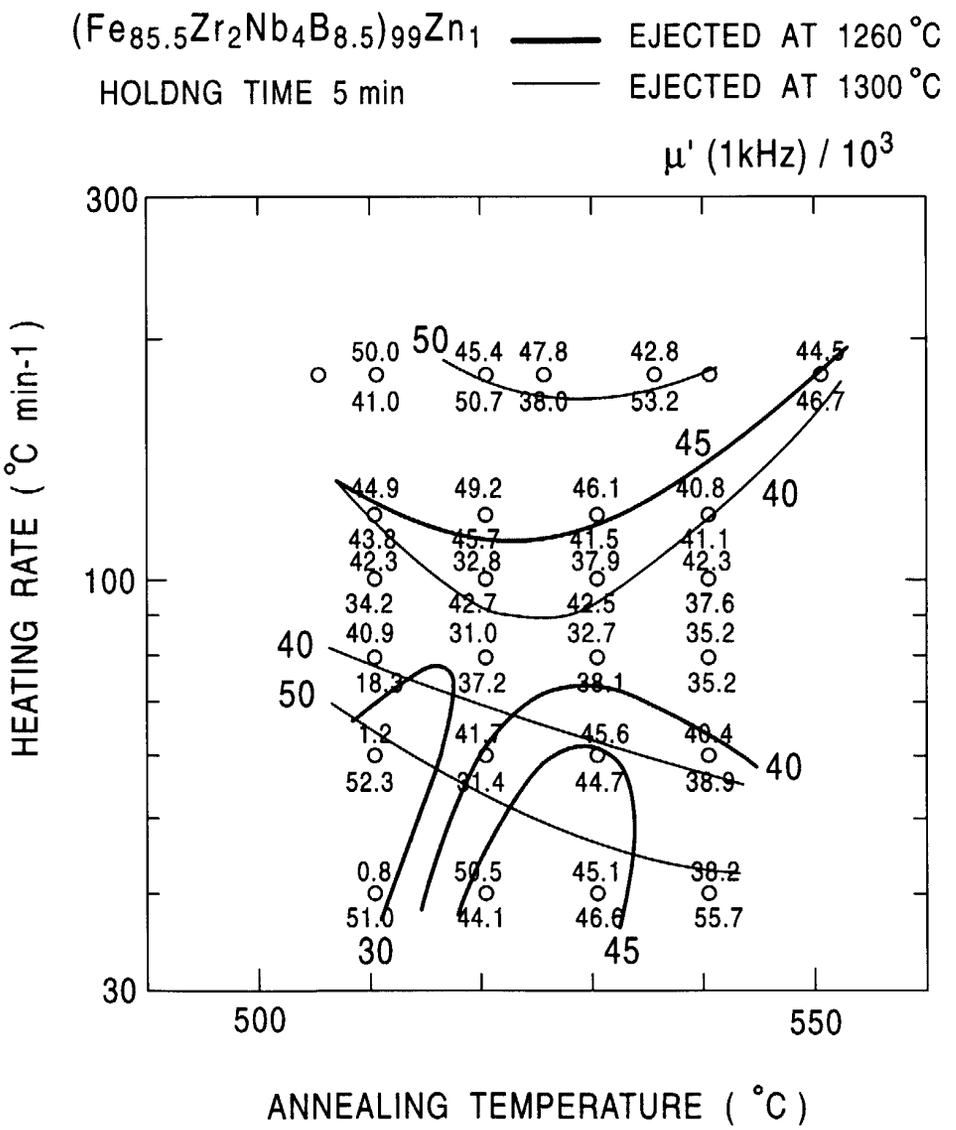
$(Fe_{85.5}Zr_2Nb_4B_{8.5})_{99}Zn_1$
HOLDNG TIME 5 min
EJECTED AT 1260 °C
EJECTED AT 1300 °C
μ' (1kHz) / 10^3
HEATING RATE (°C min-1)
ANNEALING TEMPERATURE (°C)
300
100
30
500
550
50
45
40
30
50.0
45.4
47.8
42.8
44.5
41.0
50.7
38.0
53.2
46.7
44.9
49.2
46.1
40.8
43.8
45.7
41.5
41.1
42.3
32.8
37.9
42.3
34.2
42.7
42.5
37.6
40.9
31.0
32.7
35.2
18.3
37.2
38.1
35.2
1.2
41.7
45.6
40.4
52.3
31.4
44.7
38.9
0.8
50.5
45.1
38.2
51.0
44.1
46.6
55.7

FIG. 119

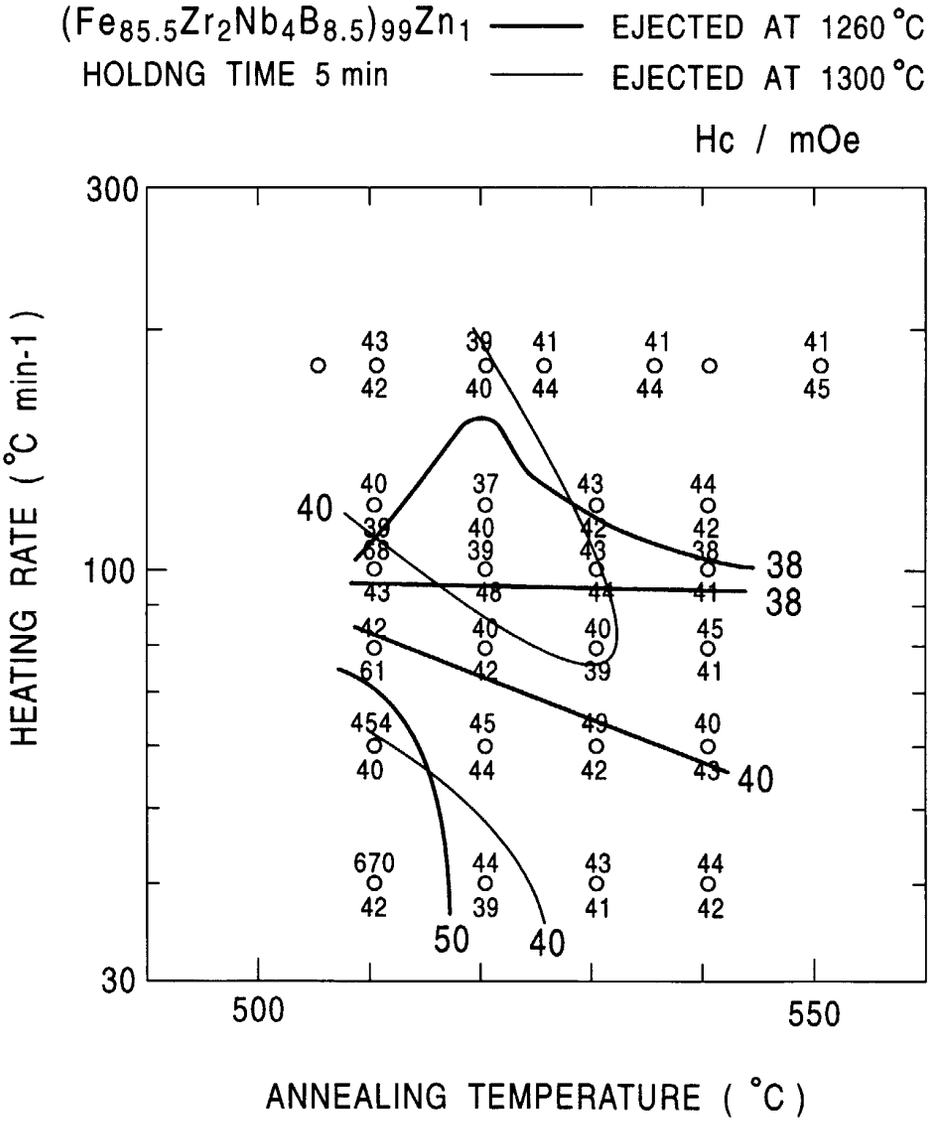
$(Fe_{85.5}Zr_2Nb_4B_{8.5})_{99}Zn_1$ —— EJECTED AT 1260 °C
HOLDNG TIME 5 min —— EJECTED AT 1300 °C
Hc / mOe
HEATING RATE (°C min-1)
300
100
30
500
550
ANNEALING TEMPERATURE (°C)
40
38
38
40
50
40

FIG. 120

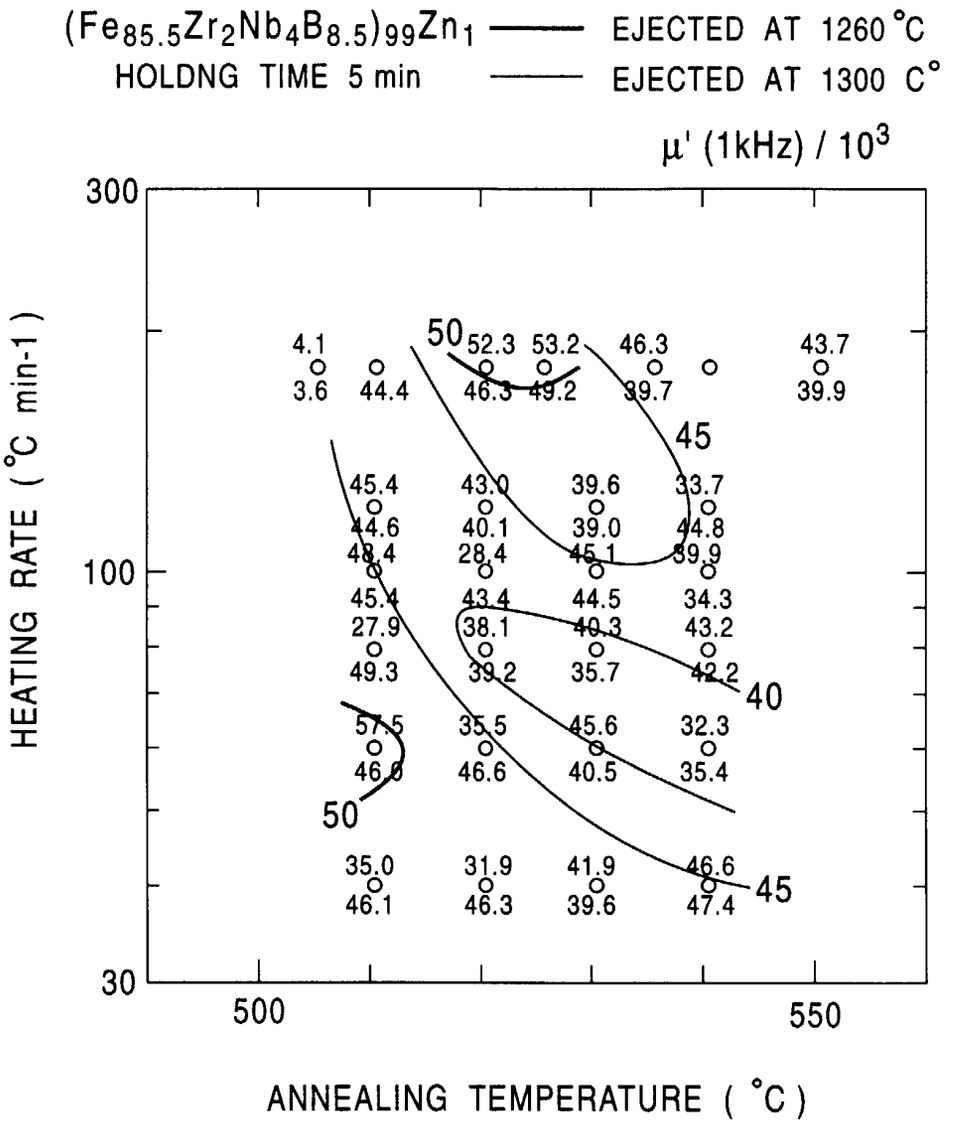
$(Fe_{85.5}Zr_2Nb_4B_{8.5})_{99}Zn_1$ —— EJECTED AT 1260 °C
HOLDNG TIME 5 min —— EJECTED AT 1300 C°
μ' (1kHz) / 10^3
HEATING RATE (°C min-1)
ANNEALING TEMPERATURE (°C)
300
100
30
500
550
50
45
40
4.1
3.6
44.4
52.3
53.2
46.3
49.2
46.3
39.7
43.7
39.9
45.4
44.6
43.0
40.1
39.6
39.0
33.7
44.8
48.4
28.4
45.1
39.9
45.4
27.9
49.3
43.4
38.1
39.2
44.5
40.3
35.7
34.3
43.2
42.2
57.5
46.6
35.5
46.6
45.6
40.5
32.3
35.4
35.0
46.1
31.9
46.3
41.9
39.6
46.6
47.4

FIG. 121

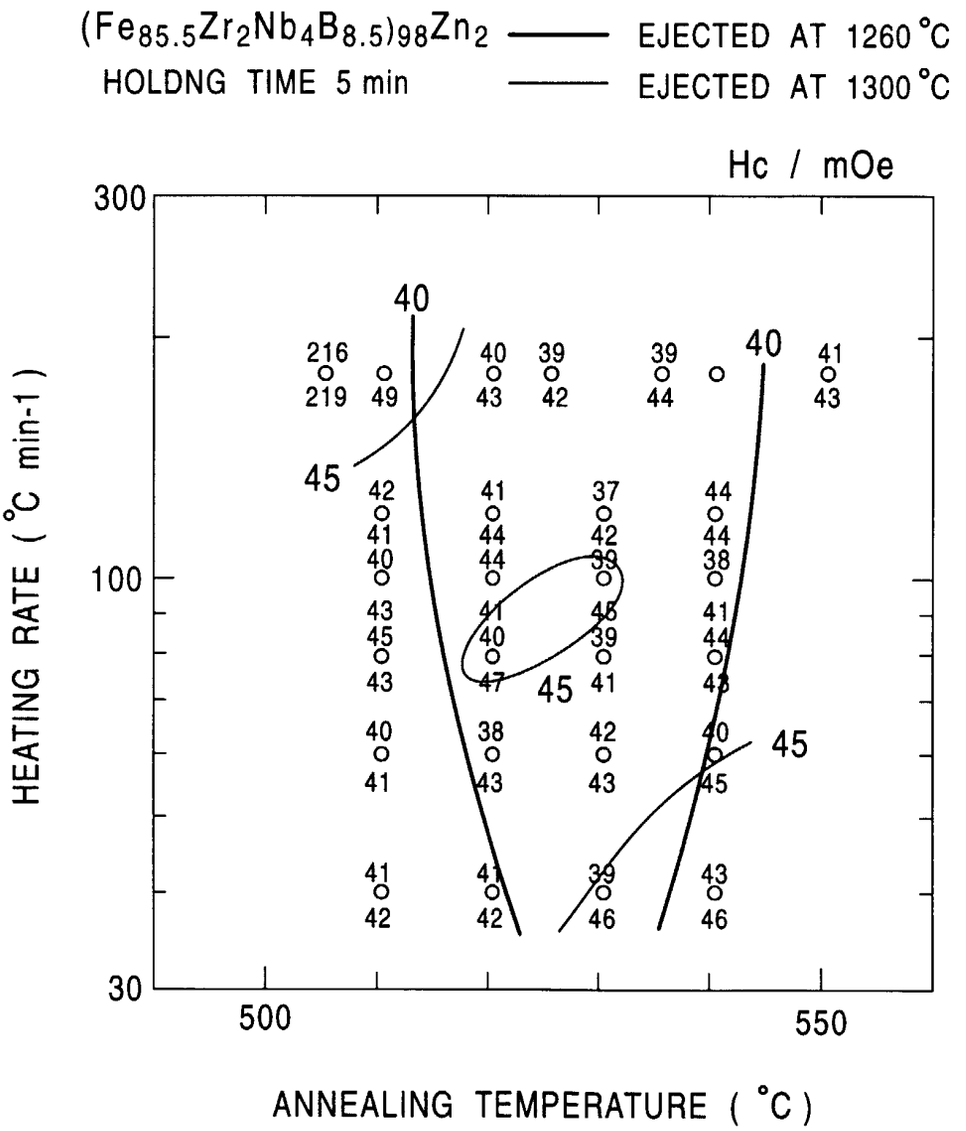
$(Fe_{85.5}Zr_2Nb_4B_{8.5})_{98}Zn_2$
HOLDNG TIME 5 min
EJECTED AT 1260 °C
EJECTED AT 1300 °C
Hc / mOe
HEATING RATE (°C min-1)
ANNEALING TEMPERATURE (°C)
300
100
30
500
550
40
45

FIG. 122

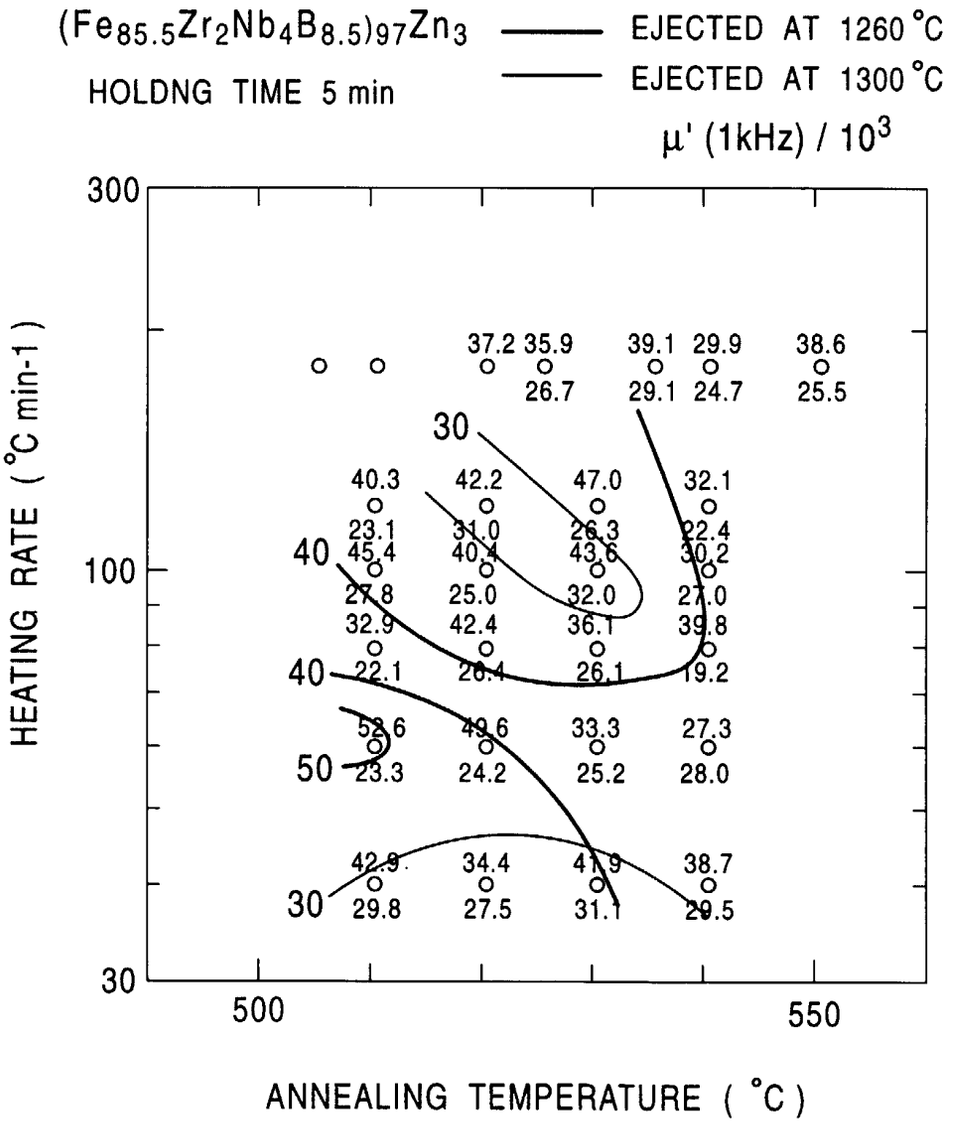
$(Fe_{85.5}Zr_2Nb_4B_{8.5})_{97}Zn_3$
HOLDNG TIME 5 min
EJECTED AT 1260 °C
EJECTED AT 1300 °C
μ' (1kHz) / 10^3
HEATING RATE (°C min-1)
ANNEALING TEMPERATURE (°C)
300
100
30
500
550
30
40
40
50
30
37.2 35.9 39.1 29.9 38.6
26.7 29.1 24.7 25.5
40.3 42.2 47.0 32.1
23.1 31.0 26.3 22.4
45.4 40.4 43.6 30.2
27.8 25.0 32.0 27.0
32.9 42.4 36.1 39.8
22.1 26.4 26.1 19.2
52.6 49.6 33.3 27.3
23.3 24.2 25.2 28.0
42.9 34.4 41.9 38.7
29.8 27.5 31.1 29.5

FIG. 123

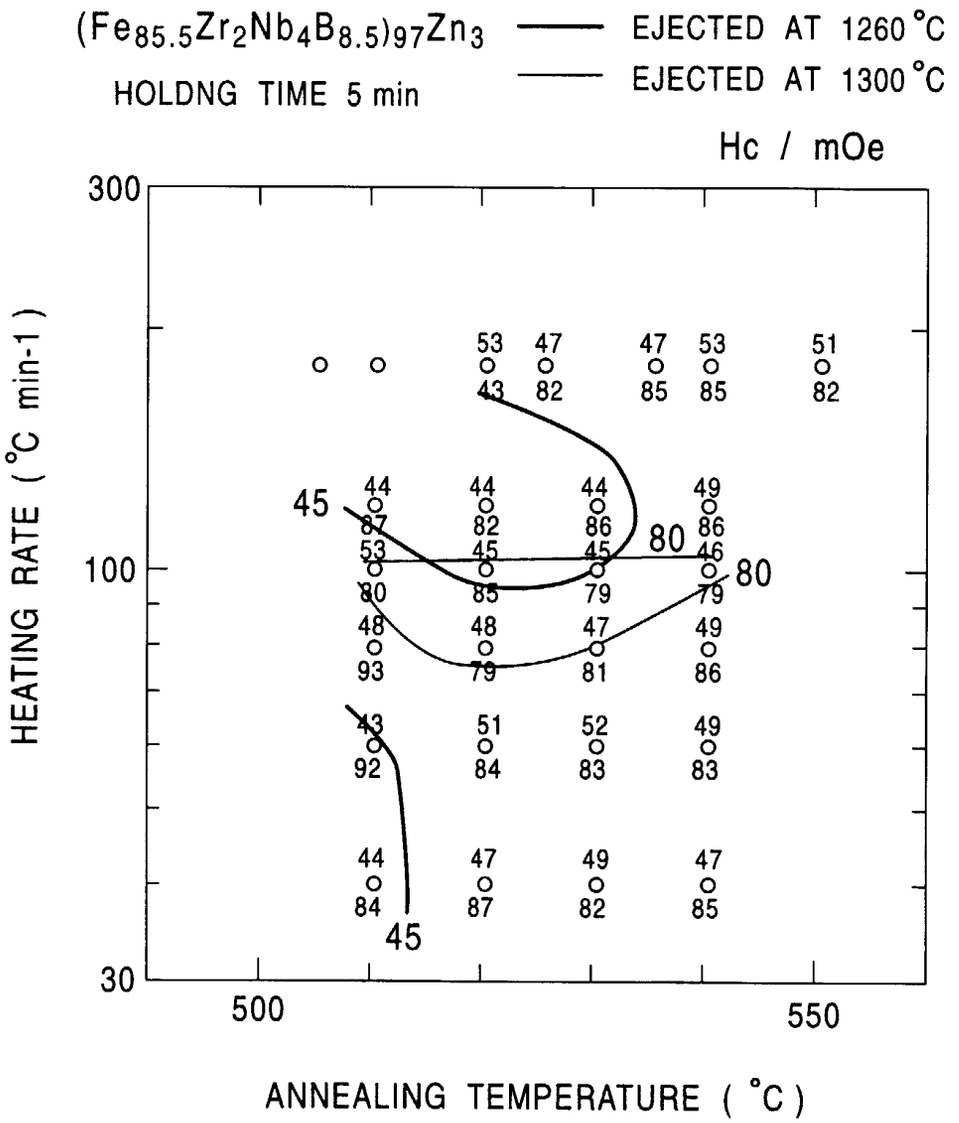
$(Fe_{85.5}Zr_2Nb_4B_{8.5})_{97}Zn_3$
HOLDNG TIME 5 min
EJECTED AT 1260 °C
EJECTED AT 1300 °C
Hc / mOe
HEATING RATE (°C min-1)
ANNEALING TEMPERATURE (°C)
300
100
30
500
550
45
80
80
45

FIG. 124

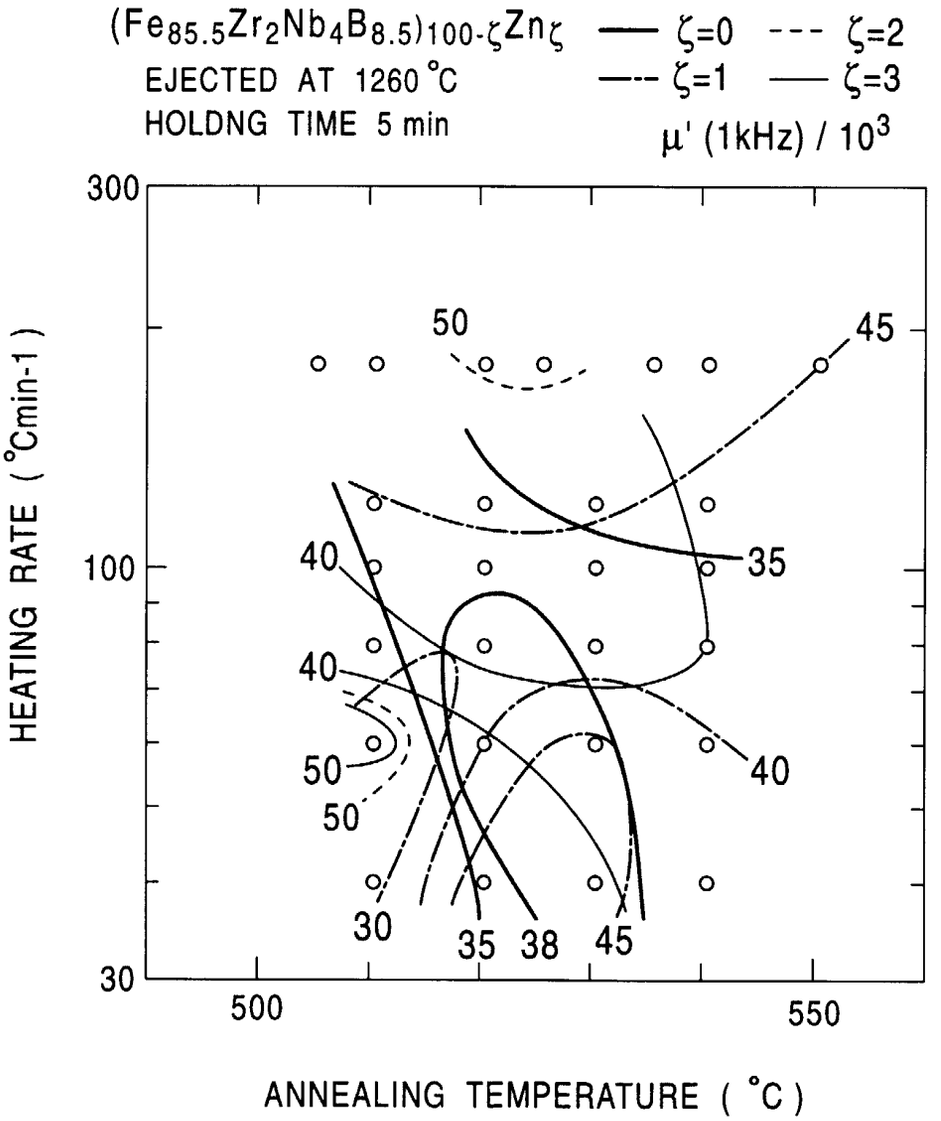
$(Fe_{85.5}Zr_2Nb_4B_{8.5})_{100-\zeta}Zn_\zeta$
EJECTED AT 1260 °C
HOLDNG TIME 5 min
ζ=0
ζ=1
ζ=2
ζ=3
μ' (1kHz) / 10³
HEATING RATE (°Cmin-1)
300
100
30
500
550
ANNEALING TEMPERATURE (°C)
50
45
40
35
40
40
50
50
30
35
38
45

FIG. 125

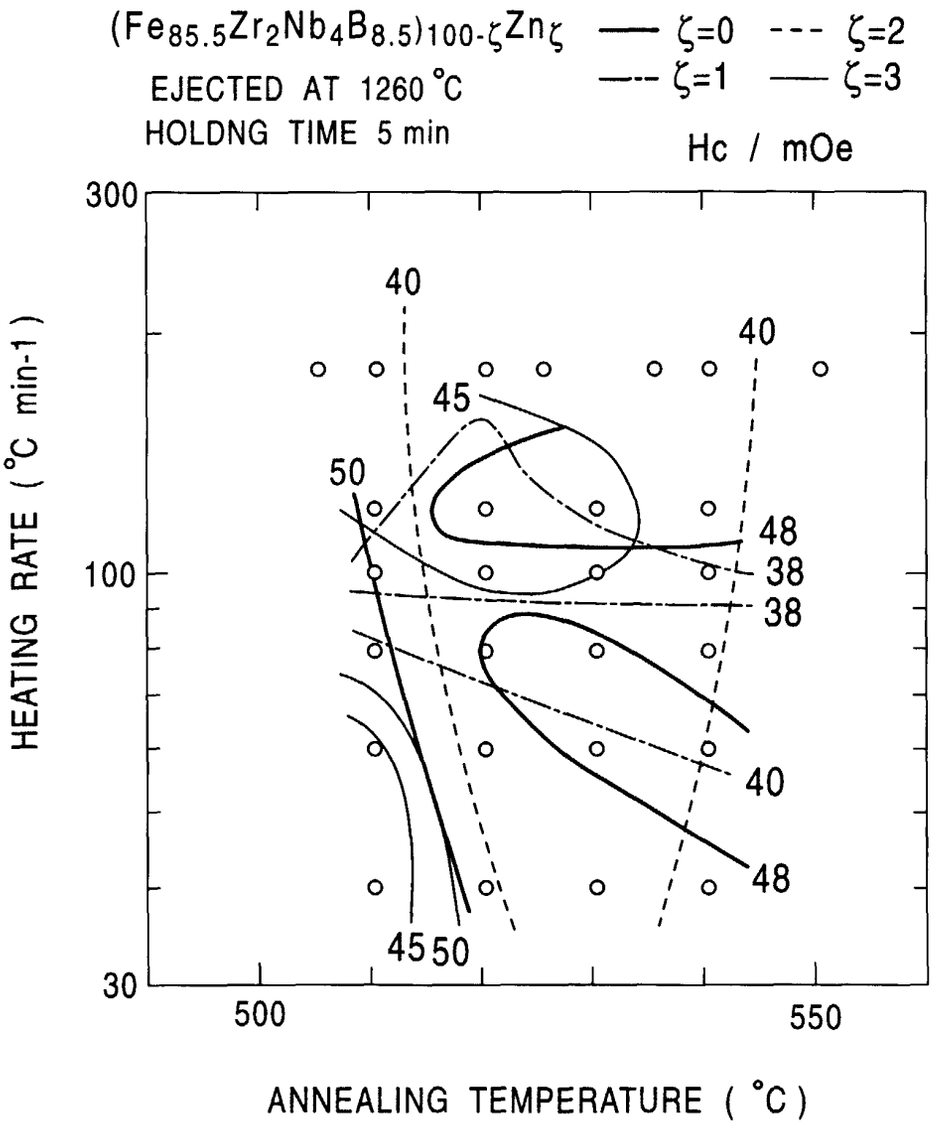
$(Fe_{85.5}Zr_2Nb_4B_{8.5})_{100-\zeta}Zn_\zeta$
EJECTED AT 1260 °C
HOLDNG TIME 5 min
ζ=0
ζ=1
ζ=2
ζ=3
Hc / mOe
300
100
30
500
550
HEATING RATE (°C min-1)
ANNEALING TEMPERATURE (°C)
40
40
45
50
48
38
38
40
48
45
50

FIG. 126

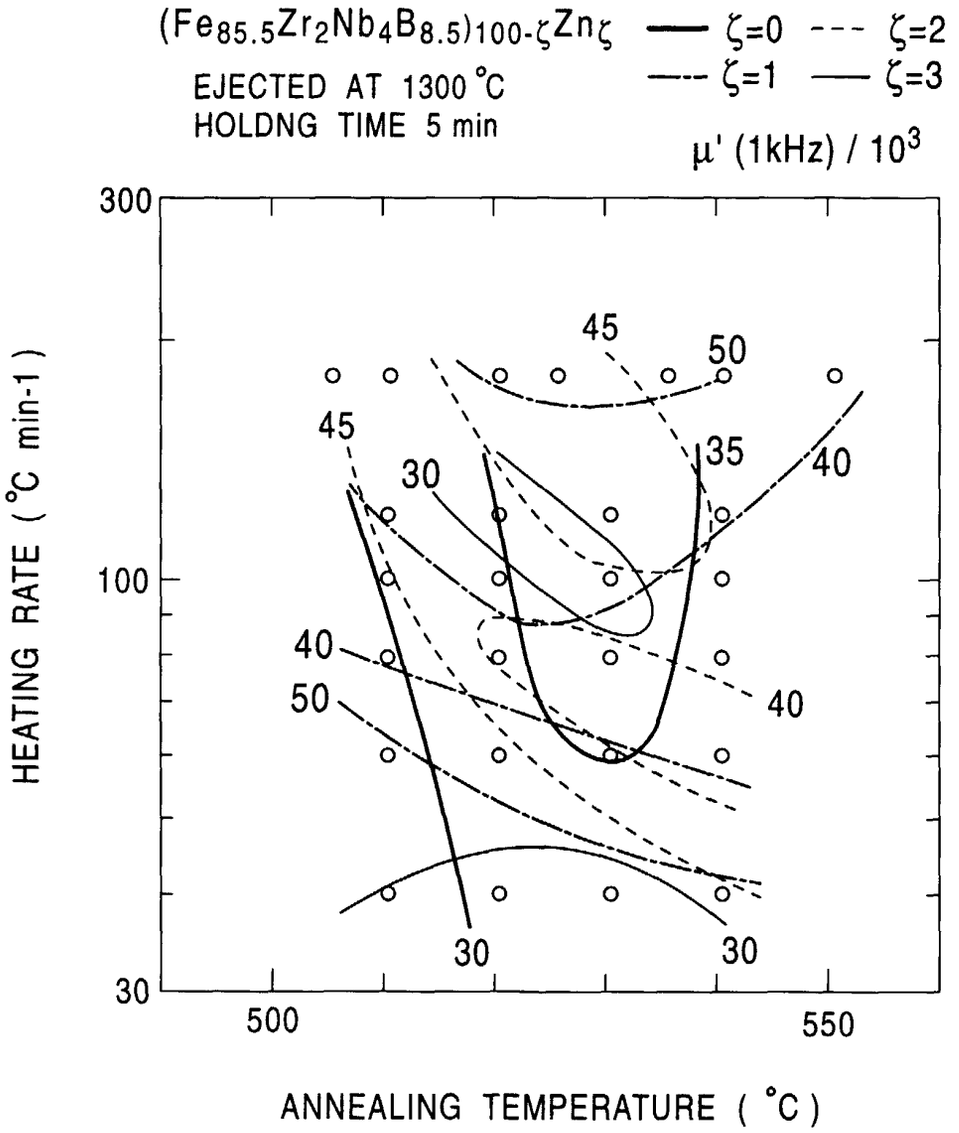
$(Fe_{85.5}Zr_2Nb_4B_{8.5})_{100-\zeta}Zn_\zeta$
ζ=0
ζ=2
ζ=1
ζ=3
EJECTED AT 1300 °C
HOLDNG TIME 5 min
μ' (1kHz) / 10³
HEATING RATE (°C min-1)
ANNEALING TEMPERATURE (°C)
300
100
30
500
550
45
50
45
30
35
40
40
40
50
30
30

FIG. 127

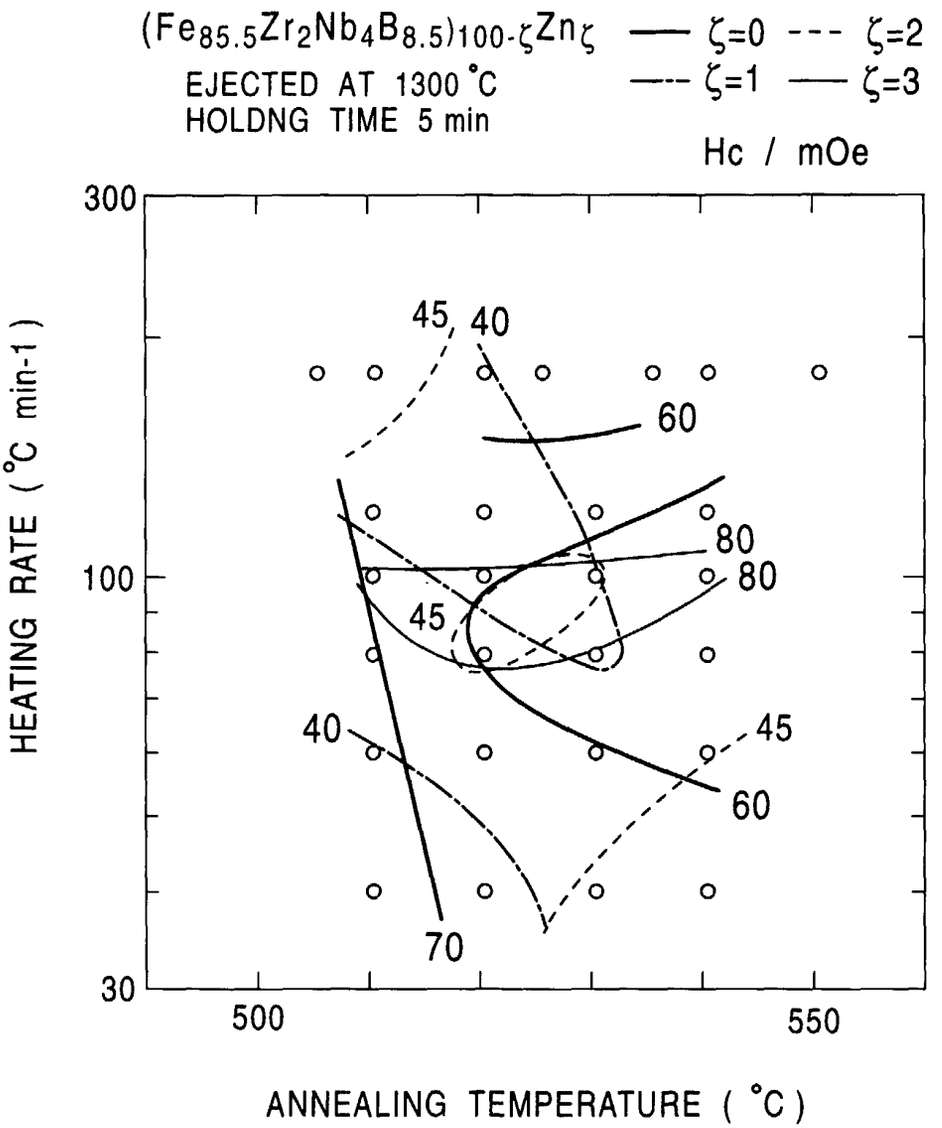
$(Fe_{85.5}Zr_2Nb_4B_{8.5})_{100-\zeta}Zn_\zeta$
EJECTED AT 1300 °C
HOLDNG TIME 5 min
ζ=0 --- ζ=2
—·— ζ=1 —— ζ=3
Hc / mOe
HEATING RATE (°C min-1)
ANNEALING TEMPERATURE (°C)
300
100
30
500
550
45
40
60
80
80
45
40
45
60
70

FIG. 128

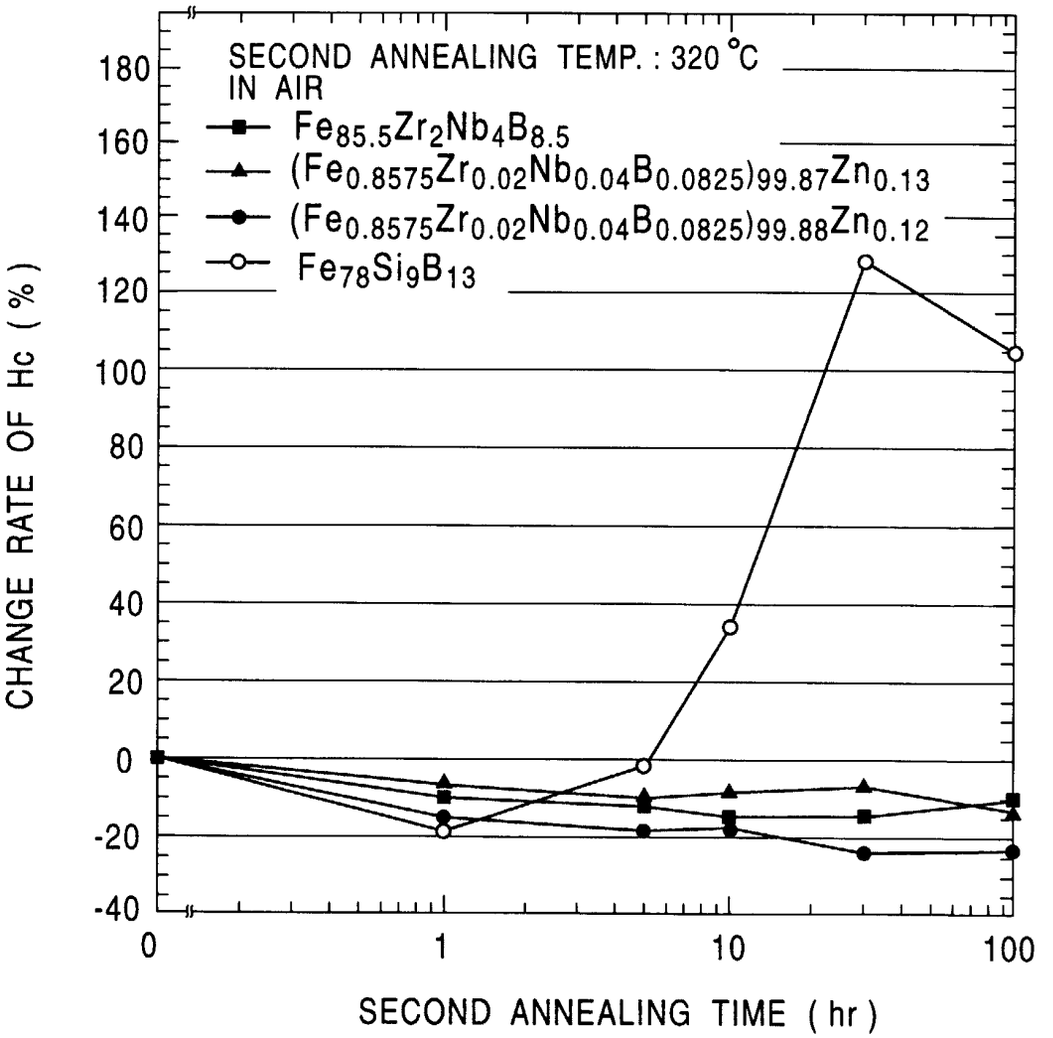
SECOND ANNEALING TEMP. : 320 °C
IN AIR
Fe85.5Zr2Nb4B8.5
(Fe0.8575Zr0.02Nb0.04B0.0825)99.87Zn0.13
(Fe0.8575Zr0.02Nb0.04B0.0825)99.88Zn0.12
Fe78Si9B13
CHANGE RATE OF Hc (%)
180
160
140
120
100
80
60
40
20
0
-20
-40
0
1
10
100
SECOND ANNEALING TIME (hr)

FIG. 129

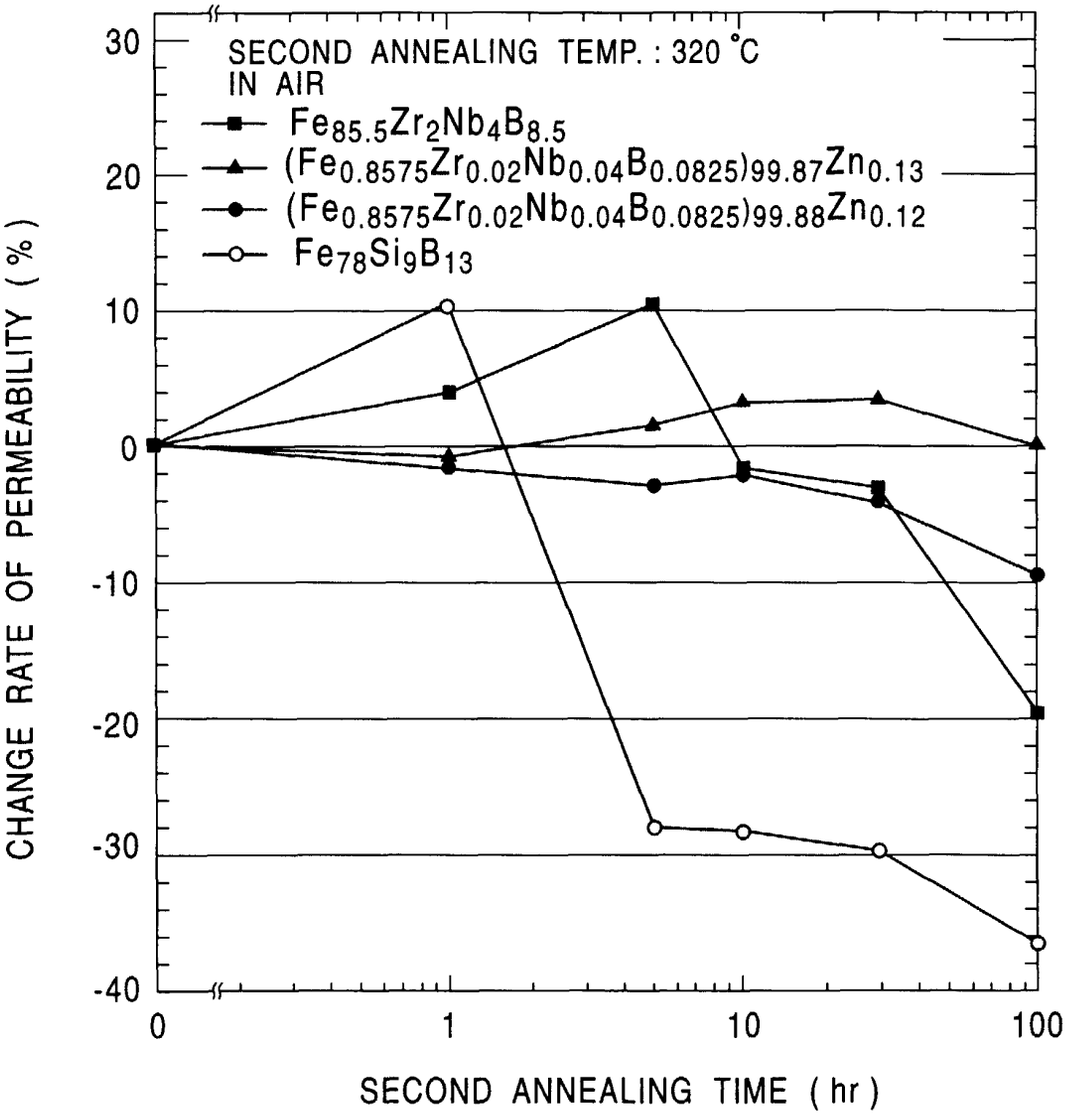
SECOND ANNEALING TEMP. : 320 °C
IN AIR
Fe85.5Zr2Nb4B8.5
(Fe0.8575Zr0.02Nb0.04B0.0825)99.87Zn0.13
(Fe0.8575Zr0.02Nb0.04B0.0825)99.88Zn0.12
Fe78Si9B13
CHANGE RATE OF PERMEABILITY (%)
30
20
10
0
-10
-20
-30
-40
0
1
10
100
SECOND ANNEALING TIME (hr)

European Patent Office

EUROPEAN SEARCH REPORT

Application Number
EP 99 30 8538

DOCUMENTS CONSIDERED TO BE RELEVANT

Category	Citation of document with indication, where appropriate, of relevant passages	Relevant to claim	CLASSIFICATION OF THE APPLICATION (Int.Cl.7)
X	PATENT ABSTRACTS OF JAPAN vol. 1995, no. 11, 26 December 1995 (1995-12-26) & JP 07 201599 A (ALPS ELECTRIC CO LTD;OTHERS: 02), 4 August 1995 (1995-08-04)	1	H01F1/153
A	* abstract * & US 5 935 347 A	2,17,18, 22,23	
A	US 5 474 624 A (SUZUKI KIYONORI ET AL) 12 December 1995 (1995-12-12)	1,6,9, 14,15, 17,24, 29,35,36	
X	* column 9, line 1 - line 59; claims 1-6; example 4 *	12,34, 41-44	
A	WO 92 15998 A (ALLIED SIGNAL INC) 17 September 1992 (1992-09-17)	1,17	
X	* page 8, line 4 - line 34 *	41	
A	HASEGAWA N ET AL: "MAGNETIC DOMAIN STRUCTURE OF NANOCRYSTALLINE FE-M-B (M=ZR,NB) ALLOYS REVEALED BY LORENTZ ELECTRON MICROSCOPY" JOURNAL OF MAGNETISM AND MAGNETIC MATERIALS,NL,ELSEVIER SCIENCE PUBLISHERS, AMSTERDAM, vol. 160, 1 July 1996 (1996-07-01), pages 249-250, XP000625253 ISSN: 0304-8853	1	TECHNICAL FIELDS SEARCHED (Int.Cl.7) H01F

The present search report has been drawn up for all claims

Place of search	Date of completion of the search	Examiner
THE HAGUE	1 February 2000	Decanniere, L

CATEGORY OF CITED DOCUMENTS

X : particularly relevant if taken alone
Y : particularly relevant if combined with another document of the same category
A : technological background
O : non-written disclosure
P : intermediate document

T : theory or principle underlying the invention
E : earlier patent document, but published on, or after the filing date
D : document cited in the application
L : document cited for other reasons

& : member of the same patent family, corresponding document

EPO FORM 1503 03.82 (P04C01)

ANNEX TO THE EUROPEAN SEARCH REPORT ON EUROPEAN PATENT APPLICATION NO. EP 99 30 8538

This annex lists the patent family members relating to the patent documents cited in the above-mentioned European search report. The members are as contained in the European Patent Office EDP file on
The European Patent Office is in no way liable for these particulars which are merely given for the purpose of information.

01-02-2000

Patent document cited in search report	Publication date	Patent family member(s)	Publication date
JP 07201599 A	04-08-1995	US 5935347 A	10-08-1999
US 5474624 A	12-12-1995	JP 6322472 A	22-11-1994
WO 9215998 A	17-09-1992	AT 137049 T	15-05-1996
		AU 1538992 A	06-10-1992
		CA 2104211 A	07-09-1992
		CN 1064561 A,B	16-09-1992
		DE 69210017 D	23-05-1996
		DE 69210017 T	05-09-1996
		DK 574513 T	28-05-1996
		EP 0574513 A	22-12-1993
		ES 2086734 T	01-07-1996
		GR 3020450 T	31-10-1996
		JP 6505533 T	23-06-1994
		MX 9200959 A	01-09-1992
		US 5340413 A	23-08-1994

EPO FORM P0459

For more details about this annex : see Official Journal of the European Patent Office, No. 12/82